Mircea Vicențiu Săceleanu

Mario Monzon Ilaria Cacciotti

Iulian Antoniac

Brain Revealed

Handbook for Students and Practitioners

Vol. I

Editura Universității „Lucian Blaga“ din Sibiu

2021

Descrierea CIP a Bibliotecii Naţionale a României
Brain reveal : hadbook for students and practitioners / coord.: Mircea Vicenţiu Săceleanu. - Sibiu : Editura Universităţii "Lucian Blaga" din Sibiu, 2021
2 vol.
ISBN 978-606-12-1860-8
Vol. 1. - 2021. - Conţine bibliografie. - ISBN 978-606-12-1861-5

I. Săceleanu, Vicenţiu Mircea (coord.)

616.8

Co-funded by the
Erasmus+ Programme
of the European Union

Preface

This handbook contains the publications presented in the *Brain Revealed – Innovative Technologies in Neurosurgery Study, BrainIT* conference (Project Reference: 2018-1-RO01-KA203-049317).

This project was coordinated by the "Lucian Blaga" University Sibiu, and was carried out during 2018-2021. Other affiliated institutions with competence in neurosurgery and bioengineering participated also. This project proposes the implementation and use of telemedicine as part of the teaching process. Several methods were used, as follows: live video transmissions from the surgery room, interactive education materials and 3D technology for cranial reconstruction. Also a free online platform with education materials for neurosurgery and bioengineering was established.

We want to thank all the implicated institutions in this project for the important role they played in achieving all our goals: "Lucian Blaga" University Sibiu, the Academic Emergency Hospital Sibiu, the *Universita degli Studi Niccolo Cusano* University Italy, and the *Universidad de las Palmas de Gran Canaria* Spain.

We are grateful to announce the release of this handbook, which is addressed to the academic teaching staff, to the neurosurgeons, but also to the residents in training and students of Medicine. This publication is available in printed and digital formats and brings new insights in the neurosurgical pathologies such as arteriovenous malformations, stroke, cerebral neoplasms, or traumatic brain injuries. It also addresses new biotechnologies and their applications in neurosurgery. Among these, biomaterials for modern cranioplasty procedures and wireless power transfer procedures for medical applications are some of the subjects

described. Case studies are also highlighted in order to accurately describe the practical approach.

All in all, this handbook supervised by **Assist. Prof. Vicenţiu Săceleanu** brings an important contribution to the science and research of the future in neurosurgery.

Professor Sorin Radu, Ph.D
Rector
Lucian Blaga University of Sibiu

Preface

The Brain IT is a project financed by the ERASMUS + Programme Strategic Partnership – Project no. 2018-1-RO01-KA203-049317 - and represents an interdisciplinary collaboration between biomaterials and neurosurgery with the ultimate goal of creating 3D molds of the skull and cranial pathology to help students apply neurosurgery techniques in the laboratory, thus becoming familiar with the notions of neurosurgery practice.

Thus, the book published within this project under the name of "Brain Revealed – Handbook for Students and Practitioners", brings together the current practical experience in the field of traumatic, vascular and tumor pathology through the collaboration and involvement in the project of personalities in the field of neurosurgery Dr. Prof. Av. Ciurea and Dr. Prof. St. Florian.

This book written by experts in neurosurgery and biomaterials, provides an excellent overview of the field of traumatic, vascular and tumor pathology and should represent a resource that will be used by neurosurgeons at every stage in their training. It is already known that the education for young people is the best investment for a better society. We hope that this book will stand for the development of the young learning people.

Assist. Prof. Dr. Mircea Vicențiu Săceleanu

Preface

Additive Manufacturing (AM) is a rapidly developing technology and the application in the medical field, and in particular neurosurgery, is a clear example of the high potential. This book presents the two options of application in the neurosurgery field, the first option is as training material for educational purpose, using realistic 3D models coming from scanned images with different pathologies (trauma, tumour, aneurism etc.). The second option is as cases studies for pre-surgery, where the surgeon can simulate the real operation, reducing the risk of failure. For both options it is very important to get realistic 3D models in terms of material and shape and this is a relevant finding of BrainIT project. The objective is either the students of medicine or the professional surgeon to feel they are manipulating real tissue when using these 3D models, which is the most challenging point of the developed training material. BrainIT is without any doubt an interdisciplinary project, working in collaboration professionals of medicine and engineers, under the same objective of improving the health and quality of life of people. On behalf of the team of Las Palmas de Gran Canaria University, who collaborated in this project, and with the thanks to the coordinator, Dr. Vicentiu Saceleanu, and the other partners, I hope you will enjoy reading this book.

Dr. Mario D. Monzón Verona
Profesor Titular de Universidad
Departamento de Ingeniería Mecánica
Universidad de Las Palmas de Gran Canaria

Preface

Despite its history of thousands of years, the modern cranioplasty still presents high postsurgery complication rate, with an elevated number of reoperations, infection and resorption of the implanted grafts. Even if autologous bone graft is still considered the gold standard material for cranioplasty, it presents a lot of drawbacks, i.e. high risk of infection, high absorption rate, and reduced strength. Thus, the formulation, development and production of new biomaterials is strongly motivated by the limits of the traditional and currently used materials. However, the design of performant and efficient biomaterials is very complicated and challenging, taking into account the need to simultaneously satisfy several requirements in terms of chemical composition, physico-chemical properties, microstructure, surface topography, mechanical behaviour, as well as biological responsiveness and interactions with cells, tissues, organs.

More viable alloplastic materials, including metals, ceramics, polymers and composites, have been developed, such as titanium, mesoporous hydroxyapatite (HAp), polymethylmethacrylate (PMMA), polyetheretherketone (PEEK) and their combination. From the comparison among the different types of alloplastic materials, poor statistical evidence justifies the choice of one material with respect to another, and, in all cases, their use leads to high infection rate that remains an open concern leading to implant failure.

Thus, it is crucial to identify materials and implantable reconstruction solutions able to mitigate the potential infection risk, as well as technologies to monitor the post-surgery infection/inflammation. New current trends in the development of innovative and efficient biomaterials involve the biomimetic and molecular biological approaches. The first one is devoted to the design of biomimetic materials able to resemble both the chemical composition, microstructure and properties of the native tissue, and characterised by suitable biomechanical properties, enhanced biodegradability, and improved osteoconductivity. On the other hand, the second strategy is based on the introduction of bone growth factors

and bone morphogenetic proteins (BMP), to guarantee immediate protection to the cranium, with aesthetical beneficies, and both osteoconductive and osteoinductive actions.

Concerning the urgent need of an appropriate post-surgery monitoring, it is pivotal to design efficient sensors for specific parameters, such as temperature, intracranial pressure, pH..., as well as innovative transfer data technologies. Indeed, wearable and implantable sensor devices can be the answer to monitor specific parameters associated to postsurgery infections. The way to access the control of the different vital parameters must be as easy as possible for the patient. The main issues, in implementing this type of health monitoring system, are the data transfer modality and how to power the implantable and wearable sensors. One possible answer to these problems is the use of the wireless power transfer (WPT) technology, which is a safe and appropriate method to provide energy for recharging biosensors and implantable electrical devices as well as for data communication in these specific applications.

In conclusion, up to date, a consensus about the optimal biomaterials and techniques has not been achieved yet, due to lack of consolidated data and contradictory evidences. Thus, the presurgical decisions strictly depend on the surgeon experience and on the individual conditions of the patient, and large scale and prospective studies are strongly demanded to accomplish more reasonable and reliable data.

Prof. Dr Ilaria Cacciotti
Ph.D. in Materials Engineering
Associate Professor of Materials Science & Technology and
Biomaterials &Tissue Engineering
Engineering Department, University of Rome "Niccolò Cusano"

Preface

Neurosurgery is a complex and cutting-edge specialty, consisting in multiple aspects that require decades of constant work to truly understand. Its complex nature derives from the relatively short history of neural science which developed gradually and slowly throughout the time and finally accumulating in the last century some of the most extremely challenging data in science. The efforts of both „Lucian Blaga" University, Sibiu and ERASMUS + Program – Strategic Partnership, led to the creation of two volumes dedicated to this complex topic: the first volume presents the applicability of biomaterials in neurosurgery and the second volume is dedicated to neurosurgical pathologies.

For medical students, residents and neurosurgery practitioners navigating through all neurosurgical information can be overwhelming. *BrainIT Revealed – Handbook for students and practitioners* is a support handbook that allows the rapid assimilation of the essential elements of neurosurgical interventions.

The authors of the two volumes collaborated with internationally recognized scientists. The first volume of biomaterials was coordinated by Prof. Mario D. Monzon (Spain), Prof. Ilaria Cacciotti (Italy), Prof. Iulian Antoniac (Romania) and Assist. Prof. Dr. Vicentiu Saceleanu (Romania). The second volume coordinated by Prof. Dr. Alexandru Vlad Ciurea (Bucharest) and Assist. Prof. Dr. Vicentiu Saceleanu (Sibiu) is divided in 4 parts (classic neurosurgical approaches, vascular, tumoral and traumatic pathologies) and provides a clear, illustrated introduction to all aspects of neurosurgery.

Prof. Dr. MSc. Alexandru Vlad Ciurea

Preface

It is a pleasure to write the preface for *BrainIT Revealed – Handbook for students and practitioners*. This book is designed in two parts: one regarding the biomaterials and another one is describing the main entities of the neurosurgical pathology; they are clearly outlined both clinically and imagistically and then the elements of neurosurgical management are presented. Written by neurosurgeons, this book is a hands-on guide that translates basic science and theories of neurosurgery into clinical practice. This monograph summarizes the main, classic data, but also the current clinical and operative elements in traumatic, tumor and vascular craniocerebral pathology. I strongly recommend *The BrainIT Revealed - Handbook* to all students of neurosurgery and to all neurosurgeon practitioners as an up-to-date, objective, and readable text that covers the full scope of neurosurgical practice. Based on the authors' own clinical practice, teaching and examination experiences in medicine, but having also a good engineering expertise in fabric the 3D molds, this book provides candidates with a firm grasp of neurosurgery and biomaterials as a support of a discipline which is knowing a rapidly developing and technically demanding. It should be mentioned that the entire material is completely original and updated with modern data from the literature.

Prof. Ioan Ștefan Florian, MD, PhD

Preface

Neurosurgery is a complex medical specialty that use a lot of advanced technologies, from microscopy to robotics and advanced biomaterials.

The efforts of „Lucian Blaga" University, Sibiu to publish a complex book dedicated to the applicability of biomaterials in neurosurgery and the neurosurgical pathologies, represent a milestone in the field of neurosurgery. The authors of the book *BrainIT Revealed – Handbook for students and practitioners* provides a clear and useful data that allows the rapid assimilation of the essential elements of actual and future neurosurgical interventions for the medical students, residents, and neurosurgery practitioners.

With the development of tissue engineering technology, there have been new developments in the treatment of nerve injury. Tissue engineering and regenerative treatment strategies require high growth factor concentrations achieve proper regeneration to sustain therapy level for a longer period.

A combination between bioengineering, biomaterials improvement, and neuroscience is needed to drive forward these guarantees.

Successful tissue regeneration strategies focus on the use new biomaterials, structures, and various control replicas cellular behaviour and promotion of regeneration.

Prof. univ. habil. dr. eng. Iulian Antoniac

TECHNOLOGIES OF ADDITIVE MANUFACTURING APPLIED IN THE MEDICAL FIELD

Rubén Paz[1]
Mario Monzón[1]

[1] Department of Mechanical Engineering, Campus de Tafira Baja, Edificio de Ingenierías, University of Las Palmas de Gran Canaria, 35017, Las Palmas, Spain

This chapter gives an overview of the Additive Manufacturing concept, the general categories of technologies according to the standard classification, and the most typical technologies in the medical field, both for the production of prostheses, scaffolds, and pre-clinical evaluation and training.

Contents

1.1. Introduction to Additive Manufacturing technologies. General classification

According to 'ISO ISO/ASTM 52900:2015 Additive manufacturing — General principles — Terminology' [1], Additive Manufacturing (AM) is the process of joining materials, usually layer upon layer, to make parts from digital data (3D model). This manufacturing concept, colloquially known as 3D printing, differs from the traditional subtractive manufacturing, which is based on the removal of material (e.g. machining processes), or formative manufacturing methodologies, which consist in causing the plastic deformation of the material (plastics or metals) into the desired shape by applying stresses and, in some cases, temperature (e.g. injection molding, rotomoulding, forming processes, bending, etc.). These conventional processes require specific tools (molds, cutting tools, etc.) which hinder or constraint the manufacturing process in terms of design freedom. Additionally, in the case of short productions, the initial investment needed for these tools leads to expensive unit costs and, in some cases, long manufacturing times due to the production of these. However, the layer-upon-layer concept that characterizes AM has the advantage of not needing these tools or molds, making it more competitive especially for short production runs or complex geometries. Therefore, AM technologies stand out compared to traditional manufacturing process due to the possibilities in terms of design freedom/customization and reduced production time and manufacturing costs for short runs due to the avoidance of additional tools.

Despite these clear advantages and possibilities, AM commercially emerged in 1987, thus being a relatively new manufacturing concept, especially when compared with other conventional processes. In 1951, Munz proposed the first AM technology, which was based on layers of photopolymer that were selectively hardened according to the cross-section by a piston mechanism. Since then, different proposals were published such as the use of a laser to carry out the photopolymerization (1968), the earliest powder laser sintering process (1981), and, about the same time, the earliest AM system that used a computer to control the laser for the polymerization of the photopolymer [2]. However, the first AM equipment was formally

invented in 1986: StereoLithography Apparatus (SLA) and commercialized in 1987, which is considered the year of the birth of AM. This equipment consists in the photopolymerization of a thin layer of light-sensitive liquid polymer (photopolymer) by the application of a laser ultraviolet light. In 1991, several new AM concepts were launched to the market, being fused deposition modeling (FDM, from Stratasys) and laminated object manufacturing (LOM, from Helisys) the most innovative. In the case of FDM, a thermoplastic material in filament format is melted/extruded and deposited/solidified layer by layer to make the part. Although FDM was the name of the specific machine of Stratasys, nowadays this concept is still used when referring to material extrusion AM. Regarding LOM technology, the material, in the form of sheets, is bonded (adhesive coating) and cut by a laser. Later on, Selective Laser Sintering (SLS), which uses the heat of a laser to fuse a powder bed, was commercially available in 1992. Many different technologies have been patented and launched since then, contributing to the development and spreading of AM technologies. Additionally, the expiration of important patents such as the most critical ones related to FDM caused an exponential expansion of material extrusion-based machines with low prices [3], affordable even for private users. As a consequence, nowadays there is an important community of private users that has broadened the knowledge and advantages of AM.

Nowadays, there are several AM technologies, both for polymers, metals, ceramics or even composite feedstock. In order to have a standard classification, ISO/ASTM launched in 2015 the standard 'ISO/ASTM 52900:2015 Additive manufacturing — General principles — Terminology' [1], which classifies the existing technologies into 7 categories. The following subsections describe each one of these categories.

1.1.1. VAT photopolymerization

VAT photopolymerization (VPP) is an Additive Manufacturing process in which a photopolymer liquid is selectively cured in a vat by light-activated polymerization (ultraviolet photopolymerization). Figure 1 shows the principle of functioning of these technologies. The build platform, initially on the top of the vat, is submerged in the

photopolymer liquid until a thin layer of liquid (according to the selected layer height) is on the platform. Then, the laser (in the case of SLA) sweeps the desired section and cures the material according to the 3D data. Once the layer has been photopolymerized, the platforms goes down, placing an additional thin layer of liquid on the platform to repeat the process.

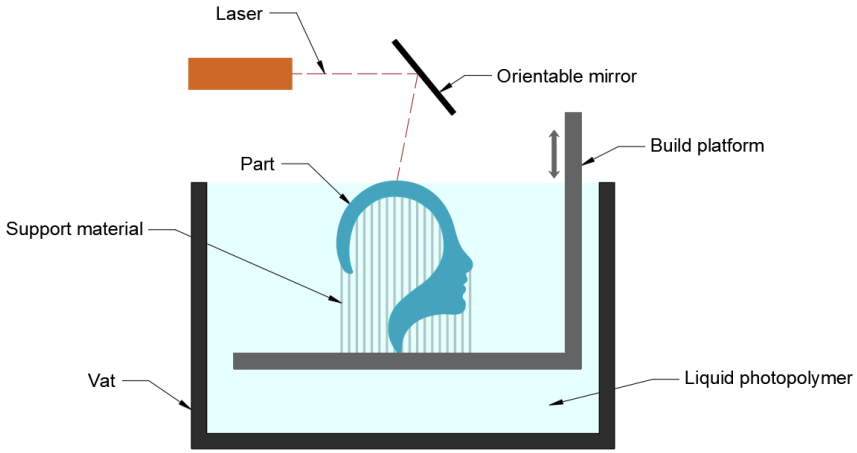

Figure 1. Vat photopolymerization scheme (stereolithography, SLA).

Within this category, there are two main technologies: stereolithography (SLA), which uses a laser that sweeps the desired section oriented by a mirror, and Digital Light Processing (DLP), which uses a light projector to cure the complete section at once. This second option is represented in Figure 2. Usually, the light projector is placed on the bottom and the part is built from the bottom to the top of the vat, thus being hanging from the build platform, which moves from the bottom to the top.

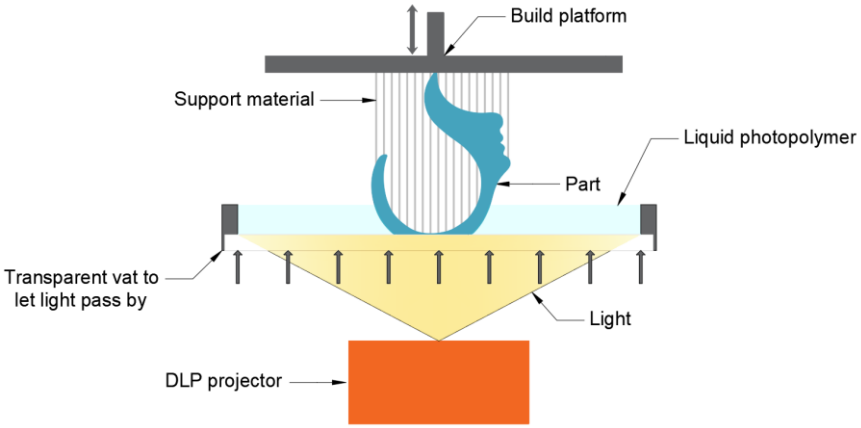

Figure 2. Vat photopolymerization scheme (Digital Light Processing, DLP).

Depending on the manufacturing configuration, this category is also divided into three different types.

The first one is the 'bottom-up printing' (according to the movement of the build platform), in which the liquid is cured through a window placed in the bottom of the vat by a light source (as depicted in Figure 2). The build platform is raised out of the resin vat and a 'peel' step is required to detach the last cured layer from the bottom of the vat. This 'peel' step is by far the slowest stage, thus being the bottle neck of the process. However, this configuration uses less resin, which means smaller vats (less material) and consequently smaller printers with fewer mechanical parts. Several printers such as Projet 1200 (Figure 3), Formlabs Form2, Envisiontec Vida or Structo Orthoform use this configuration, being the most typical due to these advantages.

Figure 3. ProJet 1200, vat photopolymerization machine with DLP technology and 'bottom-up printing'.

The second type is the 'top-down printing'. In this case, the resin is cured by using a light source placed above the vat. Therefore, the build platform is lowered down into the liquid photopolymer during the process, as depicted in Figure 1. The 'top-down printing' has the advantage of using a continuous light exposure to polymerize the photopolymer. As a consequence, the alternating light exposures and 'peel' steps are avoided and the printing speed is considerably improved, especially due to the avoidance of the 'peel' step. For this reason, this configuration is preferred for industrial printers where the speed is more important (e.g. Juell Flash OC).

The third configuration is the 'Continuous Liquid Interface Production (CLIP)'. In this configuration, the liquid photopolymer is cured through an oxygen permeable window (placed on the bottom of the vat) by a light source from below. This oxygen layer avoids the sticking of the resin to the vat and, consequently, the 'peel' step is not needed. As a result, a continuous light exposure can be used, thus improving the printing speed. Therefore, this configuration is similar to

the 'bottom-up printing' but with the advantage of not needing the 'peel' step, which leads to similar speeds to the 'top-down printing'. However, this configuration is more expensive. One example of this configuration is the Carbon M1.

1.1.2. Material jetting

Material Jetting (MJT) is an AM process in which droplets of build material (photopolymer) are selectively deposited and cured immediately by ultraviolet light. This concept is similar to a two dimensional ink jet printer, but in 3D. The material is jetted onto a build platform from a nozzle. This nozzle moves horizontally on the build platform. The material layers are then polymerized using ultraviolet light. Figure 4 shows the functioning scheme of material jetting technologies.

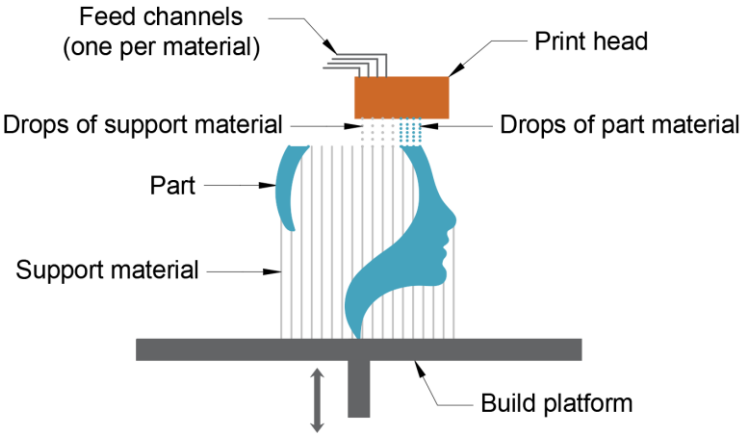

Figure 4. Material jetting scheme.

Within this category, there are two main nozzle configurations: the inkjet printing, which applies a continuous stream of material (jet of material), and the 'Drop on Demand' (DOD), in which droplets are dispensed only when needed, thus being more accurate and using less material, but also with lower printing speeds.

On the other hand, these technologies are characterized by needing support material in all the cantilever areas. However, the support material can be removed using a sodium hydroxide solution or water jet.

Additionally, material jetting technologies can print with two different configurations: matte or glossy. The matte setting will add a thin layer of support to the entire part. This provides more accuracy and uniform finish to the part (matte), but uses more material, requires more cleaning post-processing and the surface is softer. The glossy setting, otherwise, will only use support material when necessary (cantilever areas). This setting leads to higher strength on thin walls, material reduction and gives a smoother finish. However, the finish is not uniform throughout the part (the zones requiring support material will have a matte finish, while the other ones will be glossy) and small rounding are obtained at sharp corners on the top surfaces.

Polymers and waxes are the commonly used materials due to their viscous nature and ability to form drops.

1.1.3. Binder jetting

Binder Jetting (BJT) is an AM process in which a liquid bonding agent is selectively deposited to join powder materials. The binder (usually in liquid form) acts as an adhesive between the layers of the build material (in powder form). The print head moves horizontally (x-y axes) to deposit the binding material (sometimes together with colored ink to obtain different colors) on the build material. After each layer, the build platform is lowered down and a new layer is added to continue the process (Figure 5). It is a fast process even though it requires a certain cooling time for the binder to solidify. However, a porous surface finish and slow post-processing are typical due to the powder format of the build material.

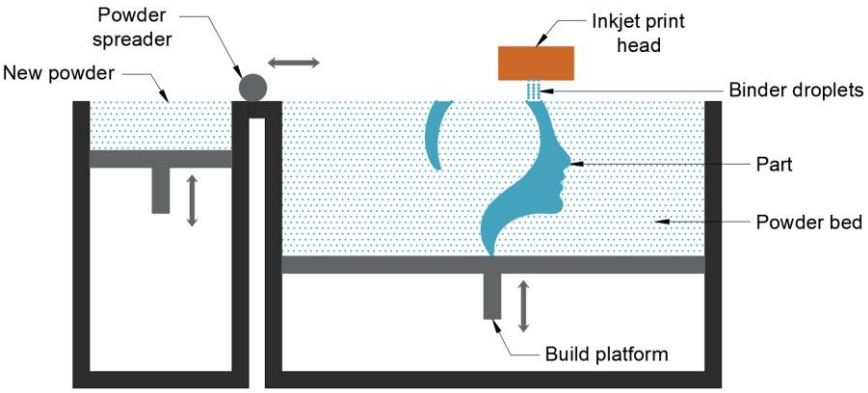

Figure 5. Binder jetting scheme.

Due to the binding method, the resulting 3D printed objects are not always suitable for structural parts. On the other hand, despite the relative speed of printing, the additional post processing required (powder removal and powder conditioning for the subsequent run) can add significant time to the overall process. The main advantage of this category is that the powder bed acts as a self-supporting structure, which allows adding complex parts in the build volume, as well as using different materials.

Additionally, apart from full-color parts, this technology allows the use of metal powder to obtain metal parts. The resulting 3D printed parts (usually known as 'green parts') are very brittle (metal powder joined by the binder) and subsequent steps such as infiltration or sintering are required to improve the mechanical properties. Both in the infiltration and sintering postprocesses, high temperatures are used to burn the binder. However, in the infiltration process, bronze infiltration is carried out by the capillary action of the melted metal, while in the sintering process, the high temperature sinters the metal particles, causing an important shrinkage (around 20 %). As the resulting parts are not 100 % dense (approximately 90% in the case of infiltration and 97 % for sintering), their mechanical properties are also limited, especially for dynamic conditions in which the voids can lead

to crack initiation and failure by fatigue. However, this process can be less expensive than other technologies for metal parts production.

1.1.4. Material Extrusion

Material Extrusion (MEX) is the AM process in which material is selectively dispensed through a nozzle or orifice. Usually, this process starts with the stock material (thermoplastic or composite material with thermoplastic matrix) in filament format (spools). The most common diameter is 1.75 mm, although 2.85 and 3 mm are also possible. The use of pellets as stock material is also possible in some technologies with screw extruders, but the deposition speed is reduced and the flow is less stable, thus leading to more defects on the deposited filament. In the most typical case, an extrusion mechanism feeds the filament into the hot end, where the filament is heated by electrical resistances and melted. The filament that is being introduced to the hot end pushes the melted material out the nozzle tip, thus depositing new material on the last deposited layer (Figure 6). The extruded filament, in a melting state, sticks to the to the previous layer (or build platform) and solidifies after a certain time. Once the entire layer has been deposited, the build platform is lowered down and the process is repeated again.

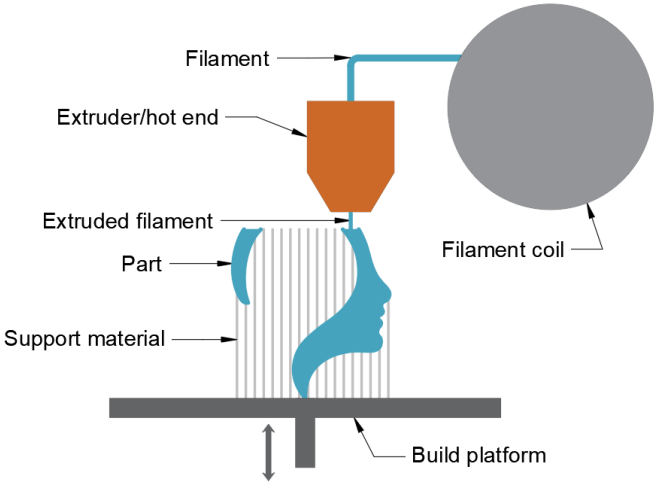

Figure 6. Material extrusion scheme.

The most common diameter of nozzle tip is 0.4 mm, but other diameters from 0.1 to 0.8 mm can be found. This value has a great influence on the speed of the process, as the layer height must be lower than the diameter to guarantee a good bonding between layers (Figure 7). As a consequence, in general, the higher the diameter of the nozzle tip, the lower the printing time. However, the accuracy of the deposited part is also dependent on the nozzle tip diameter (smaller nozzle tips lead to higher accuracy). Additionally, thicker layers can have a negative effect on the finishing of the part, as the layers can be easily noticeable, especially in near horizontal surfaces.

Figure 7. Bonding of layers. On the left, poor bonding due to too high layer height. On the right, good bonding.

This technology is also characterized by having a high anisotropy behavior due to the reduced properties in the printing direction (Z axis). The mechanical properties of the bonding between layers are usually lower than the corresponding to the deposited filaments (XY plane). This effect is typical in any other AM technologies, but in the case of MEX category the level of anisotropy is considerable.

On the other hand, some MEX printers have a heated bed or even chamber to control the environment temperature. This characteristic is crucial to avoid the warping effect (Figure 8), especially in materials with high coefficient of thermal expansion and high processing temperatures. When the upper layers solidify and cool down, the associated shrinking pulls the lower layers, producing delamination or, most commonly, detaching the corners of the first layer from the build platform. This can ruin the printing in some cases, as the corners of the part are distorted and the nozzle tip may collide with them and completely detach the part. The warping defect can be reduced by

homogenizing the temperature between layers through a controlled bed temperature and, in some industrial machines, a controlled environment temperature. In the case of 3D printers without heated bed, the common practice to reduce the warping is the use of brims [4], which are an extension of the cross section of the fist layer to increase the contact surface between the first layer and the build platform, thus enhancing the adherence. However, additional postprocessing is required (removal of the brim to obtain the desired geometry).

Figure 8. Warping defect.

This category of AM has become the most used technology for private users due to the emergence of low cost manufacturers of this type of 3D printers (Figure 9). As the initial patent was Fused Deposition Modeling (FDM), these 3D printers are also named as FDM technologies, referring to MEX AM equipment.

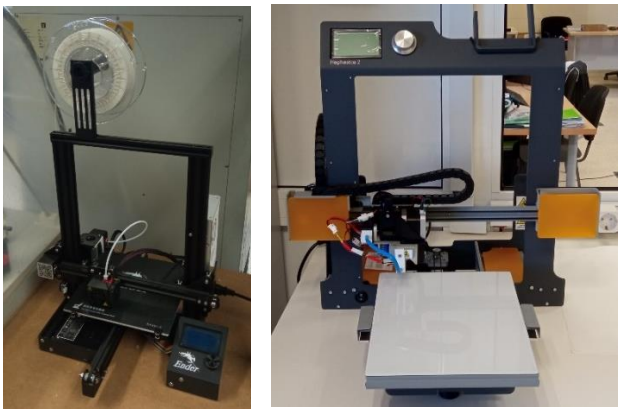

Figure 9. Low-cost MEX 3D printers (left: Creality Ender 3; right: BQ Hephestos 2).

Apart from the typical thermoplastic extrusion AM equipment, there are other AM technologies also based on extrusion but working with other materials and applications. This is the case of bioplotters or bioprinters (Figure 10), 3D printers that allow working with biomaterials and cells, in sterile environments, for AM applied in tissue engineering and tissue biofabrication. These technologies usually have several type of printheads, which allow the manufacturing of multi-material parts. Among the type of printheads, there are 2 main groups: the specific ones for hydrogels (viscous fluids that are extruded by pneumatic and mechanical mechanisms), and the specific ones for depositing thermoplastic materials (also based in the feeding, melting and extrusion of the material).

Figure 10. Bioplotter (Bio X, Cellink).

Finally, there is another group of innovative AM technologies that use an extrusion process to produce the parts: Atomic Diffusion Additive Manufacturing (ADAM) [5]. ADAM is based on a MEX AM process but using a filament with metal powder embedded in a thermoplastic matrix. The initial step of ADAM is the same as in a conventional MEX 3D printer, but obtaining a composite part with metal powder inside (also called 'green part', as in binder jetting with

metal powder). After this, the green part is submerged in a liquid (debinder) to remove almost all the plastic matrix, thus obtaining a porous part. Finally, the part is subjected to a sintering process in a high temperature oven where the remaining binder is burnt out and the metal powder is sintered to achieve an almost fully-dense part (approximately 1% of porosity). Therefore, ADAM technology allows the manufacturing of 3D printed metal parts with very competitive cost compared to metal Powder Bed Fusion AM technologies.

1.1.5. Powder bed fusion

Powder bed fusion (PBF) is an AM process in which thermal energy selectively fuses regions of a powder bed. For this to happen, a thin layer of powder material is spread by a powder spreader system on the build platform (this step is considered the most time consuming of the entire process). After that, an energy source (usually a laser beam, although it depends on the technology) sweeps the section of the part, sintering the powder particles and joining them together. Once the layer has been sintered, the build platform is lowered down and the process is repeated again until the part is completely manufactured (Figure 11).

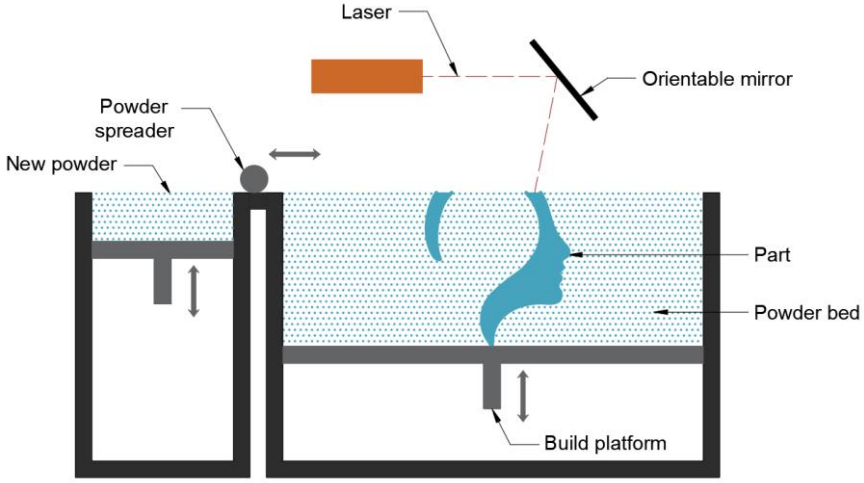

Figure 11. Powder bed fusion scheme.

As in the category of binder jetting, powder bed fusion stands out due to the use of a powder bed that acts as a self-supporting structure for the part. For this reason, support material is not usually required, except in metal technologies where the energy to join the particles is so high that the powder itself is not enough to support it. Moreover, the high temperature gradients of these metal processes are also critical for the warping effect. For this reason, support structures are not only useful to withstand the energy of the process, but also to cool down the printing area and attach the new layer to a solid base. As a consequence, in metal technologies the general rule is to add support structures in walls with less than 45° with respect to the horizontal plane. However, in the case of plastic technologies of this category, support structures are not needed and it is possible to allocate parts all over the build volume without the use of support material. This possibility is also very powerful for the production of assembled parts. The non-sintered powder acts as a support and separation element between the different components of the assembly. Once the manufacturing is finished, the powder is removed in the postprocessing step, obtaining the final assembly. As a result, no assembly steps are required.

Depending on the energy source and material type, different PBF technologies can be found. In the case of thermoplastic materials (and thermoplastic composites), the most common technology is the Selective Laser Sintering (SLS) (Figure 12). In this case, a thermoplastic is spread on the build platform and a laser sinters together the particles. In order to speed up the process, the environment is preheated, so that the laser only provides the additional energy required to sinter the particles.

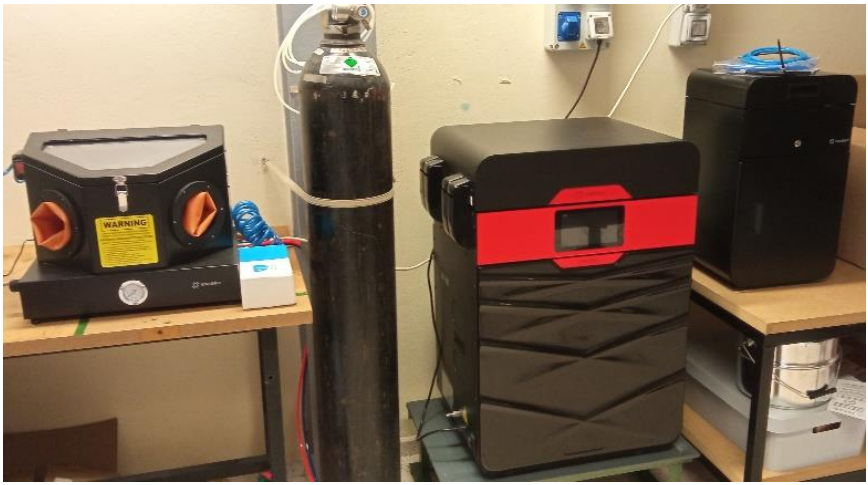

Figure 12. First Selective Laser Sintering machine with desktop format (Sinterit Lisa Pro). Left: sandblaster unit for post-processing. Middle: 3D printer with optional nitrogen atmosphere. Right: sieving unit for material preprocessing (mixing of virgin and reused material and sieving).

In the case of metal powder, there are three main technologies: Direct Metal Laser Sintering (DMLS), Selective Laser Melting (SLM) and Electron Beam Melting (EBM). DMLS is similar to SLS since the particles are sintered, but not completely melted. However, in the case of SLM, the particles are completely fused as the energy source is more powerful (leading to lower porosity parts). Moreover, an inert atmosphere is required to avoid the oxidation and reaction of the melted powder with the environment gases. Finally, EBM has a similar concept to SLM as it melts the particles, but the energy source is an electron beam instead of a laser. The main characteristic of this technology is that the surface is usually rougher compared to the previous ones. This could an advantage for some specific applications (e.g. cell attachment in the case of internal prostheses for tissue regeneration), but also a limitation for other applications and for the strength under fatigue loads.

Apart from the aforementioned technologies, there is another technique called Multi Jet Fusion (MJF) in which the fusion of the

powder is triggered by the jetting of fusing agents and the application of an energy source. This energy produces the reaction between the fusing agent and the powder bed, causing the selective melting of the material. Additionally, detailing agents are also jetted around the contours to produce accurate details and obtain smooth surface finishing.

On the other hand, it is important to note that the characteristics required in PBF powders (e.g. particle size distribution) make them expensive, especially in the case of metal materials. For this reason, one of the main design rules for these technologies is to optimize the use of powder by allocating as many parts as possible in the printing volume. The non-sintered powder can be reutilized but, as it has received a thermal cycle during the PBF process, it must be refreshed with around 30-50% of new powder (otherwise, the printed part will have lower mechanical properties). This means that the powder removal must be done very carefully to reutilize as much material as possible. Moreover, the recycled material must be blended and sieved with the new powder to be in good conditions for the following printing. All these steps are very time consuming and require manual work, which is one of the main limitations of these technologies. Apart from this, the working conditions must be appropriate and with the correct personal protective equipment as handling so small powder particles implies certain health risks.

1.1.6. Sheet Lamination

Sheet Lamination (SHL) is an AM process in which sheets of material are bonded to form a part. This process in summarized in Figure 13. A spool of material is fed into the build platform and glued to the build platform or previous layer by using compression or welding. Then, each layer is cut by a laser or cutting tool according to the desired cross section of the 3D model. Once the layer is finished, the build platform is lowered and the material spool is fed again, repeating the process and making the part layer by layer. This process is fast and low cost, but it is limited to sheet format materials and requires postprocessing to obtain the final part.

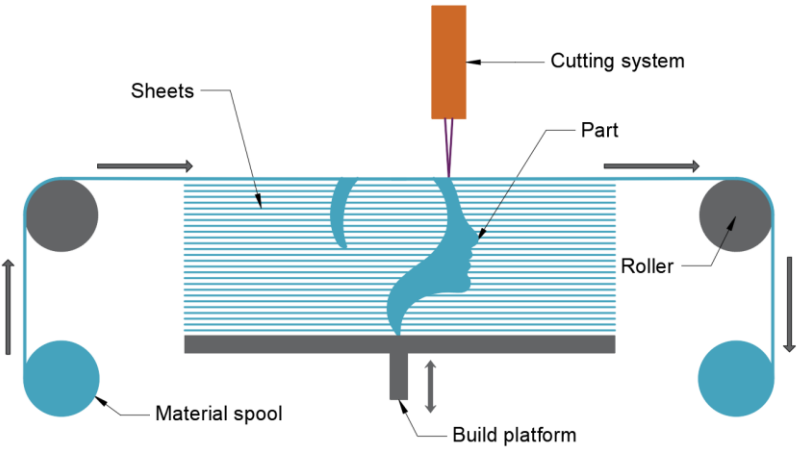

Figure 13. Sheet lamination scheme.

Within this category, there are two main technologies: Laminated Object Manufacturing (LOM) and Ultrasonic Additive Manufacturing (UAM). LOM uses adhesive paper (in sheet format) that is glued by compression and cut by a laser. In the case of UAM, metal alloy sheets (mainly of aluminum, copper, stainless steel or titanium) are used and joined by ultrasonic welding.

1.1.7. Directed Energy Deposition

Directed Energy Deposition (DED) is an AM process in which a thermal energy source such as a laser, electron beam, or plasma arc, is used to melt materials at the same time they are being deposited on the substrate (part or build platform) (Figure 14). The technologies of this category usually work with metal materials in powder or wire format.

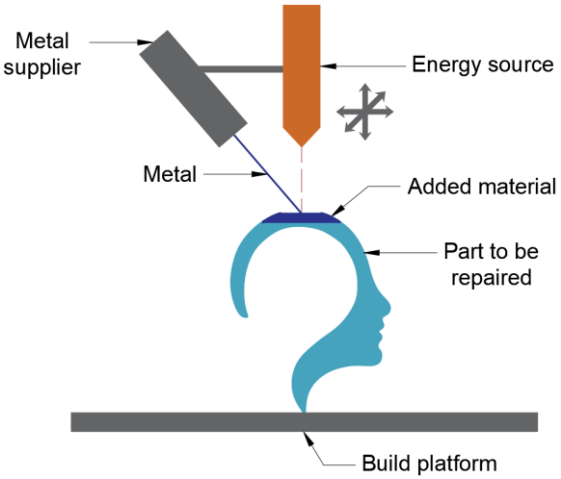

Figure 14. Directed energy deposition scheme.

The functioning of this category could be similar to a metal arc welding technology, but with controlled motion by Computer Numerical Control (CNC) in a multi axis arm (4 or 5 axis machines). This arm feeds the material (wire or powder) and deposits and melts the material, at the same time, on the surface of the part, where it solidifies. The process could be also similar to material extrusion, with the different that the beam can move in multiple directions and the material is usually a metal such as cobalt, chrome and titanium. Powder DED machines often use inert gas, which is added together with the powder or wire from the nozzles to reduce the reaction of the melted metal with the atmosphere. Moreover, these machines may have multiple nozzles to work with different metal powders at the same time, which allows mixing them to produce functionally graded components, also known as Functionally Graded Additive Manufacturing when the part is obtained by AM [6].

Depending on the format of the material and energy source, there are different technologies within this category. Regarding the energy source to melt the material, there are three main groups:

- Laser-based systems such as Laser Engineering Net Shape (LENS), Laser Metal Deposition (LDM) or Laser Cladding (LC).

- Electron beam based systems such as Electron Beam Additive Manufacturing (EBAM).
- Plasma or Electric arc based systems such as Wire Arc Additive Manufacturing (WAAM).

With regards the format of the material feedstock, there are two main groups:

- Powder-based systems (LENS, LDM or LC), which use powder material.
- Wire-based systems (e.g. WAAM), which work with wires.

These technologies are commonly used to repair parts, taking advantage of the existing part to be used as substrate for the addition of new layers. Despite the finishing is rough, these technologies are usually combined with subtractive manufacturing (multi axis machining) to improve the final surface quality. These combination of additive and subtractive manufacturing in the same equipment is known as 'hybrid manufacturing'.

1.1.8. Main advantages and disadvantages of AM by categories

Table 1 shows the main advantages and drawbacks of AM technologies, sorted by category and from the medical perspective.

Table 1. Main pros and cons of AM technologies by category [7].

AM category	Pros	Cons
VAT photopolymerization (VPP)	High resolution and accuracy, complex parts, decent surface finish and flexible printing setup	Lacking in strength and durability, sensitivity to UV light after print, and not for structural use
Material jetting (MJT)	High accuracy, low material waste and multimaterial and multicolor parts	Required support material and limited materials (only polymers and waxes)

AM category	Pros	Cons
Binder jetting (BJT)	Multicolor, multimaterial, fast AM and different binder-powder combinations to adjust mechanical properties	Not always suitable for structural parts and long postprocessing (cleaning)
Material extrusion (MEX)	Inexpensive, widespread and availability of different materials with interesting properties	Quality depends on the nozzle radius, low accuracy and speed, and contact pressure needed to increase quality
Powder bed fusion (PBF)	Large material options	Low speed, lack of structural properties in materials, limited sizes and dependence on powder size
Sheet lamination (SHL)	Speed, inexpensive, ease of handling	Dependence on paper or plastic material, need of postprocessing and limited material range
Direct energy deposition (DED)	High control of grain structure, fully dense parts and good process for part repair	Limited materials, poor surface quality and low accuracy of wire process

1.2. Additive Manufacturing technologies in the medical field

The medical industry is one of the largest users of AM since the high customization and complexity degree required in this field matches perfectly with the main advantages and capabilities of AM technologies.

For example, the manufacturing of a specific and optimized implant or scaffold (structure that serves as support for the growth of extracellular matrix of the damaged tissue) requires a unique and complex design that cannot be easily manufactured with conventional technologies. In the specific case of scaffolds (or implant areas where the tissue regeneration is important), a cellular structure with a large volume fraction of interconnected pores is needed (the greater the surface of the scaffold, the better the cell adhesion) and the shape and size of the cellular structure have a great influence on the regeneration efficiency. Therefore, the design must be tailored according to these considerations, but also ensuring the appropriate mechanical properties (trying to mimic the replaced tissue) and a minimal mechanical integrity for a proper handling during surgery [8]. As a consequence, the resulting optimal design (unique design) is usually quite complex and almost impossible to produce with conventional processing techniques. However, AM technologies and the continuous evolution of materials in this field (which must be biocompatible and, in some cases, bioresorbable) make these designs feasible to be manufactured and in a short period of time, without additional tools needed. For these reasons, the most cutting edge uses of AM are usually related to the medical field.

Apart from the direct application of AM for specific medical parts such as prostheses or scaffolds, AM technologies are also useful for the production of personalized anatomy models from patients' scans. These anatomy models can be very valuable for training and, specially, for preclinical practice since surgeons can practice tricky surgery techniques before the real operation, thus reducing risks during the surgical procedure. Finally, AM capabilities can be also applied for the production of specific and personalized tools for medical applications.

The following subsections summarize the most typical AM technologies used in the medical field and classified by category. In this case, three different medical applications have been considered for the classification of AM technologies: prostheses, scaffolds, and training/pre-clinical models production. According to the literature [9], directed energy deposition is only used in isolated cases of implants and sheet lamination rarely used for medical models or phantoms. In the

case of material jetting, this technology is not used for internal prostheses. However, the remaining AM categories (VAT photopolymerization, powder bed fusion, material extrusion and binder jetting) have been utilized in all the medical applications considered in this chapter, although some of them are more common depending on the specific application. Table 2 summarizes these medical applications of the seven AM categories.

Table 2. Application of AM technologies in the medical field sorted by AM category.

	Prostheses	**Scaffolds**	**Pre-clinical and training**
VAT photopolymerization (VPP)	☒	☒	☒
Material Jetting (MJT)	Not for implants	☒	☒
Binder Jetting (BJT)	☒	☒	☒
Material extrusion (MEX)	☒	☒	☒
Powder bed fusion (PBF)	☒	☒	☒
Sheet Lamination (SHL)	☒	☒	Rarely used
Directed Energy Deposition (DED)	Rarely used for implants	☒	☒

Table 3 also summarizes the most typical materials and medical uses of the seven AM categories.

Table 3. Common materials and medical uses of the seven AM categories [7].

AM process	Materials	Medical use
VPP	Photopolymer resin	Bone, dental models, dental implant guides and hearing aids
MTJ	Polymers (PP, HDPE, PS, PMMA, PC, ABS, HIPS, EDP)	Medical models, dental casts and dental implant guides
BJT	Stainless steel, polymers (ABS, PA, PC) and ceramic (glass)	Color parts (especially for coding anatomy models)
MEX	Polymers (ABS, PA, PC, etc.)	Medical instruments and devices and rapid prototyping exoskeleton
PBF	Powder-based materials (depending on the technology: PA, stainless steel, titanium, aluminum, cobalt chrome, steel and copper)	Models with cellular structures, medical devices such as implants and fixations
SHL	Paper, plastic and sheet metals	Limited (orthopedic modelling of bone surfaces)
DED	Metals (cobalt chrome and titanium)	Limited (used to repair existing parts and build very large parts)

1.2.1. Additive Manufacturing technologies for prostheses

Prostheses are artificial devices used to meet the biomechanical needs of people with physical disabilities. Traditionally, these devices were fabricated by time-consuming and labor-intensive processes. However, the evolution of AM technologies is changing this trend, since AM prostheses can achieve the biomechanical performance of

traditional prostheses, with the inherent advantages of AM. In the traditional fabrication of external prostheses, a negative cast mold is produced by wrapping plaster bandages around the affected part. This mold is then used to pour plaster and obtain the positive mold. Subsequently, sheets of thermoplastic are heated and adapted to the positive mold by vacuum forming. Once solidified, they are cut with the correct shape. Moreover, the final prosthesis usually requires some additional adjustments to achieve the desired comfort and functionality. All these problems can be significantly reduced by using body scanning techniques, CAD modelling and AM technologies [10].

There are several technologies used for the development of prostheses, especially depending on the location of the prosthesis. In the case of internal prostheses (implants) the materials used must be biocompatible. Moreover, in some cases the implants are designed not only to substitute the damaged tissue in the initial recovery stage, but also to biodegrade so that the regenerated tissue can replace the implant progressively. In these cases, the implant must degrade into non-toxic components easily resorbable by the body (bioresorbable materials).

In the case of internal prostheses, usually metal parts are required to achieve the desired mechanical properties, although high performance and biocompatible plastics are also used, such as PEEK (mainly with material extrusion technologies [11], [12] or SLS powder bed fusion). Among the AM technologies that can work with biocompatible metals, powder bed fusion is the preferred category for this application (SLM, DMLS or EBM technologies). The most common materials for powder bed fusion in implants applications are titanium alloys (or pure titanium), stainless steels, tantalum, NiTi, and CoCr alloys. The use of biodegradable metals in AM such as magnesium (Mg), iron (Fe), and zinc (Zn) is currently under research, although still in its initial steps. According to the literature, element loss and porosity are the most common processing problems for AM of biodegradable metals like Zn and Mg [13].

Regarding external prostheses, plastic materials are more common as the required mechanical properties can be achieved by adjusting the design. As a consequence, almost all the AM categories working with plastic material (material extrusion, SLS powder bed fusion, material

jetting, vat photopolymerization and binder jetting) can be used, especially for prosthetic arms and hands. However, other prostheses such as the ones used for lower limbs must withstand higher and dynamic loads and, at the same time, provide sufficient durability. Therefore, the application of plastic-based AM technologies is limited in these cases. For this reason, some researches focus on the development of composite materials for AM with the objective of improving the mechanical performance of the 3D printed plastic prostheses [14].

1.2.2. Additive Manufacturing technologies for scaffolds

As mentioned before, scaffolds are porous 3D structures used to replace or regenerate native tissues in human body (Figure 15 and Figure 16). These porous structures allow cell activity such as migration, proliferation, attachment, and differentiation, thus promoting the regeneration. For this to happen, the materials used for the production of scaffolds have to be biocompatible, easily sterilizable and non-toxic, as in the case of implants. The most commonly used materials are natural or synthetic polymers (e.g., hydrogels, proteins, thermoplastics, thermoplastic elastomers), metals (titanium and magnesium alloys), bioactive ceramics and glasses, and also composites of polymers and ceramics [15].

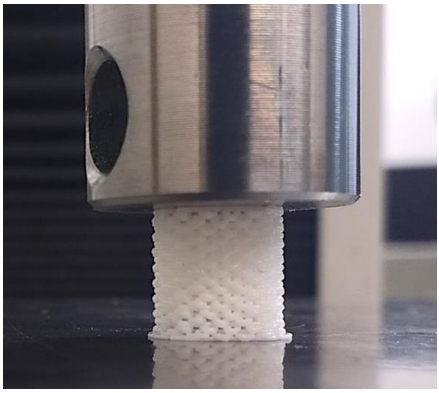

Figure 15. PLA scaffold made by MEX AM technology during compression test.

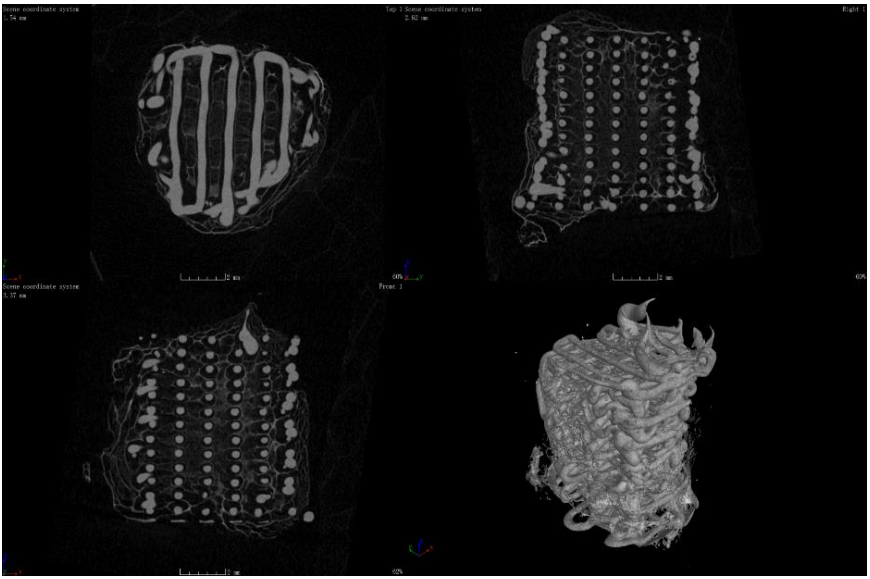

Figure 16. Micro CT scan of PCL scaffold made with extruded PCL in bioplotter and subsequent casting of alginate with nanocellulose.

As depicted in Table 2 and Table 3, not all the AM categories are commonly used for biomedical applications, mainly due to restrictive material requirements. Moreover, some AM categories apply, during the layer-upon-layer manufacturing process, high temperatures that may damage the used material for this application. In any case, different AM technologies are used for scaffolds production.

For the fabrication of metal scaffolds, the most typical technologies are those of the powder bed fusion category such as SLM, EBM [16] and DMLS [17] (as it also happens with AM metal prostheses). Among them, SLM and EBM are more used than DMLS.

Regarding AM used for the production of polymeric scaffolds, the most common technologies are binder jetting, stereolithography (SLA, vat photopolymerization category), material extrusion and SLS (powder bed fusion) [15].

Binder jetting technologies has the advantage of not needing support structures to produce complex geometries since the powder

bed does this function (as it happens in SLS). For this reason, binder jetting can be used to produce complex scaffolds with a relatively low cost. The main problem of binder jetting technologies is the lack of adhesion between layer, which limits the mechanical performance of the 3D printed parts. The print resolution is also a limitation of this technique for scaffolds production. However, binder jetting can process a wide variety of powder materials such as polymers, sand, metals and ceramics, but also cells and hydrogels, which is very interesting for scaffolds fabrication.

In the case of stereolithography (SLA), the main disadvantage for its use in scaffolds production is the limited number of potential materials that can be used. The free radicals that are formed during the photopolymerization process can damage cell membrane, protein, and nucleic acids, which limits its application in this specific field.

Regarding material extrusion, this category has many advantages, such as good efficiency, easy material replacement and low cost. However, the narrow list of available biomedical materials is a limitation for scaffolds production. The most typical materials used are acrylonitrile butadiene styrene (ABS), polylactic acid (PLA), polycaprolactone (PCL), polyethylene terephthalate glycol (PET-G), tricalcium phosphate (TCP) and polyamide (PA). The incorporation of cells or bioactive molecules is not possible in the conventional material extrusion AM equipment. Additionally, the inherent poor surface finish also limits its application for scaffolds. This can be solved by reducing the layer height, as lower values of this parameter will reduce the surface roughness and increase the mechanical properties (improved contact between layers). However, a lower layer height would also increase the production time and costs.

Despite these limitations, bioplotters, which are also based on extrusion processes, are one of the best options for the development of scaffolds, mainly due to the capability to work with biomaterials and cells in sterile environments (biomanufacturing). This capability, together with the option of producing multi-material parts with adjusted properties in different zones according to the desired functionality (e.g. combination of thermoplastic and hydrogels with embedded cells to improve the regeneration rate), places this

technology as the most promising AM equipment for scaffolds production.

Finally, Selective Laser Sintering (SLS) has the advantage of having a higher accuracy (although it depends on the size of the powder and laser spot) and better mechanical properties of the 3D printed parts compared with other technologies such as FDM or SLA. Moreover, the powder bed allows more design freedom due to the avoidance of support structures, although the powder removal can be very tedious in the case of scaffolds (structures with small interconnected porous which hinders the powder removal). On the other hand, the main drawback of SLS for scaffolds fabrication is that the use of high temperatures (laser radiation) limits the number of materials that can be used. The most typical are polycaprolactone (PCL), poly(D,Llactide) (PDLLA), poly(ether-etherketone) (PEEK), poly(lactic-co-glycolic acid) (PLGA), poly(vinyl alcohol) (PVA), composite of polycaprolactone/hydroxyapatite (PCL/HA) or poly(ether-etherketone)/hydroxyapatite (PEEK/HA).

1.2.3. Additive Manufacturing technologies for pre-clinical evaluation and training

The design freedom of AM technologies together with the capabilities of medical imaging technologies such as computed tomography (CT), magnetic resonance imaging (MRI) or ultrasound allow the production of medical models based on the patient anatomy. Therefore, the combination of scanning technologies, image treatment, 3D modelling and Additive Manufacturing can lead to very realistic synthetic models of personalized patient's anatomy. These synthetic models can be very useful for pre-operative planning/training, especially in the case of complex surgeries that require a deep analysis or practice before the operation. Additionally, these models can also be used to train medicine students, which in many cases have limited access to real cases. Therefore, AM allows increasing the practice of students as phantoms can be easily produced and managed. In fact, these synthetic models could replace, in a certain extent, the use of cadavers for training, which are more difficult to manage and expensive. Moreover, as cadavers are unique, it is not possible to train several

students exactly with same case, while AM does allow this option. Apart from this, medical models obtained by AM can also be useful to inform patients or patients' families about anomalies, surgical procedures, etc.

Although many different technologies have been used for pre-clinical evaluation and training, the most typical AM category used for this specific application is material jetting. In fact, nowadays there is a specific material jetting technology called J750 Digital Anatomy Printer (DAP, from Stratasys), which was specifically developed to produce anatomy models. The main difference between DAP and conventional material jetting printers is that the materials available try to mimic anatomy materials. In fact, the laminator used in this machine (GrabCAD Print) allows users to choose from different anatomy families and anatomy elements which are basically made of the following three type of materials [18]:

1. TissueMatrix™: ultra-soft material to mimic muscle and soft organs.
2. GelMatrix™: Gel-based material to emulate blood vessels and cavities.
3. BoneMatrix™: Material with high toughness to replicate cortical bone and connective tissue.

Depending on the specific anatomy family and anatomy element, these materials are combined to mimic the real tissue. Moreover, the softness/stiffness can be manually adjusted, thus covering a wide range of applications.

References:

1. "ISO - ISO/ASTM 52921:2013 - Standard terminology for additive manufacturing — Coordinate systems and test methodologies." [Online]. Available: https://www.iso.org/standard/62794.html. [Accessed: 17-Feb-2021].
2. Y. Zhai, D. A. Lados, and J. L. Lagoy, "Additive Manufacturing: Making imagination the major Limitation," *Jom*, vol. 66, no. 5, pp. 808–816, 2014.
3. T. Wohlers and T. Gornet, "History of Additive Manufacturing," 2016.
4. G. H. Loh, E. Pei, J. Gonzalez-Gutierrez, and M. Monzón, "An overview of material extrusion troubleshooting," *Appl. Sci.*, vol. 10, no. 14, 2020.

5. "A Revolutionary New Way to Manufacture Metal Parts." [Online]. Available: https://markforged.com/resources/blog/adam. [Accessed: 13-Mar-2021].
6. G. H. Loh, E. Pei, D. Harrison, and M. D. Monzón, "An overview of functionally graded additive manufacturing," *Addit. Manuf.*, vol. 23, no. May, pp. 34–44, 2018.
7. A. Aimar, A. Palermo, and B. Innocenti, "The Role of 3D Printing in Medical Applications: A State of the Art," *J. Healthc. Eng.*, vol. 2019, 2019.
8. R. Paz and M. D. Monzón, "Optimization methodology for the material assignation in bioprinted scaffolds to achieve the desired stiffness over time," *Int. j. numer. method. biomed. eng.*, vol. 35, no. 10, p. e3248, Oct. 2019.
9. M. Salmi, "Additive manufacturing processes in medical applications," *Materials (Basel).*, vol. 14, no. 1, pp. 1–16, 2021.
10. Y. Wang, Q. Tan, F. Pu, D. Boone, and M. Zhang, "A Review of the Application of Additive Manufacturing in Prosthetic and Orthotic Clinics from a Biomechanical Perspective," *Engineering*, vol. 6, no. 11, pp. 1258–1266, 2020.
11. P. Honigmann, N. Sharma, B. Okolo, U. Popp, B. Msallem, and F. M. Thieringer, "Patient-specific surgical implants made of 3D printed PEEK: Material, technology, and scope of surgical application," *Biomed Res. Int.*, vol. 2018, 2018.
12. P. Honigmann, N. Sharma, R. Schumacher, J. Rueegg, M. Haefeli, and F. Thieringer, "In-Hospital 3D Printed Scaphoid Prosthesis Using Medical-Grade Polyetheretherketone (PEEK) Biomaterial," *Biomed Res. Int.*, vol. 2021, pp. 1–7, 2021.
13. Y. Qin *et al.*, "Additive manufacturing of biodegradable metals: Current research status and future perspectives," *Acta Biomater.*, vol. 98, pp. 3–22, 2019.
14. E. Stenvall *et al.*, "Additive manufacturing of prostheses using forest-based composites," *Bioengineering*, vol. 7, no. 3, pp. 1–18, 2020.
15. P. Szymczyk-Ziółkowska, M. B. Łabowska, J. Detyna, I. Michalak, and P. Gruber, "A review of fabrication polymer scaffolds for biomedical applications using additive manufacturing techniques," *Biocybern. Biomed. Eng.*, vol. 40, no. 2, pp. 624–638, 2020.
16. Y. Yang *et al.*, "Additive manufacturing of bone scaffolds," *International Journal of Bioprinting*, vol. 5, no. 1. Whioce Publishing Pte. Ltd., 2019.

17. F. Mangano, L. Chambrone, R. Van Noort, C. Miller, P. Hatton, and C. Mangano, "Direct metal laser sintering titanium dental implants: A review of the current literature," *International Journal of Biomaterials*, vol. 2014. Hindawi Limited, 2014.
18. "Medical 3D Printing Software for the Stratasys Digital Anatomy Printer | GrabCAD Print." [Online]. Available: https://grabcad.com/print/digital_anatomy. [Accessed: 13-Mar-2021].

CASES STUDIES OF TRAINING MATERIAL APPLIED TO NEUROSURGERY

Rubén Paz[1], **Mario Monzón**[1], **Joshua García**[1] **Yamilet Rivero**[1]

[1] Department of Mechanical Engineering, Campus de Tafira Baja, Edificio de Ingenierías, University of Las Palmas de Gran Canaria, 35017, Las Palmas, Spain

This chapter explains all the process steps carried out to produce several synthetic models from real cases of cranial trauma, brain tumor and cerebral aneurysm. The synthetic models were mainly produced by Additive Manufacturing (AM) technologies, but also combined with conventional manufacturing processes such as silicone molding. The combination of AM (material extrusion technologies) and conventional techniques, together with the correct selection of materials, made possible to produce realistic synthetic models from the real scan data with low-cost approaches.

Contents

1.1. Training material for surgery of cranial trauma

The first summer school of the BrainIT project (July 2019) focused on trauma in neurosurgery. Two cases were developed for the practical sessions of this summer school:

- An intracranial hematoma with large skull fracture
- An intracranial hematoma, without skull fracture

Both cases were developed starting from the real scanning images of the patients and with low-cost manufacturing approaches. Material extrusion AM was used to produce 10 replicas of each case for the practical training sessions. In both cases, the students had to cut the skull in the correct area, remove the hematoma by vacuum and place/sew again the removed bone.

As the 3D printed models would be produced by material extrusion AM, the first step was to select the best 3D printable filament to mimic the properties of the skull. Among the possibilities, two main materials were considered: polylactic acid (PLA) and Smartfil® EP, which is a mixture of 30% of calcium carbonate ($CaCO_3$) and 70% of PLA. The PLA filament was selected as it is the most common plastic for material extrusion AM due to its outstanding printability. On the other hand, the EP filament was chosen due to its content in calcium carbonate, which is also present in bones and, consequently, could provide similar properties to the real bone.

To compare both materials, different tests were carried out in terms of flexural mechanical properties, drilling/milling cutting forces and chips behavior, surface hardness and the validation of a neurosurgeon.

The first analysis consisted in a flexural mechanical test. Five standard samples of each material were 3D printed and tested under three-point flexural test according to ISO 178 in a universal testing machine (Figure 1).

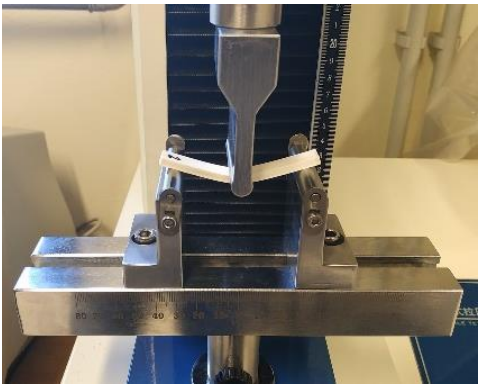

Figure 17. Three-point flexural tests on 3D printed specimens.

The results showed that the EP samples had a more fragile behavior, with higher elastic modulus (3389.46 MPa) than PLA (2743.51 MPa) and lower flexural strength (71.42 MPa) than PLA (93.53 MPa). Figure 18 represents a simplification of the flexural behavior of both materials, using the elastic modulus as the slope of the linear elastic zone until the yield point, and defining another linear behavior in the plastic zone until the point of maximum strength.

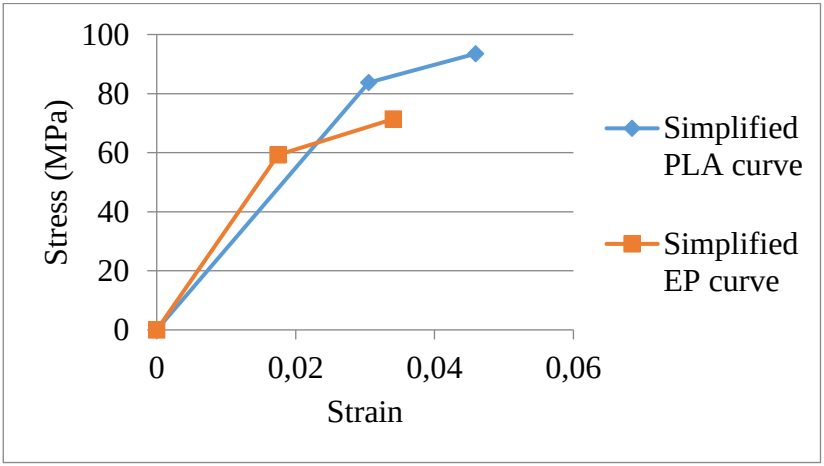

Figure 18. Simplified representative behavior of 3D printed PLA and EP under flexural loads.

According to the literature [1]–[4], the average flexural elastic modulus of the skull bone is around 9625 MPa and the flexural strength around 106.48 MPa (average values obtained from the previous references). As a conclusion, the presence of $CaCO_3$ increases the elastic modulus of EP filament (which is closer to the real bone, although still not close) and reduces the flexural strength.

The behavior of these materials during drilling and milling was also compared, but in this case also testing a cow bone to have an approximated reference value. In the case of the drilling, a load cell was installed under the specimens and the forces during the drilling were registered. The same drilling conditions were applied (4.5 mm diameter drill bit, 10 mm/min feed rate, 2000 rpm rotational speed and 10 mm depth) in four drillings of each material. Figure 19 shows one of the tests on the reference bone and Figure 20 the resulting bone with the 4 drills.

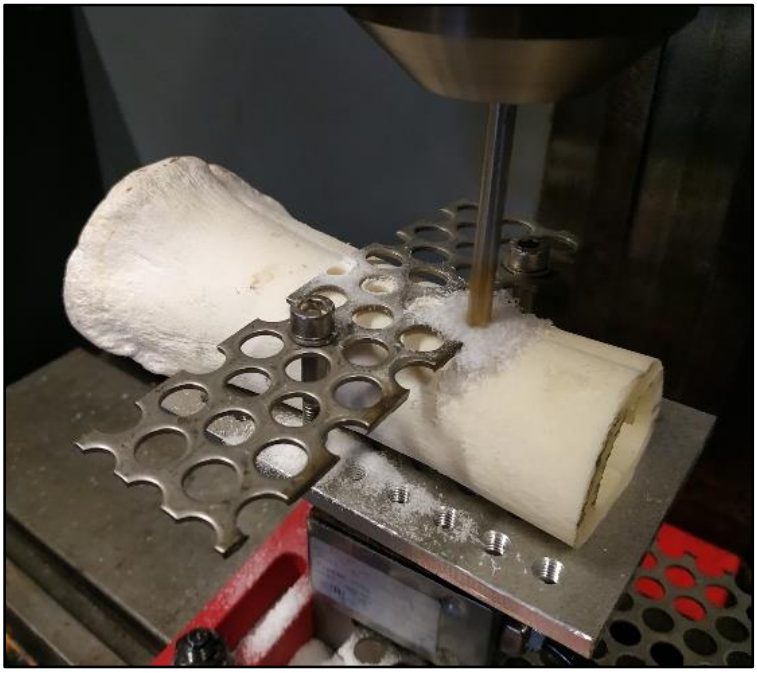

Figure 19. Cutting force measurement during drilling (in a reference bone).

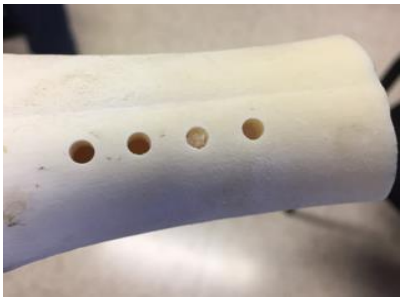

Figure 20. Reference bone after the drilling tests.

The average force-time curves of the 3 materials are depicted in Figure 21. The maximum cutting force during drilling was quite similar between EP material and bone. However, in PLA the drilling forces were higher.

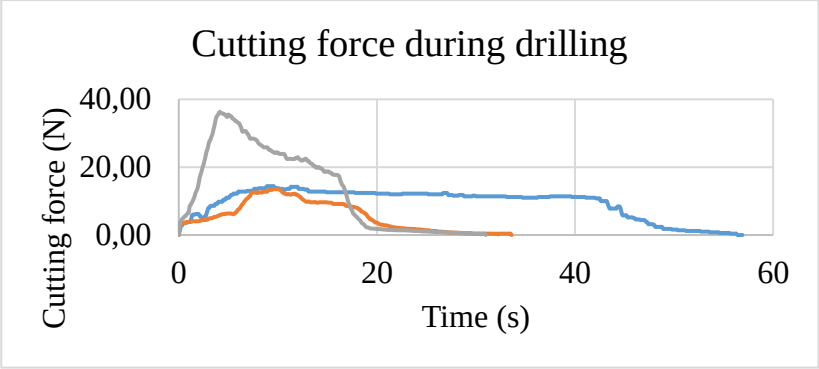

Figure 21. Cutting force during drilling in the different materials tested (blue: bone; orange: EP; grey: PLA). The maximum drilling force is almost the same in the case of EP and bone, while in PLA was higher.

For the milling test, the load cell was placed in the lateral side of the holder of the specimens (Figure 22), so that the milling tool feed rate was towards the load cell. The same milling conditions were applied for all the materials (mill tool of 4 mm diameter, 50 mm/min feed rate, 2000 rpm rotational speed, and 2 mm depth) and the resulting average curve of five millings (force-time) was calculated, as depicted in Figure 23. The

results showed that the milling forces were lower in EP material, while PLA and boner had similar values.

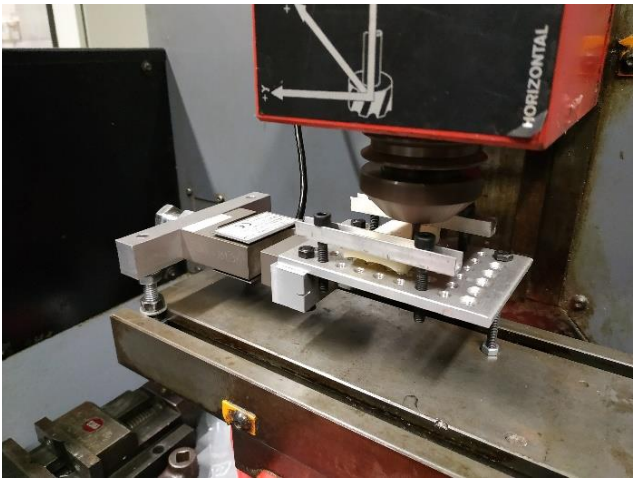

Figure 22. Cutting force measurement during milling.

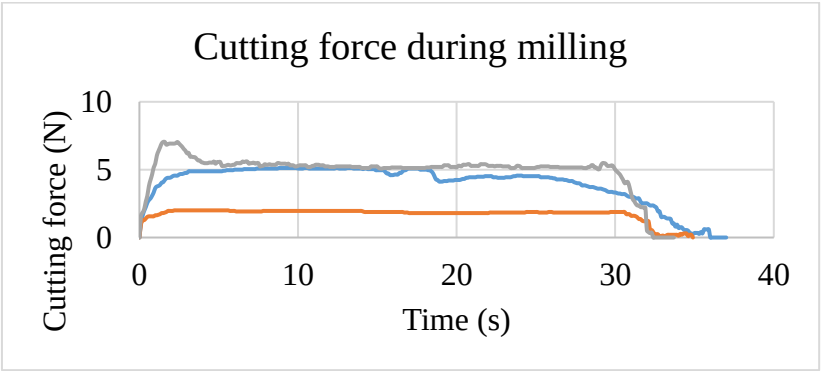

Figure 23. Cutting force during milling in the different materials tested (blue: bone; orange: EP; grey: PLA). In the case of milling, EP obtained lower values compared to PLA and real bone.

Regarding the behavior of the chips during milling and drilling, it was observed that small chips and powder were removed in the case of the bone. However, in the PLA specimens, the material tended to melt

and stick to the tool (both in drilling and milling), while in the case of EP, the behavior was more similar to the real bone (although in some cases the material also tended to melt).

With regard to the surface hardness, the Shore D hardness was measured in five tests for each material. The results showed that the hardness was relatively similar in all the cases, with an average value of 82 for PLA, 83 for EP and 77 for the bone (Shore D).

In general, the EP filament performed better than PLA. For this reason, a skull sample was manufactured with the EP filament for the validation of an experienced neurosurgeon. The neurosurgeon did some practical verification cutting the skull and validated the material with a positive feedback. Table 4 summarizes the results of the comparison between PLA and EP materials.

Table 4. Comparison of EP and PLA under the different criteria evaluated.

Analyzed criterion	**Smartfil® EP**	**PLA (without additives)**
Flexural elastic modulus	☒	☒
Flexural strength	☒	☒
Maximum drilling cutting force	☒	☒
Maximum milling cutting force	☒	☒
Chips behavior	☒	☒
Hardness (Shore D)	☒	☒
Neurosurgeon's validation	☒	☒

Regarding the hematoma material, after different tests with different concentrations, the final choice was a solution of sodium

alginate powder (from Acros Organics) with distilled water (1:20 w/w) (Figure 40). This solution was also approved by the surgeon to simulate the hematoma.

1.1.1. Case 1: Intracranial hematoma (with skull fracture)

The first case was an intracranial hematoma with skull fracture (the patient suffered a severe trauma with a large fracture).

Once selected the material for the skull and hematoma, the 3D reconstruction was made by using the CT scan images of the patient (Figure 24) and processing them in the 3D Slicer software (segmentation process). Figure 25 shows the resulting 3D model (STL file).

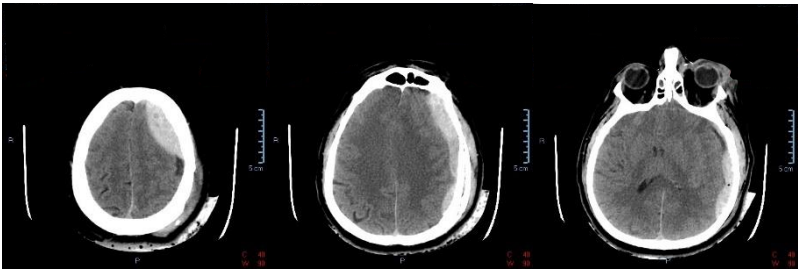

Figure 24. CT images of the patient. The DICOM files were used for the 3D reconstruction and segmentation of the skull. The hematoma is noticeable on the right side of the images (left side of the patient).

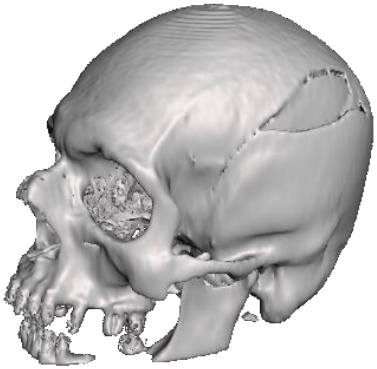

Figure 25. 3D model of the skull after segmentation of the CT images in 3D Slicer. The fracture is visible on the left side of the patient.

In order to reduce the cost and facilitate the fixation of the skulls for the practical training sessions, the skull was cut in the Meshmixer software to focus on the region of interest, thus removing the lower part of the model (Figure 26).

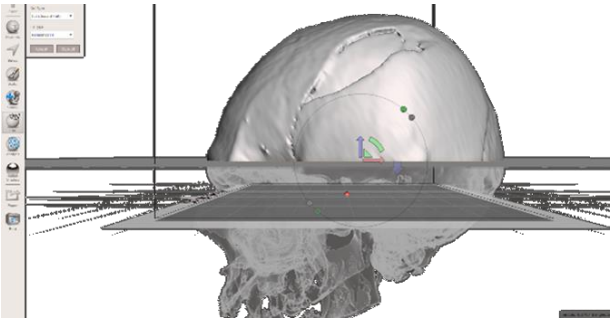

Figure 26. The 3D model of the skull was cut to keep only the region of interest for the training activity.

The resulting geometry was imported in SolidWorks software to define a completely flat plane on the bottom of the skull and to define the base (Figure 27), including four towers with internal holes for the fixation screws and an additional hole to fill the hematoma.

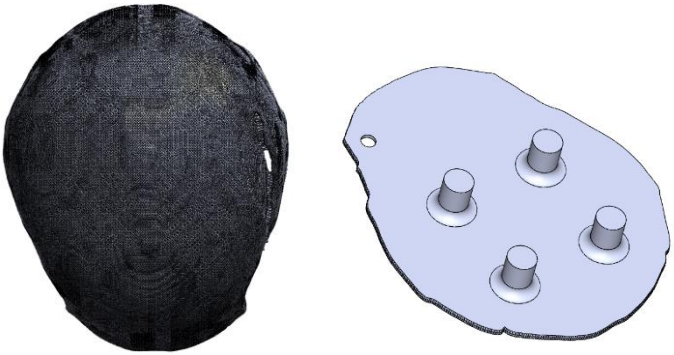

Figure 27. CAD modelling operations in SolidWorks to define the base with the fixation mechanism (right) starting from the segmented skull (left).

The base and skull were joined again in the Meshmixer software and laminated with Simplify3D to be 3D printed with PLA, just as a first trial. The printing was successfully completed, as shown in Figure 28.

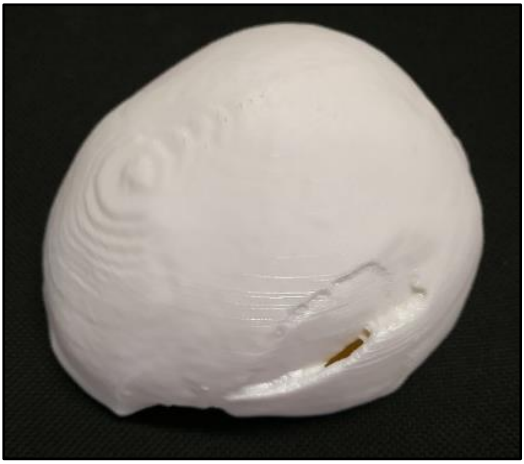

Figure 28. 3D printed skull obtained in MEX technology with PLA filament.

After that, a new wall was added in the fracture zone to serve as container bag of the hematoma (Figure 29).

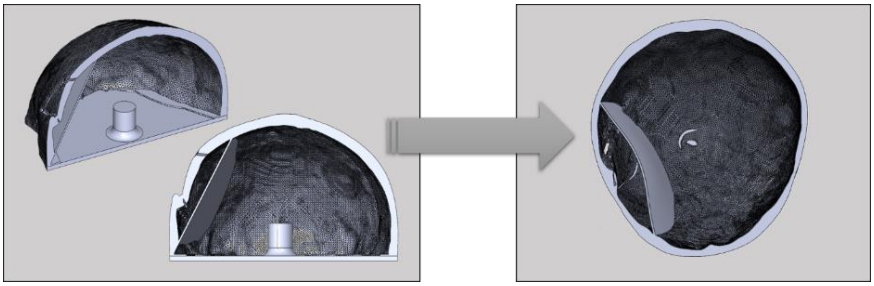

Figure 29. CAD modelling of the bag to retain the hematoma.

In parallel, a fixation mechanism was designed (Figure 30) to fix the skulls for the practical training sessions. The design consists of 4 parts that are joined by screws and with adjustable angle in one axis to the skull in the desired position.

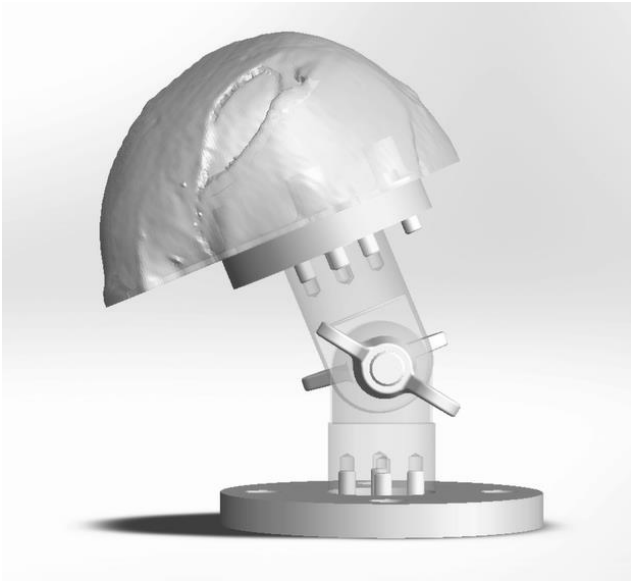

Figure 30. Design of the fixation mechanism of the skull, with adjustable angle and several possible positions of the skull.

The components of the fixation mechanism were machined (Figure 31) and a new skull with EP filament was produced (Figure 32).

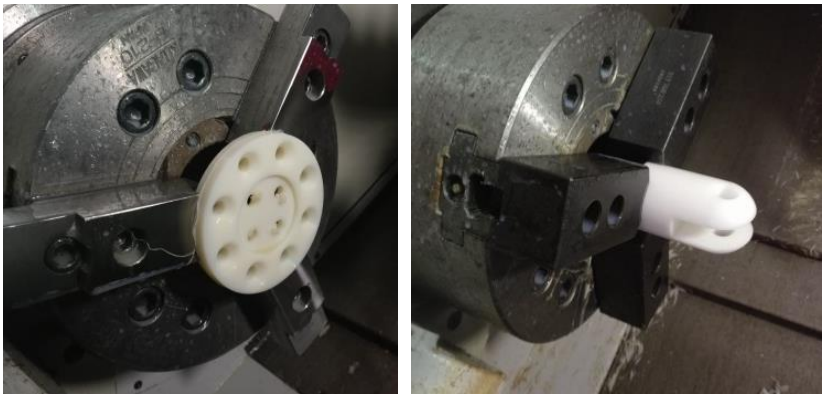

Figure 31. CNC machining (lathe) of the fixation system components.

Figure 32. 3D printed skull in MEX technology with EP filament.

The skull was screwed on the fixation system (Figure 33) and the assembly was used by the neurosurgeon to validate the geometry and material selected (Figure 34). Figure 35 shows the 3D printed skull after the validation test.

Figure 33. 3D printed skull with EP filament.

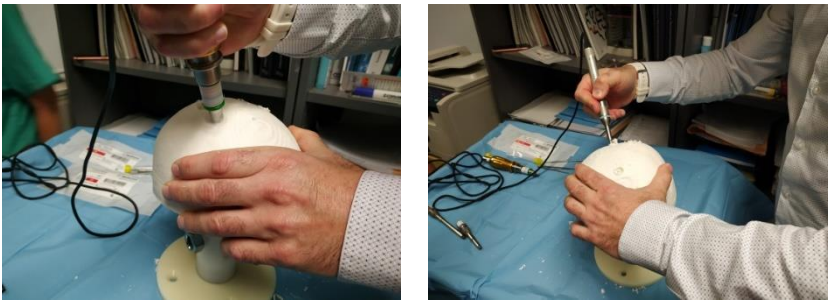

Figure 34. 3D printed skull during the validation test. The neurosurgeon gave a positive feedback of the material.

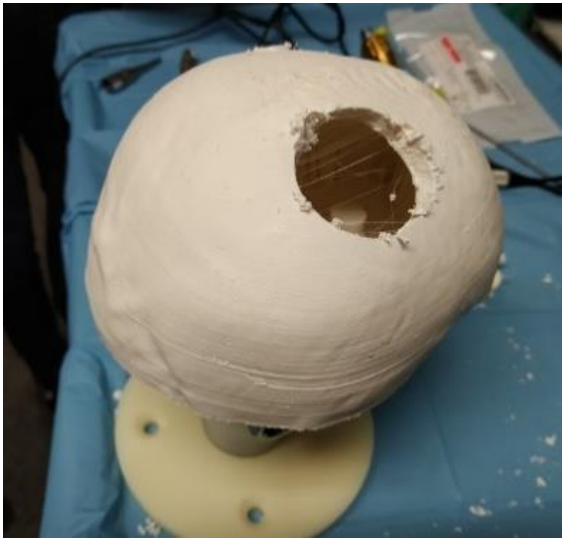

Figure 35. Skull after the neurosurgeon's test.

Although the neurosurgeon validated the material for the skull, one important detail was discussed regarding the geometry of the fracture. According to their knowledge, this fracture should have less joining points. As a consequence, the fracture was segmented again to reduce the contact area. Figure 36 shows the difference between the initial fracture and the final one.

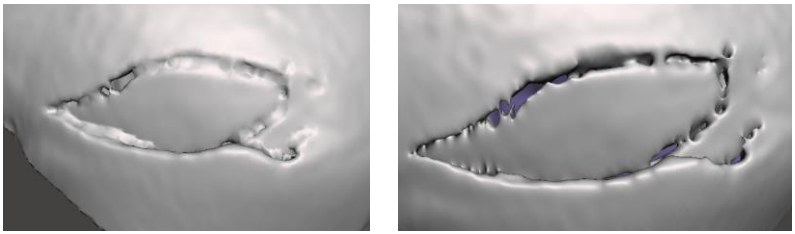

Figure 36. Modification of the fracture (left: original geometry of the fracture; right: new fracture).

Taking advantage of the new segmentation, the geometry of the hematoma bag was improved by defining a wall surrounding the hematoma, which was noticeable in the CT images (Figure 37).

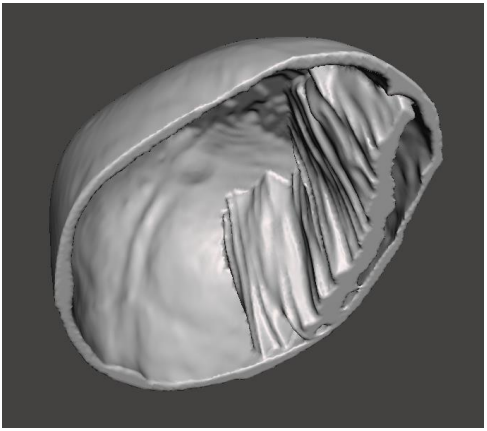

Figure 37. New hematoma bag.

The new model was 3D printed and it was observed that the hematoma cavity was not completely sealed. To solve this, the STL file after the segmentation was modified with different approaches. The first attempt consisted in adding spheres in Meshmixer all around the hematoma bag (Figure 38), but it did not work properly as in some cases the spheres were considered as removed material in the lamination software.

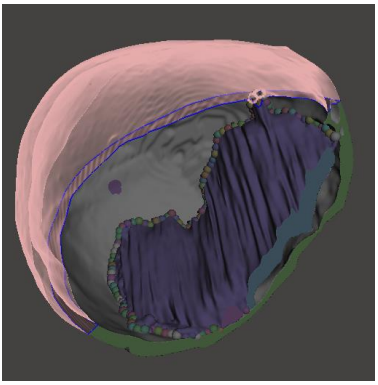

Figure 38. Hematoma bag with small spheres in the perimeter to try to seal the contour without success.

Finally, the sculpt feature in Meshmixer was the solution to seal the contour (Figure 39).

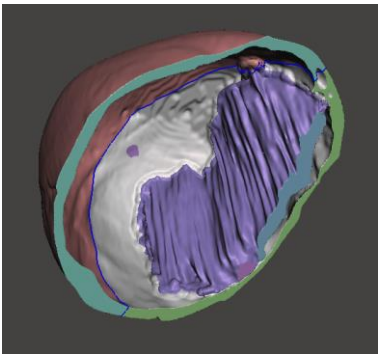

Figure 39. Hematoma bag with sealed contour (sculpt tool in Meshmixer).

With the final design of the fracture and hematoma bag, a 3D printed model was manufactured with EP to do a leakage test (Figure 40). Regarding the hematoma material, the solution of sodium alginate powder (from Acros Organics) with distilled water (1:20 w/w) was used (Figure 40). To properly fill the cavity of the hematoma, the fracture was sealed with Parafilm®.

Figure 40. Left: 3D printed model of the final geometry cover with Parafilm® for the leakage test. Right: Syringe with sodium alginate and distilled water (1:20 w/w) to mimic the hematoma.

The leakage test was successfully completed (no leaks in the cavity of the hematoma), although it was carried out in a skull without base. However, the base is needed to fix the skull to the fixation system and to seal the bottom of the hematoma cavity. Therefore, a hole was added in the base of the skull, properly located to be able to fill the hematoma cavity from the outside (Figure 41).

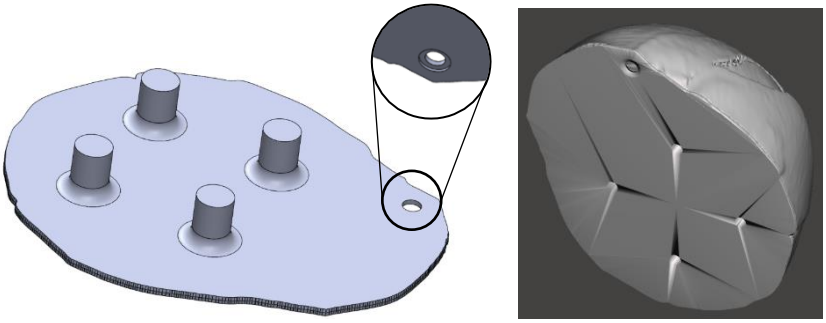

Figure 41. Left: base of the skull with the hole to fill the hematoma cavity. Right: final skull STL ready to 3Dprint, with the filling hole in the base.

The final design of the skull was laminated in Simplify3D software, using a printing temperature of 200 °C, layer height of 0.3 mm, extrusion width of 0.6 mm and infill density of 100%. The resulting

gcode file was run in an Atom 2.5 FX 3D printer, with an approximated printing time of 14 hours and 15 min. The result is depicted in Figure 42.

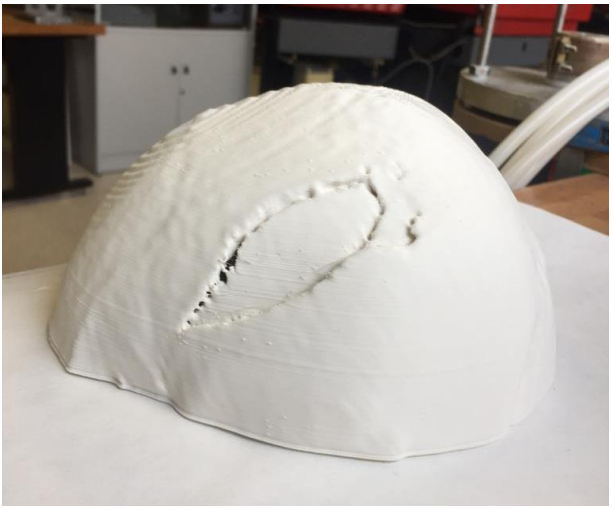

Figure 42. Final 3D printed skull of case 1 (intracranial hematoma with skull fracture).

Note that the 3D printing of the EP filament is more complex than in the case of PLA, especially for long prints. This is due to the higher brittleness of the EP filament (the teeth of the driver gear of the extrusion mechanism gradually remove small particles of the filament that lead to the blockage of the extrusion device). To avoid this, compressed air was applied in the extrusion mechanism to keep it clean (as the 3D printer uses a Bowden extrusion system, the hotend is far away from this air flow, which means that it does not affect the printing process).

The 3D printed skull was manually machined with a tap tool to make the internal thread of the four holes of the base. Then, the skull was placed and screwed in the fixation system. Figure 43 shows all the components previous to the assembly. Figure 44, Figure 45 and Figure 46 depict the assembly process.

Figure 43. 3D printed skull and components of the fixation mechanism before the assembly.

Figure 44. Assembly of the lower part of the fixation system.

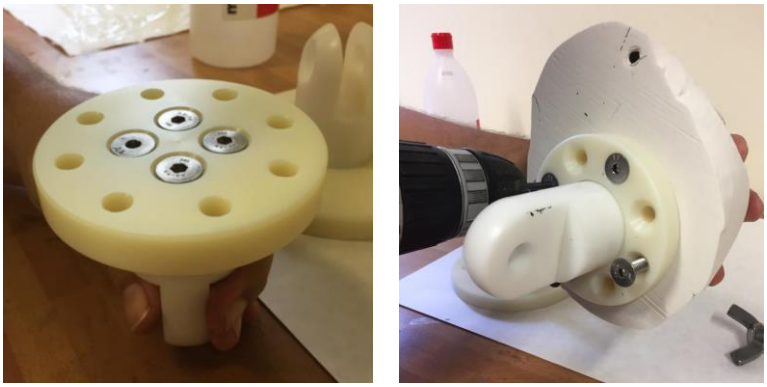

Figure 45. Assembly of the upper part of the fixation system (left) and skull (right).

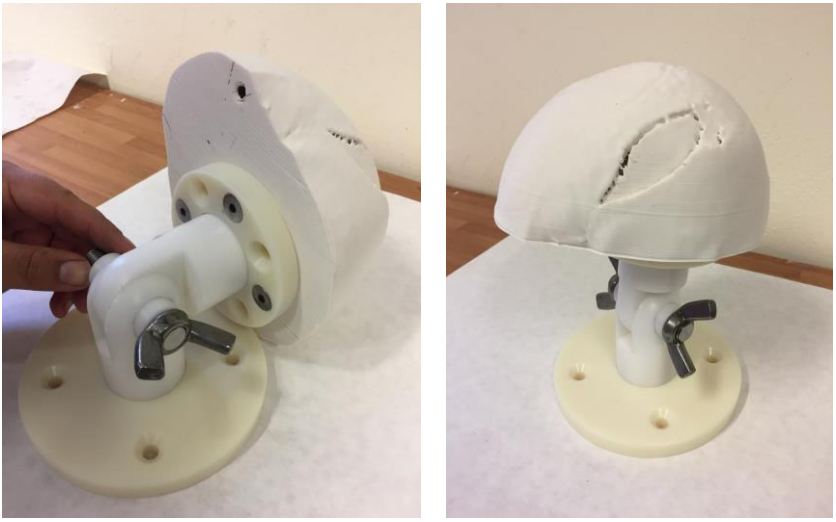

Figure 46. Skull assembled in the fixation system with adjustable angle.

Figure 47 shows the synthetic models prepared for the practical session with all the required tools for the surgery. Note that the sodium alginate solution was filled *in situ* just before the practical session and the hole was sealed with 3D printed cylindrical caps with flexible filament (Filaflex TPU).

Figure 47. Synthetic models of the intracranial hematoma with fracture prepared for the practical training (July 2019). The sodium alginate solution to simulate the hematoma was injected just before the practice in the hematoma cavity.

Figure 48 shows the developed skull being used during the training session.

Figure 48. Synthetic model during the practice.

1.1.2. Case 2: Intracranial hematoma (without skull fracture)

The second case consisted in another intracranial hematoma, but in this case the skull did not have any fracture. The process was similar to the previous one and the same materials were used (Smartfil® EP filament for the skull production in a material extrusion AM equipment and the solution of sodium alginate with distilled water at 1:20 w/w for the hematoma).

The process started with the segmentation of the real CT images (DICOM files). In this case, during the segmentation of the skull, a wall that surrounds the hematoma was also segmented to obtain the cavity of the hematoma (Figure 49). The complete segmented skull is depicted in Figure 50.

Figure 49. Segmentation of the skull from DICOM images. The hematoma is depicted in pink and the container wall of the hematoma in blue.

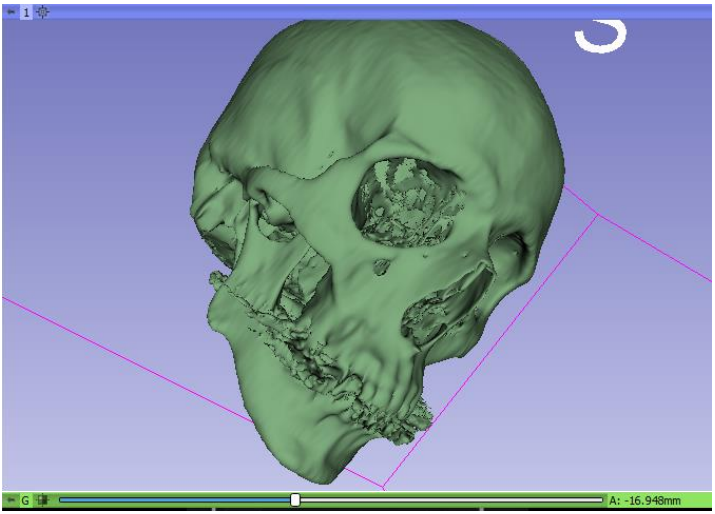

Figure 50. Reconstructed skull after segmentation.

The STL files of the skull and wall of the hematoma cavity were imported into Meshmixer and joined (combine feature). Afterwards, the lower part of the resulting skull was removed to simplify the model (the lower part was not needed for the practical training) (Figure 51).

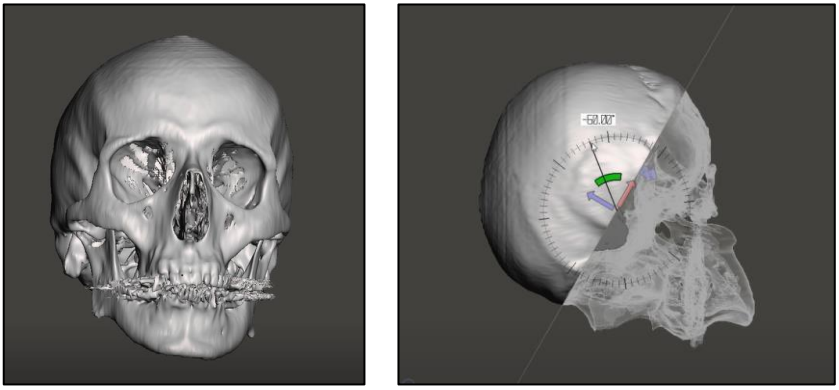

Figure 51. Cutting of the 3D skull in Meshmixer.

The resulting object was converted into solid STL and imported in SolidWorks (Figure 52).

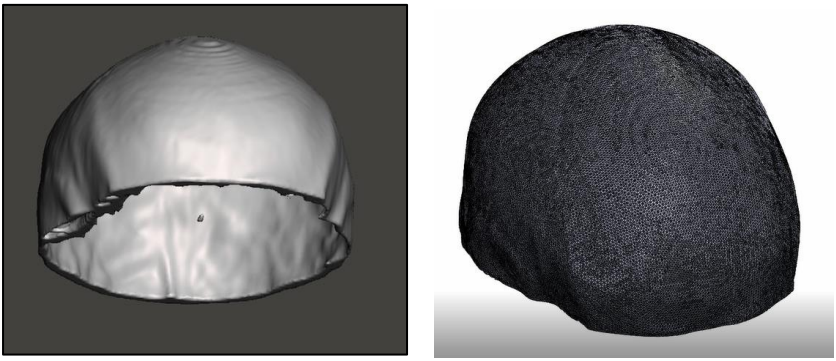

Figure 52. Cut skull in Meshmixer (left) and imported geometry in SolidWorks (right).

As the plane cut feature in Meshmixer leaves a non-planar surface, an additional cutting was carried out in SolidWorks. After this, an extrusion feature was applied to create the base of the skull (Figure 53). Apart from this, the towers and holes for the fixation screws were added (Figure 54).

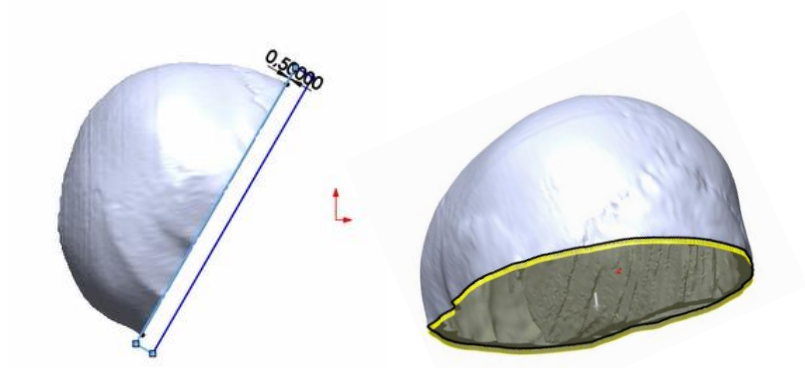

Figure 53. Cutting and extrusion features in SolidWorks to define the base of the skull.

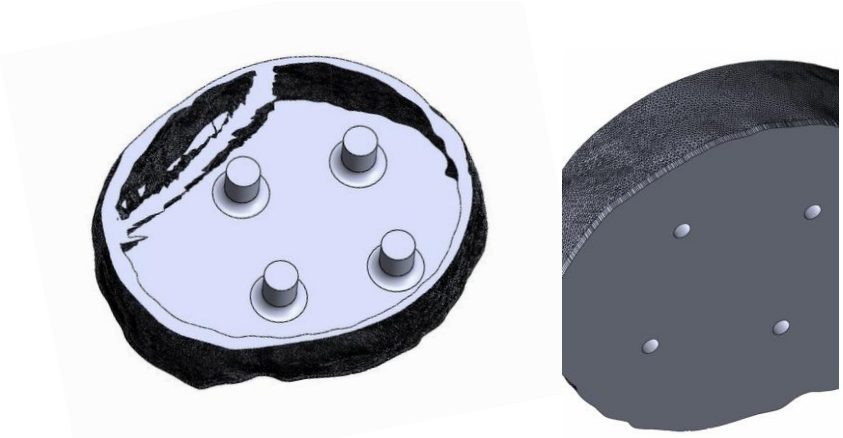

Figure 54. Towers (left) and holes (right) to fix the skull to the fixation mechanism with screws.

In this case, as the hematoma cavity did not have enough space on the base, an additional channel was added to connect the cavity with outside, so that the simulated hematoma material (solution of sodium alginate) could be injected (Figure 55). Figure 56 shows the final design of the skull, including the base and filling channel.

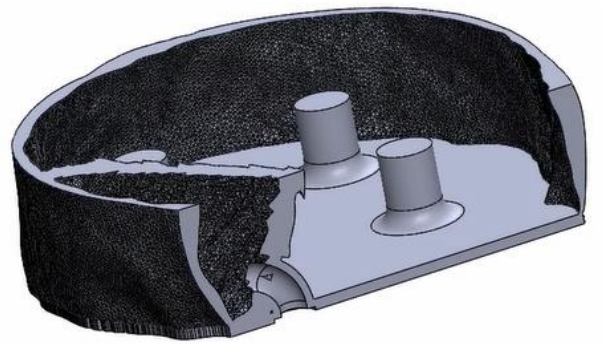

Figure 55. Section view of the 3D skull geometry with additional channel connecting the outside with the hematoma cavity to inject the sodium alginate solution.

Figure 56. Final design of the skull.

The STL file of the final design was imported in Simplify3D and laminated with the same printing parameters as case 1. Figure 57 and Figure 58 show some screenshots of this step.

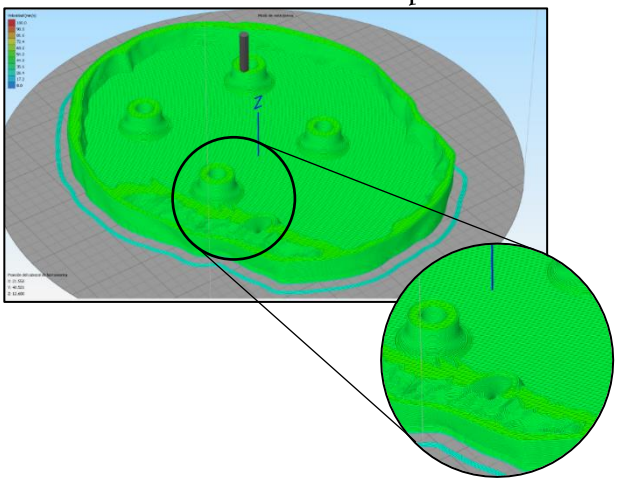

Figure 57. Lamination of the base in Simplify3D, with detail of the filling channel.

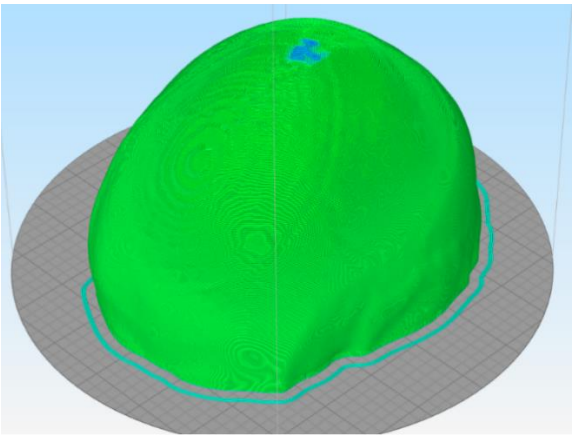

Figure 58. Complete view of the model in Simplify3D software.

The resulting manufacturing file (gcode file) was run in the 3D printer (Atom 2.5 FX) and the skull was obtained after several hours of 3D printing (Figure 59).

Figure 59. Final 3D printed skull.

Figure 60 shows the skull already assembled in the fixation mechanism.

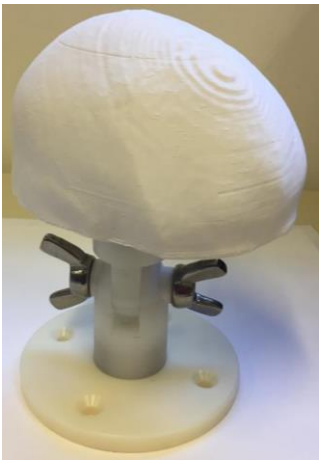

Figure 60. 3D printed skull assembled in the fixation system.

Figure 61 shows the skull during the practical training of students (after the cutting of bone, removal of the hematoma and suture of the removed bone). Note that the sodium alginate solution to emulate the hematoma was also filled *in situ* before the practical session (the hole of the base was sealed with the cylindrical and flexible 3D printed caps, as in case 1).

Figure 61. Synthetic model of case 2 during the practical training.

1.2. Training material for surgery of brain tumor

The second summer school of the BrainIT project (initially scheduled for July 2020, but delayed due to the pandemic situation) focused on neuro-oncology. For the practical sessions, two real cases of brain tumor have been developed:

- Meningioma case, which is a brain tumor arising from the meninges (the membranous layers surrounding the brain). The consistency of the tumor is higher than the one of the brain.
- Glioma case, which is a brain tumor located in any area of the brain and with lower consistency than the brain (removable by vacuum).

As in the previous section, both cases had to be developed starting from the DICOM images of the patients and with low-cost manufacturing approaches (material extrusion AM). Ten replicas of each case had to be obtained for the practical training sessions. In both cases, the students will cut the skull and access the tumor to be removed with hand tools (meningioma) or by vacuum (glioma). Finally, the removed bone will be sutured again.

The first activity to develop these cases focused on the selection of the manufacturing process and materials.

For the production of the skulls, the same approach of the previous cases was used (material extrusion AM of Smartfil® EP filament). However, since the printability of this filament is less reliable than standard PLA, the skulls were divided in two zones: the working area, where the students will cut and suture; and the rest of skull. The idea was to use Smartfil® EP filament for the working area and PLA for the rest. This way, the risk of blockage of the extrusion driver of the 3D printer would be drastically reduced, thus improving the reliability of the printing and, at the same time, keeping the quality of the synthetic models as the PLA filament would only be used in the non-working areas. Moreover, in order to facilitate the cutting process of the skull, which will be carried out with a Gigli saw, it was proposed to reduce the infill density of the printing process to avoid the blockage of the tool. To properly select the best infill density, several plates with different infill densities (10, 20, 30, 50, 75 and 100%) were 3D printed and cut with saw to qualitatively analyze the behavior (Figure 62). Therefore, the

infill density for the working area was 30%, while the rest of the skull (PLA filament) would be printed with 20% of infill density.

Figure 62. Samples with different infill densities (10, 20, 30, 50, 75 and 100%) to be cut with saw (left) and sample with the selected infill density after the cutting (right).

For the manufacturing of the brain, the approach consisted in using different liquid thermoset materials poured and polymerized in a 3D printed mold (also manufactured with material extrusion AM) to reproduce the desired geometry. Three different materials were analyzed in the preliminary tests:

- AljaSafe®: alginate used to produce molds. This material was processed in different concentrations but it was discarded due to its dimensional instability and higher stiffness compared to the real brain.
- Contor 5005: three-component silicone (A, B, C) with tin catalyst. Six cylindrical samples of five different proportions (30 samples in total) were manufactured with this material. The A:B ratio was maintained according to the manufacturer's recommendation (100:2.5) while the C content compared to A+B was modified (30, 50, 70, 90 and 100% of C component). The codes used for the five different groups were C30, C50, C70, C90 and C100.
- Ecoflex® 00-10: two-component silicone (A, B) with platinum catalyst (B). Six cylindrical samples of three different proportions were

manufactured with this silicone. The A:B ratios were 1:0.5 (codified as E0.5), 1:1 (E1) and 1:1.5 (E1.5).

Figure 63 shows samples of both silicones. These samples were subjected to compression tests with 10 mm/min of crosshead speed (Figure 64) and weighed every day for approximately one month to check their dimensional stability (no significant variations were observed).

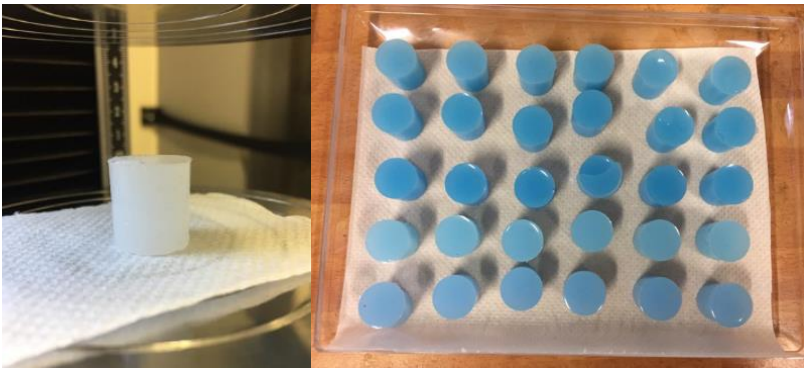

Figure 63. Sample of Contor silicone (left) and samples of Ecoflex® 00-10 (right) before the compression tests.

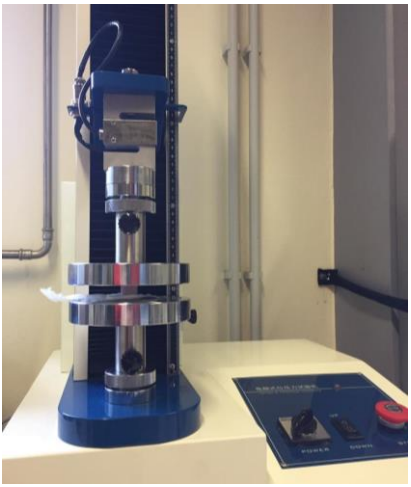

Figure 64. Sample during compression test.

The results (average value and standard deviation) of the compression tests are shown in Figure 65. According to the literature,

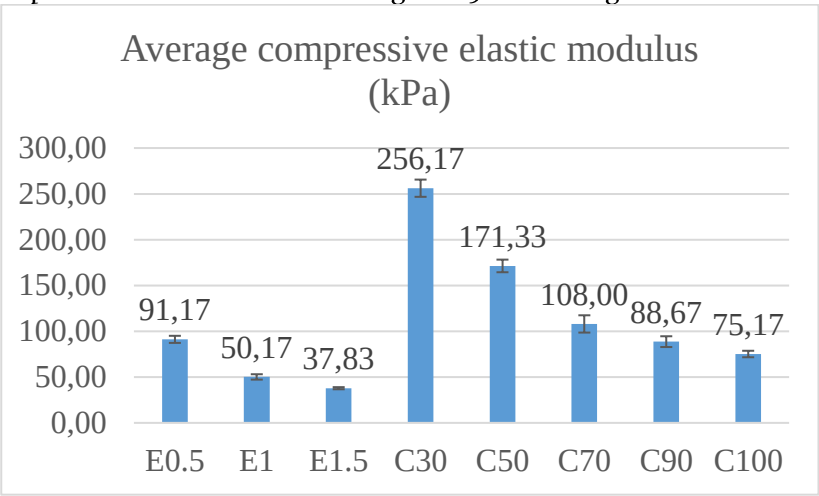

Figure 65. Compressive elastic modulus (average and error bars according to the standard deviation) of the different groups tested (Contor 5005 and Ecoflex® 00-10 silicones).

Table 5. Reference values of brain elastic modulus.

Brain elastic modulus (kPa)	**Reference**
71.7 (*Dynamic modulus value*)	[5]
5.96 (gray matter) **2.68** (white matter)	[6]
490.3 (gray matter) **49** (white matter)	[7]
10 (gray matter) **10** (white matter)	[8]
2.1 – 2.7 (gray matter) **2.1 – 6** (white matter)	[9]
3.24	[10]
73 (gray matter) **32** (white matter)	[11]
3.15	[12]

From the previous data, the average value was estimated, but considering the highest value an outlier. The obtained average value (21.16 kPa) was lower than the value of the tested silicones. In any case, one sample of each group was produced again (Figure 66) to be directly tested by an experienced neurosurgeon.

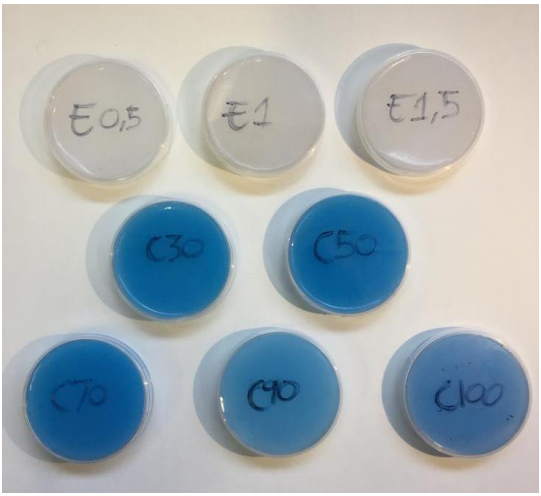

Figure 66. Silicone samples for the neurosurgeon's validation.

Among them, the preferred one was E1.5, which was the one with the lowest elastic modulus. However, other tests carried out by the neurosurgeons participating in this project recommended an even lower stiffness to improve the similarity to real brain tissue. For this to happen, a new component was included, following the recommendation of the manufacturer of this silicone. This new component, called Slacker, reduces the stiffness of the molded silicone. In order to find the best proportion, 4 different groups with different proportions of the silicone components and slacker (A:B:Slacker) were produced (Figure 67 ,six replicas of each group) and subjected to compression tests. The results are shown in Table 6.

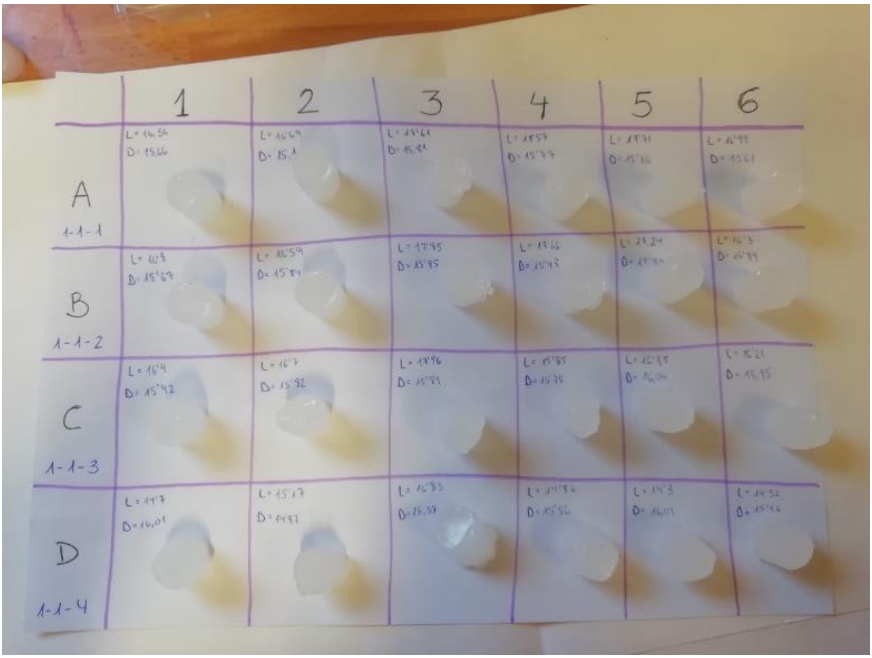

Figure 67. Final silicone samples for the compression tests.

Table 6. Average compressive elastic modulus for the four silicone groups tested.

Groups of samples (A:B:Slacker)	**Average elastic modulus (kPa)**
Group 1 (1:1:1)	40.41
Group 2 (1:1:2)	37.90
Group 3 (1:1:3)	31.29
Group 4 (1:1:4)	27.95

As expected, the slacker allowed the reduction of the elastic modulus of the samples. Among the produced samples and in accordance with the neurosurgeons' feelings, the best material to mimic the brain was group 3 (1:1:3), which had an elastic modulus of 31.29 kPa. Therefore, this mixture was selected as the optimal one for the brain. However, the Slacker component is considerably more expensive than

the other ones. For this reason and with the objective of keeping a low-cost approach, the brain of the two cases was divided into 2 different zones: the working area (zones affected during the training session), which was manufactured with 1:1:3 ratios (A:B:Slacker) of Ecoflex® 00-10; and the non-working area (the rest of the brain that will not be used by students during the surgery training), which was produced with the 1:1 ratio (A:B, without Slacker).

On the other hand, note that between the brain and the skull there are 3 membranes. In this case, the most important layer (the dura mater) will be reproduced. Dura mater is a membrane with a greater consistency than brain. For this reason, the mixture chosen to reproduce this tissue was Ecoflex 00-10 with 1:1 ratio (A:B). The dura mater was produced by pouring this mixture on a flat surface and laminating the blend with a roller to obtain a thin sheet that will be located between the skull and the brain during the assembly.

Regarding the molds and insert tools needed for the silicone molding of the different components (such as the brains and the tumor of case 1), material extrusion AM with PLA filament were used (with 20% of infill density). The PLA filament was chosen due to its stability and speed for 3D printing.

1.2.1. Case 1: Meningioma.

This type of tumor has a higher consistency than brain. For this reason, a stiffer blend compared to the brain was used to produce the tumor (1:1 rate of components A:B of Ecoflex 00-10). Furthermore, considering that this tumor is reddish in color and contains calcium deposits, it was decided to add a small amount of a red pigment (3% of the total mass), in addition to crushed PLA that simulates calcification, thus achieving a more realistic model.

Once selected the materials for the different components, the 3D reconstruction was made by using the CT scan of the patient and processing them in the 3D Slicer software (segmentation process).

First of all, the skull was segmented (Figure 68) and cut to obtain the final model (Figure 69).

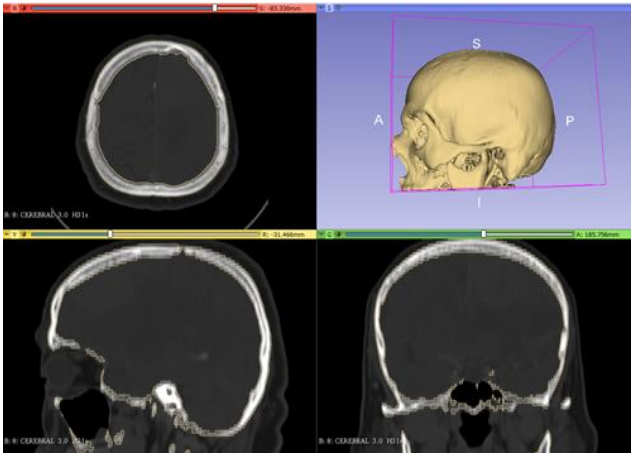

Figure 68. Segmentation of the skull from the DICOM images.

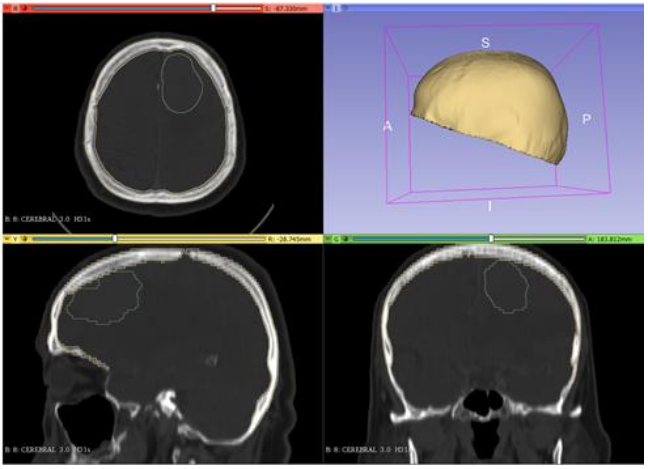

Figure 69. Cutting of the 3D skull in 3DSlicer.

As previously mentioned, the tumor mold is required to be able to pour the silicone mixture later. Therefore, once the tumor was segmented (Figure 70), a copy of this model was made with an added thickness of 10 mm. The original segment was subtracted, generating the mold of this model (Figure 71).

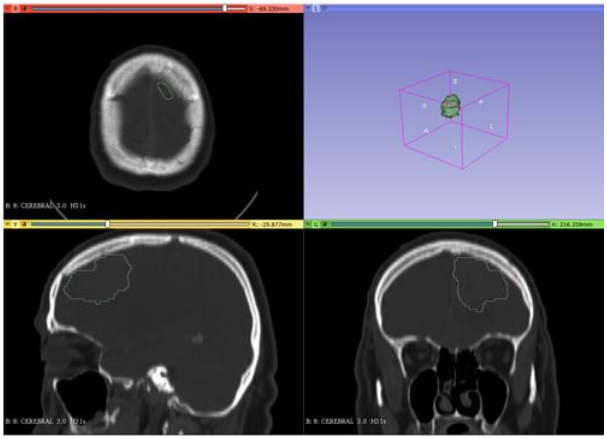

Figure 70. Segmentation of the tumor from the DICOM images.

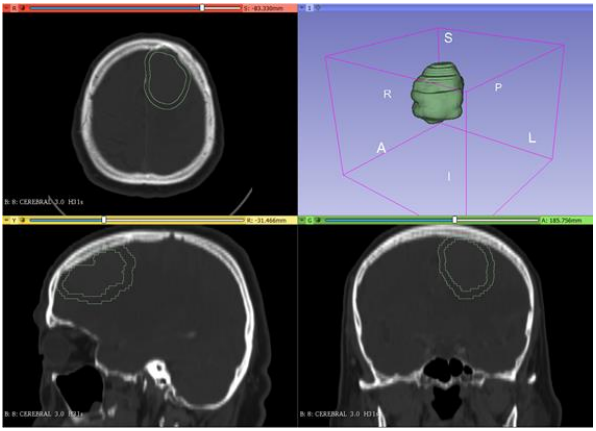

Figure 71. Segmentation of the tumor mold with a thickness of 10 mm.

To create the brain mold, the model in Figure 68 (skull) and the model in Figure 70 (tumor) were joined so that the molded brain could have the void to assemble the tumor. Moreover, the thickness of the resulting geometry was increased 3 mm so that the molded brain had 3 mm clearance with the skull (Figure 72). The resulting geometry was cut to remove the lower part of the model (Figure 73).

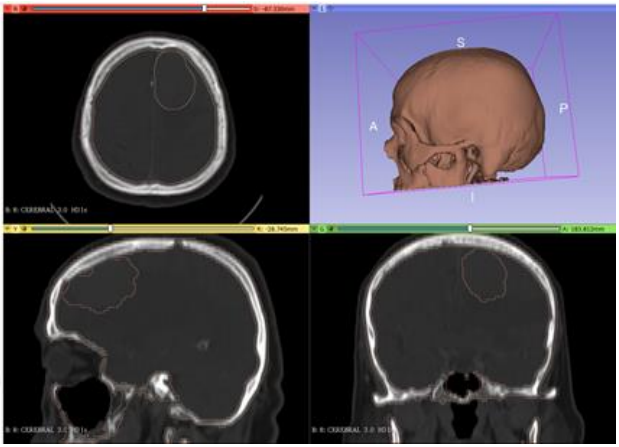

Figure 72. Segmentation of the brain from the DICOM images.

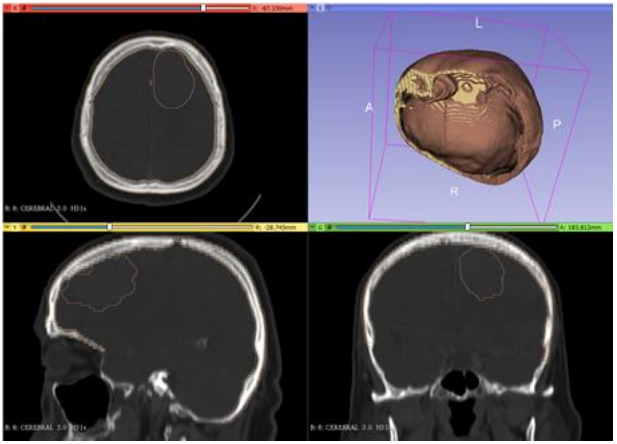

Figure 73. Brain mold obtained from the DICOM images after cutting the lower part.

Once these models were segmented, the STL files of the skull, tumor mold and brain mold were imported into Meshmixer, where all of them were converted into solid STL (Figure 74) and imported in SolidWorks.

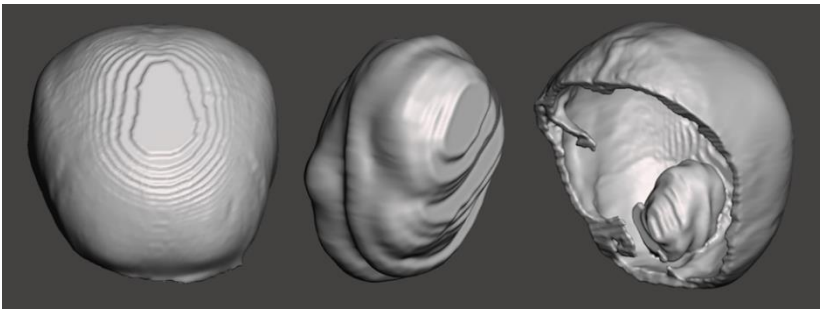

Figure 74. Models of case 1 in Meshmixer.

Regarding the skull model, the first feature carried out was a cutting operation with a well-referenced flat plane to obtain a perfectly flat surface on the bottom of the skull. Afterwards, some tabs were added to be able to assemble this part of the skull with the base (Figure 75). Note that the base of the scale is an independent part that allows assembling the dura mater, brain and tumor inside the skull and then screwing the base to fix all the components to the fixation system (Figure 30).

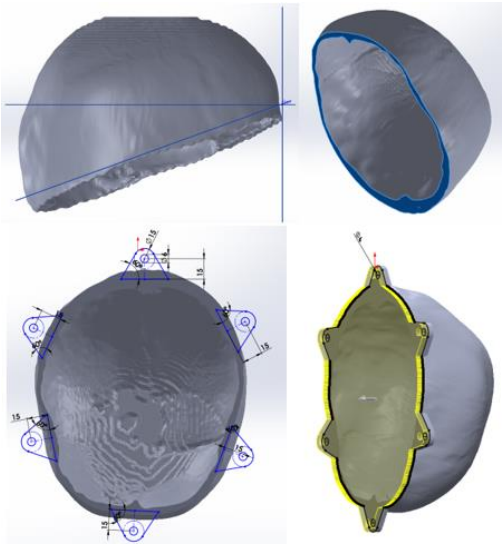

Figure 75. Initial features performed with SolidWorks for the skull design.

Afterwards, the working area was defined (Figure 76) to divide the skull into 2 parts. This way, the working area will be 3D printed with the selected EP filament and 30% infill density, and the rest with PLA filament and 20% infill density. Moreover, the tabs to screw the base of the skull were modified and placed inside the mold for aesthetics (Figure 77).

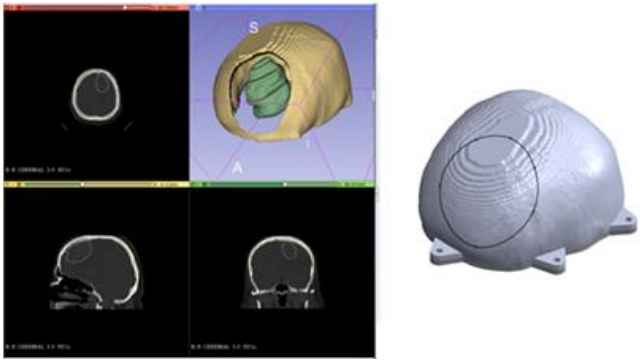

Figure 76. Image of the segmentation with a cut in the skull in the location of the tumor (left) and definition of the working area of the skull (right) to change the material during 3D printing (EP for the working area and PLA for the rest of the skull).

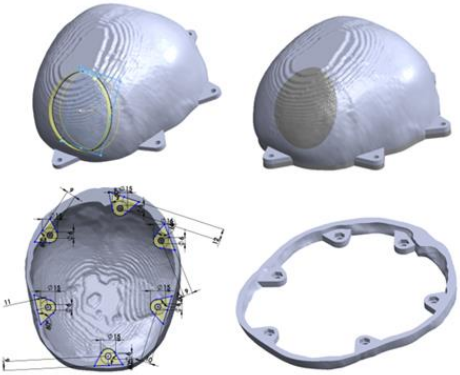

Figure 77. Features performed with SolidWorks to divide the model into the working and non-working areas (top) and modification of the housings for the assembly (hidden housing).

The base of the skull was also defined according to the screw tabs of the upper part of the skull (Figure 77). Moreover, the holes to fix the base to the fixation mechanism (holder) were also defined according to holder design (Figure 78).

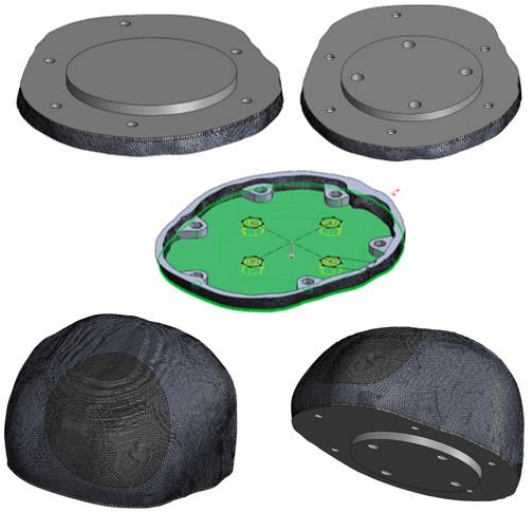

Figure 78. Features performed in SolidWorks for the skull base design.

The resulting manufacturing file (gcode file) was run in the 3D printer (Atom 2.5 FX) and the skull (Figure 79) and the skull base (Figure 80) was obtained after several hours of 3D printing.

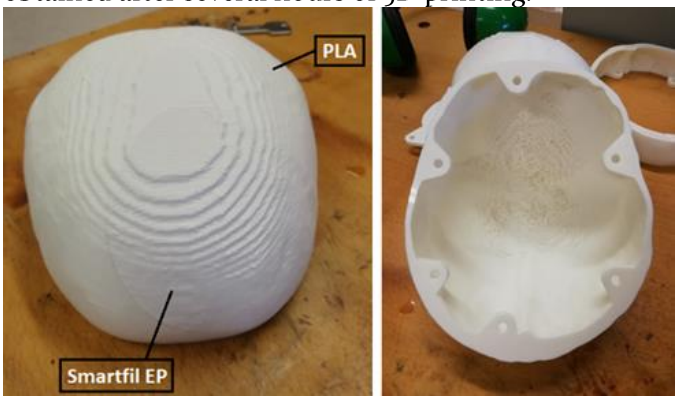

Figure 79. Final 3D printed skull.

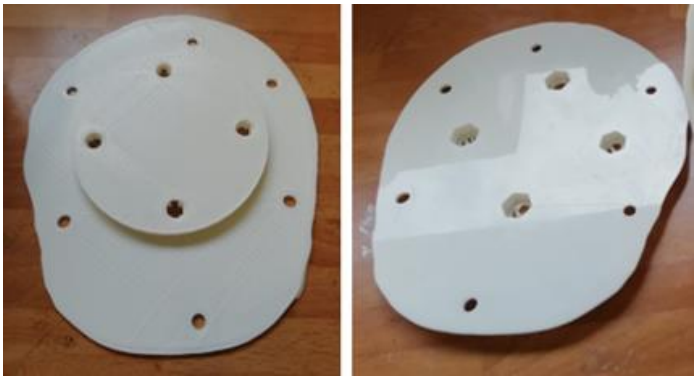

Figure 80. Final 3D printed skull base.

Regarding the brain mold model, the segmented mold (Figure 74) was cut to define a flat plane and then, divided into two parts to facilitate the demolding process, especially in the region of the tumor (Figure 81).

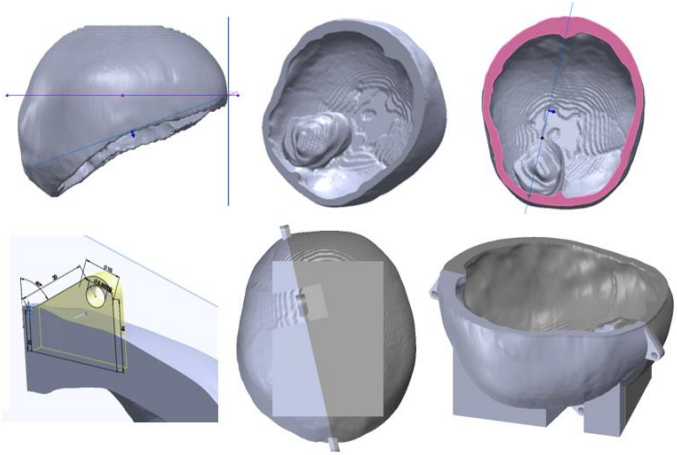

Figure 81. Design steps in SolidWorks to obtain the final geometry of the brain mold.

The result of the 3D manufacturing process of the brain mold is shown in Figure 82.

Figure 82. Final 3D printed brain mold.

Regarding the tumor mold, several features were applied to divide the initial geometry into two parts for the demolding process. Additionally, some tabs were added to join both parts of the mold and a feeding hopper to pour the silicone (Figure 83). Figure 84 shows the 3D printed tumor mold.

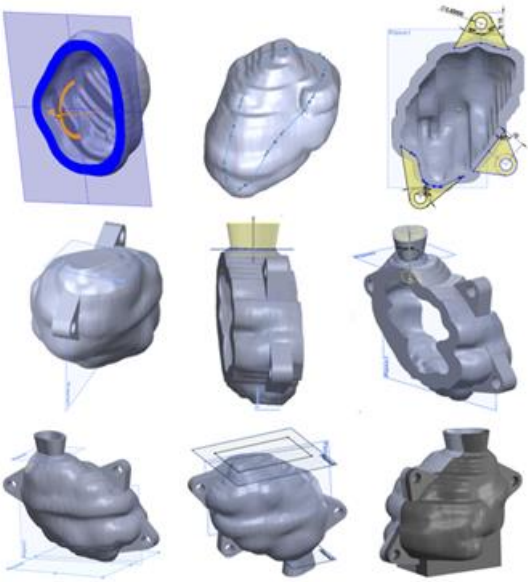

Figure 83. Design steps in SolidWorks to obtain the final geometry of the tumor mold.

Figure 84. Final 3D printed tumor mold.

As mentioned before, the brain will be produced with two different mixtures of silicone: the softest selected mixture for the working area, and the hardest mixture for the rest of the brain. Therefore, two different pouring processes must be carried out. Figure 85 shows the design steps of the mold to define the working area. This mold surrounds the tumor, leaving a certain clearance between the tumor and the mold so that the softest silicone can cover the tumor, which is

already defined in the mold of the brain. The mold of the working area also has a ring that perfectly fits with the upper part of the brain mold to correctly place it before pouring the silicone.

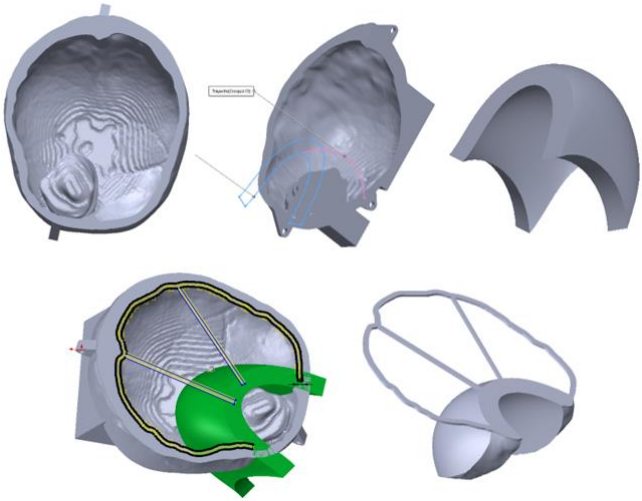

Figure 85. Design steps in SolidWorks to obtain the mold to define the working area.

Figure 86 shows the 3D printed mold of the working area and the final assembly with the brain mold.

Figure 86. Final 3D printed mold of the working area (left) and assembly with the brain mold (right).

Once all the 3D printed models were obtained, the silicone mixtures that were necessary to make the brain (with the two different mixtures: the working area and the non-working area), the tumor and the dura mater were produced.

To make the brain, the mold to define the working area was placed inside the brain mold and the first pouring was made inside this mold with the chosen mixture of 1:1:3 (Ecoflex 00-10 component A:B:Slacker) (Figure 87). Then the rest of the mix without the Slacker was poured into the brain mold (Figure 88).

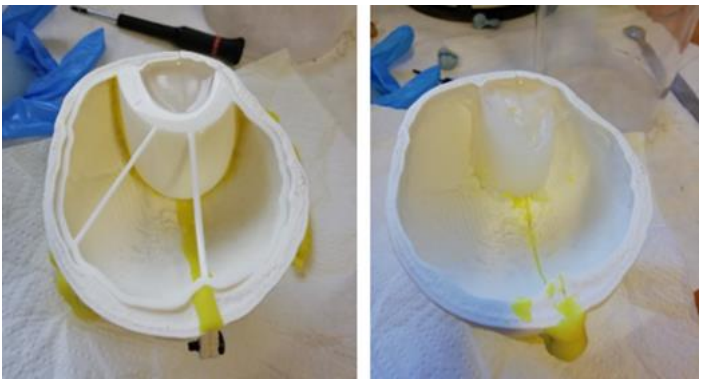

Figure 87. 1:1:3 silicone mixture inside the mold that defines the working area (left) and cured mixture (right).

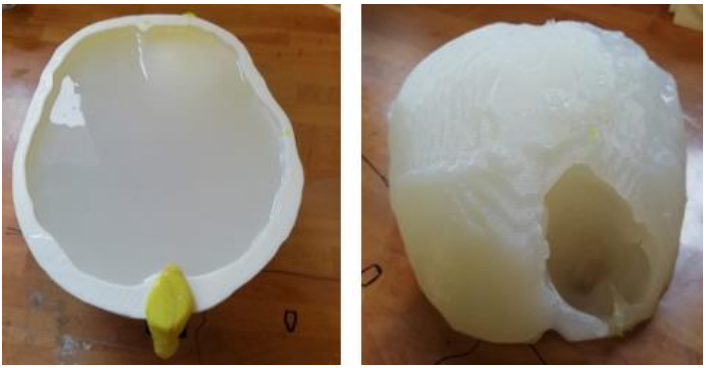

Figure 88. Pouring of 1:1 silicone mixture into the brain mold (left) and final brain model (right).

For the tumor, the 1:1 silicone mixture with pigments and crushed PLA was poured into the tumor mold (Figure 89). Figure 90 shows the final tumor model.

Figure 89. Mixture made for the preparation of the tumor (left) and mold filling (right).

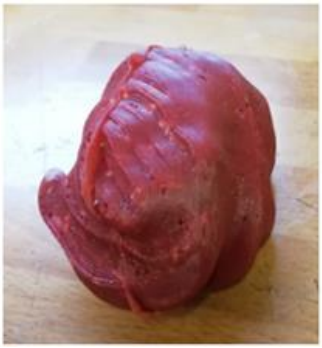

Figure 90. Final tumor model.

Finally, to simulate the dura mater, 1:1 silicone mixture was expanded on a surface, after applying a previous layer of release agent, and left as thin as possible to make a thin sheet (Figure 91).

Figure 91. Thin sheet made with 1:1 silicone mixture to simulate the dura mater.

To finish case 1, the assembly of the full-scale models was carried out, as shown in Figure 92 and Figure 93, and the model was placed in the fixation mechanism (Figure 94).

Figure 92. Skull (left) and brain model with the meningioma inside (right).

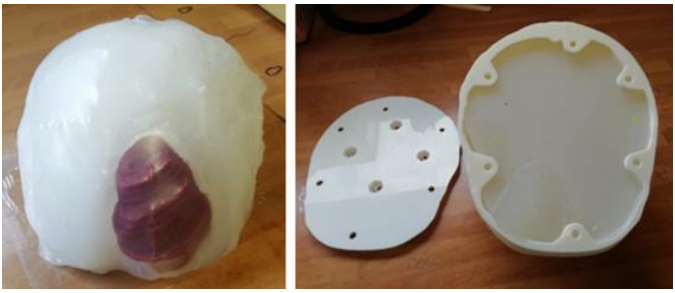

Figure 93. Incorporation of the dura mater layer on the brain model (left) and introduction of the brain into the skull (right).

Figure 94. Final model of case 1 on the stand.

1.2.2. Case 2: Glioma

This tumor has a lower consistency than brain. For this reason and with the experience obtained with the material chosen to emulate the hematoma of case 1 of the first summer school (Figure 40), it was decided to simulate this model with a mixture of sodium alginate with distilled water in a ratio of 1:20 w/w.

The process started with the segmentation of the real CT images (DICOM files). In this case, the models to be segmented will be the same as in the previous case, except the tumor, which will not be poured in a

mold, but inside the molded brain. Therefore, a cavity must be defined inside the molded brain to pour the sodium alginate solution that mimics the tumor.

The first model to be segmented was the skull (Figure 95). Also, as in Figure 69, the lower part of the skull was cut out (Figure 96).

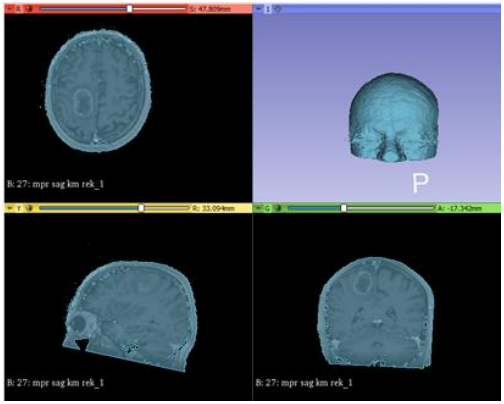

Figure 95. Segmentation of the skull from the DICOM images.

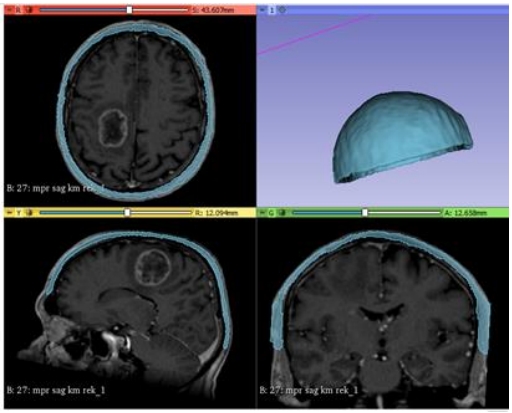

Figure 96. Cutting of the 3D skull in 3DSlicer.

To create the brain mold, the brain was first segmented by the succession of CT layers (Figure 97). Next, the thickness of this model was increased 10 millimeters and finally, the original brain model was

removed, thus leaving the interior empty and creating the mold (Figure 98).

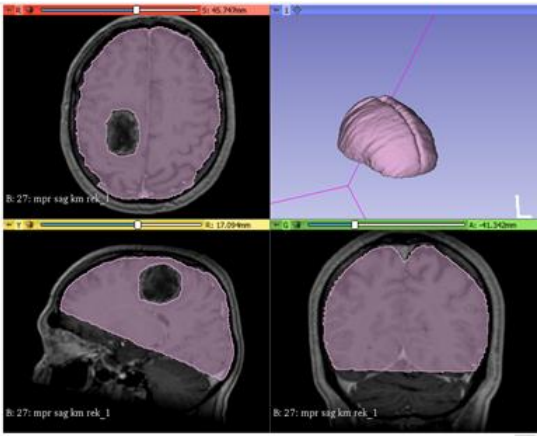

Figure 97. Segmentation of the brain from the DICOM images.

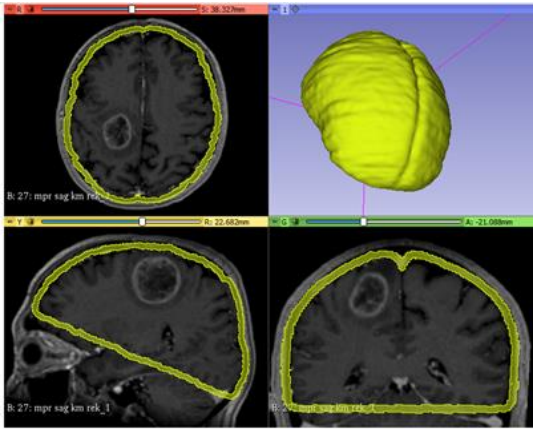

Figure 98. Segmentation of the brain mold with a thickness of 10 mm.

As in the previous models (Figure 95 and Figure 97), the tumor was segmented by the different CT layers, creating the tumor model shown in Figure 99.

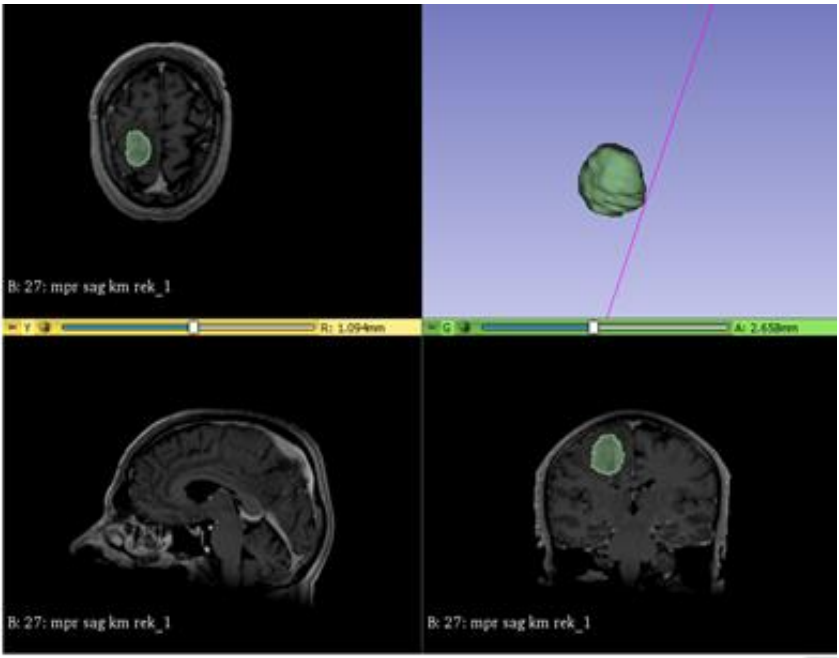

Figure 99. Segmentation of the tumor from the DICOM images.

Once the segmentation process was finished, the models were imported in STL files into Meshmixer and converted into solid STL (Figure 100).

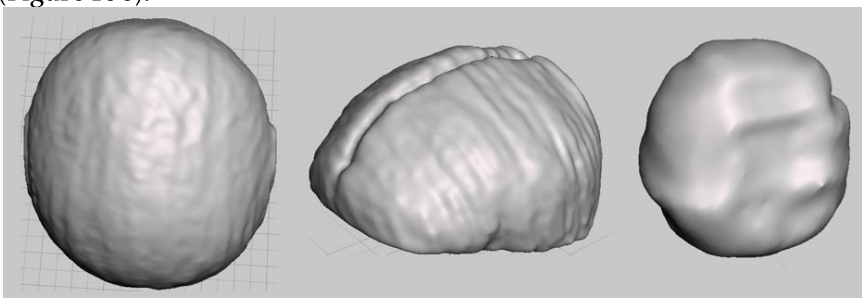

Figure 100. Models of case 1 in Meshmixer.

For the final definition of the skull, a flat cutting and the definition of the assembly tabs of the skull were designed (Figure 101).

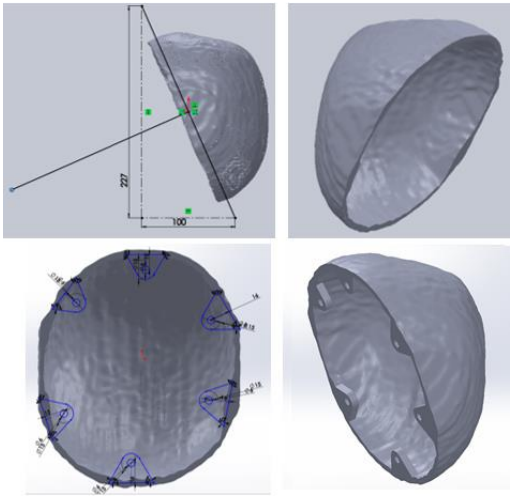

Figure 101. Initial features performed with SolidWorks for the skull design.

For the skull base, the same steps as in case 1 were followed (Figure 102).

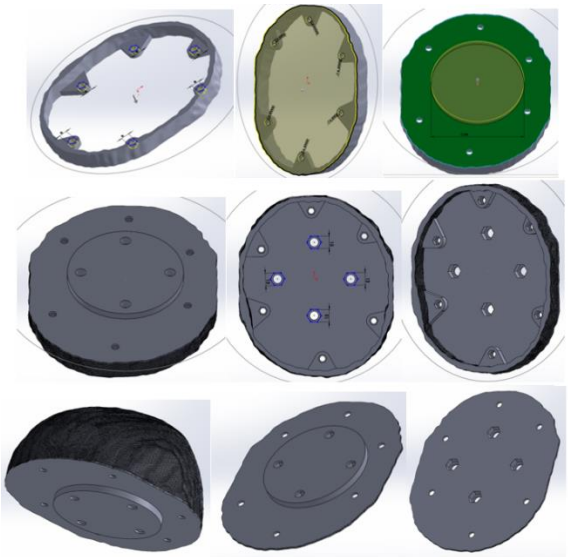

Figure 102. Features performed in SolidWorks for the skull base design.

The skull was divided into two zones: the working zone (with EP filament and 30 % infill density), and the rest (PLA filament with 20% infill density). Figure 103 shows these steps.

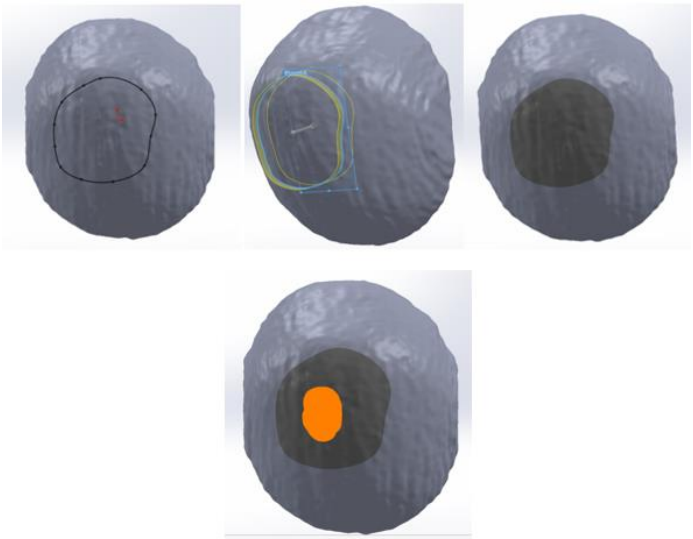

Figure 103. Features performed with SolidWorks to divide the model into the working and non-working areas (top) and image of the location of the tumor to ensure that correct the definition of the working area (bottom).

The result of the skull and the base skull model is depicted in Figure 104.

Figure 104. Final 3D printed skull.

For the brain mold, unlike the brain mold of case 1 (Figure 81), it was not necessary to divide it into two parts. Figure 105 shows the design steps (flat cut and definition of the base for stability during the silicone pouring).

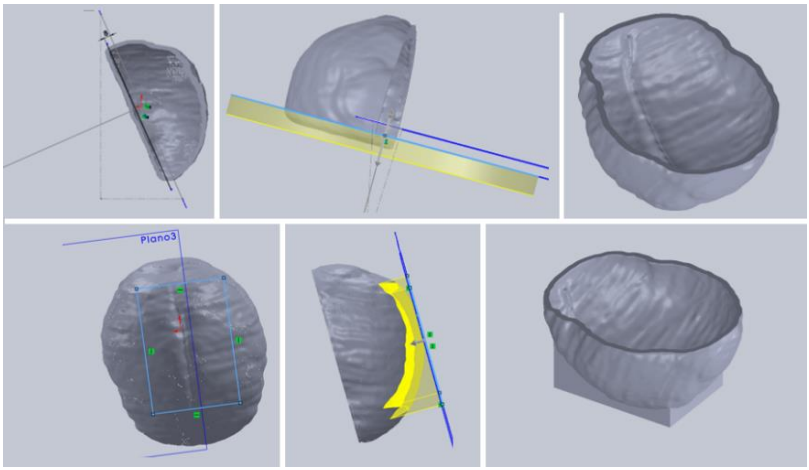

Figure 105. Design steps in SolidWorks to obtain the final geometry of the brain mold.

Figure 106 shows the 3D printed brain mold.

Figure 106. Final 3D printed brain mold.

For the design of the mold that defines the working area, a part was modeled covering the tumor with a certain clearance and adding a hopper to pour the silicone inside this mold (Figure 107).

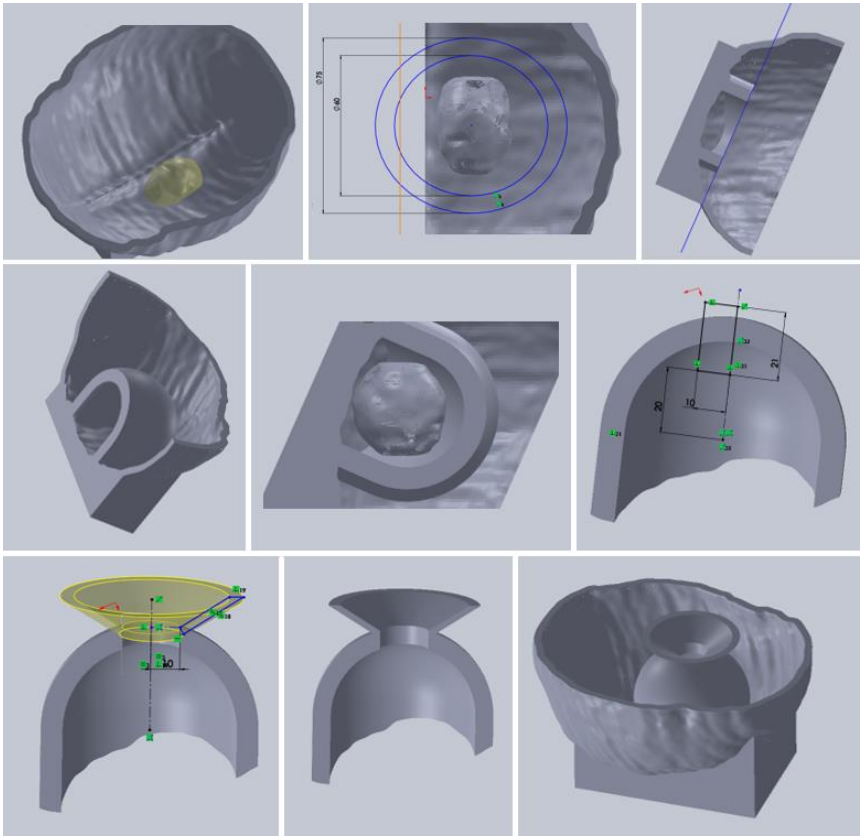

Figure 107. Design steps in SolidWorks to obtain the mold to define the working area.

With this mold that is located in the skull mold, it is possible to separate the different silicone mixtures. However, to guarantee the correct position of this mold during the pouring process, some tabs were added to be screwed in a support that will be placed on top of the brain mold (Figure 108).

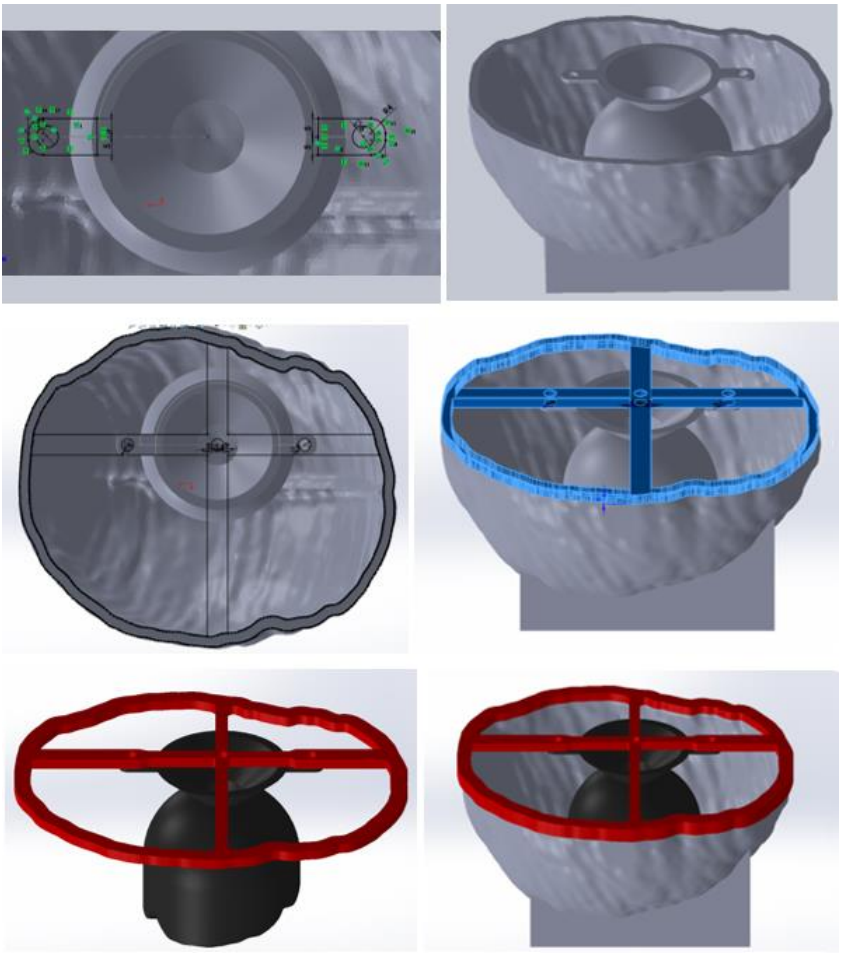

Figure 108. Design steps in SolidWorks to obtain the support (red) that is attached to the mold that defines the working area (black).

In order to keep the hematoma cavity, an insert with the segmented model of the tumor was designed to be placed inside the mold of the working area. This way, the soft silicone will fill the gap between the mold and the insert (Figure 109). Once cured the silicone, the insert will be removed thus leaving the cavity for the later infiltration of the simulated hematoma.

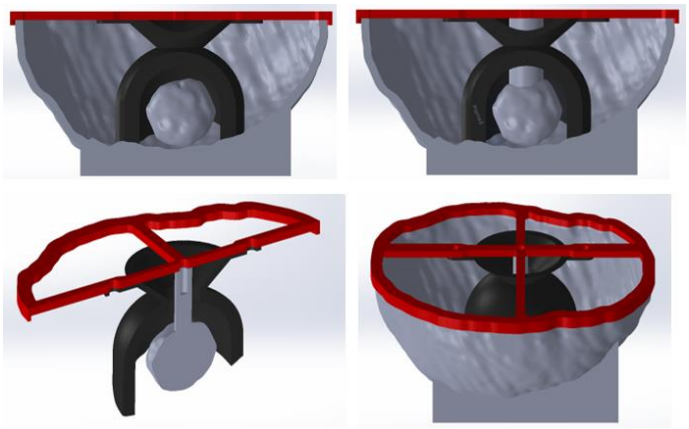

Figure 109. Design steps in SolidWorks to obtain the insert attached to the support (red).

These models were 3D printed with PLA (Figure 110).

Figure 110. Final 3D printed tools for the silicone pouring process.

Finally, an additional part (cone) was designed to be placed before the pouring of the final silicone (non-working silicone). This is a similar geometry to the tumor, but cut to reduce the demolding undercut. The objective of this part is to seal the cavity of the tumor during the pouring of the silicone of the non-working area (Figure 111).

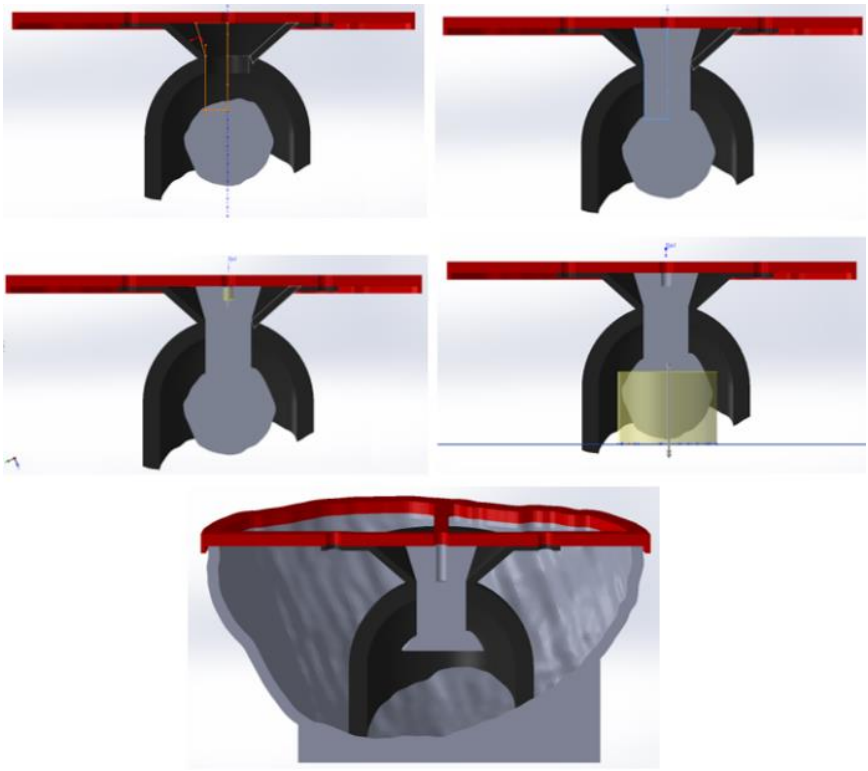

Figure 111. Design steps in SolidWorks to obtain the cone attached to support.

Once all the 3D printed models were obtained and 3D printed, the pouring process was carried out (Figure 112).

Figure 112. Brain model with the different silicone mixtures inside the skull model.

Although the initial idea was to first pour the silicone surrounding the tumor (the low consistency silicone, with Slacker component, for the working area), and then the rest (harder silicone for the non-working area), during the first trials it was observed that it was easier to do it the other way around. This means that the harder component (non-working area, outer part of the brain) should be poured before, and then the softest silicone surrounding the tumor (working area). This option was not initially considered to avoid undercuts in the demolding of the component that defines the working area. However, as the outer silicone has a high elasticity, this option was feasible and preferred to facilitate the poring process.

To do so, the mold to define the working area was designed as depicted in Figure 113. This part is fixed to the holder in the correct position and sealed in the bottom to the brain mold with modeling clay. The hardest silicone is then poured inside the mold and left to cure. Then, the mold defining the working area is removed and the insert with the geometry of the tumor is fixed to the holder and put inside the previously cured silicone. By using the available space between this part and the already cured silicone, the pouring of the working zone is accomplished. Finally, once the reticulation is finished, the mold defining the tumor is removed, once again taking advantage of the high

elasticity of the poured silicones, and the sodium alginate solution is injected into the remaining cavity.

As the sodium alginate solution that simulates the tumor may lose water over time, several tests were carried out to assess if this solution was stable once infiltrated in the simulated brain and covered with a silicone cap. The results showed good stability of the alginate solution, which means that this infiltration or filling process can be done during the preparation of the synthetic models and not necessarily just before the practical training.

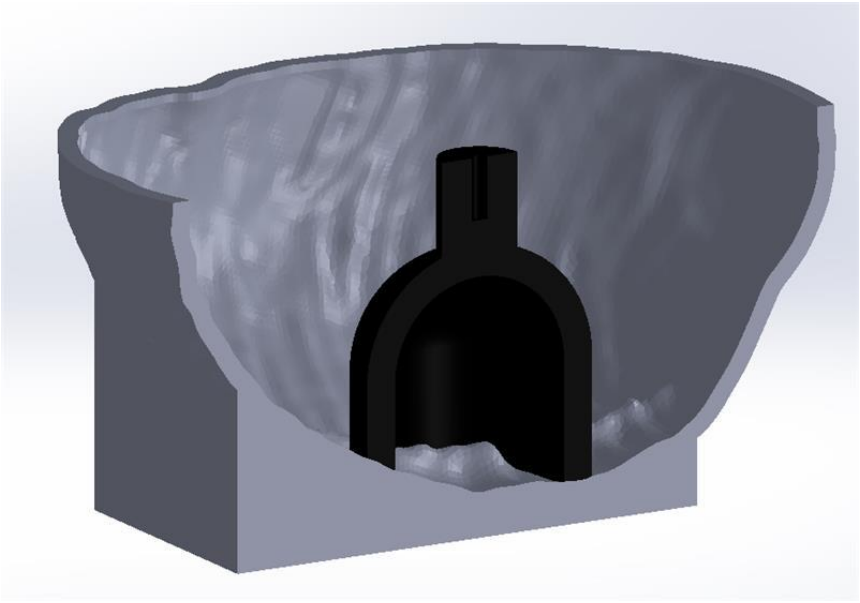

Figure 113. Design of the internal mold (black) to pour the hardest silicone and define the non-working zone. The upper part is fixed to the holder, which allows the correct positioning inside the brain mold.

Figure 114 shows the final molds and tools for the silicone pouring.

Figure 114. Brain mold with insert, holder and final design of the mold to define the working area.

Figure 115 shows the cured brain, already assembled in the skull and with the simulated tumor already infiltrated and covered with a cap.

Figure 115. Brain with tumor already infiltrated and assembled in the skull.

Figure 116 shows the final model with all the components (skull, brain with tumor inside, and base of the skull screwed).

Figure 116. Case 2 with skull and brain assembled (with tumor already infiltrated).

1.3. Training material for neurovascular surgery

The third summer school of the BrainIT project focused on neurovascular surgery. For this summer school, synthetic models of an aneurysm located in the medial cerebral artery (MCA aneurysm) were developed. As this document is being written before this summer school (August 2021), the current section shows all the design process and tests carried out so far, without having finished the complete manufacturing process.

1.3.1. Medial cerebral artery aneurysm

Synthetic models of a medial cerebral artery aneurysm was developed, starting from the real case depicted in Figure 117.

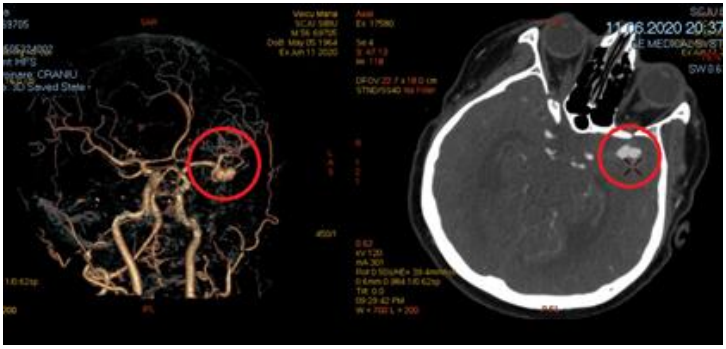

Figure 117. CT images of a real case of MCA aneurysm.

For the manufacture of blood vessels, the Digital Anatomy Printer (DAP) technology was selected, as it has a wide range of materials to mimic anatomy tissues. In order to choose the best material option and thickness of the vessels, 9 tube-shaped samples were manufactured and tested by neurosurgeons to find the best option to mimic real brain blood vessels for the surgery training. The external diameter was 3 mm (fixed value), while the internal diameter was modified with three different levels (1.8, 1.4 and 1 mm), so that the resulting minimum thickness was 0.6 mm, which is the minimum recommended thickness to guarantee the printability. For each geometry, three different hardness levels (compliance levels of 1, 3 and 6, being 1 the minimum 6 the maximum levels allowed) were used (vessel wall material, blood vessel family). Note that level 1 corresponds to the minimum hardness, and level 6 to the maximum hardness. Figure 118 shows the resulting 9 samples of the combination of the three internal diameters (or wall thicknesses) and the tree materials.

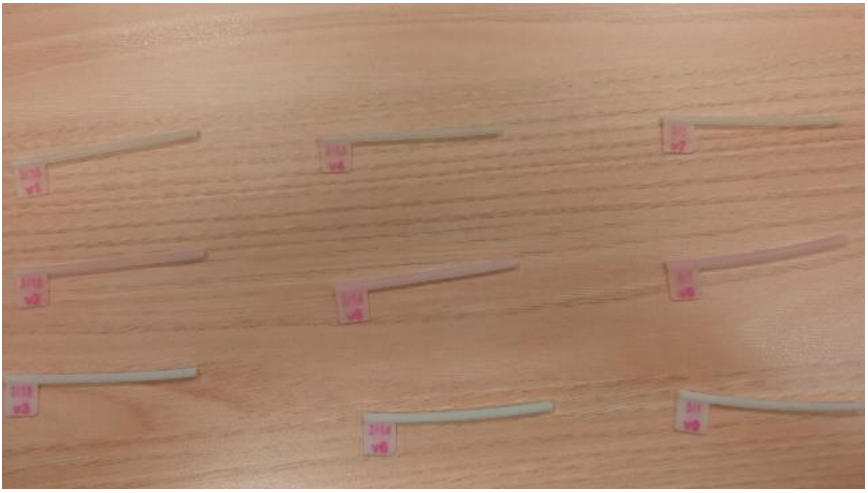

Figure 118. Tube samples with codes (vessel wall material).

Figure 119 shows the samples during the tests made by the neurosurgeons.

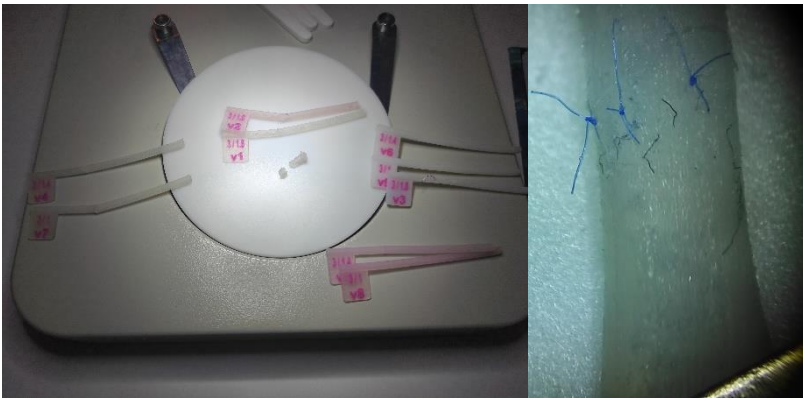

Figure 119. Tube samples during the tests. Left: general view. Right: view of sutures in the optical microscope.

Table 7 shows all the combinations with the corresponding code (from V1 to V9), diameters, materials, and also the neurosurgeons' score. According to the tests, the best combination was the one with the lowest wall thickness and the intermediate hardness (V2 option, with vessel wall thickness of 0.6 mm and slightly compliant hardness of the vessel wall material). This option provides a similar flexibility and fragile behavior to the real brain vessels.

Table 7. List of materials used for the samples.

Code	**D_{ext}/D_{int} (mm)**	**DAP material (hardness: 1-6)**	**Neurosurgeons' score (1-10) and comments**
V1	3/1.8	Compliant (1)	8
V2	3/1.8	Slightly compliant (3)	8.5
V3	3/1.8	Rigid (6)	Too hard and stiff
V4	3/1.4	Compliant (1)	6.5
V5	3/1.4	Slightly compliant (3)	6.5
V6	3/1.4	Rigid (6)	Too hard and stiff
V7	3/1	Compliant (1)	Too thick
V8	3/1	Slightly compliant (3)	Too thick
V9	3/1	Rigid (6)	Too hard and stiff

Once selected the material and thickness for the blood vessels, the 3D reconstruction was carried out by using the CT scan of the patient and processing the images in the ITK-SNAP software (segmentation process). In this case, the segmentation focused on the interior of the vessels (blood), which was obtained by removing the rest of material with the erase tool (Figure 120).

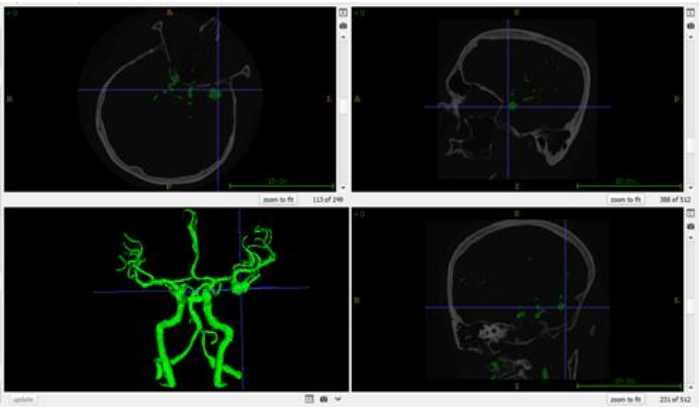

Figure 120. Segmentation of the interior of the blood vessel from the DICOM images.

Figure 121 shows the segmented model, where the aneurysm's area pecan be perfectly appreciated, as it was depicted in Figure 117.

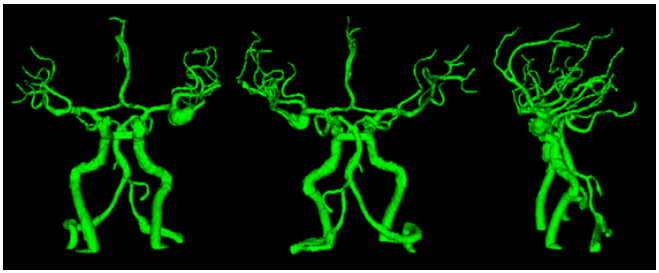

Figure 121. Different views of the 3D reconstruction of the interior of the vessels.

The STL file of the blood was imported into Meshmixer, where several operations were carried out to obtain the model of the hollow blood vessels, with a 0.6 mm thickness (Figure 122). Figure 123 shows the general dimensions of the final model.

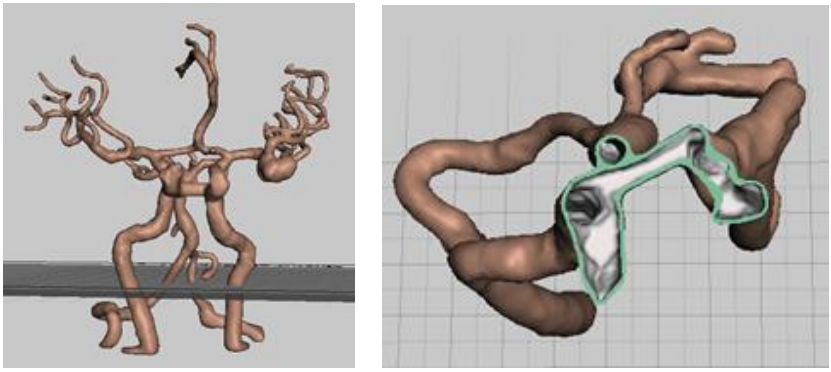

Figure 122. Blood vessels with 0.6 mm thickness. Left: general view. Right: section view (0.6mm wall thickness).

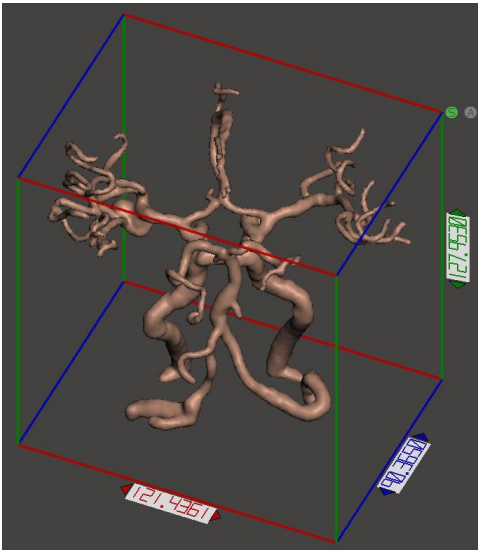

Figure 123. Dimensions of the blood vessels (approximately 121x90x128 mm).

On the other hand, in order to work with this model in the microscope, it must be cut to the region of interest (aneurysm zone) so that it can be fixed to the microscope and, at the same time, reduce the printing costs. As shown in Figure 124, the working area of the microscope corresponds to approximately 93 mm diameter if the fixation plate is used (external diameter) and 75 mm diameter if not (internal diameter). Similarly, the maximum available height from the bottom to the focal limit is 57 mm without the plate and 32 mm with the plate.

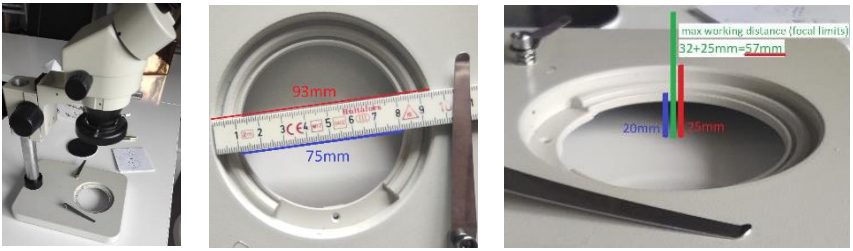

Figure 124. Optical microscope (left), dimensions of the working area (middle) and maximum heights (right).

Therefore, taking this into account, the cut was applied both to the model of the interior of the blood vessels and to the model of the blood vessels with a wall thickness of 0.6 mm. Both models were appended in the same document in Meshmixer to apply the same two plane cuts: the first on the left side and the second where the branches are located, thus reducing the model to a considerable size to be able to work with it in the microscope (Figure 125).

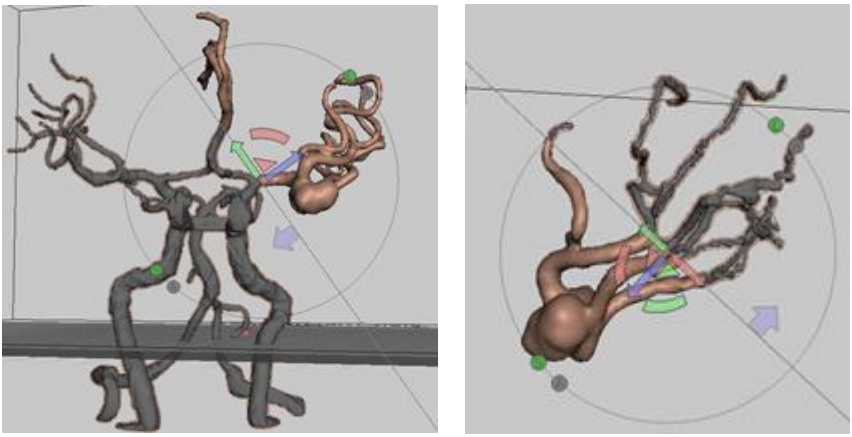

Figure 125. First plane cut to remove the lower part of the models (left) and second plane cut to eliminate the end of the vessels/blood (right).

Figure 126 shows the final models after the plane cuts (region of interest with the aneurysm). The dimensions of the reduced model were 31.8x31.8x37.9 mm, as depicted in Figure 127.

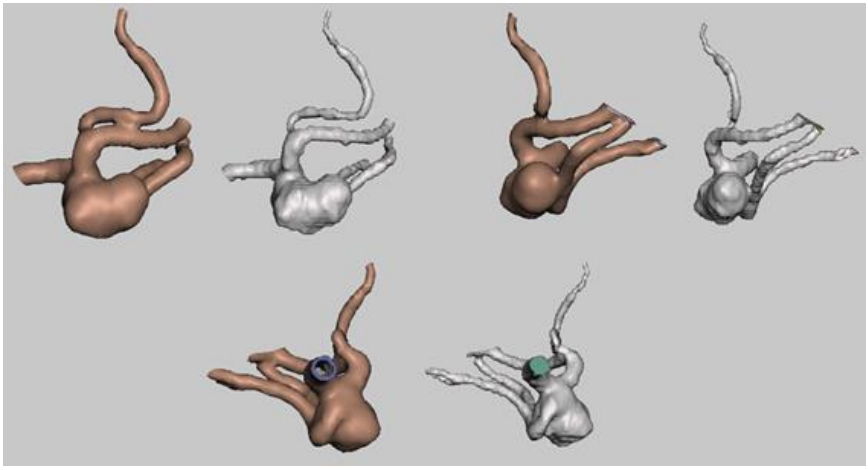

Figure 126. Reduced model of blood vessels and internal blood (in grey) seen from different angles.

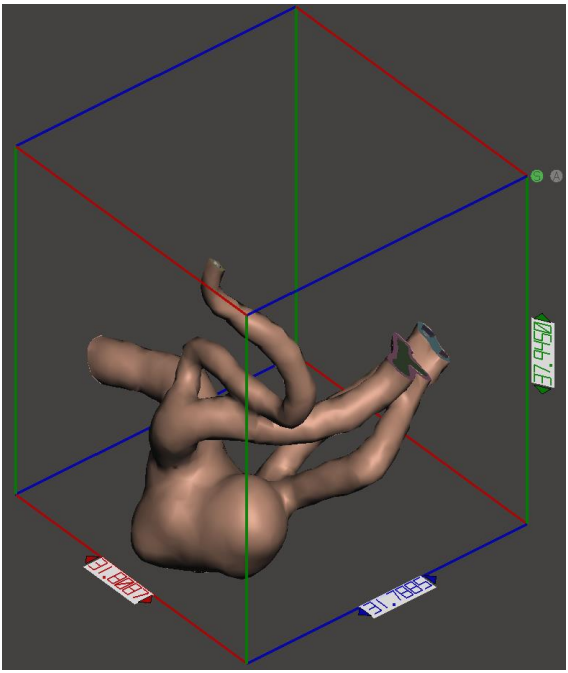

Figure 127. Dimensions of the reduced model of blood vessels and internal blood (in mm).

As the dimensions of the final reduced model do not exceed the dimensions of the working area of the microscope, the models can be properly placed and fixed in the microscope.

Once the segmentation and design of these models was carried out, 10 replicas of the reduced model and one replica of the complete vessels will be manufactured (process ongoing during the writing of this document). The complete model will serve as a reference to show all the vessels to the students, while the other 10 reduced blood vessels models will be the working models used by the trainees during the practical session. In both cases, the material to make the vessels will be the previously selected (V2 option, Table 7), and the support material that will be applied to the internal blood model will be GelMatrix. This material has a gel-like consistency that can be easily removed from the interior of the blood vessel models with water jet.

References:

1. R. P. Hubbard, "Flexure of layered cranial bone," *J. Biomech.*, vol. 4, no. 4, pp. 251–263, Jul. 1971.
2. C. Deck, S. Nicolle, and R. Willinger, "HUMAN HEAD FE MODELLING : IMPROVEMENT OF SKULL GEOMETRY AND BRAIN CONSTITUTIVE LAWS," 2004.
3. J. A. Motherway, P. Verschueren, G. Van Der Perre, J. Vander Sloten, and M. D. Gilchrist, "The mechanical properties of cranial bone," in *IFMBE Proceedings*, 2010, vol. 31 IFMBE, pp. 776–779.
4. R. Delille, D. Lesueur, P. Potier, P. Drazetic, and E. Markiewicz, "Experimental study of the bone behaviour of the human skull bone for the development of a physical head model," *Int. J. Crashworthiness*, vol. 12, no. 2, pp. 101–108, 2007.
5. J. E. Galford and J. H. McElhaney, "A viscoelastic study of scalp, brain, and dura," *J. Biomech.*, vol. 3, no. 2, pp. 211–221, 1970.
6. P. J. Basser, "Interstitial pressure, volume, and flow during infusion into brain tissue," *Microvasc. Res.*, vol. 44, no. 2, pp. 143–165, 1992.
7. Y. Tada, T. Nagashina, and M. Takada, "Biomechanics of Brain Tissue (Simulation of Cerebrospinal Fluid Flow)," *Trans. Japan Soc. Mech. Eng. Ser. A*, vol. 58, no. 551, pp. 1115–1121, 1992.
8. M. Kaczmarek, R. P. Subramaniam, and S. R. Neff, "The hydromechanics of hydrocephalus: Steady-state solutions for cylindrical geometry," *Bull. Math. Biol.*, vol. 59, no. 2, pp. 295–323, 1997.
9. M. Miga, K. Paulsen, F. Kennedy, J. Hoopes, A. Hartov, and D. Roberts, "Initial in-vivo analysis of 3D heterogeneous brain computations for model-updated image-guided neurosurgery," in *Lecture Notes in Computer Science (including subseries Lecture Notes in Artificial Intelligence and Lecture Notes in Bioinformatics)*, 1998, vol. 1496, pp. 743–752.
10. K. Miller, K. Chinzei, G. Orssengo, and P. Bednarz, "Mechanical properties of brain tissue in-vivo: Experiment and computer simulation," *J. Biomech.*, vol. 33, no. 11, pp. 1369–1376, Nov. 2000.
11. W. Goldsmith, "The state of head injury biomechanics: Past, present, and future: Part 1," *Critical Reviews in Biomedical Engineering*, vol. 29, no. 5–6. Begell House Inc., pp. 441–600, 2001.
12. Z. Taylor and K. Miller, "Reassessment of brain elasticity for analysis of biomechanisms of hydrocephalus," *J. Biomech.*, vol. 37, no. 8, pp. 1263–1269, Aug. 2004.

BIOMATERIALS FOR CRANIOPLASTY: A CURRENT VISION AND FUTURE PERSPECTIVES

Ilaria Cacciotti[1]

[1] Department of Engineering, University of Rome "Niccolò Cusano", INSTM RU, via Don Carlo Gnocchi 3 00166 Rome, Italy.
ilaria.cacciotti@unicusano.it

Contents

1. Introduction

Even if the cranioplasty has been performed for centuries, the postoperative complication rate is still very high, with the need of reoperation, the occurring of infection and resorption of the implanted grafts.

For these reasons, many efforts have been and are devoted to identify the optimal materials able to guarantee the best long-term results. However, up to date, there is no consensus regarding the ideal material to be used in cranioplasty, and the selection depends on the experience of the surgeons and the patient individual conditions [Servadei and Iaccarino, 2015; Lindner et al., 2016].

This chapter provides a complete overview about the materials used for cranioplasty, starting from the ancient time to the current period, reporting the advantages and drawbacks. Some future perspectives about cranioplastic biomaterials are discussed.

2. Cranioplasty

2.1. Cranioplasty: generalities

The cranioplasty consists in the surgical repair of a deficiency/deformity and of structural or morphological defects of the skull. Craniofacial reconstruction is a very complicated surgical process, involving brain, eyes and other sensory organs, all within a confined space [Moiduddin et al., 2017]. It is possible to identify many causes of cranial defects, such as infections with osteomyelitis, trauma with fractures, congenital malformations (e.g., craniosynostosys [Tiberio et al., 2021]), decompressive craniectomies, cranial tumor resection, degenerative pathologies [Khader & Towler, 2016; Moiduddin et al., 2017], that result in functional and esthetic deficiencies, as schematized in **Figure 1**. Around 30 thousand surgical reconstruction procedures of craniofacial bone defects are performed annually in the United States alone [Kim et al., 2012].

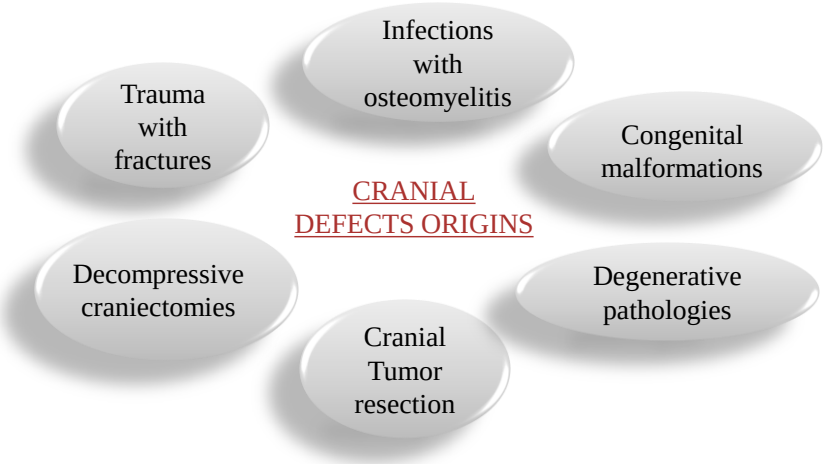

Figure 1. Main causes of cranial defects.

The main aims of cranioplasty are summarised below [Moiduddin et al., 2017]:

- ✓ to provide protection for the brain following cranial surgery;
- ✓ to alleviate the psychological disorder caused by the bone defects;
- ✓ to restore the appearance and psychological stability of the patient (cosmethic purposes);
- ✓ to avoid the recurrence of brain damage, by protecting the patient from cerebral losses;
- ✓ to increase the brain blood flow;
- ✓ to improve the brain energy metabolism and promote the brain tissue recovery.

The success of cranial reconstruction depends on the following aspects [Khader & Towler, 2016; Moiduddin et al., 2017]:

- preoperative defect evaluation;
- implant design;
- material and fabrication;
- skills of the surgeon.

2.2. Cranioplasty: historical records

The first attempts of cranioplasty have been testified by several archaeological records since the origin of human civilization [Shah et al., 2014]. However, the modern technique of cranioplasty has been introduced only since the second half of the last century [Goldstein et al., 2013].

The main important historical events are reported in **Figure 2** and are summarised below [Aydin et al., 2011; Harris et al., 2014; Alves Junior et al., 2016; Alkhaibary et al., 2020; Feroze et al., 2015]:

- Cranioplasty was practiced in many ancient civilizations, including the Incans, the Britons, the Asiatics, the North Africans, and the Polynesians [Courville, 1959], with records dating back to 7,000 BC.
- In the earliest historical cranial reconstructions locally available materials, such as gourds, coconuts, or precious metals, were used. Moreover, the selected material reflected the socioeconomic rank of the patient: precious metals were used for the nobility, and gourds for the common citizen.
- The first cranioplastic operations by using metallic materials are dated back to 3000 BC.
- A Peruvian skull, dating back to 2000 BC, was found to have a left frontal defect covered with a 1-mm-thick gold plate [Kennedy, 1987].
- The first documented description of cranioplasty in the medical literature is ascribed to Fallopius and Petronius in the 16th century, who proposed the use of gold plates [Courville, 1959].
- With the introduction of inhaled anesthesia and antiseptic practices in the late 19th century, the cranioplasty became a more viable treatment option.
- In the 18th and 19th centuries, bone grafts were mainly employed.
- In 1821, the first recorded autologous bone graft cranioplasty was performed by Walther [Munroe, 1924].
- In 1889, plastic reconstruction of the cranium was first recorded by Seydel who used pieces of tibia to cover a left parietal defect with uneventful recovery [Aydin et al., 2011].
- Morestin used the cadaver cartilage for cranioplasty in 1915, for the first time [Durand et al., 1997].

- Sicard and Dambrin experimented with cadaveric skull in 1917.
- In the last century, during the WorldWars, the use of non-biological prostheses became more common: in WorldWar I, there was a preference for gold and silver; titanium started to be used in WorldWar II and the first use in cranioplasty was ascribed to Simpson (1965).; vitallium alloys were used by Geib (1941), tantalum by Pudenz and Odom (1942), stainless steel mesh by Boldrey (1944), stainless steel by Scott, Wycis, and Murtagh (1956); since the 1940's, non-metal prostheses started to achieve more interest with the first implant of a methylmethacrylate prosthetic into a patient by Zander, in 1940.
- Starting from 1960s up to date, many efforts have been dedicated to the development of recombinant growth factors.
- Starting from 2000 to present, many researches have been focused on stem cell-based therapies in the calvarial defect repair.

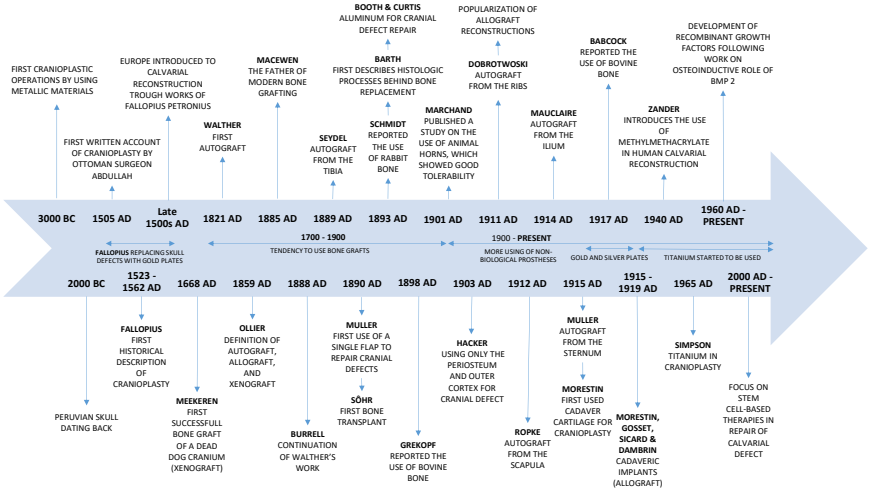

Figure 2. Timeline of the cranioplasty history.

3. Cranioplastic implants

3.1. Requirements for the ideal cranioplastic implant

The optimal implant should have high interconnected porosity, in order to promote the cell adhesion, to allow the transportation of fluids, and to provide a good interfacial adhesion with the bone, leading to

bone ingrowth formation, effective fixation and shorter healing time [Pilliar, 1998]. The ideal pore size for the bone ingrowth lies in the range of 500-1500 μm [Otsuki et al., 2006]. For example, porous titanium with a porosity of 50% is ideal for bone tissue ingrowth [Otsuki et al., 2006]. However, it is important to take into account that, even if high porosity promotes bone formation, its excessive increase can significantly decrease the strength of the implant.

3.2. Requirements for the ideal cranioplastic material

An ideal cranioplasty material must have the following features [Blake, 1994; Harris et al., 2014; Alves Junior et al., 2016]:

- physical properties similar to those of the bone;
- biocompatibility;
- bioactivity/osteoconductivity/bioresorbability;
- adequate mechanical strength;
- low heat conductivity;
- no cytoxicity and no infection risk;
- resistance to infections;
- malleability and easiness to shape and contour to properly fit the cranial defects with complete closure;
- readily availability for use at reasonable costs;
- radiolucency/radiotrasparency;
- possibly low cost.

Up to date, none material has satisfied all these requirements.

4. Materials for cranioplasty

There are four known types of grafts for cranioplasty [Mohan et al., 2015; Aydin et al., 2011; Ciurea 2010]:

- autogenic grafts (from the same patient), such as bone from cranium, ribs, shinbones, shoulder blades, sternum or ilia;
- allogenic grafts (from another human donator), such as cartilage;
- xenogenic grafts (transplanted from animals ex: bovines, pigs, etc.);

- alloplastic grafts (composed of synthetic materials) such as metals (e.g., aluminium, gold, silver, lead, platinum, titanium, tantalum and their alloys), celluloid, polymethylmethacrylate (PMMA), polyetheretherketone (PEEK), hydroxyapatite (HAp), polyethylene (PE), silicone, ceramic and other derivatives.

The main advantages and drawbacks of the commonly used materials for cranioplasty are collected in **Table 1.**

Table 1. Main advantages and drawbacks of the cranioplastic materials [Shah et al., 2014; Song et al., 2015; Khader and Towler, 2016].

Material	Advantages	Drawbacks
Natural materials		
Autograft	✓ decreased infection risk ✓ absence of host rejection ✓ capability to well integrate with the cranial cavity, resulting in lower risk of fracture ✓ minimal dislodgement or disintegration, due to higher rate of revascularisation and integration with adjacent bone	• limited/poor availability of suitable donor sites • tissue harvesting problems and prolonged operative time, • donor site morbidity • pain and infection • expensive surgeries • the bone donor site graft resorption • difficult moulding to the defect • insufficient graftable tissue to cover the defect, particularly in the case of paediatric patients

Material	Advantages	Drawbacks
Natural materials		
Allograft	✓ abundant source	• high resorption rates • unwanted immunological responses • infection
Metallic materials		
Titanium mesh/plate	✓ no inflammatory reaction ✓ no corrosion ✓ low infection rate ✓ good cosmesis ✓ high mechanical strength ✓ good biocompatibility ✓ virtually no risk of allergic reaction ✓ excellent customization ✓ higher radiolucency than many other metals ✓ lower cost than many other metals ✓ possibility to be shaped intraoperatively ✓ support to cement materials	• high cost • artifacts on CT and MRI imaging • infection • heat conduction • poor malleability • poor cosmesis • loosens over time
Polymeric materials		
PE	✓ biocompatibility	• too high softness

Material	Advantages	Drawbacks
Natural materials		
PMMA	✓ ready availability ✓ biocompatibility ✓ lightness ✓ malleability ✓ good strength ✓ durability ✓ inertia ✓ heat resistance ✓ lack of thermoconduction ✓ radiolucency ✓ easiness of use ✓ low cost ✓ excellent cosmesis	• exothermic burn reaction during its setting with possible damage to the surrounding tissues • possible inflammation reaction due to unreacted toxic monomers • risk of infection • low mechanical properties • brittleness • fracture susceptibility • low osteoconductivity • lack of osseointegration
PEEK	✓ chemically inertia ✓ stiffness ✓ strength comparable to that of cortical bone ✓ elasticity ✓ lack of thermoconduction ✓ absence of artifacts on imaging ✓ comfortability ✓ radiolucency	• very high cost • lack of osteointegrative properties • high risk of being dislodged or extruded • infection • inflammation • need for additional 3D planning and imaging

Material	Advantages	Drawbacks
Natural materials		
	✓ high heat and gamma ray tolerance, allowing for multiple sterilizations if necessary ✓ possibility to be shaped intraoperatively when needed ✓ absence of allergenic reactions ✓	
Ceramic materials		
HAp	✓ noninflammatory ✓ good chemical bonding to ✓ bone ✓ excellent cosmesis and contouring ability ✓ good biocompatibility	• low tensile strength • brittleness • infection • implant fracture/fragmentation • lack of osteointegration
Alumina ceramics	✓ hardness ✓ chemical stability ✓ tissue compatibility ✓ low infection rate	• high cost • propensity to shatter
Composite materials		
Calcium phosphate cement	✓ ease to use ✓ good biocompatibility ✓ no heat generation in use ✓ osteoconductivity ✓ no inflammatory reaction	• low mechanical strength • infection • implant fracture • inflammation • brittleness • difficult to contour

Material	Advantages	Drawbacks
Natural materials		
Cortoss™	✓ high strength	• exothermic reaction
Mineralised collagen	✓ biomimetic chemical compositions ✓ biomimetic microstructure ✓ good biocompatibility ✓ osteoconductivity ✓ bioresorbability ✓ radiolucency	• low mechanical strength

4.1. Autografts

For both paediatric and adult patients, the autologous bone graft (usually from cranium, ribs and iliac crest) is considered the gold standard, and, when available and appropriate, this is the commonest technique used [Elsalanty and Genecov, 2009; Rogers & Greene, 2012]. Many other bone harvest sites were experimented, such as sternum, scapula, fascia, and fat [Aydin et al., 2011]. Its use presents many advantages (**Table 1**), such as the decreased infection risk, absence of host rejection and capability to well integrate with the cranial cavity and the skull, resulting in lower risk of fracture [Shah et al., 2014], minimal dislodgement or disintegration, due to higher rate of revascularisation and integration with adjacent bone [Rogers & Greene, 2012]. However, its employment is restricted due to the limited/poor availability of suitable donor sites, especially for the large and complex defects, tissue harvesting problems and prolonged operative time, donor site morbidity, pain and infection, expensive surgeries, the bone donor site graft resorption, difficulty to perfectly fitting the defect, and insufficient graftable tissue to cover the defect, particularly in the case of paediatric patients (**Table 1**) [Rogers and Greene, 2012]. Indeed, an incidence of bone resorption of 2–32% has been reported in adults, and

50–66% in children [Shah et al., 2014; Goldstein et al., 2013; Servadei and Iaccarino, 2015].

4.2. Allografts and xenografts

Due to the criticisms associated to the use of autografts, such as the complications at the donor site, xenograts and allografts were attempted. For centuries, bone xenografts (obtained from species other than humans) have been used for the cranial defects reconstruction: canine bone was used by vanMeekeren in 1668 [Durand et al., 1997], rabbit bone by Schmidt in 1893, bovine bone by Grekopf in 1898 and by Babcock in 1917. In 1901, Marchand reported the use of animal horns with good tolerability. Moreover, bones from monkeys, geese, dogs, calfs, and eagles were also employed [Shah et al., 2014; Santoni- Rugiu and Sykes, 2007]. Ox horn, buffalo horn, and ivory also led to satisfactory results. However, the development of new techniques and materials made xenografts uncommon in contemporary cranioplasty. Concerning the allografts, Morestin first used cadaver cartilage for cranioplasty in 1915 [Durand et al., 1997], being cartilage able to well fill the defects and being it resistant to infection [Munroe, 1924]. However, it was not strong enough and no significant calcification occurred. In 1917 Sicard and Dambrin used cadaveric skull, treating the resected bone with sodium carbonate, xylol, alcohol, and ether and subsequently sterilizing it with heat. However, the applied treatment reduced the bone thickness and only the outer table remained, which could then be perforated for use [Grant and Norcross, 1939], with high rate of infection and bone resorption. Thus, the employment of allografts is precluded due to high resorption rates and unwanted immune responses [Goldstein et al., 2013].

4.3. Alloplastic materials

Taking into account the limits of the autografts, synthetic biomaterials were used and developed, even if their complication rates are still high in clinical practice [Arnaud, 2000]. The use of synthetic biomaterials present many advantages: unlimited availability, no donor site morbidity, biocompatibility, and reduced operating time due to ease of use [Gosain et al., 2009].

4.3.1. Metals

Metals were among the earlier known calvarial repair materials, being able to provide good cosmetic outcome and reasonable mechanical properties. The used metals varied in the strength, availability, malleability, reactivity with surrounding tissue, and conductivity of heat or electricity. The advantages and drawbacks of the main metals employed in cranioplasty are collected in **Table 2.** However, their shortcomings motivated the introduction and investigation of alternative materials for cranial reconstruction [Harris, et al., 2014].

4.3.1.1. Precious metals and alloys

Gold and silver were used in many cultures, in both Western and Incan civilizations. In particular, both of them were employed for cranial repair in World War I, but by the midcentury, they were no longer in use.

During the early 20th century, platinum, lead, and aluminum were exploited as materials for cranioplasty, but their use was discontinued, due to their drawbacks (**Table 2**).

In order to find a good compromise between the metals positive aspects (i.e. strength, availability, and malleability) and their limits (i.e. side effects, costs, and radiopacity), some alloys were proposed as potential cranial reconstructive materials. Among them, tantalum, vitallium, and steel were commonly used in the mid-20th century.

In particular, tantalum was widely used during and after World War II for a brief period, but, afterward, it was no longer used due to its high cost, limited availability, and thermoconduction, that caused painful headaches in the patients due to its heating, especially when they were outside in the sunlight. Similarly, the use of vitallium, an alloy of cobalt, molybdenum, and chromium, was limited, being too difficult to shape intraoperatively, even if it revealed reduced bone necrosis and metal corrosion with respect to pure metals.

Stainless steel presented strength and malleability comparable with respect to the tantalum, and was more radiolucent and economical than tantalum. However, the tissue incompatibility was identified for some stainless steel alloys, as well as high failure rates were recorded.

In conclusion, most of the reported metals and alloys are are no longer used, mainly for the introduction of stronger, more conformable, and osteocompatible materials, as well as for futher limitations, such as the potential for epileptogenesis, plate dislodgement and subsequent scalp erosion and perforation, and the creation of a potential dead space into which brain can herniate or hematoma can form.

Table 2. Advantages and disadvantages of metals used in the alloplastic cranioplasty [Harris et al., 2014; Khader and Towler, 2016].

Metal	Advantages	Disadvantages
Gold	✓ high strength ✓ high malleability ✓ low complication rates	• high price • high softness
Silver	✓ easy to shape ✓ less expensive	• too high softness to provide adequate protection • interaction with the surrounding tissue, causing discoloration of the skin/scalp due to its oxidation • too high malleability to confer adequate protection
Platinum	✓ good biocompatibility ✓ no tissue reaction	• too high cost
Aluminum	✓ malleability	• increased rate of infectious • complications and epilepsy • irritation of the brain

Metal	Advantages	Disadvantages
		• material degradation • insignificant bone replacement • irritation of the surrounding tissue • prompted seizures • slow disintegration
Lead		• toxicity
Tantalum	✓ inertia ✓ high malleability ✓ corrosion resistance ✓ absence of infections ✓ Resistance to tissue reaction	• high price • limited availability • thermoconduction • difficulty to shape • radio-opacity which causes problems in postoperative imaging
Vitallium	✓ No corrosion ✓ decreased bone necrosis ✓ decreased metal corrosion	• lack of malleability • difficulty of intraoperative shaping
Stainless steel	✓ strength and malleability similar to tantalum ✓ higher radiolucency than tantalum ✓ lower cost than tantalum	• tissue incompatibility for some compositions • high failure rates for some compositions

4.3.1.2. Titanium

Among all the testes metals, only titanium plates and meshes remain in current practice. Indeed, from its earliest uses during World War II, titanium remains a pillar of modern cranioplasty practice. Titanium presents many advantages: it is non-corrosive, biocompatible, relatively radiolucent, and biologically inert (without any risk of resorption), it owns high tensile strength and malleability, and has shown comparatively low inflammatory reactions (**Table 1**) [Park et al., 2016]. Moreover, the use of titanium implants leads to improved long-term outcome [Park et al., 2016], due to the absence of resorption risk, and to the lowest incidence of infection (2.6 %) with respect to all other cranioplasty materials [Matsuno et al., 2006].

However, the use of metallic cranioplasty can lead to imaging artefacts with CT scans and radiographs due to radiographic attenuations, whose degree depends on used metal the atomic number and is, thus, higher for tantalum and gold than titanium [Chandler et al., 1994]. This limit has to be taken into account in the case of patients who require radiation therapy, after cranioplasty. Indeed, the metallic backscatter could potentially lead to local overdose with consequent skin necrosis and underdosing to deeper tissues, such as tumors, resulting in an inadequate treatment. Often, titanium meshes and plates are used in combination with other cranioplasty materials to improve the implant properties, mainly its strength [Shah et al., 2014]. For example, the reinforcement of hydroxyapatite with Ti mesh allows to treat larger cranial defects, providing improved osteointegration and suitable aesthetic restoration of cranial contours, with minimal side effects, and can be also applied also in pediatric procedures [Wiggins et al., 2013; Ducic, 2002; Cabraja et al., 2009].

4.3.2. Polymers

4.3.2.1. Polyethilene (PE)

Polyethylene (PE) was developed in 1936, and proposed for the cranial defects repair, for the first time, in the middle of 20th century [Busch et al., 1949]. In details, after World War II, the pediatric neurosurgeon Franc Ingraham tested several materials, e.g., PE, fibrin film, methyl methacrylate, and tantalum, in animal cranioplasty

experiments, concluding that polyethylene was the most effective due to its biocompatibility. In 1948, Busch reported the employment of polyethylene in humans. However, polyethylene was too softer with respect to acrylic resins, and, thus, its use was limited to small cranial defects.

For these reasons, PE was not extensively used until the development of porous polyethylene that may allow the native tissue in-growth and collagen deposition through pores with enhanced biocompatibility [Liu et al., 2004]. These commercially available PE implants can be easily cut into different shapes, and could be used for repairing cranial defects of different sizes [Lin et al., 2012; Wang et al., 2012a; Wang et al., 2012b].

4.3.2.2. Polymethylmethacrylate (PMMA)

Polymethylmethacrylate (PMMA), also called acrylic glass or plexiglass, is a thermoplastic and transparent polymer and is the second material of choice after the autograft for the cranioplasty with long term results in adults. The PMMA prosthetic was implanted into a patient by Zander in 1940 for the first time [Sanan and Haines, 1997].

It presents many advantages: ready availability, low cost, good strength, light weight, malleability, radiolucency, lack of thermoconduction, flexible intraoperative application, unlimited possibilities of adaptation to individual anatomy, and biocompatibility (**Table 1**) [Goldstein et al., 2013].

However, its employment, particularly for the pediatric patients, is limited due to its drawbacks: the exothermic reaction which occurs during its setting with possible severe damage to the underlying and surrounding tissues (brain, dura mater, cortex) coud be severely damaged due to the heat [Azmi et al., 2004; Pang et al., 2005], possible inflammation reaction due to unreacted monomers that are toxic, the absence of integration with the growing bone [Pang et al., 2005], its low mechanical properties, brittleness, brittle nature and lack of osseointegration (**Table 1**). Thus, these criticisms prevent its application in permanent cranioplasty in the growing skull and are potential risks for fracture and fragmentation [Goldstein et al., 2013].

In order to overcome these limits, custom made PMMA implants, obtained by 3D printing technique, have been proposed, since this approach presents many advantages with respect to the traditional *in situ* polymerization to produce mouldable PMMA [Fiaschi et al., 2016]. Indeed, the custom made strategy allows to obtain a well-fitting implant, to avoid the exothermic reaction, and, thus, the exposure of brain tissue to heat, the presence of possible unreacted toxic monomer residues or dust produced during intraoperative moulding. Moreover, this production technique guarantees an easy remanufacturing of the pre-existing model, in the case of complications, and shorter operative time and, consequently, reduced intraoperative blood loss [Fiaschi et al., 2016].

4.3.2.3 Polyetheretherketone (PEEK)

Polyetheretherketone (PEEK) is a technopolymer, is semicrystalline, radiolucent, chemically inert, and can be sterilized by steam or gamma irradiation [Marcacci et al., 1999].

PEEK implants were originally developed for spinal surgery and hip replacement surgery in 1998. Afterwards, they were also used in craniofacial reconstruction.PEEK based implants present many advantages (**Table 1**), as summarised below [Marcacci et al., 1999]:

- strength and elasticity comparable to cortical bone;
- capability to be precisely integrated within the defect without the use of miniplates;
- possibility to be processed by 3D printing technologies in order to obtain custom made implants, designed on the basis of the patient's craniotomy defect;
- absence of artifacts on computed tomography (CT) or magnetic resonance imaging (MRI), being PEEK translucent to x-rays and nonmagnetic;
- high comfortability, due to PEEK very low density and weight;
- the absence of heat conductivity which could lead to negative impacts on the brain, as in the case of metals.

However, they present some drawbacks (**Table 1**):

- very high cost;
- lack of osteointegrative properties;

- high risk of being dislodged or extruded, being not able to integrate themselves with the surrounding native bone.

4.3.3. Ceramics

4.3.3.1. Hydroxyapatite

Hydroxyapatite (HAp, $Ca_{10}(PO_4)_6(OH)_2$) consists in the inorganic component of the hard tissue extracellular matrix [Bianco et al., 2007; Bianco et al., 2009; Bianco et al., 2010; Cacciotti et al., 2009; Cacciotti, 2016; Cacciotti, 2019] and constitutes around 60% of human bone [Shah et al., 2014].

It can be synthesised and can also be reinforced with titanium mesh to obtain a stronger prosthesis [Shah et al., 2014].

The employment of HAp shows several advantages (**Table 1**):

- it can be easily moulded and does not create artefact on imaging [Shah et al., 2014], whereas metals and other synthetic materials are difficult to contour to the natural skull shape and hinder the brain CT scanning;
- It promotes new bone formation on the implant surface due its similar composition to bone, and propensity to accumulate calcium and phosphate ions [Stefini et al., 2013];
- it has acceptable chemical bonding with bone [Shah et al., 2014];
- it produces minimal inflammation [Shah et al., 2014];
- it causes little foreign body reaction;
- it provides excellent cosmetic results, since it can be smoothly contoured and shaped as required [Shah et al., 2014];
- it can be used in paediatric patients, since it allows expansion of the growing cranium, in contrast to PMMA [Shah et al., 2014],

However, it also presents some drawbacks (**Table 1**):

- brittle nature (it can disintegrate or fragment, are easily displaced or fractured,);
- low tensile strength;
- high infection rates;
- lack of integration with the bone.

Indeed, even if HAp has demonstrated osteointegration in animal models [Martini et al., 2012], there is not clear evidence for osteointegration in humans *in vivo*, as evidenced by Frassanito et al. who reported remarkably limited osteointegration without lamellar organization, as well as the HAp tendency to break down into many fragments over time *in vivo* [Frassanito et al., 2013].

Thus, it is not possible to repair large defects with HAp due to its compromised structural integrity in contact with the cerebrospinal fluid and the blood and due to the lack of osteointegration [Grant et al., 2004].

4.3.3.2. Alumina

Alumina bioceramics are usually employed in dental implants and have been applied in cranioplasty (with the addition of yttrium to make the alumina slightly radiopaque) within the last decades due to their stable physicochemical properties, high mechanical strength, biocompatibility and aesthetic benefits (**Table 1**) [Kobayashi et al., 1987].

However, alumina owns some deficiencies, such as relative high brittleness and low plasticity (**Table 1**) [Sanan and Haines, 1997].

It has been reported that custom-made alumina implants present a very low postoperative infection rate (i.e. 5.9 %) [Matusno et al., 2006], but they are very expensive, need to be preformed, and tend to fragment [Grant et al., 2004].

4.3.4. Composites

4.3.4.1. Mineralised collagen

Mineralized collagen is the fundamental unit of vertebrate's bone [Cui et al., 2007], and is composed of collagen and nano-sized hydroxyapatite [Weiner et al., 1992].

Many efforts have been devoted to the development of biomimetic materials to resemble the natural mineralized collagen [Zhang et al., 2003; Wang et al., 1995; Du et al., 2000; Kikuchi et al., 2001; Constantz and Gunasekaran, 1993; Bradt et al., 199; Qiu et al., 2014], using different preparation methods. The mineralized collagen materials are bioresorbable and osteoconductive, and, thus can be gradually replaced by new bone, simultaneously degrading.

Some of the produced materials are commercially available as bone substitutes [109–112], such as SkuhealTM (Beijing Allgens Medical Science and Technology Co., Ltd., Beijing, China) that consists in a series of commercialized mineralized collagen bone repair materials for cranial defects, approved for marketing by the China Food and Drug Administration (CFDA).

4.3.4.2. Bioactive fibre-reinforced composite

Recently, glass fiber-reinforced composite (FRC) material, loaded with a bioactive glass particulate filling, has been proposed for bone reconstruction, allowing to overcome the criticisms associated to the bone resorption with autologous bone flap. Bioglasses particles are added due to their This new composite material presents many advantages [Aitasalo et al., 2014; Piitulainen et al., 2015]: biocompatibility, high strength and toughness, lightweight, relative radiolucency, initial malleability, nonmagnetic properties, low thermal conductivity, long-term stability, and osteoinductivity/osteoconductivity/ability to chemically bond to the bone/bacteriostaticity due to the bioglass component [Cacciotti, 2017].

However, Piitulainen et al. [Piitulainen et al., 2015] evidenced a 29 % of infection rate using this composite material, and, thus, it is strongly suggested to carry out a long-term follow up, with a larger sample size, to provide more statistically significant results and evidences regarding the associated disadvantages and possible complications.

4.3.4.3. Calcium phosphate cements (CPCs)

CPC is similar to inorganic component of natural bone, in terms of composition, and, thus, presents good biocompatibility and resulted osteoconductive in cranioplasty [Kuemmerle et al., 2005; Pang et al., 2005].

However, it also shows some drawbacks, such as the low mechanical properties, the high incidence of fracture and of related infection, the absence of bone ingrowth.

Indeed, it has been reported that CPC underwent fragmentation and, consequently, induced infection at an average of 2 weeks after the minor trauma [Matic and Manson, 2004], and that the use of CPC led

to worst performances with respect to PMMA cements and autografts [Moreira-Gonzalez et al., 2003; Afifi et al., 2010].

The induced inflammatory reactions caused the skin thinning and erosion, exposing the material, and making secondary repair difficult [Moreira-Gonzalez et al., 2003].

Based on these considerations and clinical studies, CPC is unsuitable for large, full-thickness skull defects due to unacceptable high overall complication rate [Zins et al., 2010].

4.3.4.4. Cortoss™

Cortoss™ consists in a synthetic bone void filler, composed of bis-glycidyl methylmethacrylate, bisphenol, trethylene glycol dimethylacrylate monomer, and bioactive glass, in order to simulate the cortical bone composition [Sanus et al., 2008]. Initially, it was proposed as an alternative to PMMA for dental applications, and later was also applied for cranial defects [Ozlen et al., 2010]. Cortoss™ polymerizes in a three-dimensional network, acquiring the consistency of toothpaste, and mixing it with blood, during the polymerization, allows to delay the hardening time, allowing for its injection.

It is characterised by an elastic modulus comparable to that of bone [Aydin et al., 2011], higher values for compressive strength, bending modulus, and shear strength, bioactivity, ability to promote the bone apposition at the cement-bone interface interface without any fibrous interposition [Sanus et al., 2008], and its use leads to lower incidents of inflammation with respect to PMMA [Aydin et al., 2011].

In some clinical applications, good surgical and cosmetic results were achieved [Sanus et al., 2008], without infections and/or foreign body reactions or Cortoss leakage, suggesting a safe and effective use of Cortoss in calvarial defects [Sanus et al., 2008].

5. Concluding remarks and future perspectives

Despite the modern cranioplasty has been in practice since the second half of the last century and despite its history of thousands of years, it still presents many complications and the optimal materials and approaches have not been defined yet. The postsurgery complication rate continues to be high, with elevated rates of

reoperation, infection and resorption of the implanted grafts. Specifically, it ranges from 16 % to 40 %, with a general reoperation rate of 25% [Feroze et al., 2015; Bobinski et al., 2013; De Bonis et al., 2012; Gooch et al., 2009; Sobani et al., 2011].

Currently there is no consensus about the optimal cranioplastic materials and techniques, and the presurgical decisions strictly depend on the experience of surgical service and the individual conditions of the patient [Servadei and Iaccarino, 2015; Lindner et al., 2016]. Autologous bone graft is still considered the gold standard material for cranioplasty since it avoids the introduction of foreign materials into the body, and can be readily accepted by the host and integrated back into the skull. However, its drawbacks, i.e. high risk of infection, high absorption rate, and reduced strength, have motivated the study, the employment and development of more viable alloplastic materials, including metals, ceramics, polymers and composites. More recent technologies include the use of PEEK implants and titanium mesh that can be specifically designed and custom made taking into account the patient's craniotomy defect with 3D printing technologies. Titanium meshes are employed in combination with other materials, such as HAp and PMMA, in order to obtain stronger implants. From the comparison among the different types of alloplastic materials, poor statistical evidence justifies the choice of one material with respect to another. For example, titanium resulted more acceptable in clinical practice with respect to PEEK due to its lower cost [Thien et al., 2015], whereas lower rates of infection were revealed for HAp compared to titanium, even if the difference was not significant. In all cases, among the materials properties, infection remains a central and open concern leading to implant failure and patient health, as evident from **Table 3**, where the mainly used materials are also compared in terms of infection rate. The average infection rate following cranioplasty is 10 %. It depends on the used material: for example, the infection rate associated to PMMA implants ranges from 5.8 to 18.4 %, that related to titanium implants from 2.6 to 18.4 %, that ascribed to PEEK from 8.3 to 22%, while the lowest percentage was o bserved for hydroxyapatite, i.e. 2.05% [Alves Junior et al., 2016]. Concerning the risks of infection with PEEK implants, there are not many evidences in literature, and further studies

are needed [Servadei and Iaccarino, 2015]. Thus, it is pivotal to identify materials and implantable reconstruction solutions able to mitigate the potential infection risk, as well as technologies to monitor the post-surgery infection/inflammation [De Santis and Cacciotti, 2020].

Future advances in cranioplasty will widely involve the biomimetic approach that has been proposed as a new trend in the development of innovative and efficient biomaterials [Song et al., 2015; Chronopolou et al., 2021; Tiberio et al., 2021]. The idea is to design biomimetic bone substitutes, able to resemble both the chemical composition and the microstructure of the native cranial bone.

Mineralized collagen bone substitute material can be considered a pioneer of biomimetic concept for repairing cranial bone defects [Song et al., 2015].

Actually, many efforts are devoted to the development of biomimetic materials for cranioplasty with suitable biomechanical properties, enhanced biodegradability, and improved osteoconductivity [Song et al., 2015].

In parallel, in the research about the optimal cranioplastic materials, the actual trend is focused on molecular biological approaches, with the introduction of bone growth factors and bone morphogenetic proteins (BMP) [Feroze et al., 2015; Shah et al., 2014], to promote the bone deposition and growth within a graft, as well as of stem cells in a regenerative medicine/tissue engineering vision [Lehmann et al., 2010; Lehmann et al., 2012; D'Angelo et al., 2012; Bianco et al., 2011]. This new strategy could guarantee immediate protection to the cranium, with aesthetical beneficies, and both osteoconductive and osteoinductive actions [Shah et al., 2014].

Some studies reported on the use of recombinant growth factors, such as transforming growth factor β, insulin-like growth factor–I, and BMP-2, in augmenting the calvarial closure in animal and human models [Feroze et al., 2015].

Thesleff et al. combined the beta-tricalcium phosphate and autologous adipose-derived stem cells (ADSCs), that can be easily harvested, expanded *in vitro* and undergo adipogenic, osteogenic, chondrogenic, neurogenic, and myogenic differentiation, for cranioplasty applications in four adult patients, achieving well ossified

constructs post operatively without any complications [Thesleff et al., 2011].

This approach is very innovative and novel, and currently there is no documented and published work about its application in paediatric patients. Similarly, the use of BMP in the paediatric population needs further investigation [Feroze et al., 2015].

In terms of processing techniques, the additive manufacturing strategy is gaining a lot of interest for the fabrication of custom made cranial implants [Tiberio et al., 2021]. Nowadays, customized implants made of the traditional materials for cranioplasty are clinically available, whereas the customized manufacture of biomimetic materials, such as mineralized collagen, has not been developed yet and is under study and in progess [Song et al., 2015].

In this regard, up to date, the main concerns to be urgently addressed are related to the cost reduction and the need to shorten the manufacturing process [Song et al., 2015].

In conclusion, up to date, there is no strong evidence about the optimal material for adult and, mainly, paediatric cranioplasty, due to lack of consolidated data and contradictory evidences. Thus, large scale and prospective studies are required and recommended to achieve more reasonable and reliable data on this topic.

Table 3. Comparin among the most used materiasl for cranioplasty.

Material	Cost	Osteocon-duction	Infection rate (%)	Resis-tance	Radiolu-cency
Autograft	low	high	moderate	high	no
Titanium 	high	low	moderate	high	no
PMMA 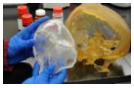	moderate	low	high	low	yes

Material	Cost	Osteocon-duction	Infection rate (%)	Resis-tance	Radiolu-cency
PEEK 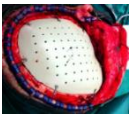	high	low	moderate	high	yes
HAp 	moderate	high	moderate	low	no

References:

1. Afifi A M, Gordon C R, Pryor L S, et al. Calcium phosphate cements in skull reconstruction: a meta-analysis. Plastic and Reconstructive Surgery, 2010, 126(4): 1300–1309.
2. Aitasalo, K. M., Piitulainen, J. M., Rekola, J., & Vallittu, P. K. (2014). Craniofacial bone reconstruction with bioactive fiber-reinforced composite implant. Head & neck, 36(5), 722-728.
3. Alkhaibary, A., Alharbi, A., Alnefaie, N., Aloraidi, A., & Khairy, S. (2020). Cranioplasty: A Comprehensive Review of the History, Materials, Surgical Aspects and Complications. *World neurosurgery*.
4. Alves Junior, A. C. A., Hamamoto Filho, P. T., Neto, A. A. P., & Zanini, M. A. (2016). Biomaterials for reconstruction of cranial defects. Arquivos Brasileiros de Neurocirurgia: Brazilian Neurosurgery, 35(04), 291-295.
5. Arnaud E. Advances in cranioplasty with osteoinductive biomaterials: summary of experimental studies and clinical prospects. Childs NervSyst 2000;16(10–11):659–668.
6. Aydin, S., Kucukyuruk, B., Abuzayed, B., Aydin, S., & Sanus, G. Z. (2011). Cranioplasty: review of materials and techniques. Journal of neurosciences in rural practice, 2(2), 162.
7. Azmi A, Latiff AZ, Johari A: Methyl methacrylate cranioplasty. **Med J Malaysia 59:**418–421, 2004.
8. Bianco, A., Cacciotti, I., Lombardi, M., Montanaro, L., & Gusmano, G. (2007). Thermal stability and sintering behaviour of hydroxyapatite

nanopowders. Journal of thermal analysis and calorimetry, 88(1), 237-243.
9. Bianco, A., Cacciotti, I., Lombardi, M., & Montanaro, L. (2009). Si-substituted hydroxyapatite nanopowders: synthesis, thermal stability and sinterability. Materials research bulletin, 44(2), 345-354.
10. Bianco, A., Cacciotti, I., Lombardi, M., Montanaro, L., Bemporad, E., & Sebastiani, M. (2010). F-substituted hydroxyapatite nanopowders: thermal stability, sintering behaviour and mechanical properties. Ceramics international, 36(1), 313-322.
11. Bianco, A., Bozzo, B. M., Del Gaudio, C., Cacciotti, I., Armentano, I., Dottori, M., ... & Kenny, J. M. (2011). Poly (L-lactic acid)/calcium-deficient nanohydroxyapatite electrospun mats for bone marrow stem cell cultures. Journal of bioactive and compatible polymers, 26(3), 225-241.
12. Blake DP, The use of synthetics in cranioplasty: a clinical review. Mil Med. 1994 Jun; 159(6):466-9.
13. Bobinski L, Koskinen LO, Lindvall P: Complications following cranioplasty using autologous bone or polymethylmethacrylate—retrospective experience from a single center. Clin Neurol Neurosurg 115:1788–1791, 2013.
14. Bradt J H, Mertig M, Teresiak A, et al. Biomimetic mineralization of collagen by combined fibril assembly and calcium phosphate formation. Chemistry of Materials, 1999, 11(10): 2694–2701.
15. Bruens ML, Pieterman H, de Wijn JR, Vaandrager JM: Porous polymethylmethacrylate as bone substitute in the craniofacial area. J Craniofac Surg 14:63–68, 2003.
16. Busch E, Bing J, Hansen E H. Gelatine and polythene film as dura substitutes and polythene plates as bone substitute in skull defects. Acta Chirurgica Scandinavica, 1949, 97(5): 410–416.
17. Cabraja M, Klein M, Lehmann TN: Long-term results following titanium cranioplasty of large skull defects. Neurosurg Focus 26(6):E10, 2009.
18. Cacciotti, I., Bianco, A., Lombardi, M., & Montanaro, L. (2009). Mg-substituted hydroxyapatite nanopowders: synthesis, thermal stability and sintering behaviour. Journal of the European Ceramic Society, 29(14), 2969-2978.
19. Cacciotti I. (2016), Cationic and Anionic substitutions in hydroxyapatite, In: Handbook of Bioceramics and Biocomposites, Iulian Vasile Antoniac Editor, Springer International Publishing 2016, 1

January 2016, Pages 145-211. ISBN 978-3-319-12459-9, DOI: 10.1007/978-3-319-09230-0_7-1.
20. Cacciotti, I. (2019). Multisubstituted hydroxyapatite powders and coatings: The influence of the codoping on the hydroxyapatite performances. International Journal of Applied Ceramic Technology, 16(5), 1864-1884.
21. Cacciotti I., Bivalent cationic ions doped bioactive glasses: the influence of magnesium, zinc, strontium and copper on the physical and biological properties, Journal of Materials Science 52(15) (2017): 8812–8831.
22. Chandler CL, Uttley D, Archer DJ, MacVicar D: Imaging after titanium cranioplasty. Br J Neurosurg 8:409–414, 1994.
23. Chronopoulou, L., Cacciotti, I., Amalfitano, A., Di Nitto, A., D'Arienzo, V., Nocca, G., & Palocci, C. (2021). Biosynthesis of innovative calcium phosphate/hydrogel composites: physicochemical and biological characterisation. Nanotechnology 32(9) (2021): 095102.
24. iurea A.V., Tratat de Neurochirurgie Vol. 1. Bucharest Medical Publishing House 2010 pp 160-70,242-243.
25. Constantz B R, Gunasekaran S. Mineralized collagen. US Patent, 5 231 169, 1993-07-27.
26. Courville CB. Cranioplasty in prehistoric times. Bulletin of the Los Angeles Neurological Society, 1959, 24.1: 1-8.
27. Cui F Z, Li Y, Ge J. Self-assembly of mineralized collagen composites. Materials Science and Engineering R: Reports, 2007, 57(1–6): 1–27.
28. D'Angelo, F., Armentano, I., Cacciotti, I., Tiribuzi, R., Quattrocelli, M., Del Gaudio, C., ... & Orlacchio, A. (2012). Tuning multi/pluri-potent stem cell fate by electrospun poly (L-lactic acid)-calcium-deficient hydroxyapatite nanocomposite mats. Biomacromolecules, 13(5), 1350-1360.
29. De Bonis P, Frassanito P, Mangiola A, Nucci CG, Anile C, Pompucci A: Cranial repair: how complicated is filling a "hole"? J Neurotrauma 29:1071–1076, 2012.
30. De Santis, M., & Cacciotti, I. (2020). Wireless implantable and biodegradable sensors for postsurgery monitoring: Current status and future perspectives. Nanotechnology, 31(25), 252001.
31. Du C, Cui F Z, Zhang W, et al. Formation of calcium phosphate/collagen composites through mineralization of collagen matrix. Journal of Biomedical Materials Research, 2000, 50(4): 518–527.

32. Ducic Y: Titanium mesh and hydroxyapatite cement cranioplasty: a report of 20 cases. J Oral Maxillofac Surg 60:272–276, 2002
33. Durand JL, Renier D, Marchac D: [The history of cranioplasty.] Ann Chir Plast Esthet 42:75–83, 1997 (Fr).
34. Elsalanty, M. E., & Genecov, D. G. (2009). Bone grafts in craniofacial surgery. Craniomaxillofacial trauma & reconstruction, 2(3-4), 125-134.
35. Eppley BL: Biomechanical testing of alloplastic PMMA cranioplasty materials. J Craniofac Surg 16:140–143, 2005.
36. Feroze, A. H., Walmsley, G. G., Choudhri, O., Lorenz, H. P., Grant, G. A., & Edwards, M. S. (2015). Evolution of cranioplasty techniques in neurosurgery: historical review, pediatric considerations, and current trends. Journal of neurosurgery, 123(4), 1098-1107.
37. Fiaschi, P., Pavanello, M., Imperato, A., Dallolio, V., Accogli, A., Capra, V., ... & Piatelli, G. (2016). Surgical results of cranioplasty with a polymethylmethacrylate customized cranial implant in pediatric patients: a single-center experience. Journal of Neurosurgery: Pediatrics, 17(6), 705-710.
38. Frassanito P, De Bonis P, Mattogno PP, Mangiola A, Novello M, Brinchi D, et al: The fate of a macroporous hydroxyapatite cranioplasty four years after implantation: macroscopical and microscopical findings in a case of recurrent atypical meningioma. Clin Neurol Neurosurg 115:1496–1498, 2013
39. Goldstein, J. A., Paliga, J. T., & Bartlett, S. P. (2013). Cranioplasty: indications and advances. Current opinion in otolaryngology & head and neck surgery, 21(4), 400-409.
40. Gooch MR, Gin GE, Kenning TJ, German JW: Complications of cranioplasty following decompressive craniectomy: analysis of 62 cases. Neurosurg Focus 26(6):E9, 2009.
41. Gosain, A. K., Chim, H., & Arneja, J. S. (2009). Application-specific selection of biomaterials for pediatric craniofacial reconstruction: developing a rational approach to guide clinical use. Plastic and reconstructive surgery, 123(1), 319-330.
42. Grant FC, Norcross NC: Repair of cranial defects by cranioplasty. Ann Surg 110:488–512, 1939
43. Grant GA, Jolley M, Ellenbogen RG, Roberts TS, Gruss JR, Loeser JD: Failure of autologous bone-assisted cranioplasty following decompressive craniectomy in children and adolescents. J Neurosurg 100 (2 Suppl Pediatrics):163–168, 2004.
44. Harris, D. A., Fong, A. J., Buchanan, E. P., Monson, L., Khechoyan, D., &

Lam, S. (2014). History of synthetic materials in alloplastic cranioplasty. *Neurosurgical focus*, *36*(4), E20.
45. Johnell, O. (2003). Economic implication of osteoporotic spine disease: cost to society. European Spine Journal, 12(2), S168-S169.
46. Kennedy KAR: Primitive Surgery: Skills Before Science. Spencer L. Rogers. Am Anthropol 89:217–218, 1987
47. Khader, B. A., & Towler, M. R. (2016). Materials and techniques used in cranioplasty fixation: A review. Materials Science and Engineering: C, 66, 315-322.
48. Kikuchi M, Itoh S, Ichinose S, et al. Self-organization mechanism in a bone-like hydroxyapatite/collagen nanocomposite synthesized in vitro and its biological reaction in vivo. Biomaterials, 2001, 22(13): 1705–1711.
49. Kim J, McBride S, Fulmer M, et al. Fiber-reinforced calcium phosphate cement formulations for cranioplasty applications: a 52-week duration preclinical rabbit calvaria study. J Biomed Mater Res B ApplBiomater 2012;100(4):1170–1178
50. Kobayashi S, Hara H, Okudera H, et al. Usefulness of ceramic implants in neurosurgery. Neurosurgery, 1987, 21(5): 751–755
51. Kuemmerle J M, Oberle A, Oechslin C, et al. Assessment of the suitability of a new brushite calcium phosphate cement for cranioplasty – an experimental study in sheep. Journal of Cranio-Maxillo-Facial Surgery, 2005, 33(1): 37–44.
52. Lehmann, G., Palmero, P., Cacciotti, I., Pecci, R., Campagnolo, L., Bedini, R., ... & Montanaro, L. (2010). Design, production and biocompatibility of nanostructured porous HAp and Si-HAp ceramics as three-dimensional scaffolds for stem cell culture and differentiation. Ceramics-Silikaty, 54(2), 90-96.
53. Lehmann, G., Cacciotti, I., Palmero, P., Montanaro, L., Bianco, A., Campagnolo, L., & Camaioni, A. (2012). Differentiation of osteoblast and osteoclast precursors on pure and silicon-substituted synthesized hydroxyapatites. Biomedical Materials, 7(5), 055001.
54. Lin A Y, Kinsella C R, Rottgers S A, et al. Custom porous polyethylene implants for large-scale pediatric skull reconstruction: early outcomes. The Journal of Craniofacial Surgery, 2012, 23(1): 67–70.
55. Lindner D, Schlothofer-Schumann K, Kern BC, Marx O, Müns A, Meixensberger J. Cranioplasty using custom-made hydroxyapatite versus titanium: a randomized clinical trial. J

Neurosurg 2016;26:1–9
56. Liu J K, Gottfried O N, Cole C D, et al. Porous polyethylene implant for cranioplasty and skull base reconstruction. Neurosurgical Focus, 2004, 16(3): 1
57. Marcacci M, Kon E, Zaffagnini S, Giardino R, Rocca M, & Corsi A, Reconstruction of extensive long-bone defects in sheep using porous hydroxyapatite sponges. *Calcif Tissue Int* 64:83–90, 1999
58. Martini L, Staffa G, Giavaresi G, Salamanna F, Parrilli A, Serchi E, et al: Long-term results following cranial hydroxyapatite prosthesis implantation in a large skull defect model. Plast Reconstr Surg 129:625e–635e, 2012
59. Matic D B, Manson P N. Biomechanical analysis of hydroxyapatite cement cranioplasty. Journal of Craniofacial Surgery, 2004, 15(3): 415–422.
60. Matsuno, A., Tanaka, H., Iwamuro, H., Takanashi, S., Miyawaki, S., Nakashima, M., ... & Nagashima, T. (2006). Analyses of the factors influencing bone graft infection after delayed cranioplasty. Acta neurochirurgica, 148(5), 535-540.
61. Mohan D., Munteanu V., Moisa H., Ciurea A.V.; A medical insight on the use of biomaterials for cranioplasty surgery. Key Engineering Materials, Vol. 638 (2015) pp 205-209.
62. Moiduddin, K., Darwish, S., Al-Ahmari, A., ElWatidy, S., Mohammad, A., & Ameen, W. (2017). Structural and mechanical characterization of custom design cranial implant created using additive manufacturing. electronic Journal of Biotechnology, 29, 22-31.
63. Moreira-Gonzalez A, Jackson I T, Miyawaki T, et al. Clinical outcome in cranioplasty: critical review in long-term follow-up. The Journal of Craniofacial Surgery, 2003, 14(2): 144–153.
64. Munroe AR: The operation of cartilage-cranioplasty. Can Med Assoc J 14:47–49, 1924.
65. Oliver, J. D., Banuelos, J., Abu-Ghname, A., Vyas, K. S., & Sharaf, B. (2019). Alloplastic cranioplasty reconstruction: a systematic review comparing outcomes with titanium mesh, polymethyl methacrylate, polyether ether ketone, and Norian implants in 3591 adult patients. Annals of plastic surgery, 82(5S), S289-S294.
66. Otsuki, B., Takemoto, M., Fujibayashi, S., Neo, M., Kokubo, T., & Nakamura, T. (2006). Pore throat size and connectivity determine bone and tissue ingrowth into porous implants: three-dimensional micro-CT based structural analyses of porous bioactive titanium implants. Biomaterials, 27(35), 5892-5900.

67. Ozlen, F., Abuzayed, B., Dashti, R., Isler, C., Tanriover, N., & Sanus, G. Z. (2010). Low-profile 1-piece bifrontal craniotomy for anterior skull base approach and reconstruction. Journal of Craniofacial Surgery, 21(1), 233-238.
68. Pang, D., Herman, H. T., Zwienenberg-Lee, M., Smith, M., & Zovickian, J. (2005). The combined use of hydroxyapatite and bioresorbable plates to repair cranial defects in children. Journal of Neurosurgery: Pediatrics, 102(1), 36-43.
69. Park, E. K., Lim, J. Y., Yun, I. S., Kim, J. S., Woo, S. H., Kim, D. S., & Shim, K. W. (2016). Cranioplasty enhanced by three-dimensional printing: custom-made three-dimensional-printed titanium implants for skull defects. Journal of Craniofacial Surgery, 27(4), 943-949.
70. Piitulainen, J. M., Posti, J. P., Aitasalo, K. M., Vuorinen, V., Vallittu, P. K., & Serlo, W. (2015). Paediatric cranial defect reconstruction using bioactive fibre-reinforced composite implant: early outcomes. Acta neurochirurgica, 157(4), 681-687.
71. Pilliar R.M., Overview of surface variability of metallic endosseous dental implants: textured and porous surface-structured designs, Implant Dent, 7 (1998), pp. 305-314.
72. Qiu Z Y, Tao C S, Cui H, et al. High-strength mineralized collagen artificial bone. Frontiers of Materials Science, 2014, 8(1): 53–62.
73. Rogers, G. F., & Greene, A. K. (2012). Autogenous bone graft: basic science and clinical implications. Journal of Craniofacial Surgery, 23(1), 323-327.
74. Sanan A, Haines SJ: Repairing holes in the head: a history of cranioplasty. Neurosurgery 40:588–603, 1997
75. Santoni- Rugiu P.. Sykes P.J. A history of Plastic Surgery. Springer-Verlag, Berlin, 2007
76. Sanus, G. Z., Tanriverdi, T., Ulu, M. O., Kafadar, A. M., Tanriover, N., & Ozlen, F. (2008). Use of cortoss™ as an alternative material in calvarial defects: The first clinical results in cranioplasty. *Journal of Craniofacial Surgery*, *19*(1), 88-95.
77. Servadei F, laccarino C. The therapeutic cranioplasty still needs an ideal material and surgical timing. World Neurosurg 2015;83(2):133–135.
78. Shah, A. M., Jung, H., & Skirboll, S. (2014). Materials used in cranioplasty: a history and analysis. Neurosurgical focus, 36(4), E19.
79. Sobani ZA, Shamim MS, Zafar SN, Qadeer M, Bilal N, Murtaza SG, et al: Cranioplasty after decompressive craniectomy: an institutional

audit and analysis of factors related to complications. Surg Neurol Int 2:123, 2011 .
80. Song, T., Qiu, Z. Y., & Cui, F. Z. (2015). Biomaterials for reconstruction of cranial defects. Frontiers of Materials Science, 9(4), 346-354.
81. Stefini, R., Esposito, G., Zanotti, B., laccarino, C., Fontanella, M. M., & Servadei, F. (2013). Use of "custom made" porous hydroxyapatite implants for cranioplasty: postoperative analysis of complications in 1549 patients. *Surgical neurology international*, *4*.
82. Thesleff, T., Lehtimäki, K., Niskakangas, T., Mannerström, B., Miettinen, S., Suuronen, R., & Öhman, J. (2011). Cranioplasty with adipose-derived stem cells and biomaterial: a novel method for cranial reconstruction. Neurosurgery, 68(6), 1535-1540.
83. Thien A, King NKK, Ang BT, Wang E, Ng I. Comparison of polyetheretherketone and titanium cranioplasty after decompressive craniectomy. World Neurosurg 2015;83(2):176–180.
84. Tiberio, F., Cacciotti, I., Frassanito, P., Nocca, G., Tamburrini, G., Arcovito, A., & Lattanzi, W. (2021). Personalized Bone Reconstruction and Regeneration in the Treatment of Craniosynostosis. Applied Sciences, 11(6), 2649 (35 pages).
85. Wang J C, Wei L, Xu J, et al. Clinical outcome of cranioplasty with high-density porous polyethylene. The Journal of Craniofacial Surgery, 2012a, 23(5): 1404–1406.
86. Wang J C, Wang S Y, Gui L, et al. Porous polyethylene combined with split calvarial bone graft to cover complex calvarial defect. The Journal of Craniofacial Surgery, 2012b, 23(6): 1802–1804.
87. Wang R Z, Cui F Z, Lu H B, et al. Synthesis of nanophase hydroxyapatite/collagen composite. Journal of Materials Science Letters, 1995, 14(7): 490–492.
88. Weiner S, Traub W. Bone structure: from angstroms to microns. FASEB Journal, 1992, 6(3): 879–885.
89. Wiggins A, Austerberry R, Morrison D, Ho KM, Honeybul S: Cranioplasty with custom-made titanium plates—14 years experience. Neurosurgery 72:248–256, 2013
90. Zhang W, Liao S S, Cui F Z. Hierarchical self-assembly of nanofibrils in mineralized collagen. Chemistry of Materials, 2003, 15 (16): 3221–3226.
91. Zins J E, Langevin C J, Nasir S. Controversies in skull reconstruction. The Journal of Craniofacial Surgery, 2010, 21(6): 1755–1760.

WIRELESS POWER TRANSFER METHODOLOGIES FOR MEDICAL APPLICATIONS

Michele De Santis

Department of Engineering, University of Rome "Niccolò Cusano", Via Don Carlo Gnocchi 3 00166 Rome, Italy
michele.desantis@unicusano.it

Contents

1. Introduction to Wireless Power Transfer systems in biomedical applications

The improvements in the manufacturing and information technologies are opening new avenues for hospital stay. Due to the increase of healthcare costs, the wards are moving towards the reduction of hospitalization times. Many patients, staying at home, require continuous heath monitoring after surgery or for chronic diseases. The population is also ageing, and many older people cannot afford to, or do not want to, live in an assisted living facility. Some citizens also stay home alone and then, need to be able to look after their health.

Wearable and implantable sensor devices can be the answer either to control specific parameters of various diseases or to check for an infection after surgery. These devices can really improve the quality of

life for people with previous pathologies or those resulting from a recent surgery. The way to access the control of the different vital parameters must be as easy as possible for the patient. One device used by most people regardless of their age is the mobile phone. Today, cell phones at a computational level can be considered as real small computers, so being able to run software applications on them is quite easy. So, cell phones can be the tools to communicate with the implantable devices; clearly, cell phones are not the only devices that can be used for this communication.

The main issues, in implementing this type of health monitoring system, are both the data transfer mode and how to power the implantable and wearable sensors. One possible answer to these problems is the use of the wireless power transfer (WPT) technology. WPT is a safe and appropriate method to provide energy for recharging biosensors and implantable electrical devices as well as for data communication in these specific applications [1].

WPT can be divided into two main parts in relation to the transmission distance of the perturbation: near-field and far-field transmissions. First of all, a transmitting and a receiving device must be present in order for the transmission of energy to take place. The conditions that distinguish near field from far field are related to the distance between transmitter and receiver in relation to the wavelength of the perturbation and to the dimensions of the transmitter.

The region of application is considered to be of the near-field type if:

- the distance between transmitter and receiver (d) is less than a wavelength (λ), determined by the operating frequency ($d< \lambda$);
- the largest size of the transmitter (D) must be less than half the disturbing wavelength ($D < \frac{\lambda}{2}$).

In contrast, the region is considered to be far-field if the relationship ($D > \frac{\lambda}{2}$) holds. Furthermore, a further watershed between these two regions refers to the Fraunhofer distance ($d_F = 2D^2/\lambda$): in fact, if the two conditions $d_F \gg D$ and $d_F \gg \lambda$ are satisfied, the region is considered to be far-field.

In general, the transmitter and receiver are represented by coils of metallic material. Considering two coils, transmitter and receiver, three major methodologies to create a near-field WPT are:

- capacitive coupling between the coils, this coupling is based on the electric field;
- inductive coupling between the coils, this coupling is based on the magnetic field;
- magnetic resonant inductive coupling, which must consider that both the coils, transmitter and receiver, must be part of a resonant circuit.

The far-field technology is instead mainly based on microwave coupling. In biomedical applications also hybrid wireless power transfer (HWPT) methodologies are used; the functioning of these systems involves both near- and far-field technologies.

The main applications of biomedical sensors include biology studies, medical therapies and diagnoses. The latest generation biological materials make it possible to exploit biocompatibility, especially in the case of sensors implanted in the human body, at a lower cost than in the past. Implantable medical devices (IMD) can be divided into two main types, according to the methodology used for the transmission of their power supply. The first classification considers inductive and capacitive coupling, and optical and ultrasound charging; these methodologies consider also, if necessary, the data transfer. The second classification includes two sub-branches that differ according to the mode of energizing the sensor: battery mode, such as lithium technology, or natural energy supply which may include bio-fuel cells, piezoelectricity, electrostatics, and electromagnetics.

The latter category can also be seen as divided into active and passive devices, respectively. Active IMDs (AIMDs) are generally more powerful in terms of the functions they can perform since the power system (the battery module) is integrated with the sensor circuitry. In fact, the most common way, of powering the electronic circuitry of large implants, such as pacemakers, is the use of batteries.

On the other hand, batteries place a limit on the miniaturization of the device, which is therefore heavier and can occupy a greater volume: in this regard it must be borne in mind that the IMDs devices must not

exceed 2% by mass of that of the patient. Furthermore, batteries introduce a further problem which is that of recharging. Non-rechargeable batteries, once exhausted, need to be replaced by accessing the region where they were implanted: this involves a small invasive intervention. A good alternative can be the use of rechargeable batteries, which however require a charging system that can be wireless. However, the use of these systems is not recommended due to the high-power transfer and the low transfer efficiency that leads, at radio frequencies (RF), to realize antennas of considerable sizes. Finally, it is not certain that the elements that make up the chemistry of the battery are biocompatible; even by making a casing to prevent contact, in case of deterioration or breakage of the latter it would still be necessary to intervene surgically to extract the battery.

Another possibility is to use passive devices that do not need to integrate the power supply system, so they can be easily miniaturized. The passive IMD (PIMD) is powered by an electromagnetic field, generated by an external electric circuit, and radiated by a transmitting antenna. The receiving antenna of the passive system acts, at that moment, as the supply system of the implanted sensor. The PIMD is powered only when it is interrogated by the external electromagnetic field.

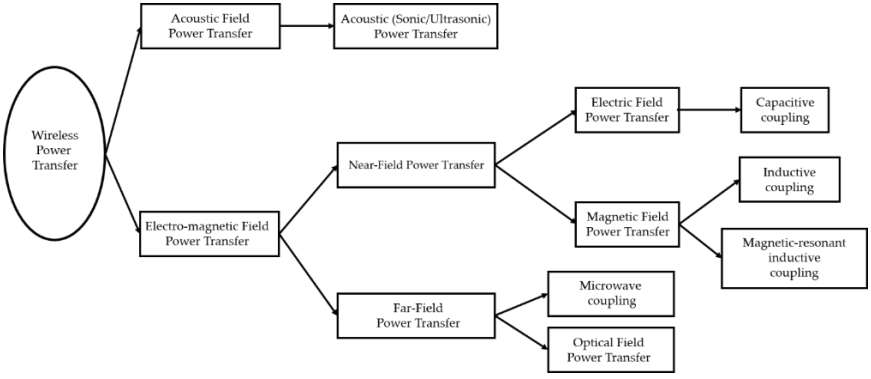

Figure 128. Different methodologies to perform the wireles power transfer.

As reported in Figure 1, the electromagnetic field is not the only mean to transfer the power between the transmitter and the receiver. Another methodology considers the acoustic field. The acoustic technique takes the acronym of APT (acoustic power transfer) or ultrasonic-based power transfer. The APT is an alternative method with respect to the electromagnetic one, capable of providing good performance.

Figure 1 shows that the properties of the electromagnetic field can also be exploited, for far-field applications, by means of the optical power transfer (OPT). However, the OPT methodology is dependent on precise alignment of the transmitter and receiver. Therefore, an optical connection can only be used for applications where the transmitter and receiver can be kept stationary.

2. Wireless Power Transfer System: different methodologies.

A typical electric scheme of a WPT system is reported in Figure 2.

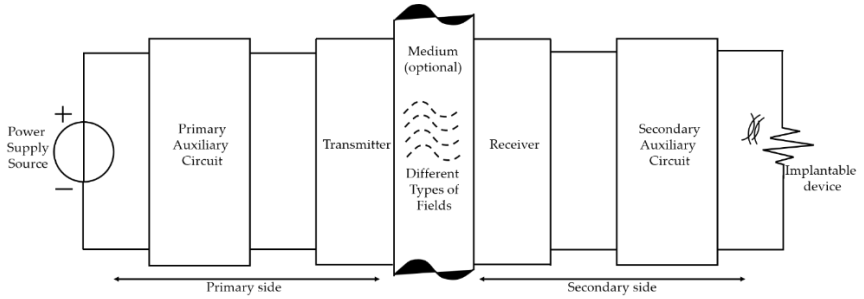

Figure 129. The layout of a Wireless Power Transfer system

At the primary side, the power supply energizes the transmitter through the primary auxiliary circuit. The transmitter, excited by the electric energy, generates the transmitting field that travels through the medium, which may be optional for the propagation of some types of fields, to reach the receiver. At the secondary side, the energy stored in the transmitting field is converted back into electric energy that, through the secondary auxiliary circuit, is suitable to power the IMD.

The nature of the transmitting field, that connects transmitter and receiver, defines the typology of WPT. Different categories of WPT systems exist, as reported in Figure 2.

Going more in detail, when the magnetic-field properties are exploited a switching electric current is generated by the power source, at the primary side, at a given frequency. This current flows through the transmitting coil, producing a magnetic field that oscillates at the same frequency of the current. When the receiving coil is positioned in the proximity of the generated magnetic field, a potential difference is induced at the ends of the receiving coil. The establishment of a potential difference involves a passage of alternating current in the integrated circuit with the receiving coil. The switching current can be rectified in the receiving circuit, allowing to use both direct voltage and current to recharge the battery in case of AIMD or simply power the circuit in case of PIMD.

It goes without saying that the efficiency of the WPT decreases as the distance between the receiving and transmitting coil increases. The strength of the magnetic field diminishes exponentially with the distance from the field source. The most efficient WPT methodology is the magnetic resonant inductive coupling which occurs when the two coils, transmitter and receiver, are tuned to the same frequency, which turns out to be the resonant frequency. The resonant frequency is calculated with the total inductance and capacitance of the transmitting circuit (including the transmitting coil). In fact, the maximum power transfer (impedance matching condition) occurs when the imaginary part of the total impedance of the circuit is brought to zero. If both the transmitter and receiver are tuned at their resonant frequency, which must concur, the two coils will couple and the power transmission will operate at a greater distance and with greater efficiency, having available the power supplied by the source to the primary side.

Exams routine diagnostics that patients generally undergo primarily require wearable sensors. Some examples can be represented by rest and exercise electrocardiography, heart rate measurement, blood pressure measurement, oxygen saturation, galvanic skin response, and many others. The first two examinations can be carried out by affixing

electrodes, in specific positions, on the surface of the body; the methodology involved could be the capacitive coupling for both measurements, although the second one could be also performed using an optical technology to monitor the pulsation of blood in the veins. The tool, used to measure oxygen saturation, measures the amount of hemoglobin bound in the blood and, therefore, obtain an estimate of the amount of oxygen present in the blood: the measurement is carried out using an optical technology. Galvanic skin response represents a simple measure of skin conductivity and it is made by applying two electrodes, for example on two fingers: the methodology involved is the capacitive coupling.

On the other hand, most of the used IMDs base their functioning on the electromagnetic principles. The development of electrical / electronic circuitry compatible with biological systems has made it possible to power the IMDs, which can be represented by sensors of physical parameters of medical interest: biological sensors (pressure and infection sensors, based on pH measurement), pacemakers, implanted pumps, neurostimulator and ultrasound imaging. A fairly popular medical pump is the ventricular assist device (VAD) which helps the defective ventricle to pump blood around the body.

The operation of these sensors requires power absorption which can range from a few microwatts to units of watts. From Section 1, it is clear that making a wireless battery recharging or power supply is safer from a patient health point of view, even when using an active IMD, such as a VAD or a pacemaker. Figure 3 shows the range of the power absorbed by the IMDs.

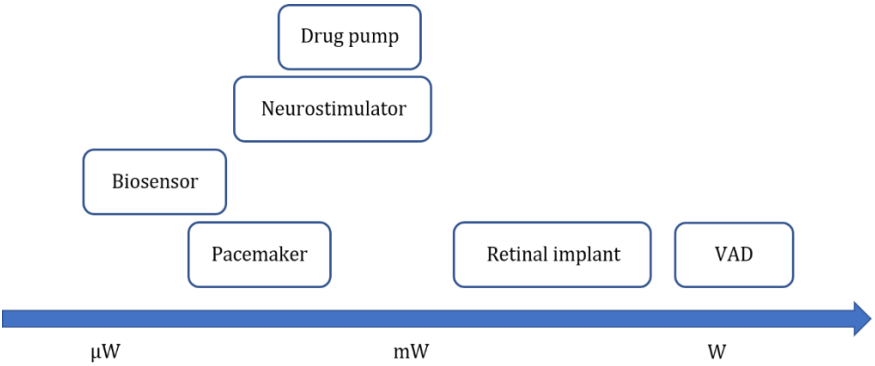

Figure 130. The range of the power absorbed by mostly used IMDs.

The exposure to both radio frequencies and microwaves can be harmful to the human body. For this reason, the maximum permissible exposure (MPE) to electromagnetic field strength values has been regulated by the assessment of the specific absorption rate (SAR). The IEEE C95.1 Edition-1999 – "IEEE Standard for Safety Levels with Respect to Human Exposure to Radio Frequency Electromagnetic Fields, 3 kHz to 300 GHz" provides SAR limitations. In recent years, many studies have been conducted to improve the safety of inductive WPT [2].

Focusing on wireless biological sensors, as the other types of IMDs, they can be categorized based on their communication methodology. The employed technology can vary based on the physical principle used to transfer the electrical energy from the transmitting device to the receiving one. In Table I, some of the WPT methodologies, considered in Figure 1, are reported, when considering biological sensors, together with the devices used to implement the corresponding technology.

Table 8. WPT methodologies for biological sensors.

Technology	Energy transfer	Device enabling power transfer	Application	Reference
Capacitive coupling	Electric fields	Conductive coupling plates	pressure sensor	[3-5]
Inductive coupling	Magnetic fields	Coils of wire	--	[6]
Resonant inductive coupling	Magnetic fields	Resonant circuits	pressure sensor	[4],[7-12]
Microwave radiation	Microwaves	Single antenna cell & Phased arrays	infection detecting sensor	[13]

2.1. Capacitive coupling

In the last years, many studies focused on wireless sensors for biomedical applications have been presented. During the 90s the leading technology for communicating between medical devices, placed inside the skin, and the electronic circuitry, located above the skin, was the capacitive coupling, whose acronym is capacitive power transfer (CPT) technology.

The typical structure of a CPT system is reported in Figure 4. The capacitive coupler is realized by the four metal plates: the two metal plates on the left represent the transmitter and the two metal plates on the right the receiver. As visible from Figure 4, the primary auxiliary circuit is realized by one inverter step and a network compensation made of capacitors and inductors; a similar structure is used for the secondary side, where the compensation network is followed by a rectifier device. The system reported in Figure 4 is composed of four metal plates to form a bipolar structure, however other types of schemes are possible as unipolar architecture, where only one pair of metal plates

is used: one plate for the transmitter and one for the receiver. The value of the coupling capacitance depends on the area of the metal plates, the distance of one from the other, and the material present between them. If an alternating current (I) of varying frequency is injected in the tissue via the surface electrodes, thus inducing a voltage drop (V) across the tissue; the ratio of the resulting voltage drop to the injected current defines the bio-impedance of the tissue:

$$Z = \frac{V}{I} = z' + jz'' = \frac{1}{\sigma + \mathrm{j}\omega\varepsilon_0\varepsilon_r}$$

where z' and z'' represent the tissue's real and imaginary components respectively, ω is the angular frequency, ϵ_0 is the permittivity of free space ($8.85 * 10^{-12} F/m$) and j = √-1.

The conductivity (σ) and the relative permittivity (ϵ_r) of the tissue can be extracted from these impedance measurements by correcting the data to account for the measurement geometry. The value of the permittivity constant of the air is like the one of free space, being this value small, the resulting coupling capacitance also assumes a limited value.

This is the reason to look for resonance conditions between the electrical circuits of the compensation network and the capacitive coupler. The resonant condition is characterized by a higher value in the flowing current that can increase the potential difference between the plates of the capacitive coupler: the direct consequence is a higher electric field that can be sufficient for power transfer.

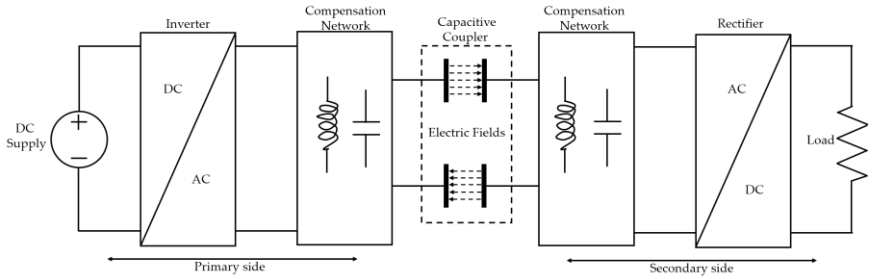

Figure 131. Layout of the capacitive coupling methodology for WPT.

This communication technique is called "intrabody communication" because it exploits the conductive properties of the body to carry the signal from the transmitter to the receiver.

In the early stages of this study, that can be considered in 1995 by Zimmermann et al. [14], the intrabody technology was used for surface-based communication, by means of two sets of electrodes. The first set of electrodes consisted of one positioned by the receiver and the other by the transmitter, both located close to the skin, capacitively coupled to the body; the second set of electrodes, one for the receiver and one for the transmitter, were oriented away from the body and they were capacitively coupled to the ground, realizing the return track of the signal. the architecture described is shown in Figure 5 for clarity.

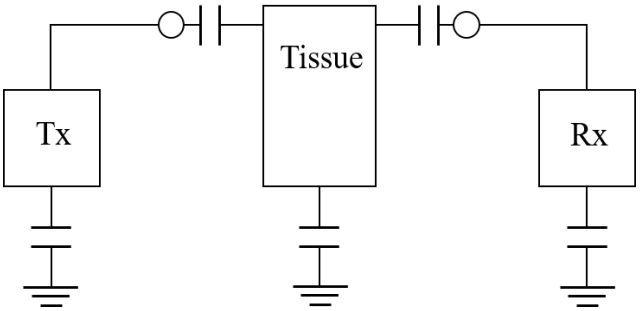

Figure 132. The classical architecture of intrabody communication: one set of electrodes located close to the skin, the other set oriented away from the body and capacitive coupled to the ground.

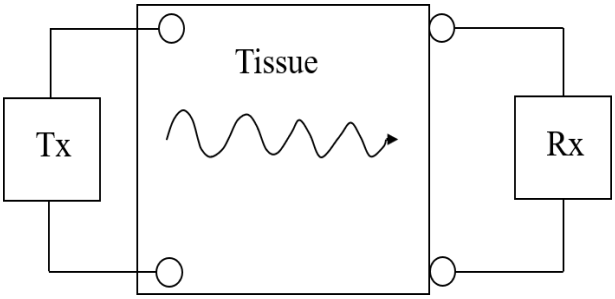

Figure 133. Both electrodes directly coupled to the body.

he capacitive intrabody communication could be used as telemetry but its main limitation is the capacitive connection to both the body and the ground, such that it cannot be used to communicate with IMDs but only with equipment placed close to the skin [15,16]. In medicine, telemetry refers to the process of monitoring a patient's vital signs where that information is collected and displayed in a central location for healthcare.

In 1997 Handa et al. [17] developed the second type of intrabody communication, called “galvanic coupling communication”.

Indeed, in this kind of communication, the coupling is of galvanic type: a small alternating current flows through the body from the transmitter to the receiver and both the transmitting and receiving electrodes are in contact with the body (Figure 6).

The main advantage of this technique is that galvanic telemetry only requires the power of 8 μW to be established; furthermore, the absence of the ground connection allows the communication with implantable devices. The galvanic coupling technique can be divided in two different communication types: implant-to-skin transmission, and implant-to-implant transmission (Figure 7).

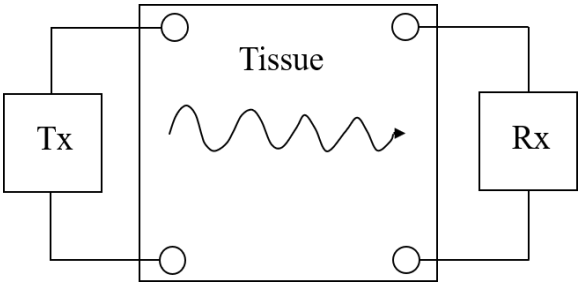

Figure 134. Implant-to-implant transmission

The latter is by far the most used as intrabody telemetry for implantable devices: the signals can be transmitted from the transmitter electrodes located inside the body to the receiver electrodes, which also are placed inside the body. The implanted receiver can then be connected to external circuitry outside the body through a wireless radio frequency telemetry.

In the case of implant-to-implant communication less power is needed to transmit the signal with comparison to implant-to-skin technique. In the study developed by Wegmueller et al. [18], the two electrodes of the transmitter were galvanically coupled with the body and they let an alternating current, of less than 1μA, at different frequencies in the range of 100-500 kHz, to flow through the body (muscle-tissue analog) to be finally detected by the two receiver electrodes. In the experiments two different types of electrodes were used, the first pair was composed of copper cylinders (10 mm in length and 4 mm for the diameter) and the second one of copper circles (4 mm in diameter). The sites of the electrodes were located 50 mm away one from the other; the signal losses along the communication medium were 32 dB over 50 mm for the first kind of electrodes and 47 dB over 50 mm for the second type. The higher percentage of signal loss was due to the presence of two pairs of electrodes, one for the transmitter and the other for the receiver. In fact, the four electrodes scenario showed quite high communication losses due to the flowing back to the source of most of transmitted current.

During the same year, Al-Ashmouny et al.[19] considered a two electrodes design for implant-to-implant intra-brain communication

(Figure 8). As shown in Figure 8, only one transmitting electrode and only one receiving electrode are in contact with the tissue. The other two ground electrodes are insulated from the tissue, so that the path, for the alternating-current signal to go back to the transmitter, is characterized by much higher impedance with respect to the path to reach the receiver. The electrodes, in this case, were realized with platinum-iridium wire of 50 μm in diameter. The transmitter was an insulated metal-oxide-semiconductor chip of less than 1 mm^3 in volume: both the transmitter and receiver were implanted in a rat's brain. Using this two-electrodes system a neural signal was transmitted through the brain tissue with 20 dB of signal attenuation; that is almost half the losses with respect to the four-electrodes scenario.

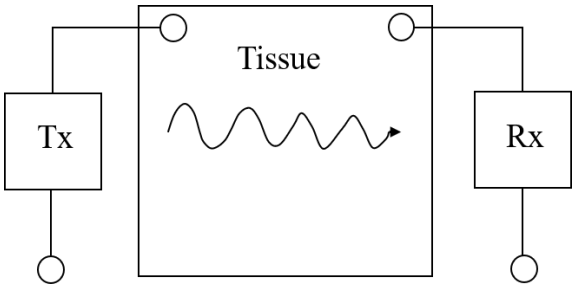

Figure 135. two electrodes design for implant-to-implant intra-brain communication.

The advantage of intrabody communication is the possibility of using low frequency carrier wave below few megahertz, as in the previous reported experiments. In fact, the higher the frequency the more dissipated power in the tissue, which can cause localized heating of the body tissue used as signal conductor [20].

However, in recent years the intrabody communication has not found great success for applications involving IMDs for clinical applications as physiological monitoring. The main flaw of this technology is related to the fact that communication between transmitter and receiver can take place if both are in contact with the patient's body.

Usually, the receiving device for health diagnosis is located at distance from the patient. In fact, if it is true that miniature devices can be implanted in multiple body structures, these implants would need to be interrogated using an RFID (Radio Frequency IDentification) telemetry system.

The necessary step of using anyway higher frequency, such as radio frequency, in the telemetry process has limited the adoption of intrabody communication for health monitoring to only particular applications such as wearable devices or short-distance, low-power and low-cost IMDs.

2.2. Inductive coupling and resonant inductive coupling

Inductive coupling is the process used for the transfer of power between a primary coil, placed outside the body tissue and connected to a variable magnetic field generator, and a secondary receiving coil which is located inside the body tissue. An inductor coil is integrated with the implanted sensor to get the electric power from the external-source magnetic field; in fact, the biological sensor is powered through the mutual inductance between the secondary integrated coil and the primary external one. Figure 9 shows the inductive coupling principle.

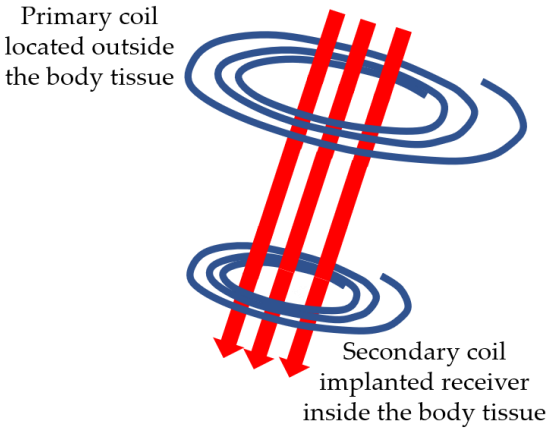

Figure 136. Inductive coupling configuration, the red arrows represent the magnetic field lines.

The induced voltage in the implanted coil (V_{is}) is obtained by the following equation:

$$V_{is} = -N\frac{d\Phi}{dt} = jN\omega\Phi = jN\omega\mu \int \vec{H} \cdot \overrightarrow{ds} \qquad (1)$$

where N is the number of the coil turns, ω is the operating angular frequency, Φ is the magnetic flux, $\vec{H}$ is the vector magnetic field, and μ is the permeability of the transfer medium. It is apparent that the value of V_{is} depends on the amount of magnetic flux lines that are concatenated with both coils, primary and secondary, respectively. Clearly as the distance between the transmitter and receiver coils decreases, the amount of concatenated magnetic flux increases.

The amount of power transferred between external coil and implanted coil can be maximized by using a capacitor in order to obtain the resonance conditions. In the IMD, the coil (L_{is}) is integrated with the capacitive sensor that usually uses a variable capacitor (C_{mim}) which changes its capacitance linearly with the quantity to be measured: pressure, temperature, presence of ions, such as pH measurement. Figure 10 describes the simplified diagram of the resonant inductive WPT circuit.

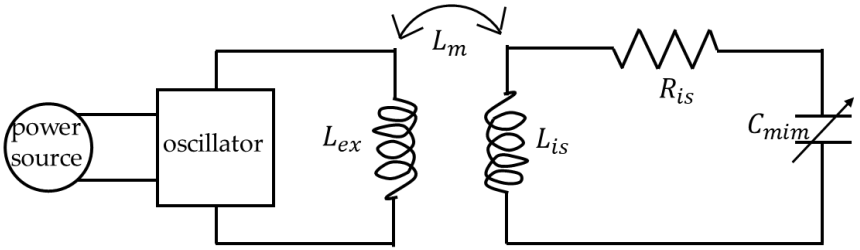

Figure 137. Simplified diagram of the resonant inductive WPT circuit.

L_{ex} represents the inductance of the external (or primary) transmitter coil, L_{is} is the coil of the IMD (or secondary coil) integrated with the implant electronics. L_m represents the mutual inductance between L_{ex} and L_{is}; the inductance L_{is} is integrated with the resistor R_{is} and the metal-insulator-metal capacitor C_{mim}, to form an RLC

circuit. Also, in the primary side circuit a resistor and capacitor are present because the coil winding has parasitic capacitance and resistance, associated with it, which are not shown in Figure 10.

From the previous consideration of Section 1, the highest value of transferred power and, hence, the highest voltage gain is obtained when in both sides (primary and secondary) the reactive part of the circuit impedance is zero. This resonant condition is met for the frequency value of:

$$\omega_0 = 2\pi f_0 = \frac{1}{\sqrt{L_{is} C_{mim}}} \quad (2)$$

which represents the tuned frequency for both sides, that is the link resonant frequency. The power transferred between the external coil and that of the IMD is regulated by the L_m. The coupling coefficient (k) is defined as:

$$k = \frac{L_M}{\sqrt{L_{is} L_{ex}}} \quad (3)$$

To improve the efficiency of the power transfer from the transmitter to the receiver circuit, it is necessary to optimize the coupling factor between the two coils of inductances L_{ex} and L_{is}, respectively.

The majority of current studies are focused on wireless systems that use the RF telemetry system to communicate from the IMD to the external energizing/interrogating circuitry. The inductive coupling is a methodology that is commonly used for power transfer to both active and passive IMDs; in particular, this type of power supply is used for cardiac pacemakers, cardioverter implanted defibrillators, biological sensors, neuromuscular stimulators.

When an inductive coupling is intended, two important parameters are the working frequency of the electromagnetic field and the distance between the primary and secondary coils. Generally, the most used frequencies are in the range that goes from hundreds of kHz to tens of MHz and the size of the implanted coils ranges from millimeters to a

few centimeters. As the frequency increases it is true that the power transfer increases but the energy dissipation due to the signal transmission through the human tissue also increases. The absorption of power by the biological tissue can create attenuations in the propagation of the electromagnetic field, this can worsen the efficiency of the inductive link. as the frequency increases, the wavelength of the electromagnetic field becomes commensurable with the size of the coils and the distance between them. According to Faraday's law, to increase the efficiency of the inductive coupling it is necessary to increase the size of the coils and increase the number of turns. When the dimensions of the transmitting and receiving coils are practically the same, it is possible to maximize the coupling. However, generally the dimensions of the implanted coil are smaller than the external transmitting coil.

In [21] the authors have developed a 5mm × 7.5mm neurostimulator implant that works at a frequency of 198 MHz and allows for a distance of about 140 mm between the IMD and the external transmitter circuit, the output power is 1000 mW. The stimulator takes the energy stored in a switched capacitor and releases it as an output stimulus once the voltage reaches a certain threshold. An in vivo experiment was performed to test the effectiveness of the neurostimulator. Two electromyography (EMG) recording electrodes were implanted into the gastrocnemius muscle of a rat, the ground electrode was attached to the skin.

In [22], a free-floating neural implant is proposed as an inductive link for WPT. The efficiency of the inductive link is 2.4%, the output power is 1.3 mW, the operating frequency is 60 MHz, the distance between the transmitter and the receiver is 16 mm, the transmitter and receiver dimensions are 45 mm and 1.2 mm, respectively.

In [23], the authors propose a wirelessly powered dielectric sensor for medical applications. The proposed dielectric sensor is based on LC resonance and offers a digitized measurement of the dielectric constant proposed for implantable applications such as bladder urine monitoring and other body fluid analysis. The resonant frequency is about 13 MHz, the rectifying efficiency is close to 75%, the transmitter and receiver dimensions are the same and equal to 30×29.6 mm^2.

In [24] a fully integrated power management application specific integrated circuit (ASIC) for efficient inductive power transmission is presented, suitable for inductive powering IMDs, with a resonant frequency of 2 MHz, power output of 1450 mW, efficiency value of 27% and transfer range of 80 mm.

Besides the applications for brain and spinal cord stimulators, the resonant inductive coupling is used for biological sensor IMDs. That is the case where the coil is integrated with the capacitive sensor that usually uses a variable capacitor which changes its capacitance linearly with the quantity to be measured: pressure, temperature, presence of ions, such as pH measurement.

In [7], the inductor is selected to have a sensor resonance frequency around 200 MHz, while the area of the sensor was of 3 mm^2; the pressure range measured by the sensor is 0-230 mmHg (where 0 mmHg is referred to the atmospheric pressure), the corresponding change in the capacitance C_{mim} was between 0.21 pF and 0.24 pF and the resonance frequency varies from 183 MHz to 173 MHz with a step of the sensor's sensitivity of 0.043 MHz/mmHg. A network analyzer is used as an impedance measuring device linked to an external antenna (L_{ex}), to measure the resonance frequency of the sensor.

The same type of technology was used by Park et al. [9] that developed a battery-less pressure sensor based on an LC resonant circuit. The sensor was integrated onto the 3D-printed polymeric stent for the purpose of wireless monitoring of pressure in a blood vessel. The experimental results of the pressure sensor were evaluated in the pressure range of 0 - 220mmHg. The resonance frequency of the sensor ranged from about 185 MHz for 0mmHg to around 130 MHz for 220mmHg, and the sensitivity was about 160 kHz/mmHg.

In [8], Luo et al. designed and realized a miniaturized resistor–inductor– capacitor (RLC) resonators with sizes of approximately 10-17 mm, using biodegradable materials and proposed as an RF component of wireless biosensors. They considered the 10-100 MHz range as operating frequencies suitable for in-vivo wireless measurements. Both the inductor and capacitor followed specific design guidelines to achieve such resonant frequencies while maintaining the device area below a nominal value of 1 cm^2. The sensor was tested in the pressure

range 0-23kPa, with a shift of the resonance frequency from about 31.9 MHz to about 31 MHz, respectively.

In [10], Boutry et al. designed a miniaturized wireless circuit which consisted of an LCR resonator circuit wherein the capacitive sensor (about 2mm × 2mm) is connected in series with an inductor coil. Due to the pulsatile nature of the artery experiences a change in vessel diameter over time that is measured by the capacitive sensor. The change in capacitance results in a shift of the resonant frequency f_0 of the LCR circuit, which is monitored wirelessly through the skin via inductive coupling with an external reader coil in a battery-free approach. The equivalent electrical circuit is shown in Fig. 11.

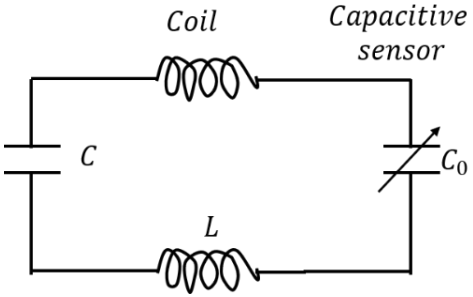

Figure 138. LCR resonator equivalent circuit: the capacitive sensor is connected in series with the inductor coil.

The shift in resonance frequency, Δf_0, due to capacitance change, ΔC_0, is calculated using the following equation, where L and C correspond to the inductance and the capacitance of the device, respectively:

$$|\Delta f_0| = \frac{\Delta C_0}{4\pi\sqrt{LC^3}} \quad (4)$$

The resonance frequency of the RLC electrical circuit was set to be at about 700 MHz for 2.2 pF value of C_0.

2.3. Microwave-based WPT

Another methodology to wirelessly transfer power from one point to another, in the order of meters up to kilometers, is the microwave power transfer. In this scenario the transmitting and receiving tools are called transmitting and receiving antennas. Generally, as in Section 2.2., there will be the external and the implanted antennas. From Figure 12, it is possible to see that the down-link is the case when the external antenna acts as transmitter and the implanted one as receiver, whereas the up-link represents the opposite case.

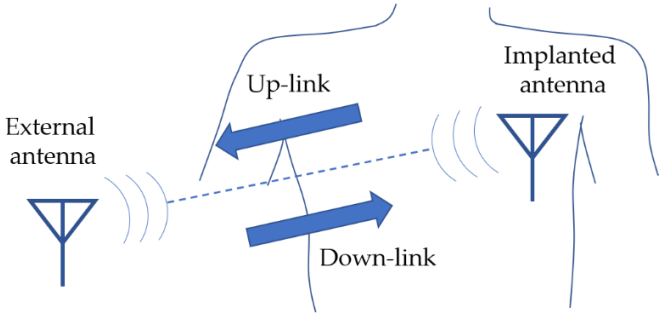

Figure 139. The schematic of a microwave WPT.

In the microwave-based WPT the communication between the two antennas is performed at much higher frequency with respect to the inductive coupling WPT; the former WPT can be established at the industrial-scientific-medical (ISM) band (2.4-2.485 GHz), the advantage of using this frequency range is that a transceiver is commercially available for this band, being the same as the wireless frequency band also used by cell phones. [Performances of an Implanted Cavity Slot Antenna Embedded in the Human Arm]. The high frequency communication band allows the power transfer to be performed over longer distances, which is why it is important to consider some parameters that characterize the performance of the established link between transmitter and receiver antennas.

In [25], an H-shaped cavity slot antenna is proposed as implanted antenna operating in the ISM frequency band, the dimensions of the antenna are 2.8 mm × 4.0 mm × 1.6 mm in volume, the input power to

the implanted antenna is 25 μW, due to limitations by the European Research Council (ERC)[26]. This implanted antenna is in the short-range communication, being the maximum distance between the transmitter and the receiver within 4 m. The condition to establish a wireless communication channel, going under the expression of $^{C}/_{N_0}$, where N_0 is the noise power density measured in dB/Hz (power per unit of bandwidth), is that the ratio $^{C}/_{N_0}$ must be greater than the required density power for the link (required $^{C}/_{N_0}$). Defining G_t and G_r as the gains of the transmission and receiving antennas, P_t the antenna transmission power, L_{feed} the transmission and receiving feeding loss, L_f the free space loss, and L_a the air propagation loss, all expressed in dB per unit of bandwidth, it is possible to calculate the $^{C}/_{N_0}$ as:

$$\text{Link } {}^{C}/_{N_0} = P_t - L_{feed} + G_t - L_f - L_a + G_r - L_{feed} - N_0 \text{ [dB/Hz]} \quad (5)$$

where:

$$L_f = 10 \cdot \log_{10}\left(\frac{4\pi d}{\lambda}\right)^2 \text{ [dB]} \quad (6)$$

$$N_0 = 10 \cdot \log_{10}(k) + 10 \cdot \log_{10}(T_i) \text{ [dB/Hz]} \quad (7)$$

$$T_i = T_0 \cdot (NF - 1) \quad (8)$$

NF is the noise figure of the receiver, T_0 is the equivalent noise temperature (generally set at 290 K), k is the Boltzmann constant, d is the distance between the transmitter and receiver, and λ the wavelength of microwave. The value of the link $^{C}/_{N_0}$must be greater than the required $^{C}/_{N_0}$, that can be calculated as:

$$\text{Required } {}^{C}/_{N_0} = {}^{E_b}/_{N_0} + 10 \cdot \log_{10}(B_r) - G_c + G_d \text{ [dB/Hz]} \quad (9)$$

where E_b/N_0 represents the phase-shift keying (PSK) signal quality (dB/Hz), B_r is the bit rate (kb/s) of the signal, G_c is the coding gain (dB/Hz) and G_d is the fixing deterioration (dB/Hz), both parameters are referred to the quality of the signal.

In [25] the link C/N_0 is equal to 50.84 dB/Hz and the Required C/N_0 is equal to 50.55 dB/Hz, so the calculated margin of the link is equal to 0.29 dB per bandwidth.

Considering the impedance mismatch losses, as:

$$L_{impedance} = -10 \cdot \log_{10}(1 - r^2) \text{ [dB/Hz]} \quad (10)$$

where r is the reflection coefficient. For a more accurate evaluation both $L_{impedance}$ and L_f can be considered to calculate the power received by the receiver, as follows:

$$P_r = P_t + G_t + G_r - L_f - L_{impedance} - e_p \quad (11)$$

where e_p is the polarization mismatch loss between the transmitter and the receiver. The previous equation (11) can also be expressed as function of the scattering parameters:

$$P_r = \frac{G_t \cdot G_r \cdot \lambda^2}{(4\pi d)^2} \cdot (1 - |S_{11}|^2) \cdot (1 - |S_{22}|^2) \cdot e_p \cdot P_t \quad (12)$$

The equation that links the transmitted power and the received power through the scattering parameters is:

$$|S_{21}|^2 = \frac{P_r}{P_t} \quad (13)$$

where $S_{21}$and S_{21} are the reflection coefficients and S_{21} is the forward scattering coefficient.

The power transmission is proportional to frequency which suggests that power efficiency is proportional to frequency. However, the Debye model for tissue shows that the absorption coefficient is

higher for higher frequency. These two opposite behaviors of the magnetic field properties in power transfer lead to the conclusion that there are optimal frequencies for energy transfer [27]; the ISM band is one of those.

In [28] the authors considered a miniaturized implantable antenna with three frequency bands (902-928, 2400-2480 and 1824-1980 MHz) working at the ISM band and at the midfield band. This antenna is equipped with electronics, batteries and sensors for different stimulation applications. This IMD is tried for different tissues such as the scalp, heart, colon, large intestine and stomach.

In [13] the authors propose a passive biodegradable implant for subcutaneous soft-tissue trauma monitoring. The authors study the possibility of using an array of antennas to increase the amplitude of the frequency response with respect to a single antenna: the array is composed of a 3x3 cell matrix. The results show that increasing the number of elements improves the frequency response of the array but it has the drawback to increase the size of the final tag. Two main techniques exist to improve the tag response while keeping limited the size of the tag: folding and intertwining the tag shape, as shown in Figure 13.

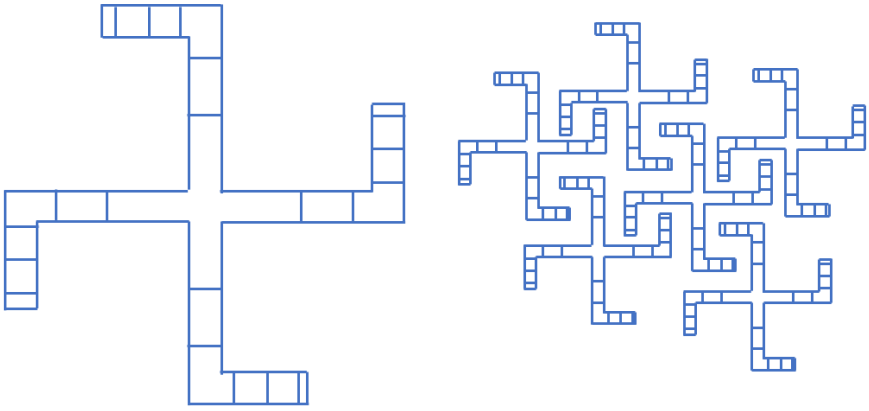

Figure 140. Shaping and intertwining of antenna-array configuration.

2.4. Ultrasonic-based WPT

Ultrasound waves have been used for several decades as a diagnostic technique. In the ultrasound imaging, the ultrasound waves emitted by the transmitter probe propagate along the body tissue and the generated echo, due to the reaction of the acoustic properties of the body tissue to sound waves propagation, is backscattered and recorded by the passive receiver. Since the sound waves can propagate in body tissues, they can also be used to wirelessly power active and passive IMDs. The functioning of the ultrasound methodology is linked to having a transducer that converts the electrical signal into an acoustic signal (by means of the piezoelectric effect), in transmission, and a transducer that performs the inverse conversion in reception, again through the piezoelectric effect. The basic principle of the ultrasonic WPT coupling is shown in Figure 14.

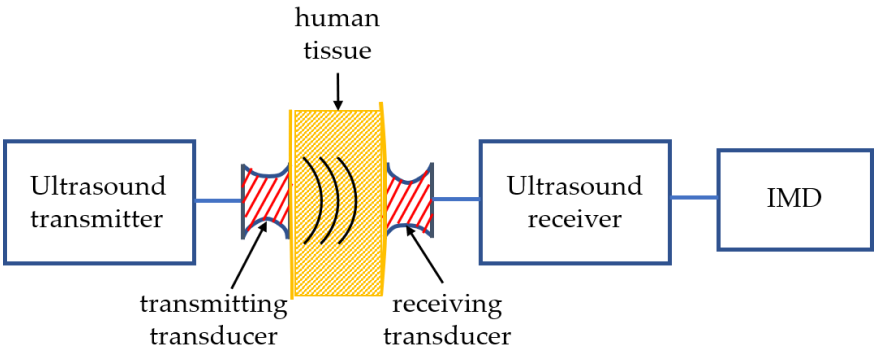

Figure 141. The basic schematic of the ultrasonic WPT coupling for IMDs.

Considering a circular piston type of transmitter and if the transmitter and the receiver are located the one in front to the other, it is possible to express the axial distribution of the sound pressure as function of the distance from the transmitter, as follows:

$$p(r,0,t) = \rho_0 c U_0 e^{-\alpha r}\left\{1 - e^{-jk(\sqrt{r^2+a^2}-r)}\right\} e^{j(\omega t - kr)} \qquad (14)$$

where ρ_0 is the density of the medium, c is the sound speed in the medium, U_0 is the speed of piston source at the transmitter side, α the attenuation coefficient, ω is the angular velocity, $k = \frac{\omega}{c}$ the wave number, r is the distance from the transmitter, a is the radius of the transmitter. To improve the transfer power efficiency it is better to focus the acoustic waves; to do that, the receiver should be located from the transmitter at the Rayleigh distance, defined as:

$$R_d = \frac{\pi a^2}{\lambda} \tag{15}$$

where λ is the wavelength of the sound wave.

The ultrasonic-based WPT methodology is an effective technique to be used as stimulator device for cardiac defibrillators and deep brain stimulators [29] [30]. The ultrasonic-based WPT methodology shows no limitations for the safety of the body exposure to ultrasound waves and generally is insensitive to misalignment between transmitter and receiver. Usually the receivers are able to produce power in the range of few milliwatts with an active range of about hundreds of millimeters.

In [29], the authors establish that the acoustic-based WPT is implementable with good performance in biocompatible applications.

The authors build an experimental setup to assess the efficiency of an ultrasonic-based WPT through the tissue medium. The ultrasonic resonance transmitter and receiver are manufactured with 50 mm diameter and 250 kHz resonance frequency. In tissue medium, it is obtained 21% power transfer efficiency in 23 mm skin depth at 255 kHz driving frequency. The power delivered by the transmitter is of 15.5 mW and the power available at the receiver is of about 3 mW.

2.5. Hybrid WPT

It is possible to combine different WPT methodologies to achieve a hybrid WPT technique that could exploit the technical advantages of each single methodology. For istance, CPT shows two main advantages with respect to the inductive WPT (IPT). The first advantage is the absence of eddy current loss [31], in fact CPT achieves power transfer by the electric field which does not generate the eddy current loss in the

nearby metal. The second advantage is that the implementation of the CPT is more economical and light with respect to IPT. On the other hand, the CPT methodology is generally limited to the transfer of small powers and for short distances, due to the usually small coupling capacitors. Considering the IPT, the high voltage generated in the coils could be used as the driving source for the CPT coupler, this way the IPT and CPT methodologies can be combined into a hybrid system.

A purely IPT connection can be therefore changed to a hybrid link that constitutes of two channels: one continues to be of IPT type, the other is instead of CPT nature. Adding the CPT link introduces minimal addiotional cost and weight; on the other hand, the addition of the CPT link guarantees greater power transfer under the same conditions compared to the simple IPT.

The basic functioning of the hybrid WPT methodology can be summarized as follows: the IPT link is active when the currents flow through the coils and generate the alternating magnetic field which provides the transmission medium. The currents produce high-voltage stress on the transfer coil because of the self inductance, while the CPT system requires high input voltage to set up the electric field for the capacitive link. In this way, the voltage stressed on the coil of the IPT system can be used as input for the CPT system, so that IPT and CPT can be combined to realize a hybrid system for WPT. Figure 15 shows the schematic of the described architecture.

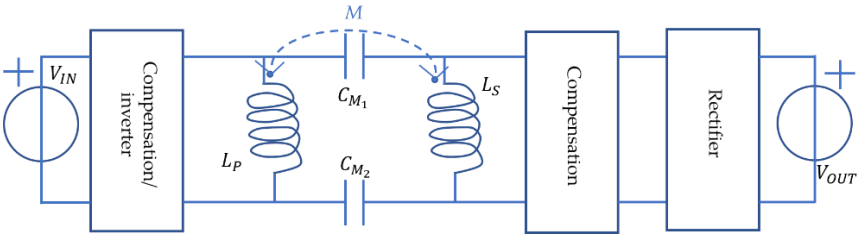

Figure 142. The generic schematic of a hybrid WPT: ICT and CPT in the same wireless system.

The compensation blocks on the primary side and secondary side, reported in Figure 15, are used to bring the system to resonance

conditions and improve the voltages of the plates, for the CPT coupling. The M represents the mutual inductance between the primary inductance L_P and the secondary inductance L_S. C_{M_1} and C_{M_2} are the two capacitive couplers, the rectifier block on the secondary side is used to obtain a direct voltage at the output to power the IMD or to recharge the implanted battery.

In [32], the authors propose a hybrid inductive and capacitive WPT system to achieve high-power transfer by combining IPT and CPT. The authors show that their hybrid solution is able to achieve the performance range between 70% and 90% of DC-DC efficiency, for the corresponding output range of 100W and 1100 W, respectively. The distance between the IPT coupler and the CPT coupler is of 300 mm. The capacitance values of the CPT couplers is in the order of a couple of hundred of pF; the switching frequency of the system is of 800 kHz.

In [33], the authors propose a hybrid system based on the combination of inductive and microwave methodologies; wherea in [34], the authors propose a hybrid system based on the combination of inductive and ultrasonic methodologies.

3. Final discussion

The WPT methodologies are gaining interest as alternative technologies to power IMDs which can be either active or passive devices. The possibility of assessing the vital parameters of patients without the necessity to use wires, that can cause infections, connected to the implanted sensors, it is a big step ahead for health control applications. The IMDs have wide room for improvement both from the poit of view of biocompatibility within the human body and from the point of view of connection with the external electronic devices.

Wireless medical instruments can be classified into two categories: short-range, such as inductive implants and medical body area networks, and long-range, such as wireless medical telemetry (WMTS) [35]. One of the first objective of Healthcare Administration, which is the field relating to management, and administration of public health systems, health care systems, hospitals, and hospital networks, is to check if the proposed medical devices guarantee the factors of safeness

and effectiveness for patient usage. Generally thiese medical devices are split into three categories of risk:

1. The first level considers the lowest-risk devices;
2. The second level is the one that includes wireless technologies: that is a sort of low/medium-risk range;
3. The third level includes high-risk devices.

In light of this, it is clear that an IMD that uses wireless technology must be classified as safe before being marketed.

The overview of the different methodologies most used, in medical applications, for WPT, provides a first guide on which technology is convenient to choose based on the type of control to be carried out. This chapter showed that most of the ultrasound-based WPT systems work at a low operating frequency, ranging from a few hundred kHz up to few MHz. The inductive-based WPT systems can operate within the RF range, so generally at a higher frequency compared to ultrasound-based technique and can reach up to a few hundred MHz. It can be concluded that the operating frequency for most of medical applications based on inductive WPT is located below 50 MHz.

In the RFID (Radio Frequency Identification) sector, the most used frequency is the one that operates at 13.56 MHz and is called NFC (Near Field Communication). Compared to other RFID frequencies, NFC has the enormous advantage of being able to be read with a smartphone equipped with an NFC sensor. For this reason, NFC is also exploited in the majority of inductive WPT medical applications.

On the contrary, the microwave-based WPT works at a higher operating frequency, compared to both ultrasound-based and inductive-based WPT. This latter methodology ranges from hundreds of MHz to hundreds of GHz. Finally, the hybrid WPT applications variy from low to high frequency: this behavior is due to the combination of methodologies of different nature.

Figure 16 shows where the considered different WPT methodologies can be found in the efficiency-versus-frequency plot. The resonant-inductive WPT shows the highest values of efficiency, which can reach up to 90%. Microwave and ultrasound based WPT generally follow in the efficiency range between 40% to 70%. The hybrid WPT techniques can show lower efficiency values, although the one

described in section 2.5 can achieve, according to authors of [32] 70% of efficiency; however, it must be underlined that this last study was conducted for high-power applications and not strictly for medical applications, where the power involved is much lower. In fact, the study shows that the efficiency of the hybrid system decreases as the power incolved decreases.

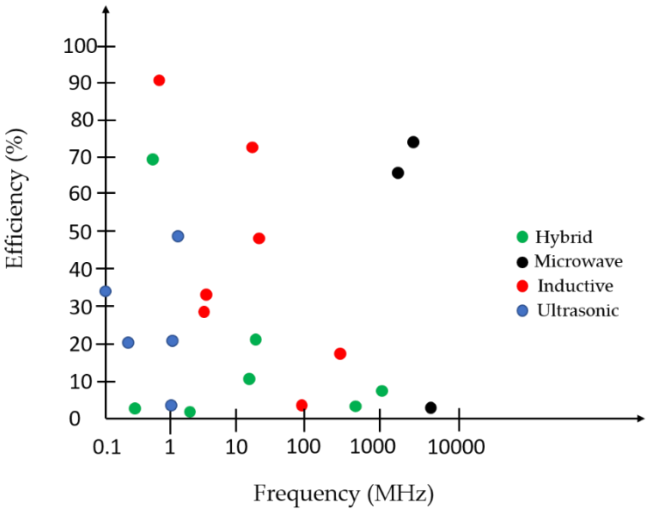

Figure 143. The efficiency versus frequency plot of the different WPT methodologies.

References:

1. Haerinia, M.; Shadid, R., Wireless Power Transfer Approaches for Medical Implants: A Review, Signals, **2020**, 1, 209–229; doi:10.3390/signals1020012.
2. Brizi, D.; Fontana, N.; Barmada, S.; Monorchio, A. A Multi-Transmitter Configuration for High-Safety Wireless Power Transfer Applications. In Proceedings of the 2019 International Applied Computational Electromagnetics Society Symposium (ACES), Miami, FL, USA, 14–19 April 2019; pp. 1–2.
3. Jegadeesan, R.; Agarwal, K.; Guo, Y.; Yen, S.; Thakor, N. Wireless power delivery to flexible subcutaneous implants using capacitive coupling. IEEE Trans. Microw. Theory Tech. 2017, 65, 280–292.

4. C.M. Boutry, H. Chandrahalim, P. Streit, M. Schinhammer, A.C. Hanzi, C. Hierold, Characterization of miniaturized RLC resonators made of biodegradable materials for wireless implant applications, Sensors and Actuators A 189, 2013, 344-355.
5. Wegmueller M.S., Nuclova S., Froehlich J., et al. Galvanic coupling enabling wireless implant communications. IEEE Trans. Instrum. Meas. 2009; 58(8):2618-2625. Report of galvanic intrabody communication between implants.
6. Covic, G.; Boys, J. Inductive power transfer. Proc. IEEE 2014, 6, 1276–1289.
7. Jongsung Park, Ji-Kwan Kim, Swati J. Patil, Jun-Kyu Park, Sua Park and Dong-Weon Lee, A wireless pressure sensor integrated with a biodegradable polymer stent for biomedical applications.
8. M. Luo, A. W. Martinez, C. Song, F. Herrault and M. G. Allen, "A microfabricated wireless RF pressure sensor made completely of biodegradable materials", Journal of microelectromechanical systems, vol.23, no. 1, February 2014.
9. J. Park, J.-K. Kim, S.A. Park, D.S. Sim, M.H. Jeong, D.-W. Lee, 3D-printed biodegradable polymeric stent integrated with a battery-less pressure sensor for biomedical applications, Transducers 2017, Kaohsiung, TAIWAN, June 18-22, 2017.
10. C.M. Boutry, L.Beker, Y. Kaizawa, C. Vassos, H. Tran, A.C. Hinckley, R. Pfattner, S. Niu, J. Li, J. Claverie, Z. Wang, J. Chang, P. M. Fox and Z. Bao, Biodegradable and flexible arterial-pulse sensor for the wireless monitoring of blood flow, Nature Biomedical engineering, Vol. 3, january 2019, 47–57.
11. Mark G. Allen, MICROFABRICATED IMPLANTABLE WIRELESS MICROSYSTEMS: PERMANENT AND BIODEGRADABLE IMPLEMENTATIONS, MEMS 2014, San Francisco, CA, USA, January 26 - 30, 2014.
12. J. Park, J.-K. Kimb, Su A. Park, D.-W. Lee, Biodegradable polymer material based smart stent: Wireless pressure sensor and 3D printed stent, Microelectronic Engineering 206, (2019),1-5.
13. J. M. Rigelsford, B. F. Al-Azzawi, C. J. Davenport, and P. Novodvorsky, A Passive Biodegradable Implant for Subcutaneous Soft-Tissue Trauma Monitoring, IEEE JOURNAL OF BIOMEDICAL AND HEALTH INFORMATICS 2015.
14. Zimmerman, TG. PhD thesis. Massachusetts Institute of Technology; MA, USA: 1995. Personal area networks (PAN): near-field intra-body communication.

15. Meoli D., May-Plumlee T. Interactive electronic textile development: a review of technologies. J. Text Apparel Technolog. Manag. 2002; 2(2):1-12.
16. Hyoung, CH., Sung, JB., Hwang, JH., Kim, JK., Park, DG., Kang, SW. A novel system for intrabody communication: touch-and-play. Proceedings of the IEEE International Symposium on Circuits and Systems; 2006.pp. 1343-1346.
17. Handa T., Shoji S., Ike S., Takeda S., Sekiguchi T. A very low-power consumption wireless ECG monitoring system using body as a signal transmission medium. Int. Solid St. Sensor Actuator Conf. 1997: 1003-1006.
18. Wegmueller MS, Huclova S., Froehlich J., et al. Galvanic coupling enebling wireless implant communications, IEEE Trans. Instrum. Meas. 2009; 58(8):2618-2625. Report of galvanic intrabody communication between implants.
19. Al-Ashmouny, K.M.; Boldt, C.; Ferguson, J.E.; Erdman, A.G.; Redish, A.D.; Yoon, E. IBCOM (intra-brain communication) microsystem: Wireless transmissin of neural signals within the brain. Proceedings of the Annual International Conference of the IEEE Engineering in Medicine and Biology Society; 2009, pp.20154-2057. First report of an in vivo test of galvanic communication through the brain.
20. De Santis M, Cacciotti I. Wireless implantable and biodegradable sensors for postsurgery monitoring: current status and future perspectives. Nanotechnology. 2020 Apr 3;31(25):252001. doi: 10.1088/1361-6528/ab7a2d. Epub 2020 Feb 26. PMID: 32101794.
21. Lyu, H.; Wang, J.; La, J.-H.; Chung, J.M.; Babakhani, A. An Energy-E cient Wirelessly Powered Millimeter-Scale Neurostimulator Implant Based on Systematic Codesign of an Inductive Loop Antenna and a Custom Rectifier. IEEE Trans. Biomed. Circuits Syst. 2018, 12, 1131–1143.
22. Mirbozorgi, S.A.; Yeon, P.; Ghovanloo, M. RobustWireless Power Transmission to mm-Sized Free-Floating Distributed Implants. IEEE Trans. Biomed. Circuits Syst. 2017, 11, 692–702.
23. Lyu, H.; Jian, Z.; Liu, X.; Sun, Y.; Babakhani, A. Towards the Implementation of a Wirelessly Powered Dielectric Sensor with Digitized Output for Implantable Applications. IEEE Sensors Lett. 2019, 3, 1–4.
24. Kiani M, Lee B, Yeon P, Ghovanloo M. A Q-Modulation Technique for Efficient Inductive Power Transmission. IEEE J Solid-State

Circuits. 2015 Dec;50(12):2839-2848. doi: 10.1109/JSSC.2015.2453201. Epub 2015 Nov 26. PMID: 27087699; PMCID: PMC4830506.
25. W. Xia, K. Saito, M. Takahashi and K. Ito, "Performances of an Implanted Cavity Slot Antenna Embedded in the Human Arm," in *IEEE Transactions on Antennas and Propagation*, vol. 57, no. 4, pp. 894-899, April 2009, doi: 10.1109/TAP.2009.2014579.
26. "ERC recommendation 70-3 relating to the use of short range devices (SRD)," in Eur. Postal Telecommunications Administration Conf.,Tromsø, Norway, 1997, CEPT/ERC70-03, Annex 12.
27. Poon A, O'Driscoll S and Meng T 2010 Optimal frequency for wireless power transmission into dispersive tissue IEEE Trans. Antennas Propag. 58 1739–50.
28. Zada, M.; Yoo, H. A Miniaturized Triple-Band Implantable Antenna System for Bio-Telemetry Applications IEEE Trans. Antennas Propag. **2018**, 66, 7378–7382.
29. Lee, S.Q.; Youm,W.; Hwang, G. Biocompatible wireless power transferring based on ultrasonic resonance devices. Proc. Mtgs. Acoust. **2013**, 19, 30030.
30. Kim, A.; Powell, C.R.; Ziaie, B. An Implantable Pressure Sensing System with Electromechanical Interrogation Scheme. IEEE Trans. Biomed. Eng. **2014**, 61, 2209–2217.
31. Lu, F., Zhang, H., Hofmann, H., *et al.*: 'A double-sided *LC* compensation circuit for loosely-coupled capacitive power transfer', *IEEE Trans. Power Electron.*, 2017, **33**, (2), pp. 1633–1643.
32. Luo, B.; Long, T.; Mai, R.; Dai, R.; He, Z.; Li, W. Analysis and design of hybrid inductive and capacitive wireless power transfer for high-power applications. IET Power Electron. **2018**, 11, 2263–2270.
33. Shadid, R.; Haerinia, M.; Sayan, R.; Noghanian, S. Hybrid Inductive Power Transfer andWireless Antenna System for Biomedical Implanted Devices. Prog. Electromagn. Res. C **2018**, 88, 77–88.
34. Meng, M.; Kiani, M. A Hybrid Inductive-Ultrasonic Link forWireless Power Transmission to Millimeter-Sized Biomedical Implants. IEEE Trans. Circuits Syst. II Express Briefs **2016**, 64, 1137–1141.
35. Wireless Medical Technologies: Navigating Government Regulation in the New Medical Age. Available online:https://www.fr.com/files/Uploads/attachments/FinalRegulatoryWhitePaperWirelessMedicalTechnologies.pdf (accessed on 20 March 2021).

BIOMATERIALS AND SCAFFOLDS FOR NEURAL TISSUE ENGINEERING

Prof. dr. Antoniac Iulian[1],
Dr. Adriana Săceleanu[2]

[1] University Politehnica of Bucharest, Romania
[2] Faculty of Medicine, "Lucian Blaga" University, Sibiu

Contents

1. Clinical aspects regarding the neural system

Therapeutic neuroscience is a fast-advancing domain mainly as far as the cellular quality and treatment are concerned, which guarantees improved outcomes for patients. A series of clinical preliminaries is underway, referring to the intense conditions in the case of neuronal injuries, such as stroke or spinal damage. It is therefore necessary to understand the way in which these therapies are needed in restoring the tissue and the latter's capacity to regenerate, to further convey this information to the patient. The areas of biomaterials, tissue design and regenerative medication are seen today as powerful instruments for the resolution of the issues emerging in case a scaffold is accepted; this should be regarded as an attempt to improve agreement and adequacy of the therapeutic systems.

With the onset of tissue engineering, new developments have occurred in the treatment of nerve injuries. High concentrations of

growth factors are needed for tissue engineering and regenerative treatment strategies to reach appropriate restoration, able to sustain the therapy level for a longer period. Moreover, the domain of biomaterials is undergoing a process of improvement as far as medication transport and cellular treatment are concerned. A combination of bioengineering, material improvement and neurosciences is necessary to obtain better results in the future.

Research has shown that many youths are currently harmed by nerve injuries and their lives change afterwards. In any case, significant improvements have been seen lately in cellular progress, alongside with the development of stem cells and the parallel upgrade of pharmaceutical regeneration and tissue construction products, as well as with the range of biomaterials compatible with the central nervous system (CNS). These last few years, the development of tissue engineering has offered a new strategy for repairing tissue damage. The purpose of tissue engineering is to design new replacements out of biological materials and cells, able to better fit the restoration and preservation of the human body features. Cell-based tissue repair offers a potential component of the repair and recovery of the damaged CNS.

After many years, the progress in cellular innovation combined with the emergence of various biomaterials based on regenerative medication and tissue design has suggested that there is exceptional potential for many of these obstacles to be overcome. The biopolymer used, the cells, and the physiological or physical shocks are the three primary components of tissue construction. Up to now, brain injuries have been a theoretically unsolved issue. This is because the three most important principles of neurobiology are opposed to post-damage brain recovery: no new neurons appear, the axons in the CNS cannot grow and no new connections among neurons are set.

A variety of factors can influence the CNS deterioration, such as injuries, stroke or diseases like Alzheimer's or Parkinson's Disease. Parkinson's disease (PD) is the second most common neurodegenerative disease in the world, and it is related to a variety of factors like the dopaminergic neuron's degradation in the substantia nigra. The essential clinical features of the disease are sleep disorders, hypokinesia, strong inflexibility and postural insecurity. The stroke is

produced by a decrease in the blood supply to one part of the brain and is the second cause of death worldwide. Alzheimer's disease (AD) is the most common neurodegenerative issue, characterized by memory disability and mental decay.

The neural system is an important part of the body and consists of two major components: the central nervous system (CNS) and the peripheral nervous system (PNS). An efficient treatment requires tissue engineering; this option makes it possible to design a scaffold, a suture and surgery. The CNS comprises the brain, the spinal cord, the retina and has several functions, such as receiving and interpreting signals. The spinal cord acts like a bridge between the brain and the rest of the body. Although the spinal cord's structure is simpler than the brain's, it is more damaged by trauma.

The regeneration of the neural system in adults is limited as compared to other tissues. These limitations are caused by a lack of neuron growth and recovery, which prevents the right connections from being made. PNS and SNC have different regenerative responses. Because of the presence of Schwann cells (SC), which provide nutrients, direct and myelinated peripheral axons, and other factors, PNS regeneration is more active.

The brain's complex structure is made up of a very well organized, interconnected neural structure, which interacts with the extracellular matrix (ECM) to form complex networks [4]. During development, the neural cells reproduce and migrate to individual locations within the networks. The brain responds to different trophic signals [5]. The neurons also change the topographic excitability through growth interactions, set up nerve endings with the proximal environment [6] and transmit mechanical signals which can lead to increased neuritis [7]. Diluted neuritis and axon growth guarantee appropriate and regulated connectivity at the nerve level, so that a circuit is created which makes a special nucleus with a specific function in the brain.

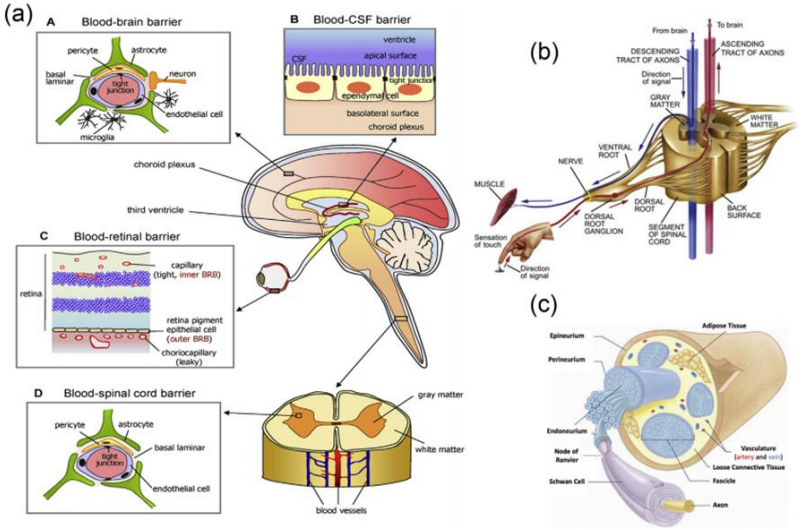

Figure 1. The schematic representation of the human neural system's main parts. (a) the brain anatomy and the blood-brain barrier [1], (b) cross section of the spinal cord [2] and (c) the peripheral nerve anatomy [3].

Traumatic brain injuries (TBI) can cause a variety of symptoms, ranging from headache to paralyzed. TBIs, spinal cord injury (SCI), and strokes are all examples of trauma. There is no effective way to reclaim the role that has been lost.: the clinical method is symptomatic and relies on minimizing the negative effects or strengthening recovery of plasticity in the affected area.

The adult brain is limited as to the regeneration capacity [8,9]. Consequently, the tissue harm caused by the disease or the TBIs is perpetual and can bring about some displays of symptoms at the psychological level. The current clinical treatment systems attempt to prevent and contain tissue incidents, along with the alleviation of the emerging side effects, by means of some biomaterials which are biocompatible and preserve motility even after restoration takes place. Despite these properties, some materials had undesired side effects [10].

The purpose of designing the brain-level tissue is to stabilize and recover the affected tissue to restore the latter's usefulness both at cell and organ level. Cellular harm disturbs the availability to convey the

message among neurons, and thereby has a negative impact upon their operation.

Stroke is caused by a decreased blood supply to one part of the brain and is the second cause of death worldwide. The two main types of strokes are: ischemic, accounting for 80%, is the point in which the blood supply has stopped because of blood or hemorrhagic clots, so that a bursting out vein causes death.

The brain tissue lost post-stroke does not regenerate, although it is commonly associated with restorative response and neurogenesis onset. The inability to regenerate functional brain tissue is not caused by the lack of available brain cells, but rather by the lack of structural support which might allow to refill the cavity of the injury. The decay mechanism of the biological folds and its main task to allow for the invasion of brain cells are debated against the cure of peripheral injuries.

The main difference between the regenerative and non-regenerative tissues refers to the progressive context, special attention being given to the neurogenic aspect. To regenerate the CNS, many researchers use aliphatic polyesters in their experiments. This family of synthetic polymers could be produced by ring opening polymerization and seems appropriate as biomaterials to cause brain damage. The SCI is caused by wound or incomplete/complete spinal cord severance, leading to deficiency of the tactile or potentially motor activity.

Cell transplant is investigated as a restoration technique for SCI by different components, e.g., affected cell replacement which provides neurotrophic resistance, balancing the host's resistant reaction.

Tissue engineering is a modern technology to repair the damaged areas; it allows for the latter's regeneration and includes many materials, both natural and synthetic, to produce scaffolds. Many studies in the neural tissue engineering have reported a wide range of scaffolds.

2 Ideal properties of a scaffold

In recent years, a scaffolding combination, biomaterials, and cellular therapy used in CNS regeneration have aroused the interest of researchers. The combination of the two therapies makes it possible to regenerate both cells and repair of connections among them.

The use of new biomaterials, structures, and various methods of monitoring cellular activity are all used in tissue regeneration strategies to improve results. Research in the field of biomaterials/structures as chemical biomaterials, the hardness of the material, the surface topography, the porosity, and nature of decay all play an important part in monitoring cellular events which influence recovery, both in vitro and in vivo. Bioactive elements, such as proteins, peptides, and even small molecules, should be included in advanced biomaterial structures and techniques to affect cell activity and regeneration.

For decades, biomaterials have been studied in various aspects of tissue engineering. They are normally shaped like a skeleton and perform the same function as the tissue and extracellular matrix (ECM) during the regeneration process. The skeleton has a direct influence upon cellular behavior insofar as the phenotype adherence, proliferation, migration, differentiation, and maintenance are concerned. Furthermore, biomaterials used in neural tissue engineering can be modified to induce these changes in cellular behavior. Additionally, the skeleton can be useful in monitoring and boosting axon growth, with a neuroprotective impact in the toxic microenvironment of the damaged CNS, as well as encouraging glial migration In recent decades, scientists have looked into the signals connected to axon development and direction through *in vitro*, covering cell substrate, physical stimulation, cellular signaling and also favoring the inhibition of axon growth molecules.

There is a variety of cell sources which can be used to repair the CNS, including the primary nervous tissue dissected on the developing embryo or the foetal brain, or different types of stem cells, the embryo stem, mesenchymal, neural and pluripotent induced cells included. Although these cells can become an efficient source of donors for cellular therapies, they are ethically and logistically limited; if this aspect is not achieved, there is a risk of teratoma development after implanting the appropriate distinction.

The cell-based remedies have proved the possibility of another treatment option to target the CNS-level injuries and to improve further deficiencies by direct substitution of the damaged tissue or by other systems, the neuroprotection upgrade and pathological measures

decrease included. Despite all this, the approaches based on cell fixation are facing many deterrence methods which impede upon extended clinical accomplishments. Preclinical exams using cell transport to recover the central neural tissue have also experienced unassisted cell resistance and coordination in the post-transplant host tissue. The cell-based treatment is expected to provide and maintain the damaged cell appropriateness and to substitute them while tissue regeneration develops. Even if the cell-based treatments are likely to moderate the obsessive results of injuries at the CNS level, of strokes and neurodegenerative disorders, they are linked with the critical constraints which prevent them from being interpreted in the clinical practice. Biomaterials can solve part of these constraints to improve mental support, remedial and recovery. Within this framework, their essential application refers to scaffolds, meant to help improve cell transport and weight.

The cell-based treatment facilitates provision and maintenance of the damaged cell feasibility or the latter's replacement, while tissue regeneration develops. Even if cell-based treatments may improve the neural results of CNS injuries, strokes, and neurodegenerative disorders, they are linked to the critical constraints which prevent their interpretation in the clinical practice. Biomaterials can overcome part of these constraints and can be approached to improve brain provision, correction, and recovery. Their critical application in this framework is as a scaffold which assists and improves cell transport and weight. Scaffolds based on biomaterials are completed as a proper design for the cells to adhere during and after transplant as an actual boundary against the transplant invulnerable reaction and as a source of transfer-restorative biomolecules.

In practice, cell transmission into a biomaterial can potentially offer the incorporated cells a more stable, defensive, and trophic microenvironment when contrasted to the adult and diseased mind into which they are moved. Biomaterials have been efficiently used for remedial and regenerative purposes in many diseases for many years now.

The planning of biomaterials for brain remedy is remarkable due to the limited brain opening and the self-regulation limit, the presence of

brain limits in blood, the brain cell complexity and usefulness. The brain unavailability, vulnerability and complexity contest the planning and advancement of biomaterials for cell-based repair. Although the brain biomaterials planning is mainly recommended by their application and the target area, there are some fundamental requirements.

If biomaterials are to be used for cell-based brain fixing, they should be meant to be transmitted in a significantly intrusive way. Under this specific circumstance, although the examinations have used implantable scaffolds, the covered area of the brain has caused the improved modelling of injectable substances, the so-called hydrogels, which can be incorporated using an insignificantly intrusive medical procedure.

Biomaterials should be produced artificially and genuinely stable for a sufficient time to carry out their ideal organic capacity; also, they should be totally biodegradable, with no excessive accumulation no matter how many times they are used [12]. Additionally, they should have long-term biocompatibility with the host tissue; neither the base material, nor any of its degradation results should cause an immunogenic reaction in the host. This is specifically significant when designed biomaterials are used. Eventually, the created biomaterials should be versatile enough, so they are mass delivered to initiate clinical practice. To choose the suitable biomaterial for a remedial approach, its combined properties – physical and material – should be considered, alongside with its possible cooperation with the target tissue. In the context of synapse correction, hydrogels and nanoparticles have aroused most interest.

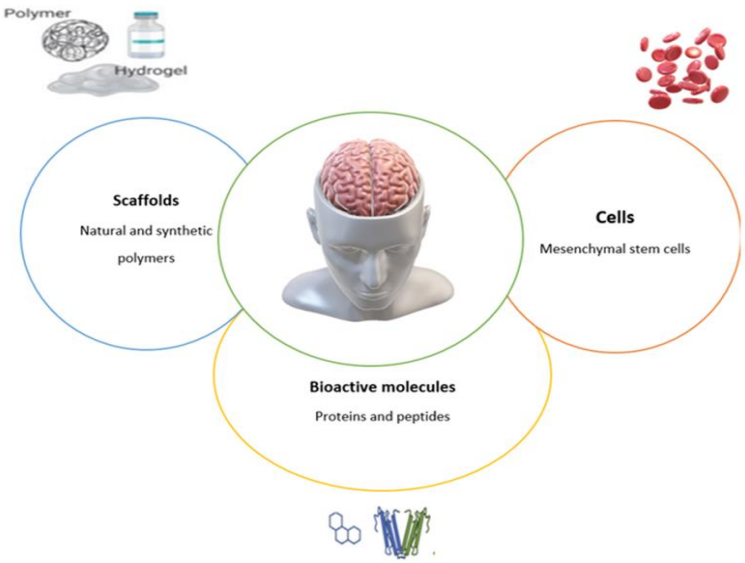

Figure 2. The schematic representation of the main participants in the neural tissue engineering process

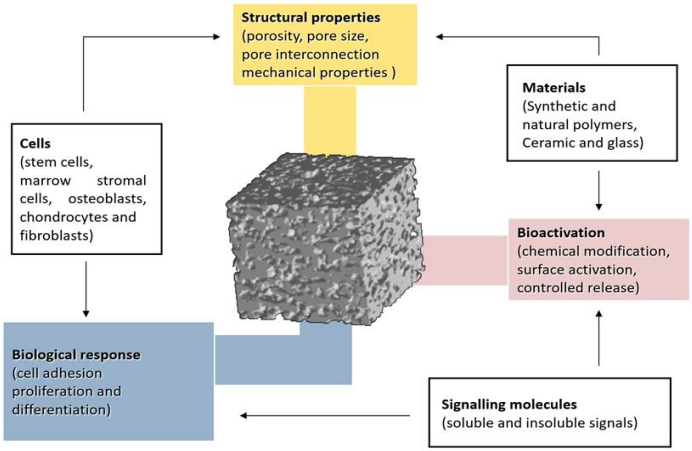

Figure 3. The relationship among molecules, cell-based materials in the case of scaffolds based on biomaterials for the neural tissue engineering [11].

The development of biomaterials normally means to provide a physical and permissive environment which strengthens or enhances axon development. There are two main areas to be focused on, i.e., the supply and upgrade of cell-based treatments, medication and bioactive particles, and also the control of the scaffold projects in order to manage neuritis growth.

The reconstituted biomaterial is produced using a variety of techniques which do not require compatibility [12,13]. Delivery is on-site and is useful for the application of the SCI / hemi transition model to animals and possibly to SCI human transition. Nevertheless, it will be more difficult to apply the prefabricated scaffold to the most clinically advanced ones. Injectable and viscous biomaterials can complement and tune the shape of SCI damage and can be less invasively interpretable for SCI.

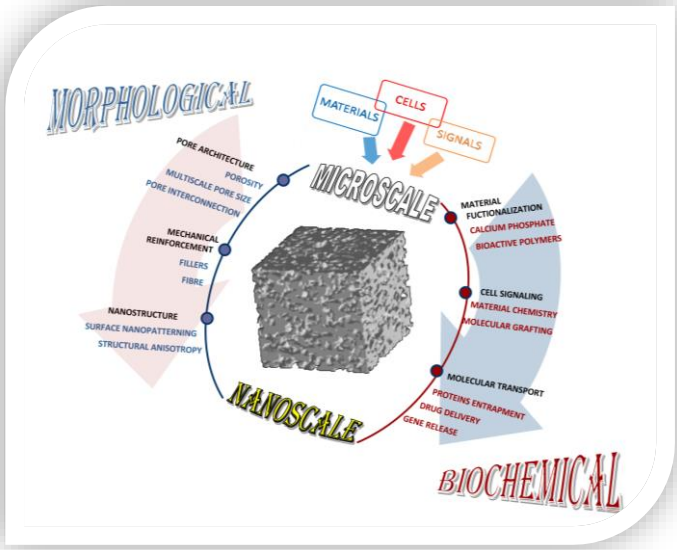

Figure.4. Correlations between the morphological and biochemical aspects at micro- and nano-scale in the case of scaffolds based on biomaterials for the neural tissue engineering [12].

To promote neural regeneration in an unfavorable environment, the scaffold must adjust cell adherence, cell proliferation migration and neuritis development, among which some are grouped together, events occurring during embryogenesis. Additionally, for an appropriate reform of the network, this must be performed in a 3D architecture.

To preserve cell functionality and promote neural circuits repair, the skeleton should facilitate the liquid flood and fuel the cell power, while removing metabolic residue. This also requires cells with appropriate synchronization and spatial display molecular guidelines to reach maturity and integration into the targeted cells. Consequently, an interconnected porosity framework consisting in sufficiently large and adequate pores ensures the proper operation of the surface for cell migration. Besides this, the physical support for cells and axons must be provided as physical features, as if it were the natural environment.

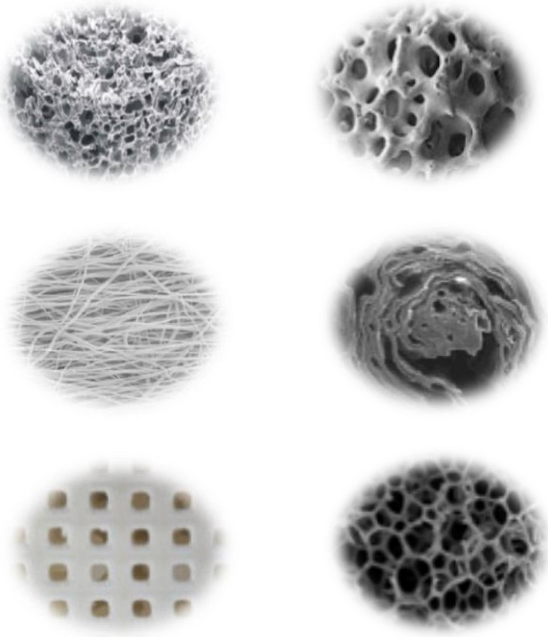

Figure 5. Various scaffold textures made by different biomaterials and processing techniques.

To overcome the traditional constraints of cell therapy, medication and bioactive molecules, biomaterials are widely used in the dedicated literature to offer these therapeutic agents. Many recent clinical studies have referred to the scaffold biomaterials used to release the cells as a material which can protect resistance to cell shear strength when injected through a needle and shield the cells from environment inhibition against damage, thereby improving implanted cells survival and functional recovery on animal models.

The brain's incongruence, frailty and complexity foster the design and development of biomaterials to regenerate neural cells. Although the biomaterial design criteria depend firstly on the latter's specific applications and aims, there are some possible basic requirements.

Nevertheless, if the biomaterials are used to repair the brain cells, they must be designed to be delivered in a minimally invasive way. Although the implant framework has been used in current studies, the enclosed position of the brain encourages the development of *in situ* injection-type scaffolds, also known as hydrogel, which can be implanted upon a minimally invasive surgery.

In addition, the biomaterials should be stable chemically and physically on long term and carry out the desired biological function, but should also be fully biodegradable, without any residue after having served the purpose [12]. Also, they should be long-term biocompatible with the host network, not with the basic material or any of the sort, and the degradation by-product should trigger an immunogenic response in the host. This is particularly important when synthetic biomaterials are used, liable to more complex degradation models. Finally, the biomaterials should be scalable to be produced on a large scale, to be finally released in the clinical practice.

Biocompatibility is an important feature, as it facilitates cell implantation, proper cell operation as well as skeletal cell migration and proliferation [13]. Bioactive molecules may be used to modify the surface of skeletons to create biocompatible materials. Bioactive molecules such as fibronectin, laminin, vitronectin, and short peptide sequences are protected biomaterials.

The alteration of the surface supports cell implantation and proliferation. The alteration of the groups of biomaterials is more useful

than that of the surface. In case the mass is modified, the peptides signal cell-integrates in the biomaterials. The implantation feature of the cell depends on the surface characteristics, e.g., umectability and charge density [14]. When met together, due to their biocompatibility, the toxicity profile also plays an important part in the implantation, growth, and proliferation of the scaffold cells.

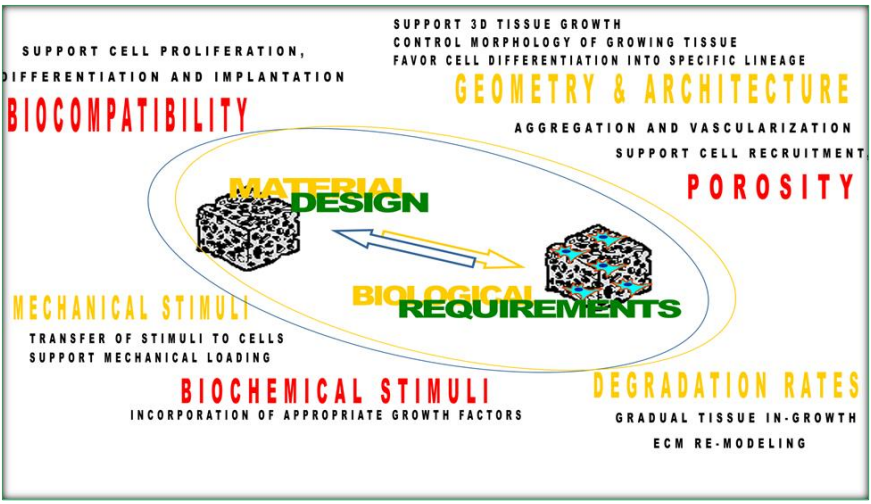

Figure 6. Design criteria for biomaterial-based scaffolds [11].

One of the most substantial advantages of bioabsorbable products is that they do not need to be surgically removed because they are absorbed by existing body tissues. [15]. For neural tissue engineering, the biodegradable skeleton is monitored, because the scaffold should support the neural cell growth. The latter are further broken down in the body during a subsequent repair. The biodiversity scaffold also favors the production of neighboring cells having their own extracellular matrix (ECM). Neuromas can also appear because of the cytotoxic effects. Biodegradability should also support removal of chronic inflammation [11, 13]. To reproduce the original network, the ideal scaffold should have the right shape and porosity [11, 12]. Both the scaffold and the surrounding tissues require high porosity and

sufficient pore size to promote cell recruitment, vascularization, and the aggregation of growth factors and nutrients [12].

Enzymatic degradation is another biomaterial degradation system, in which the biomaterial is degraded by organic chemicals found in the body. New enzymatically degradable biomaterials have been developed in response to slow progress in the design of polymers and hydrogels. Enzymatic degradation can be used for a variety of purposes.

Physical properties of biomaterials, such as pore topography, size and volume, structure architecture, and mechanical hardness, have been shown to play an important role in interactions between biomaterials and cell behavior [20]. Researchers now can design and produce biomaterials with desired nano topography or microtopography due to the availability of advanced manufacturing methods such as 3D printing. Aside from that, the availability of a variety of procedures and biosynthetic biomaterials enables the development of 3D and porous structures with variable mechanical hardness.

Pore size and architecture are important in the regeneration of other tissue types, in addition to bone technology. For neural regeneration, the built-up of neural networks there should be an additional network between the two severed nerves with sufficient porosity to support the nutrient supply to prevent external macrophages and fibroblast invasion. This necessitates a regeneration with a 50 percent higher porosity while retaining a flexible and resilient modulus of 8-16 MPa, identical to that of human nerves.

The rugosity of the biomaterial surface may be changed to induce cell proliferation, implantation, or differentiation. The rugosity of the biomaterial surface is essential for osteoblasts and bone technology in general to support implantation and differentiation from focal and adhesive complexes that accumulate ECM.

The mechanical properties of the scaffold should be like those of the tissue at the implantation site. Since this is not always possible, materials with mechanical properties that protect the cell from compression or tensile force without interfering with biomechanical replicas are used [14]. Polymeric nanofibers are particularly useful in this regard. Mechanical properties such as tensile modulus, resistance to

tensile, and shearing modulus have been demonstrated. This parameter has been observed to increase with the next parameter, due to a reduction in fiber diameter. Despite the underlying explanations, this phenomenon is still not clear; it is believed that the orientation of macromolecular chains has risen with the decrease of the fiber diameter, which further leads to a nanofiber of higher crystallinity. These unique mechanical properties facilitate the modulation of cell behavior and provides the power to the scaffold to resist the forces exerted by the cytoskeletal elements.

A selection of the best available biomaterials should be considered for a certain approach to the therapeutical agent, based on their physical, chemical, and biological properties and their interaction with the target network. As regards the brain cells repair, hydrogels and nanoparticles are beyond any doubt arousing the highest interest. Both biomaterials can be designed in keeping with the afore mentioned characteristics. This is not the whole picture of all available materials used in cell therapy or in medicine administration, but rather a combination of the benefits of using carefully designed biomaterials for regeneration purposes.

3. Scaffold biomaterials for neural tissue engineering

The biomaterial or material used for the scaffold assumes a significant role in tissue recovery. Apart from the characteristics of the biomaterial surface, the general design and architecture of the biomaterial can significantly impact cell behavior and tissue recovery. The construction of the pores of a framework can be a restrictive variable in the transport of supplement and general cell recruitment. The platforms designed with an insufficient pore structure have a restricted supplements flood, wasteful discharge, corrosion development from dissemination flaws. These features do not allow cell resistance inside the scaffold which favors cell recruitment at the surface level of the incorporated scaffolds.

In designing bone tissue scaffolds, previous research has shown the link between cell relocation and separation as regards the general pore size and width [12, 15]. Pore size and architecture, in addition to bone tissue structure, play an important role in the recovery of other tissue

types. The nerve control channels used to recover the neural tissue in the center of two severed nerves should have enough porosity to allow additional transport while preventing attack by external macrophages and fibroblasts while designing neural tissue [16]. This necessitates a combination of over half porosity, adaptability, and an elastic modulus of 8-16 MPa, like those observed in human nerves. To meet these requirements, some studies have led to the creation of highly permeable scaffolds that are completely compatible with pore properties [16, 17].

The chemical properties of biomaterials may influence their ability to recover target tissue in general. Cell growth, replication, and differentiation are all affected by the properties of a biomaterial surface, which vary depending on the sections of the surface and how they degrade. The aim of local research is to design and manufacture biomaterials using synthetic guidelines that promote cytocompatibility. Although there are different substances which have part of these features, this segment will be limited to the knowledge of the biomaterial surface, the degradation perspectives, and the way in which these synthetic signs influence cell activity and bone recovery.

The design of interfacial tissue, such as osteochondral tissue, for example, necessitates explicit pore construction to enable the recovery of two distinct tissue types while maintaining acceptability between the two layers. The distinction between cell types is especially evident in osteochondral tissue, where the scaffolds can support in the improvement of hard bone tissue, soft ligament tissue, and the interface between the two. The nature of monophasic, biphasic, and triphasic scaffolds has already addressed this problem [16]. Nevertheless, osteochondral scaffolds have been produced lately, with additional porosity and synthesis angles to speed up the recovery of bone or ligament tissue alongside an interface within a solitary scaffold [17, 18, 19]. In one design, a scaffold made from layers of polymer and gel coincides with an opposed proclivity design, in which the polymer layer supports the rigid one, and the gel layer precedes the cartilage one.

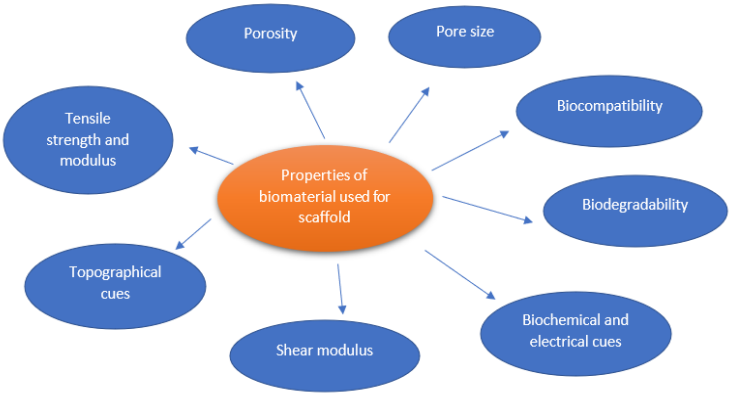

Figure 7. The schematic representation of the properties required from the biomaterials used in scaffolds

The tissue design systems often incorporate natural factors as guidelines for the progress and direction of ideal tissue development. These variables also include protein development factors, lesser marking particles which can select cells or reinvigorate cell proliferation and differentiation. Consequently, huge efforts have been made in tissue engineering to successfully use the growth factors related to biomaterials.

The biomaterials architecture and topography, the borders and pores included, can also impact non-differentiated cells implantation, proliferation, and differentiation. Moreover, the topographic guidelines can be used for cell adjustment and relocation control. As to neural differentiation, the topographic guidelines have been used time and again to coordinate the neuritis and axon growth. For example, NSC culture in lithographically designed areas influences neuron display and neuritis augmentation all along the area.

For a larger area, control over the biomaterial construction can be used to impose mathematical requirements on the non-differentiated organisms, which can also modify differentiation, thereby influencing the tissue engineering in which morphogenesis occurs.

Each scaffold is made by some procedures and has different morphological types. The same as in considering the mechanical properties of the scaffold to design brain tissues, it is imperative that the properties of its surface be optimized to support the endogenic or incorporated cells and to provide guided axon growth. Compromise related the weight and surface properties may require the progress of the scaffold by means such as biomolecule fusion and surface treatment techniques for improved bio recognition. The resulting areas will analyze different scaffolds and strategies to improve neural combination and recovery after implantation in the target area.

Identifying the organic structures that control both CNS and PNS has progressed over the last few decades. Because of their unmatched versatility, polymers have been frequently used in neural tissue design. The physical, significant, structural, and internal properties of each polymer change based on its application in 3D-cell culture, medicine transport vectors, hydrogels, neural channels, and scaffolds. Efficient polymer developments also provide structural support for neuritis growth and scarring retention, but also regulate biological guidance for axon development, advanced regeneration, and energizing implantation in existing tissue [11, 12, 13].

3.1. Scaffolds made from natural polymers

Scaffolds made from biomaterials and natural scaffolds are the two basic platforms used in CNS recovery. The two scaffold types have a 3D topological structure which can carefully mirror the local extracellular network (ECM). Despite this, although the scaffolds made from biomaterials are made from combined polymers or normal purified polymers, the organic scaffolds are usually mammal decellularized tissues [22]. Moreover, the scaffolds made from biomaterials are better than the natural ones, so that in certain situations related to design, biocompatibility, porosity, stiffness, their rate of degradation can be adjusted more efficiently and accurately [11, 12].

Considering the required design, as well as the physical and natural properties of the future tissues to be applied in CNS injuries, the scaffolds made from biomaterials used in CNS recovery can continue to be classified into hydrogels and biodegradable scaffolds.

Even though biomaterials have efficiently been used for repair and regenerative purposes in many conditions, diseases and tissues for many years, their usage at the brain level is still restricted. Biomaterial design for mental recovery has challenges of its own, due to the limited brain availability and its constraints for self-regulation, the presence of blood–brain barriers (BBB) and cell or practical complexity of the brain.

Biomaterials comprise a profitable technique for the heterogeneous area of neural cell implantation due to their variety and high tissue flexibility. The new expansion and production of biomaterials in the clinical area is due only to a small extent to the biomaterial used for each specific tissue, condition, and application.

The tissue implantation reaction interceded with the endogenic neurogenesis does not trigger any injury intrusion to replace the lost tissue. The tissue boundary undergoes a physical reaction which seals the injury and is expected to protect the tissue from the harmful effects of liquefactive necrosis. Unlike injury recovery, no substrate, e.g. a granulation tissue, is accessible in the affected area which can support synapse relocation to repopulate the tissue.

A proper substrate is required for cell support in the affected area. Almost the same as in foetal tissue transfer, this rule is provisionally illustrated by incorporating NSCs in the scaffold in an incision in the latter modelled by a blow. A subjacent scaffold accomplishment managed the costs of additional raw tissue development by NSC, although vascularization of this tissue was problematic. It was also noted that highly degradable particles produced a spider web-like tissue, which further created the undesired conditions to obtain a homogeneous tissue incorporated in the host.

Table 1. Some natural polymers proposed to be used for scaffolds in neural tissue engineering

Biomaterials	Method of fabrication	Properties
Chitosan	- precipitation method - surface modification	- Mechanical durability - injectability
Collagen	- freeze-drying - surface modification	- Biological properties

Biomaterials	Method of fabrication	Properties
		- porosity
Poly-lactic acid (PLA)	- injection molding - surface modification	-Hydrophilicity - porosity
Poly Lactic-*co*-Glycolic Acid (PLGA)	- precipitation method - surface modification	-Hydrophilicity - porosity
Poly (caprolactone)	- electrospinning - surface modification	- Biological properties - adhesion
Poly (Glycerol Sebacate) (PGS)	-Replica molding	- Biological properties
Poly (sialic acid)	- surface modification	- Biological properties

Interestingly enough, NSC implantation in a hydrogel made from ECM from the scaffold and in the brain tissue have contributed excellent cell resistance inside the tissue, at the same time producing homogeneous tissue mainly formed in the brain tissue. These studies have shown that a hydrogel addition to a bio scaffold is ideal for the brain tissue replacement. Hydrogel scaffolds quickly adapt to the injured spots topography if there is an accurate approach to RMN guided infiltration.

The extracellular grid has different capacities in the body. It offers primary and mechanical assistance to the tissues, supports cell transport, keeps the cells together, encourages cell correspondence so that cell recovery and wound repair can be performed daily and uninterruptedly [16, 19]. The specific polymers have advantages in scaffold design, insofar as they carefully mirror the macromolecules to which cells connect *in vivo*. In most situations usual polymers are used in neural tissue scaffold design for, as follows: collagen, hyaluronic acid chitosan, alginate, elastin, and gelatin.

Collagen has been used as a biomaterial in the development of neural tissue, and as a result, many collagen-based neural guides for

peripheral nerve recovery are available. For clinical testing in neural tissue architecture, collagen is currently the only biopolymer that has been authorized.

A fascinating use of collagen is disturbance, that is the utilization of type I attractively adjusted collagen, after the discovery of the collagen gel, by molding the latter in a high-resistance area as a filling material for collagen tubes. This technique was efficient in the case of minor injuries located in neural areas, controlling neuritis degree and Schwann cell interference both in vitro [24] and in vivo [25] and improving nerve recovery in a 6mm neural area in mice [23].

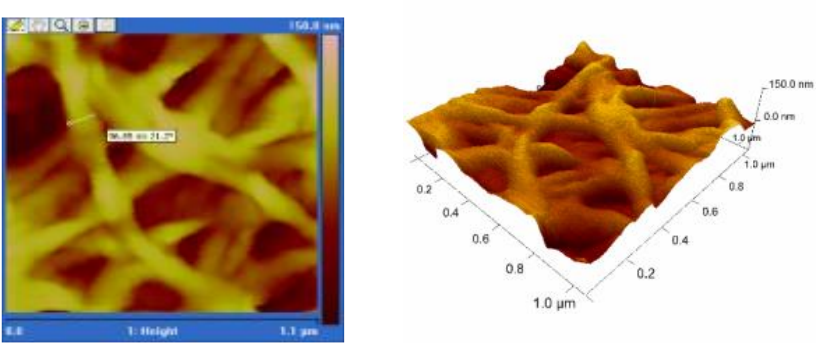

Figure 8. Collagen scaffold characterization using Atomic Force Microscopy: fibrils measurement (right); topography (left).

Fish collagen has received a great deal of attention as a possible replacement for bovine collagen. Fish collagen can be made from by-products of the processing of fish and invertebrates, such as skin, bones, and scales [60]. Fish collagen was chosen as a possible biomaterial because of its beneficial organic properties, such as exceptional biocompatibility, low antigenicity, unrivaled cell integration, and incredible biodegradability [26] Fish collagen scaffolds, including 2D or 3D, have considerable cell feasibility, comparable to bovine collagen, and have been used for both delicate and hard tissue applications. In any case, there has been practically no research on using fish collagen to develop neural tissue, and despite its promising aspects as a biomaterial, some research has shown that, although hydrolyzed fish

collagen predictions osteogenic and endothelial separation from non-differentiated stem cells species, it does not function as a neural activation factor [26]. 28 collagen types have been identified, and all can be described by a triple helicoidal structure [27]. Three interconnected alpha chains cover the collagen particles. The amino-corrosive group is named Gly-X-Y-, to glycine being essential in any third situation to enable collagen to form securely. 4-hydroxiproline is a collagen marker used in the post-translational process [29]. Collagen is a scaffolding material which corresponds to a wide variety of tissues; it is used in bone tissue, skin, cornea engineering, possibly for heart valve improvement, and possibly for other cardiovascular infections [11, 29]. Collagen's flexibility is due to the body's natural collagen dispersion. Low antigenicity, low cytotoxic reaction, biocompatibility, high water absorption, accessibility to certain segregation techniques from different sources, and the ability to adjust mechanical and transverse connection properties to the needs are all extremely valuable features of this architecture. Collagen 1 can be safely implanted in the body because few people are sensitive to it.

A simple serologic examination can also determine if use of this biomaterial would cause the patient to develop a hypersensitive response [30].. Phillips and co. designed a self-sorting collagen management conductor, which is a Schwann cell containing a pipeline that must be used on the injury spot inside the PNS. The incorporation was done to show the neuritis expansion in a separate dorsal-root ganglion and resulted in a more prominent recovery as compared to the previous methods [31]. Electrospinning, among other methods, is used to create collagen-based platforms. Collagen does not have a lot of mechanical or primary water in it. Collagen can be used in combination with other common polymers to change properties including mechanical resistance, porosity rate, compressive modulus, cell number, cell metabolic movement, e.g. Collagen domains have a variety of properties that make them ideal for scaffolds [11, 26].

Hyaluronic acid (HA) is a non-sterilized glycosaminoglycan made up of (-1, 4-D-glucuronic corrosive) and (-1, 3-N-acetyl-glucosamide). It is non-immunogenic and capable of implementing cells [32]. HA is used in cell development for a variety of reasons, most specific of those are

hydrogel scaffolds. Insofar as it offers biodegradability of hydrogels made from non-biodegradable materials, such as poly-ethylene-glycol, HA is one of the most important segments of hydrogels (PEG). It has an application for the treatment of osteoarthritis and the recovery of injuries. It is also used in the sensitive tissue substitution and has some indicative applications. It is associated to a symptomatic marker of malignity, rheumatoid articular inflammation, and some liver pathologies [33].

Similarly, it has been researched as a vector of medicine transportation via some routes, e.g. nasal, oral, aspiration, ocular, cutaneous and parenteral. The remarkable concentration of cells in diseases for which HA is used has equally been investigated [34]. Some benefits of using HA for scaffold building are its extraordinary biocompatibility, the high contents of water, its capacity to be corrupted into safe products, as well as its limited immunogenicity.

HA hydrogel has an extremely permeable structure, with interconnected pores, which permits food transportation, and cell, vein, and nerve penetration. The *in vivo* use of HA scaffolds has shown smaller glial healing, lower gliosis thickness and less positive GFAP cells around the scar area. The fact that cells do not adhere to the surface of HA is a weakness in its application. To address this problem, it is combined with other biomaterials that improve cell boundaries and help increase bone tissue recovery.

The HA-collagen scaffold [35] is one model that has physical properties for CNS recovery and advanced differentiation of neural stem cells (NSCs) that is needed for in vitro recovery. Another flaw of HA is that it dissolves in water, necessitating the addition of a reticula agent to help convert the HA into an injectable solution [36]. During one experiment, non-differentiated mesenchymal mice cells were cultured with a HA hydrogel that could be damaged by compounds released by cells.

One benefit of hydrogels resides in the fact that their mechanical properties can be adjusted to resemble those of the original tissues. This can encourage the exchange of mechanical stimuli to the cells, which matches the one in the local tissue. The mechanical properties of hydrogels are adjusted by guiding the reticula density. By supporting

neuritis development, differentiation, and expansion on various substrata, HA is a true advancement in neuronal regenerative medicine. HA hydrogels increase resistance rates and neural precursor multiplication, making them suitable for peripheral nerve regeneration and CNS restoration approaches [37, 38]. HA hydrogels have suitable mechanical properties that influence the selection of all who generate neurons, resulting in a new approach to neurodegenerative infection treatments [39].

Due to the comparative capabilities of the two biomaterials, HA can be correlated with other traditional biopolymers, most importantly collagen. Zhang et al., for example, used neural stem cells implanted in a HA/collagen stream to help rabbits recover from a neural 5mm-face injury [40]. The HA and chitosan composites were also helpful in the recovery of peripheral nerves. For the recovery of peripheral neural injuries, Xu et al. used an injectable biodegradable hydrogel chitosan/HA [41].

HYAFF is a hyaluronic acid-based product created by esterifying hyaluronic acid with benzyl alcohol. Biocompatibility, maximum degradability, dissolution in DMSO, stability to hydrolysis, efficient contact with polar atoms, and the ability to advance cell connections and the expansion of various cell types are some of HYAFF's strong points . HYAFF can also be used to configure films, gauze, bandages, tubes, and microspheres, while extending its applications. Bone implantation, managed drug release, nerve regeneration, and growth factor transmission are all possible applications.

As to cell implantation, the basic properties of hydrogels have many benefits as compared to other scaffold materials. Injectable hydrogels set an option by contrast to complex medical procedures, insofar as they are administered *in situ* to the brain as fluids and polymerase, in the relocated area. The main objective that calls for the use of scaffolds is the improvement of the practical character of the relocated cells. All things considered, biomaterials can improve different parts of the microenvironment, and are worthy of attention in certain domains. As cell transporters, hydrogels can represent a source for the controlled acquisition of growth factors, presenting the cells with an improved growth factor. Improvement of the microenvironment, i.e., the

implementation spot, by using hydrogels both as cells and growth factors, can significantly increase the relocated cells' resistance.

Artificial hydrogels are organically latent and consequently have fragile cell implementation. Anyway, artificial hydrogels are usually stable from the synthetic viewpoint and can be simplified for neural design applications. Hydrogels modified by tissue engineering avoid some disadvantages related to characteristic polymers, as a prevailing adjustment of the mechanical properties can be performed, while the absence of biological functionality can be reached by connecting peptides of cell cement and, in addition, by strengthening the common polymers.

The brain is protected by the skull, which makes it difficult to implant materials at this level. The materials applied in brain injuries are often incorporated with high accuracy. The usual materials, e.g. hyaluronic acid HA [42], collagen [143], chitosan and methylcellulose [44, 45], have been used to combine the hydrogels applied in such cases. Moreover, hydrogels have been demonstrated to diminish inflammation by decreasing inflammatory cytokine emissions [46]. These tools can support cells and axons to infiltrate in hydrogels and to continue to fix the harmed brain tissue. The same as in the case of hydrogels applied in SCI, the ones used in the brain can also be associated to practical peptides, such as IKVAV and RGD, to improve their cell implementation and the recovery effects of axons. Similarly, hydrogels can be modified to transport neutralizers or medication to improve recovery.

The use of biodegradable scaffolds and cell therapy in mental recovery is also a recently developed topic. Chitosan scaffolds are the best-known scaffolds used in brain injuries. Shi and co. designed a kind of mixed BDNF scaffold of chitosan to transmit mesenchymal stem cells with umbilical cord (hUC-MSC) by a drying method, through freezing. They discovered scaffolds can build the differentiation rate of NSCs and of the normal neural limit [47]. The *in vivo* interaction of the cells implanted in the brain is significant for the clarification of the implementation systems.

Chitosan is very biocompatible and non-cytotoxic; it induces antibacterial, antifungal, and antitumor movements [48]. Additionally,

chitosan is an adaptable biopolymer, prepared effortlessly in napkins, membranes, points, and scaffolds, and can be very well adapted for a certain application. Chitosan hydrogels have proved useful and reliable in neural tissue design, by supporting cell implementation, cell connection, cell resistance and neuritis growth [49]. In addition, 3D permeable chitosan scaffolds united with NGF have synergistically influenced the non-differentiated neural cells differentiation and shown potential to repair damage both in CNS [50] and in PNS [51].

Chitosan is often used to enhance the biocompatibility of polymers with improved mechanical properties. Antitumor treatment and growth factors have been successfully delivered to the CNS using nanochitosanic vehicles. Chitosan nanoparticles have also been engineered to transport restoring agents to the brain intranasally [52, 53]. Later, chitosan was developed as a new bio ink for neural applications and 3D printing of neural structures.

Gu et al. developed a bio ink cultured with non-differentiated human neural frontal cortical cells using a mixture of extruded chitosan, alginate, and agarose. 25% of the cultured cells died immediately after printing; however, cell expansion persisted, and 3 weeks later, an immunohistochemical examination indicated neuron regeneration [54].

Chitin is commonly found in the cell divisors of the different animal categories, e.g., insects, crabs, shrimps and is similar to the cellular mass of bacilli and parasites [55]. Chitosan is obtained by chitin deacetylation. The chitin deacetylation level is a subordinated measure. The deacetylation level along with the sub-atomic weight influences some properties such as solubility, mechanical resistance, and degradation. Chitosan evaluation as to its mechanical properties and transmission of growth factors has shown it is an excellent scaffold material [56]. Bone tissue design, skin tissue design, and other applications have been identified. Biocompatibility, biodegradability, inhibition of parasite, yeast, and microbe growth, and non-immunogenicity are some of the advantages of chitosan. Any neutralizer can be produced against chitosan because it needs any protein or lipid in its structure. Chitosan has also proven to be an effective recovery agent for neural tissue [57]. The chitin found in various materials prefers neural cells. In the case of

long incisions, chitin-based neural cameras may be used for serious neural recovery. A chitosan-based scaffold was used to repair a 50mm damage to the canine sciatic nerve.

The components of biodegradable scaffolds in the progress of brain recovery are mainly concentrated on their effects in improving support for microenvironments, axon growth and cell movement control. PCL-based scaffolds are considered the best in the recovery of the brain area. Wong et co. researched the link between the PCL scaffolds channel stream and cell implementation [58]. Their study discovered that the pores or channels displayed towards the parenchyma will increase astrocytic infiltration and that the microgrooves oriented to the ideal mode of cell movement, as well as the neural architecture will also be beneficial for recovery. In addition, Wong et co. discovered that the full interconnection channels for cell migration and tissue implementation can generate recovery.

Schwann cells can be implanted and relocated using the chitosan-based scaffold. This is important, because Schwann cells release neurotropic components, express neuro-explicit ligands, and direct neuritis development, all of which apply to the recovery of neural tissue. ECM is absorbed and maintained by Schwann cells. They also have the necessary mechanical resistance for successful neural recovery. Chitosan channels have produced myelinated axon growth and the efficient operation of the brain [59]. In the recovery of peripheral nerves, a chitosan-based scaffold pre-cultured with Schwann cells has been incorporated as a bio-mediated neural mixture. Yuan et al. discovered that Schwann cells and chitosan filaments do it splendidly [60]. In another research made by Ao, the chitosan stream cultured with stromal cells of the bone marrow (BMSC) was produced, deducted from Schwann cells. The results showed the significant viability of the stream in the treatment of basic neural injuries by sustaining nerve transmission, myelin recovery and myelinated axon recovery [61].

Alginate is a biopolymer derived from sea algae that is anionic in composition. It is particularly interesting in tissue design because of its biocompatibility, ease of gelation, and properties [62]. In either case, one of alginate's flaws is the daily existence of contaminants derived from its sea roots, such as base metals, endotoxins, proteins, and

polyphenol compounds. Therefore, alginate must be purified in an extraction system in several stages up to high immaculacy, to contain harming impacts, the immunogenic reactions to implantation included.

Alginate is used in a variety of biomedical applications, including medicine and protein transportation, injury treatment, and cell culture substratum. Alginate gels have proven to be extremely useful in tissue engineering, allowing veins, bones, ligaments, muscles, the pancreas, liver, and peripheral nerves to be restored.

Suzukia et co. also showed the way in which the non-tubular implantation solution using alginate supports peripheral neural injury recovery, and the fact that it can be successfully used as a regenerative method [62]. These discoveries were endorsed by Hashimoto et co., whose studies did not show electrophysiological or morphological differences between the alginate cylindrical constructs and the non-rounded ones used in neural recovery [63].

Alginate has recently been used to construct neural application matrices. The use of alginate in neural tissue architecture has shown promising results in the treatment of spinal cord injuries in rodents, where it became effective in repairing small neural holes (2-4mm) [64].

Because of their unique properties, elastin-based biomaterials have generated a lot of interest in tissue design. Elastin is a simple protein that has the characteristics of stability, self-collection, long-distance dependability, and organic action. Elastin is an ECM protein that gives tissues and organs flexibility and is abundant in organs where elasticity is essential, such as veins, flexible ligaments, the lungs, and the skin [65].

Elastin does not enjoy large-scale use in neural tissue design. ELPs have long been investigated for new matrices which play a role in medication transportation; promising applications have been identified in the containment of neuro-degenerative disorders. In this sense, elastin may have discovered a space in neural tissue architecture, and applications in the field of regeneration techniques may develop.

Gelatin is a hydrolyzed protein obtained by hydrolyzing collagen with an antacid or an acid. Because of its advantages, quality, high biocompatibility, and, most importantly, biodegradability, gelatin has been used safely in drugs, cosmetics, and food for a long time. Furthermore, gelatin is less antigenic than collagen since it is inhibited,

and its synthetically modifiable design allows for cell implantation modification and multiplication, thereby enhancing the action of a polymer after implantation [64]. Essentially, electrospinning mixtures of gelatin and other polymers have found to be effective in neural design applications. Electrospinning as a method of generating gelatin-based neural channels is advantageous because it allows for the enhancement and regulation of mechanical, natural, and motor properties. More specifically, electrospinning allows for orientation in the direction of the nanofiber, which is an important part of creating a functional matrix [66].

Gelatin combined with PCL helps develop the neural tissue and allows *in vitro* Schwann cell culture and multiplication [68-72]. Rodents with a 15mm hole in their sciatic nerve were treated with a PCL/collagen mixture enforced in a gelatin channel [67].The efficiently combined and PLA electrospinned gelatin leads to an increased differentiation into genealogies of the motor neurons and sustains neuritis growth. Gelatin is often reticulated with requires an ability, a non-toxic protein reticulation agent that enhances biocompatibility and consistency. An interesting application refers to electrospinned gelatin platforms reticulated with genipin as a stage in obtaining biochemical stress from the cells cultured in a decellularized neural ECM of rodents. This method demonstrated biocompatibility, cytocompatibility, and differentiation ability, as well as providing clear indications of tissue orientation toward neural precursor cell communication. To recover the peripheral nerve, Yang et al. created a direct biodegradable nerve stream containing gelatin reticulated with genipin and calcium phosphate particles. A short 10mm hole in the sciatic nerve of rodents was used to evaluate the duct, and histomorphometry evaluations verified its prevalence when compared to synthetic tubes [69, 70]. To increase the biocompatibility of polymeric matrices for bone tissue development, gelatin nanoparticles have recently been used.

Keratin is a polypeptide protein made up of various amino acids that has shown exceptional ability as a biomaterial and has a long history of use in the biomedical field due to its numerous functions. Keratin's ability to form matrices is related to its ideal biodegradability and, most importantly, its tolerability. Furthermore, keratin's organic properties

support cell implantation and replication, and its adaptable amino-corrosive architecture can be easily adapted to fit a particular tissue. Because of its biological properties that promote Schwann cell proliferation, keratin was one of the first biomaterials to show the ability to develop brain tissue [71].

Specifically, keratin-based hydrogels can achieve biocompatible constructions which support neural cell implantation and axon growth, at the same time being biodegradable. Different investigations showed the way in which keratin hydrogels support the *in vivo* rapid recovery of peripheral nerves, thereby improving movement, connectivity, and expansion of Schwann cells. The tests underway attempted to connect a larger neural hole. For instance, Lin et al. developed a keratin-based hydrogel that, when combined with PCL nervous guides, allowed a 15mm nerve root injury in a rodent model to be connected while maintaining Schwann cells and axon migration.

Silk has become a primary protein developed by silkworms and bugs that has unique properties that make it suitable for use as a biomaterial. Silk has exceptional mechanical resistance, biocompatibility, immunogenicity, bacterial implementation, and controllable biodegradability [72]. Silk is also a versatile material that can be used to make biocompatible structures, hydrogels, nanofibers, and matrices.

3.2. Scaffolds made from synthetic materials

Polymers have been considered by researchers for applications in the neural tissue and regenerative medications design. These polymers are beneficial for tissue engineering, considering that the design of their degradation depends on the simple hydrolysis and remains constant for every host tissue [73].

Biodegradable or non-biodegradable polymers may be used in neurological applications. While biomaterials containing methacrylate are not biodegradable in general, lactic, and glycolic corrosive polymers, PLA, PGA, and their co-polymer PLGA, are considered biodegradable, as are hydrogels, when considering the polyethylene glycol.

In the beginning, neural matrices were made from synthetic materials like those used for peripheral nerves fixation and skin recovery. Thanks to the progress in science and biomaterial innovation,

new materials have been found which re better matched for the neural environment [74].

The use of such polymers for neuronal tissue design is more favorable due to their resistance to compressive damage and adaptability strengthened by their capacity to adjust and adapt, insofar as their basic properties can be changed in different perspectives, by considering co-polymerization as well. Industrial polymers are also suggested with different production procedures, e.g., liquid casting, lyofilization and electrospinning. There are some basic issues in using design polymers. No matter if processed polymers are not harmful in practice, there are still worries as to the persisting harmful monomers resulting from fragmented polymerization, the same as plasticizers.

Polymers type *α-hydroxide acid* have been used as biomaterials for various biomedical applications. The main examples are poly-lactic acid (PLA), poly-glycolic acid (PGA) and their co-polymers (poly-lactic-co-glycolic acid PLGA). PLA and PGA are thermoplastic polymers described by polyester links, biocompatible and biodegradable, who could be hydrolyzed *in vivo*. They have been the first biopolymers tested for sensory tissue recovery, being recently used as an absorbent material for stitches [75] and sutures for laceration recovery [76]. PLA has been efficiently used in the design and manufacture of frameworks sustaining Schwann cells, allowing axon extension, and supporting vascular development [77]. Nevertheless, PLA matrices have proven unstable dimensionally or fundamentally: they usually break and fold. Similarly, PGA-based nano-pipelines have high mechanical properties, which favors them to be used in clinical environments, but they have been demonstrated to lose resistance 1 or 2 months after implantation [78]. The research work continues around PLA or PGA co-polymers, due to their high reliability.

PLGA has been used on a large scale in neural tissue design based on its qualities, porosity, growth, and degradation included, because they can be controlled by modifying the PLA:PGA ratio to match explicit applications, i.e., medication transportation particles and neural recovery. For example, PLGA multichannel matrices cultured with Schwann cells seemed to have a synergistic effect on neural recovery, but further investigations are expected to show even greater impact.

Polycaprolactone is a cost-effective biodegradable and biocompatible polymer with a wide range of applications, low toxicity, and excellent mechanical properties [79, 80]. It has been utilized in a wide range of tissues, including bone and neural tissue. Electrospinning has been used to make PCL filaments in the past [81]. Anyway, it was noticed that the manufacture of bioactive particles using natural solvents can induce cytotoxic effects when incorporated in the body.

Conductive polymers have been used for a wide range of applications, including condensers, adaptable electronic devices and organic light emitting diodes (OLEDs), but the absence of water solubility, the mechanical execution and the slow processing after polymerization have restricted their use for biomedical applications. Consequently, the conductive polymer composites have been designed to overcome a part of these constraints by improving solubility and degradation and, thereby, the 3D matrices for biosensors, medication transfer matrices, neural interfaces, and tissue design.

Polyprol (PPy) is a pyrrole monomer polymerized natural polymer that is one of the most used conductive polymers in neural tissue design. To increase biocompatibility, PPy is typically combined with other non-characteristic biodegradable polymers including PLA, PLGA, and PCL. PPY-PCL films have been developed to support cell growth and neuritis growth by electrical stimulation. In the end, a PPy-PDLLA nervous route was used to treat spinal cord injuries in rats, resulting in the best clinical outcome in terms of functional recovery. When associated with characteristic polymers, e.g. HA, PPy has been used to develop tridimensional electro-conductive hydrogels meant to improve recovery after injuries and traumatic stroke. Recently, the PPy immersion in plasma seems to reduce unfavorable response and to favor tissue regeneration.

Polyaniline (PANi) is a useful conductive polymer with a few attractive characteristics, including high conductivity, convenience of combination, and availability. A fundamental issue in use of PANi in neural tissue architecture, as with PPy, is its biocompatibility. PANi is often combined with more rational biodegradable polymers in this regard to minimize rash or immunogenic responses. Electroactive PANi or PLA-PCL fibers made by electrospinning have augmented neuritis

growth instigated by the NGF of PC12 cells and have shown extraordinary regeneration potential for nerves as a material.

Carbon nanotubes (CNT), graphene (G) and fullerenes are called carbon-based nanomaterials (CNM). Carbon nanomaterials contain sp2 reinforced carbon. Carbon-based nanomaterials fall into three types as to their size, such as zero- (fullerene-1985), uni- (CNT-1991) and bi-dimensional (graphene-2004). Carbon-based nanomaterials are attractive for different applications due to their new physical-chemical, optical, mechanical, and electric properties [82, 83]. Carbon-based nanomaterials are now focused on biomedical application and promising materials for neural engineering [84, 85]. They are used as materials for surface cover, neural support and regeneration, neuritis separation and growth [86]. Different types of nanocomposites and platforms are delivered using carbon-based nanomaterials for tissue design and regenerative medication, neural design included. Their application is restricted due to their physical-chemical properties [87].

Carbon-based nanomaterials are therefore promising materials for tissue design. Even so, cytotoxicity is a significant issue associated to their application. The toxicity level of carbon-based nanomaterials is difficult to follow, but it is more important to grasp carbon-based nanomaterials before their application in neural design. Several reports on their cytotoxicity are available.

Graphene is a carbon allotrope comprising a solitary carbon stratum in a bidimensional hexagonal cross section. It effectively guides heat and power, is bactericide and antiviral and is exceptionally biocompatible. Despite this, it is noteworthy that in the case of 2D and 3D use of graphene, network cells harmfulness has been reported [88, 89], the 3D networks being better for the development and multiplication of neural cells.

Graphene has been used in the construction of brain tissue in a variety of structures, including graphene foams and nano-networks. Graphene networks have been designed as 3D scaffold electric conductors which sustain and accelerate separation and proliferation of human neural fundamental microorganisms.

Table 2. Synthetic materials proposed to be used in the neural tissue engineering

Used synthetic materials & cells	Advantages	Disadvantages
PLLA & neural stem cells	- Biodegradability; - High porosity; - Varied distribution of pore size.	- Low biodegradability; - Early deterioration of the mechanical characteristics during degradation.
PLGA & neural progenesis cells	- Biodegradability; - Non-toxic.	- Plastic deformation
PCL & human mesenchymal stem cells	- Biodegradability; - Biocompatibility.	- Cytotoxic effects to the use of organic solvents
PPY & Schwann cells	- Good properties of biocompatibility and cell implementation; -Non-toxic; -Non-allergic.	- Insoluble; - Biodegradable; - low stability of the process.
PANI & human mesenchymal stem cells	-Versatility; -Conductivity; - High biocompatibility.	- Incapacity to degrade; - Chronic inflammation.
CNT & human embryo stem cells	- Higher conductivity; - Maintains the structural stability of the matrix.	- Cytotoxicity; - Non-biodegradable.

Carbon nanotubes (CNTs) are chemical allotropes with a tube-shaped construction and exceptional conductivity, as well as ideal mechanical and electrical properties. Because of their biocompatibility, conductive properties, and non-biodegradability, carbon nanotubes (CNTs) are a strong competitor for neuronal tissue architecture. CNTs

essentially operate as implants in situations where long-distance signals are required for neuritis development, such as in the recovery of the spinal cord or the treatment of neural injuries [90].

4. Cells used for neural tissue engineering

Mesenchymal stem cells are acquired in different areas of the human body tissue and proliferate efficiently *in vitro*. At the same time, their low immunogenicity and the versatility of the microenvironment qualify them for *in vitro* grafting [91]. Mesenchymal stem cells can turn into a main point for neural recovery and spinal cord injury recovery.

Schwann cells contain neuroprotective factors that cause neuritis to cells, which aids in the healing of neural injuries. During axon formation, Schwann cells play an important role. They are needed for the recovery of PNS injuries. N-cadherin, neutrophils, gamma ligands, Neural Cell Grip (N-CAM) particles, collagen, and lamina are all secreted by Schwann cells to produce ECM [92]. According to Rodrigues et al., the reaction caused by Schwann cells influenced the re-innervation interaction. Furthermore, allogeneic SCs did not provide the same results as autologous.

Olfactory cells (OECs) are glial cells which support the growth of olfactory neurons in well-evolved beings. These cells move through the glial scar tissue along the harmed targets, providing ECM and the neurotropic components necessary for nerve development and recovery. Research on OEC use in the injured human spinal cord is developing fast. The OEC continuous autologous graft in the injured human spinal cord spinal cord has shown positive results, with progress in the tactile and motor capacities. The successful use of OEC in the spinal cord recovery has encouraged different applications in the bionic engineering field. OECs cultured on or inside periprosthetic terminations are supposed to provide the microenvironment important to the undeveloped neural cells or to the local neural tissue to ensure resistance and foster cell division. The proof also advances that OECs can also help the development of neural cycles through the astrocitary scar tissue.

In situ, mammal OECs (ON) show a constant neurogenesis model. The task of OECs within the olfactory framework is to help the ON

recovery and development from the olfactory bulb unto the olfactory mucosa. Morphological similarities between OECs and astrocytes and Schwann cells are commonly noticed [97]. OECs have the interesting capacity to pass from CNS to PNS. In this way, the cells secrete neurotrophic factors and yield ECM, offering a proper environment for neuritis growth.

The morphology of olfactory cells changes to a great extent both *in vivo* and *vitro*. Inside a isolated culture, the morphology of these cells can differ, with an extended flat cytoplasm (Fig. 9, a-b), modelled on the axis of bipolar and starred cycles (Fig. 9, c-f) [97].

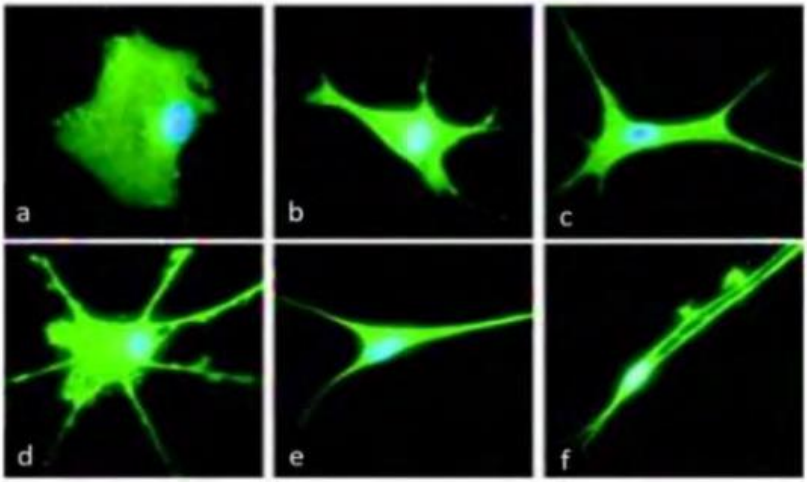

Figure 9. Variable OEC morphology. (a-b) extended flat cytoplasm, (c-f) fusiform [97].

OECs have been noticed to undergo sudden morphological alterations, the shape of the cell being affected by the present intracellular and extracellular atoms. Little can be perceived of the relationship between the distinctive morphological qualities of these cells and their useful properties. Among the various OEC morphologies, the antigenic behavior associated in-between the complementary astrocytes and the resulting tree were described, resembling the

Schwann cells. The OECs resulting from the trees showed more significant centralization of the neurotrophic receptor with low affinity (p75NTR), contrasted to the CEO complement subtype [97]. This cell form was also linked with the higher articulation of the connecting fibula-3 protein by OEC. *In vitro*, OEC was noticed to have several axes formed in serum-less media which are complementary to the serum.

Mesenchymal stem cells are glial cells that can differentiate into a variety of cell types and may thus be studied as an alternative to SC use. Such as it has multidirectional differentiation capacity, this cell type overcomes most of the disadvantages; additionally, it has numerous clinical benefits, such as ease of availability, emergence in a culture, and rapid implementation in the host tissue without fostering any rejection reaction.

Although mutated SCs are more productive than BM-MSC for axon recovery, BM-MSCs can be differentiated from Schwann cells (SLCs), which could entirely improve neural recovery. Anyway, BM-MSCs are also considered to have a lower differentiation limit as well as expansion potential, as compared to various MSC types. Studies have shown BM-MSCs differentiation into neural cell types *in vitro* in rodents.

Differentiation in a SC-like aggregate may be used to recover glial cell from stem cells from various sources. The SC stem cell type aggregate is differentiated by corrosive retinoic -mercaptoethanol, foetal serum, forskolin, human recombinant bFGF, growth factor of AA recombinant human platelets, and -1 recombinant human heregulin.

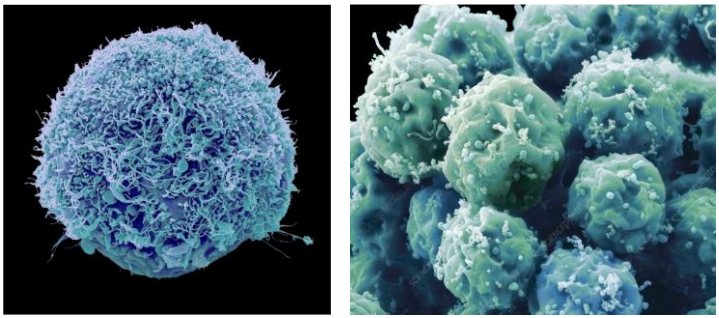

Figure 10. Human mesenchymal stem cells (left); human embryo stem cells (right)

The ECM proteins presence such as collagen, laminine, and fibronectin orientated proteins influence the recovery process. In addition, the expression of the neural growth factor (NGF), the glial cell line-derived neurotrophic factor (GDNF), the brain-derived neurotrophic factor (BDNF), the ciliary neurotrophic factor (CNTF) and neurotrophin-3 (NT-3) was represented by differentiated non-developed cells. SLCs obtained from the human umbilical cord blood mesenchymal cells (hUCBMSC) were examined as a seed for fixing the sciatic nerve. This type of cells sustains axon recovery and regional regeneration on the place of the sciatic nerve injury. The ECM discharged by this type of cells was also examined and proved the peripheral nerve fixation. Immature microorganisms are non-differentiated pluripotent cells picked from the human blastocyst having a huge multiplication limit.

The benefit of using these cells is that they are independent of disease symptoms and do not cause injury after extracted. Nonetheless, these stem cells are likely to be tumorigenic and immunogenic, and their use can cause valid questions. Treatments based on embryo microorganisms - paramount in some neurodegenerative disorders such as Parkinson's or Alzheimer's – are used [108]. Despite this, the fact that their application in neural tissue recovery is limited was considered and, consequently, mesenchymal precursors were identified. Neural immature microorganisms are intrinsically multipotent microorganisms which produce different cell types within the neural heredity, such as astrocytes, oligodendrocytes, etc. besides BM-MSC, immature mesenchymal microorganisms can be also obtained from the adipose tissue, fetal tissue, e.g. Although it was once thought that mesenchymal fundamental microorganisms could only differentiate from mesodermal cells, it is now known that they can differentiate in cell types not related to mesoderm. The contact test of markers of neural cells from disconnected human mesenchymal non-differentiated organisms was used as evidence [108]. The required non-differentiated pluripotent organisms are produced from substantial cells, e.g., fibroblasts, by bottom-up adjustment of the explicit quality's expression (Oct3 / 4, Sox2, c-Myc and Klf4), in these physical cells, it adopts pluripotency characteristics. This will cause pluripotency in

former physical cells and enable the patient to use his or her own cells, eliminating the risk of invulnerability to rejection. There are several ongoing studies that show iPSC differentiation in different types of neural cells.

Table 3. Cell types used for neural tissue engineering

Cell types	Graphic representation
Schwann cells	
Olfactory cells	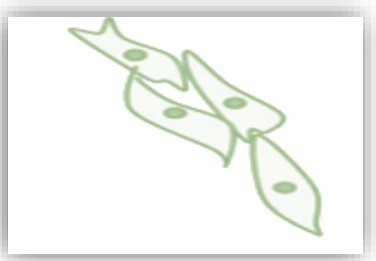
Mesenchymal stem cells	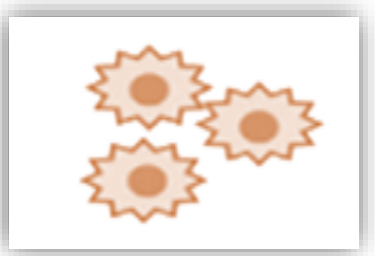

Cell types	Graphic representation
Embryo stem cells	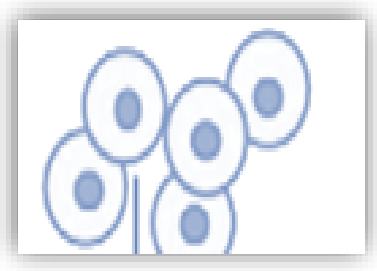

5. Bioactive molecules for neural tissue engineering

In the field of bone tissue development, peptide-based self-collecting systems (SA) have emerged in recent years, capable of replicating ECM conditions and providing a stage for drug transportation. Their nanostructures are constantly modified by physiological salts, and they are dedicated to self-collection in fluid environments. Their development is basic and effective, and it can be done with the help of machines to achieve high purities [99]. Bioactive ligands and drug discharge structures may be combined and coordinated by cells or tissues for a cautious and changed reaction due to comparative biophysical self-collection. One of the main advantages of SA systems is their ability to move naturally as individual atoms across the body, with the ability to assemble in critical locations made possible by their protection to concentrate in patches. When following an adequate plan, these atoms might have the option to go round the BBB and to accumulate as nano matrices in the significantly harmed brain spots [100]. This chapter is a survey of the SA peptide atoms used in neural tissue engineering applications, peptide ligands and drug used as neural impulses, and possible medication discharge schemes in pro-inflammatory neural cells and tissues, based on these advantages.

Numerous SA peptide nano-matrices have been studied over the last decade. The Stupp group cultured peptide amphiphiles (PA) and demonstrated their suitability for neural tissue engineering applications. Cell-based treatments were seen to reconstruct neural cells in the injured spot in a limited extent and to encourage intellectual

capacity. A type of matrices was conceived to offer a small artificial environment for resistance, improved cell expansion, etc. Hydrogels, SAPNS and nanofiber matrices were investigated for potential *in vivo* applications in the injured neural tissue maintenance, replacement, and recovery. Every platform variation has strong points as well as constraints which should be receptive to augment morphology, even bioactivity of the construction to advance cell implementation and tissue generation. Matrix bioactivity is paramount to enforce cell-to-network and cell-to-cell communication. This was achieved by connecting biomolecules, such as ECM proteins and trophic elements, to coordinate cell development and multiplication. It is beyond any doubt that matrices should exemplify key elements to sustain relocated cells survival and to hold cell coordination in the same way in which they approach some prospects of injury physiopathology by an individualistic methodology based on combination.

A bio-functional hydrogel or a self-assembling matrix may be inappropriate as to the plan. A modern half-matrix may rather be the key to the neural adjustment advance. As regards matrix improvement, research is still in the initial stages and more iterative work implying both *in vitro* and *in vivo* experiments is considered important before the clinical preliminaries. Nevertheless, the use of matrices in injured brain tissue recovery will probably be an achievable treatment option.

While the highest quality level for the brain injuries treatment is worth considering when the 5mm length is exceeded, it is supposedly the autologous neural unit. They present some weak points, including the limited accessibility of the joining tissue, the neuroma architecture, the spot of the cross nerve and, in some cases, the absence of useful recovery. Allogenic units have the obvious disadvantage of resistance loss. Fabricated matrices that copy the exact organic and material characteristics of the ECM cells in vivo are designed to overcome the disadvantages of these units. Polymer matrices express the qualified matrices materials due to the minimal adaptability of the polymer composition and design. In vivo and in vitro, matrices made of polymer biomaterials can be used to treat neural injuries. Degradation, corrosion, porosity, and other mechanical properties can all be

conveniently built into these polymer matrices to satisfy the in vivo characteristics of the tissue where they will be used.

Although the added development of such systems for the neural cells and tissues is still necessary, hydrogels offer a promising direction for tissue design and cell grafting, mainly in the brain in which the regeneration capacities are be restricted.

Biomaterial polymerization and degradation add to the hydrogel overall usefulness. These two measures are influenced by the compound qualities of hydrogel, which additionally sustain the mechanical and physical characteristics, the same as the general condition of hydrogel does. The properties of a designed hydrogel can be altered effortlessly to imitate the ECM of most body tissues, the brain included. We can conclude that these attributes will directly impact the material boundary to meet the requirements for which it was designed – no matter if it comes to medication delivery, cell summary for implementation, circuit recovery or a combination of these treatments.

6. Conclusions

The scaffold to be used should resemble the common tissue ECM and sustain the 3D cells scaffolds. To design an appropriate matrix for tissue regeneration, one must consider the tissue's mental, chemical, and material characteristics. The data that goes with the properties is based on a major basis, which is the choice of biomaterial for the application. The biomaterial is chosen in accordance with the previous matrix conditions.

Electrospinning has been the largest used technique for top scaffold manufacture, based on directed polymers and polymers such as PCL, PLA and PLGA. Also, these scaffolds can identify ECM design and, at the same time, can provide electric pulses to the scaffolds. Application of an electric improvement on a conductive substratum can sustain cell operation (cell proliferation and differentiation), refined on the matrix. Further research effects, both *in vitro* and *in vivo*, have highlighted that conductive biomaterials such as the scaffolds are promising possibilities for bone, muscle, nerve, heart, and skin tissue regeneration.

The ideal degradation pace is comparable to that of tissue regeneration, the same as in the case of other biomaterials in the

regenerative domain. The excessively fast or belated platform degradation can harm efficient tissue implementation or regeneration. *In vivo* studies are expected to evaluate different moments to decide the pace of material degradation to coordinate with the regeneration pace. Additionally, effects such as reaction and harmfulness to developed conductive biomaterials and individual components should also be accounted for.

Both in PNS and CNS, the unique spatial-temporal nature of the ECM synthesis and architecture helps to manage the numerous neural cycles by counting the cell movement, differentiation, and recovery. In this way, a better comprehension of the subjacent life structures and of the sensorial nano- or micro-environment systems is mandatory for an appropriate design planning. The connection between the chemical part and the usable design should be solved, along with a higher understanding of the topographic capacities of the surface. These days, neural scaffolds are mainly represented by highly fluid hydrogels, sensitive polymers which have similarities or similar properties to the neural tissue as well as high flexibility. The functionality of polymers manufactured by surface modification and neurotrophic factor implementation strategies has extended the use of scaffolds in the design of transportation and high-quality vectors to the CNS.

References:

1. Y.K. Choi, K.W. Kim, Blood-neural barrier: its diversity and coordinated cell-to-cell communication, Bmb Rep. 41 (2008) 345–352.
2. J.W. McDonald, V. Belegu, D. Becker, Chapter 64-Spinal Cord, in Principles of Tissue Engineering (Fourth Edition), Academic Press, 2014, Pages 1353-1373.
3. C.A. Kuliasha, B. Spearman, E.W. Atkinson, A. Furniturewalla, P. Rustogi, S. Mobini, E.B. Nunamaker, A. Brennan, K. Otto, C. Schmidt, J.W. Judy, Robust and Scalable Tissue-Engineerined Electronic Nerve Interfaces, Teeni), 2018, pp. 46–49.
4. T. Wang, M. Spector, Development of hyaluronic acid-based scaffolds for brain tissue engineering, Acta Biomater. 2009, 5(7), 2371-84.
5. H. T. Ghashghaei, C. Lai, E. S. Anton, Nat. Rev. Neurosci. 2007, 8, 141. doi:10.1038/NRN2074

6. C. A. Blizzard, M. A. Haas, J. C. Vickers, T. C. Dickson, Eur. J. Neurosci. 2007, 26, 1100. doi:10.1111/J.1460-9568.2007.05750.X
7. N. Leipzig, M. Shoichet, Biomaterials 2009, 30, 6867. doi:10.1016/J.BIOMATERIALS.2009.09.002
8. D. Nisbet, A. Rodda, M. Horne, J. Forsythe, D. Finkelstein, Biomaterials 2009, 30, 4573. doi:10.1016/J.BIOMATERIALS.2009. 05.011
9. C. E. Schmidt, J. B. Leach, Annu. Rev. Biomed. Eng. 2003, 5, 293. doi:10.1146/ANNUREV.BIOENG.5.011303.120731
10. Y. Zhong, R. Bellamkonda, J. R. Soc. Interface 2008, 5, 957. doi:10.1098/RSIF.2008.0071
11. Antoniac Iulian, Biologically Responsive Biomaterials for Tissue Engineering, Ed. Springer, ISBN: 978-1-4614-4327-8, 2013.
12. Filippo Causa, Paolo A Netti, Luigi Ambrosio, A multi-functional scaffold for tissue regeneration: the need to engineer a tissue analogue, Biomaterials, 28 (34), 5093-5099, 2007.
13. F.J. O'brien, Mater. Today 14 (2011) 88. [16] A. Subramanian, U.M. Krishnan, S. Sethuraman, J. Biomed. Sci. 16 (2009) 1.
14. A. Subramanian, U.M. Krishnan, S. Sethuraman, J. Biomed. Sci. 16 (2009) 1.
15. H. Patel, M. Bonde, G. Srinivasan, Trends Biomater. Artif. Organs 25 (2011) 20.
16. Nukavarapu SP, Dorcemus DL: Osteochondral tissue engineering: current strategies and challenges. Biotechnol Adv 2013 Oct, 31:706–721.
17. A Iulian, L Dan, T Camelia, M Claudia, G Sebastian, Synthetic materials for osteochondral tissue engineering, Osteochondral Tissue Engineering, Springer, 2018
18. Du Y, Liu H, Yang Q, Wang S, Wang J, Ma J, et al.: Selective laser sintering scaffold with hierarchical architecture and gradient composition for osteochondral repair in rabbits. Biomaterials 2017 Aug, 137:37–48.
19. Zhang B, Huang J, Narayan R J: Gradient scaffolds for osteochondral tissue engineering and regeneration [Internet] J Mater Chem B 2020.
20. Willerth SM, Sakiyama-Elbert SE. Approaches to Neural Tissue Engineering Using Scaffolds for Drug Delivery. Adv Drug Deliv Rev. 2007;30:325–38.
21. Ai J, Kiasat-Dolatabadi A, Ebrahimi-Barough S, Ai A, Lotfibakhshaiesh N, Norouzi-Javidan A, Sabero H, Arjmand B, Agayan HR. Polymeric Scaffolds in Neural Tissue Engineering: a Review. Arch Neurosci. 2014;1:15–20

22. A. S. Hofman, “Hydrogels for biomedical applications,” Advanced Drug Delivery Reviews, vol. 64, pp. 18–23, 2012
23. Ceballos D, Navarro X, Dubey N, Wendelschafer-Crabb G, Kennedy WR, Tranquillo RT. Magnetically Aligned Collagen Gel Filling a Collagen Nerve Guide Improves Peripheral Nerve Regeneration. Exp Neurol. 1999;158:290–300.
24. Dubey N, Letourneau PC, Tranquillo RT. Guided Neurite Elongation and Schwann Cell Invasion into Magnetically Aligned Collagen in Simulated Peripheral Nerve Regeneration. Exp Neurol. 1999;158:338–50.
25. Eguchi Y, Ogiue-Ikeda M, Ueno S. Control of orientation of rat Schwann cells using an 8-T static magnetic field. Neurosci Lett. 2003;351:130–2.
26. Yamada S, Yamamoto K, Ikeda T, Yanagiguchi K, Hayashi Y. Potency of Fish Collagen as a Scaffold for Regenerative Medicine. Biomed Res Int. 2014;vol 2014(Article ID 302932):8.
27. I Titorencu, MG Albu, M Giurginca, V Jinga, I Antoniac, V Trandafir, C Cotrut, F Miculescu, M Simionescu, In vitro biocompatibility of human endothelial cells with collagen-doxycycline matrices, , Molecular crystals and liquid crystals, 2010, 523, 1, 82-96.
28. T.Petreus, B.A.Stoica, O.Petreus, A.Goriuc, C.E.Cotrutz, I.V.Antoniac, L.B.Tudoran, Preparation and cytocompatibility evaluation for hydrosoluble phosphorous acid-derivatized cellulose as tissue engineering scaffold material, Journal of Materials Science: Materials in Medicine, 2014, 25 (4), 1115-11237.
29. R. Parenteau-Bareil, R. Gauvin, F. Berthod, Materials (Basel) 3 (2010) 1863.
30. Jafar Ai, Anahita Kiasat-Dolatabadi, Somayeh Ebrahimi-Barough, Armin Ai, Nasrin Lotfibakhshaiesh, Abbas Norouzi-Javidan, Hoshang Saberi, Babak Arjmand, Hamid Reza Aghayan, Arch. Neurosci. 1 (2014) 15.
31. J.B. Phillips, S.C.J. Bunting, S.M. Hall, R.A. Brown, Tissue Eng. 11 (2005) 1611.
32. J. Lam, N.F. Truong, T. Segura, Acta Biomater. 10 (4) (2014) 1571–1580.
33. A. Borzacchiello, L. Russo, B.M. Malle, K. Schwach-Abdellaoui, L. Ambrosio, Biomed. Res. Int. (2015) 2015.
34. S. Arpicco, P. Milla, B. Stella, F. Dosio, Molecules 19 (2014) 3193.
35. X. Wang, J. He, Y. Wang, F.Z. Cui, Interface Focus 2 (2012) 278.
36. S.M. Willerth, S.E. Sakiyama-Elbert, Adv. Drug Deliv. Rev. 59 (2007) 325

37. Pan L, Ren Y, Cui F, Xu Q. Viability and differentiation of neural precursors on hyaluronic acid hydrogel scaffold. J Neurosci Res. 2009;87:3207–20.
38. Liang Y, Walczak P, Bulte JWM. The survival of engrafted neural stem cells within hyaluronic acid hydrogels. Biomaterials. 2013;34:5521–9.
39. Seidlits SK, Khaing ZZ, Petersen RR, Nickels JD, Vanscoy JE, Shear JB, Schmidt CE.The effects of hyaluronic acid hydrogels with tunable mechanical properties on neural progenitor cell differentiation. Biomaterials. 2010;31:3930–40.
40. Zhang H, Wei YT, Tsang KS, Sun CR, Li J, Huang H, Cui FZ, An YH., Implantation of neural stem cells embedded in hyaluronic acid and collagen composite conduit promotes regeneration in a rabbit facial nerve injury model. J Transl Med. 2008;6:67.
41. Xu H, Zhang L, Bao Y, Yan X, Yin Y, Wang X, Huang Z, Peihu X. Preparation and characterization of injectable chitosan–hyaluronic acid hydrogels for nerve growth factor sustained release. J Bioact Compat Pol. 2016;32:146–62.
42. D. J. Cook, C. Nguyen, H. N. Chun et al., "Hydrogel-delivered brain-derived neurotrophic factor promotes tissue repair and recovery afer stroke," Journal of Cerebral Blood Flow & Metabolism, 2016.
43. J. Guan, Z. Zhu, R. C. Zhao et al., "Transplantation of human mesenchymal stem cells loaded on collagen scafolds for the treatment of traumatic brain injury in rats," Biomaterials, vol. 34, no. 24, pp. 5937–5946, 2013.
44. A. Richter, Y. Xie, A. Schumacher et al., "A simple implantation method for fexible, multisite microelectrodes into rat brains," Frontiers in Neuroengineering, vol. 6, 2013.
45. C. J. Rivet, K. Zhou, R. J. Gilbert, D. I. Finkelstein, and J. S. Forsythe, "Cell infltration into a 3D electrospun fber and hydrogel hybrid scafold implanted in the brain," Biomatter, vol. 5, p. e1005527, 2015.
46. M. Sirova, S. V. Vlierberghe, V. Matyasova et al., "Immunocompatibility evaluation of hydrogel-coated polyimide implants for applications in regenerative medicine," Journal of Biomedical Materials Research Part A, vol. 102, no. 6, pp. 1982–1990, 2014.
47. W. Shi, D. Nie, G. Jin et al., "BDNF blended chitosan scaffolds for human umbilical cord MSC transplants in traumatic brain injury therapy," Biomaterials, vol. 33, no. 11, pp. 3119–3126, 2012.
48. Crompton KE, Goud JD, Bellamkonda RV, Gengenbach TR, Finkelstein DI, Horne MK, Forsythe JS. Polylysine-functionalised

thermoresponsive chitosan hydrogel for neural tissue engineering. Biomaterials. 2007;28:441–9.
49. Valmikinathan CM, Mukhatyar VJ, Jain A, Karumbaiah L, Dasari M, Bellamkonda RV. Photocrosslinkable chitosan based hydrogels for neural tissue engineering. Soft Matter. 2012;8:1964–76.
50. Wang A, Ao Q, Cao W, Yu M, He Q, Kong L, Zhang L, Gong Y, Zhang X. Porous chitosan tubular scaffolds with knitted outer wall and controllable inner structure for nerve tissue engineering. J Biomed Mater Res A. 2006;79A:36–46.
51. Li G, Xiao Q, McNaughton R, Han L, Zhang L, Wang Y, Yang Y. Nanoengineered porous chitosan/CaTiO3 hybrid scaffolds for accelerating Schwann cells growth in peripheral nerve regeneration. Colloids Surf B Biointerfaces. 2017;158:57–67.
52. Raj R, Wairkar S, Sridhar V, Gaud R. Pramipexole dihydrochloride loaded chitosan nanoparticles for nose to brain delivery: Development, characterization and in vivo anti-Parkinson activity. Int J Biol Macromol. 2018;109:27–35.
53. Liu SH, Ho PC. Intranasal administration of brain-targeted HP-β-CD/chitosan nanoparticles for delivery of scutellarin, a compound with protective effect in cerebral ischaemia. J Pharm Pharmacol. 2017;69:1495–501.
54. Gu Q, Tomaskovic-Crook E, Lazano R, Chen Y, Kapsa RM, Zhou Q, et al. Functional 3D neural mini-tissues from printed gel-based bioink and human neural stem cells. Adv Healthc Mater. 2016;5:1429–38.
55. T. Ikeda, K. Ikeda, K. Yamamoto, H. Ishizaki, Y. Yoshizawa, K. Yanagiguchi, S. Yamada, Y. Hayashi, Biomed. Res. Int. 2014 (2014) 786892 (8 pp.).
56. M. Rodriguez-Vázquez, B. Vega-Ruiz, R. Ramos-Zúñiga, D.A. Saldaña-Koppel, L.F. Quiñones-Olvera, Biomed. Res. Int. 2015 (2015) 821279 (15 pp.).
57. S. Gnavi, C. Barwig, T. Freier, K. Haastert-Talini, C. Grothe, S. Geuna, Int. Rev. Neurobiol. 109 (2013) 1.
58. D. Y. Wong, P. H. Krebsbach, and S. J. Hollister, "Brain cortex regeneration afected by scaffold architectures: laboratory investigation," Journal of Neurosurgery, vol. 109, no. 4, pp. 715–722, 2008.
59. T.L. Yang, Int. J. Mol. Sci. 12 (2011) 1936.
60. Y. Yuan, P. Zhang, Y. Yang, X. Wang, X. Gu, Biomaterials 25 (2004) 4273.

61. Q. Ao, C.K. Fung, A.Y.P. Tsui, S. Cai, H.C. Zuo, Y.S. Chan, D.K.Y. Shum, Biomaterials 32 (2011) 787.
62. Suzukia Y, Taniharab M, Ohnishic K, Suzukia K, Endod K, Nishimuraa Y. Cat peripheral nerve regeneration across 50 mm gap repaired with a novel nerve guide composed of freeze-dried alginate gel. Neurosci Lett. 1999;259:75–8.
63. Hashimoto T, Suzuki Y, Suzuki K, Nakashima T, Tanihara M, Ide C. Review Peripheral nerve regeneration using non-tubular alginate gel crosslinked with covalent bonds. J Mater Sci: Mater Med. 2005;16:503–9.
64. Golafshan N, Kharaziha M, Fathi M. Tough and conductive hybrid graphenePVA: Alginate fibrous scaffolds for engineering neural construct. Carbon. 2017;111:752–63.
65. Daamen WF, Veerkamps JH, van Hest JCM, van Kuppevelt TH. Elastin as a biomaterial for tissue engineering. Biomaterials. 2007;28:4378–98.
66. Sill TJ, van Recum HA. Electrospinning: Applications in drug delivery and tissue engineering. Biomaterials. 2008;29:1989–2006.
67. Kriebel A, Hodde D, Kuenzel T, Engels J, Brook G, Mey J. Cell-free artificial implants of electrospun fibres in a three-dimensional gelatin matrix support sciatic nerve regeneration in vivo. J Tissue Eng Regener Med. 2017;11:3289–304.
68. Binan L, Tendey C, De Crescenzo G, El Ayoubi R, Ajji A, Jolicoeur M. Differentiation of neuronal stem cells into motor neurons using electrospun poly-l-lactic acid/gelatin scaffold. Biomaterials. 2014;35:664–74.
69. Yang YC, Shen CC, Huang TB, Chang SH, Cheng HC, Liu BS. Characteristics and biocompatibility of a biodegradable genipin-cross-linked gelatin/βtricalcium phosphate reinforced nerve guide conduit. J Biomed Mater Res part B: Appl Biomater. 2010;95:207–17.
70. Yang YC, Shen CC, Cheng HC, Liu BS. Sciatic nerve repair by reinforced nerve conduits made of gelatin-tricalcium phosphate composites. J Biomed Mater Res part A. 2011;96:288–300.
71. Hill PS, Apel PJ, Barnwell J, Smith T, Koman LA, Atala A, Van Dyke M. Repair of Peripheral Nerve Defects in Rabbits Using Keratin Hydrogel Scaffolds. Tissue Eng Part A. 2011;17:1499–505.

72. Kundu B, Kurland NE, Bano S, Patra C, Engel FB, Yadavalli VK, Kundu SC. Silk proteins for biomedical applications: Bioengineering perspectives. Prog Polym Sci. 2014;39:51–267.
73. Ratheesh G, Venugopal JR, Chinappan A, et al. 3D fabrication of polymeric scaffolds for regenerative therapy. ACS Biomater Sci Eng. 2017;3:1175–119.
74. Ricks CB, Shin SS, Becker C, Grandhi R. Extracellular matrices, artificial neural scaffolds and the promise of neural regeneration. Neural Regen Res. 2014;9:1573–7.
75. Lou CW, Yao CH, Chen YS, Hsieh TC, Lin JH, Hsing WH. Manufacturing and Properties of PLA Absorbable Surgical Suture. Text Res J. 2008;78:958–65.
76. Chong EJ, Phan TT, Lim IJ, Zhang YZ, Bay BH, Ramakrishna S, Lim CT. Evaluation of electrospun PCL/gelatin nanofibrous scaffold for wound healing and layered dermal reconstitution. Acta Biomater. 2007;3:321–30.
77. Farzamfar S, Esmailpour F, Rahmati M, Vaez A, Mirzali M, Garmabi B, Shayannia A, Ebrahimi E, Vahedi H, Salehi M. Poly-lactic Acid/Gelatin Nanofiber (PLA/GTNF) Conduits Containing Platelet-Rich Plasma for Peripheral Nerve Regeneration. Int J Health Stud. 2017;3:29–32.
78. Carriel V, Alaminos M, Garzón I, Campos A, Cornelissen M. Tissue engineering of the peripheral nervous system. Expert Rev Neurother. 2014;14:301–18.
79. H. Patel, M. Bonde, G. Srinivasan, Trends Biomater. Artif. Organs 25 (2011) 20.
80. S.L. Bechara, A. Judson, K.C. Popat, Biomaterials 31 (2010) 3492.
81. Y.S. Lee, T. Livingston Arinzeh, Polymers (Basel) 3 (2011) 413.
82. V. Georgakilas, J.A. Perman, J. Tucek, R. Zboril, Broad family of carbon nanoallotropes: classification, chemistry, and applications of fullerenes, carbon dots, nanotubes, graphene, nanodiamonds, and combined superstructures, Chem. Rev. 115 (2015) 4744–4822.
83. T. Vats, S. Dutt, R. Kumar, P.F. Siril, Facile synthesis of pristine graphene-palladium nanocomposites with extraordinary catalytic activities using swollen liquid crystals, Sci. Rep. 6 (2016).
84. C. Cha, S.R. Shin, N. Annabi, M.R. Dokmeci, A. Khademhosseini, Carbon-based nanomaterials: multifunctional materials for biomedical engineering, ACS Nano 7 (2013) 2891–2897.

85. R Guazzo, C Gardin, G Bellin, L Sbricoli, L Ferroni, FS Ludovichetti, Graphene-based nanomaterials for tissue engineering in the dental field, Nanomaterials 8 (5), 349, 2018.
86. A.M. Monaco, M. Giugliano, Carbon-based smart nanomaterials in biomedicine and neuroengineering, Beilstein J. Nanotechnol. 5 (2014) 1849–1863, https://doi. org/10.3762/bjnano.5.196.
87. A.M. Jastrzębska, P. Kurtycz, A.R. Olszyna, Recent advances in graphene family materials toxicity investigations, J. Nanoparticle Res. 14 (2012) 1320, https://doi. org/10.1007/s11051-012-1320-8.
88. Zhang Y, Ali SA, Dervishi E, Xu Y, Li Z, Casciano D, Birist AS. Cytotoxicity Effects of Graphene and Single-Wall Carbon Nanotubes in Neural Phaeochromocytoma-Derived PC12 Cells. ACS Nano. 2010;4:3181–6.
89. Song Q, Jiang Z, Li N, Liu P, Liu L, Tang M, Cheng G. Anti-inflammatory effects of three-dimensional graphene foams cultured with microglial cells. Biomaterials. 2014;35:6930–40.
90. Lee W, Parpura V. Carbon nanotubes as substrates/scaffolds for neural cell growth. In: Sharma HS, editor. Progress in Brain Research; 2009. p. 110–25.
91. D. J. Maltman, S. A. Hardy, S. A. Przyborski, Neurochem. Int. 2011, 59, 34
92. W.L. Fodor, Reprod. Biol. Endocrinol. 1 (2003) 1.
93. M.C.O. Rodrigues, A.A. Rodrigues, L.E. Glover, J. Voltarelli, C.V. Borlongan, Sci. World J. 2012 (2012).
94. S. Kyle, A. Aggeli, E. Ingham, M.J. McPherson, Production of self-assembling biomaterials for tissue engineering, Trends Biotechnol. (2009) 423–433.
95. S. Miar, A. Shafiee, T. Guda, R. Narayan, Additive manufacturing for tissue engineering, in: A. Ovsianikov, J. Yoo, V. Mironov (Eds.), 3D Printing and Biofabrication, Springer International Publishing, Cham, 2018, pp. 1–52
96. F.P.W. Melchels, J. Feijen, D.W. Grijpma, A review on stereolithography and its applications in biomedical engineering, Biomaterials 31 (2010) 6121–6130.
97. Vincent, A.J., A.K. West, and M.I. Chuah, Morphological plasticity of olfactory ensheathing cells is regulated by cAMP and endothelin-1. Glia, 2003. 41(4): p. 393-403.
98. Na Liu, Zhouping Tang, Zhiyuan Yu, Minjie Xie, Yu Zhang, Erfang Yang, and Shabei Xu, Morphological properties and proliferation analysis of olfactory ensheathing cells seeded onto three-

dimensional collagen-heparan sulfate biological scaffolds, Neural Regen Res. 2012 Jun 5; 7(16): 1213–1219.
99. C.J. Flaim, S. Chien, S.N. Bhatia, An extracellular matrix microarray for probingcellular differentiation, Nat. Methods 2 (2) (2005) 119–125.
100. G.S. Nowakowski, M.S. Dooner, H.M. Valinski, A.M. Mihaliak, P.J. Quesenberry,P.S. Becker, A specific heptapeptide from a phage display peptide library homes to bone marrow and binds to primitive hematopoietic stem cells, Stem Cells 22 (2004) 1030–1038

TELE-MEDICINE SOLUTION FOR NEUROSURGERY STUDIES AT LUCIAN BLAGA UNIVERSITY OF SIBIU

Prof. Dr. Eng. Remus Brad[1]
Dr. Adriana Săceleanu[2]

[1] Computer Science Department, Lucian Blaga University of Sibiu, Romania
[2] Faculty of Medicine, "Lucian Blaga" University, Sibiu

Contents

1. Introduction

Tele-medicine IT solutions have shown their viability, especially in the last year of the human existence, in which the direct interaction between human subjects was stopped by the absolutely necessary epidemiological barrier. For this reason, but also for the evolution distance learning facilities for teaching especially in the field of medicine, telemedicine solutions have proved their usefulness in universities around the world.

From a strictly medical point of view, a last-minute review of telemedicine practical instruments and applications was made by the authors of the paper [1]. Being an extensive and up to date material, one can observe the number of patients and how the interventions or consultations performed had an impact on the proposed telemedicine solutions. It can be seen that although neurosurgery has been less suitable for virtual interventions, in recent years, the share of medical interventions with IT and virtual support has increased. The same

conclusion can be drawn from the paper in [2], which emphasizes the same kind of applications in the post-COVID-19 era. The need for a strict and long-term isolation, characteristic of a pandemic like the one we are experiencing, means that both the solutions for surgical processes assistance, but also for university teaching, have a virtual component for distance teaching. The authors of a study from the pre-COVID-19 years highlight it in the paper [3], as well as the possibility of wider and long-term access to the procedures presented to students.

The 2019 ERASMUS + project "Brain Revealed: Innovative Technologies in Neurosurgery Study, BrainIT" aims to offer students from Lucian Blaga University of Sibiu, as well as those from partner universities among other medical related objectives, an e-Learning Platform for Telemedicine solution. In this sense, we started on the idea of integrating several requirements and functionalities in a telemedicine platform for students' use, both during the project implementation period and after that. Mainly, they were:

- web 2.0. features (discussion forums for the students; chatting functionalities, Ffacebook and twitter feeds)
- a role concept allowing the visualization of different types of content depending on the user role
- a network feature allowing users to work together on different tasks and topics
- streaming functionalities for the telemedicine applications in broadcasting surgical procedures

The implemented platform involved the creation of a dedicated hardware infrastructure, as well as a set of software applications. In the following, we will describe from a technical point of view the adopted solution, with the mention that it also involved certain physical, technical or financial constraints.

2. The hardware platform

The possibility of interactive and collaborative operation, but also the need to work with large series of students led to the implementation of the proposed solution on a dedicated hardware, namely a server from the HP family Proliant DL380G7 type. In order to be able to host the different application platform, but also due to the mentioned constraints, VmWare virtualization was employed for two operating systems. The e-learning solution was hosted on a CentOS Linux 7 architecture for the x86_64, and the streaming server on Windows Server 2016. The use of a virtualization environment allows an easier and scalable management of hardware resources but also the possibility of relocating them in the case of new needs or constraints, such as a large number of users or the existence of failures. The server was hosted in the consolidated Data Center of the university, with redundant power supplies, the possibility of replication on the redundant secondary site, as well as with redundant access to the computer network.

a) b) c)

Figure 1. Hardware components: a) HP Proliant server; b) Ubiquiti airMAX ; c) 25x optical zoom PTZ IP camera

a) b)

Figure 2. Ip streaming cameras positions in the OR; a) camera for close-up view; b) camera for general view of the OR

Because the Operating Room from which the live transmissions were expected to take place is located in the Sibiu Emergency Clinical Hospital, it was necessary to establish a point-to-point wireless connection between the hospital's and the university computer network. The relatively small distance between the two locations allowed us to use equipment from the Ubiquiti family, which could support the high traffic required for streaming, namely airMAX Nanostation LOCO M2 (figure 1). A VLAN from the university was transported in the hospital network, on which two PTZ IP cameras were connected in the operating room, a PC system for monitoring and controlling the rooms, and a large display for following the procedures in a room of the Neuro Surgery Department.

In order to achieve video transmissions, two cameras were positioned, with the possibility of adjusting remotely Pan Tilt Zoom, namely HIKVISION 4 MP type, 25x optical zoom. The two cameras were placed as shown in figure 2, one allowing the visualization of the operating field, above the operating table and having attached an omnidirectional ambient microphone. The second was intended to provide an overview of the operating room, with the ability to reorient

and zoom as needed. The two can be controlled from an adjoining room, so as to provide relevant images for the ongoing procedures.

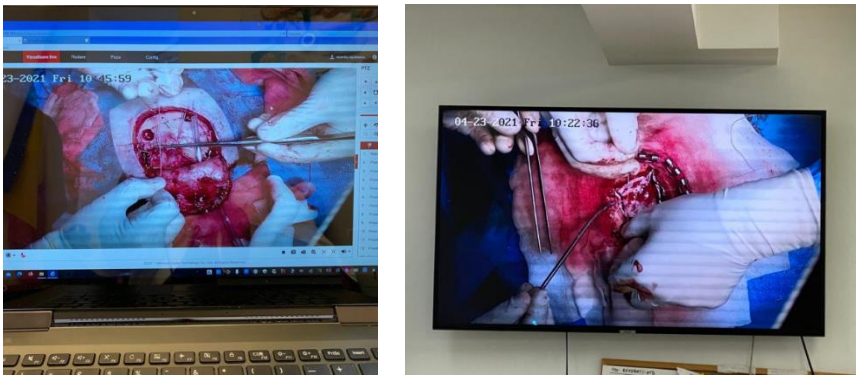

a) b)

Figure 3. Controlling the IP cameras: a) interface on a local desktop; b) remote view for side room students

For the groups of students accompanying the teachers on site, as well as to avoid entering the operating room, we opted for a display system connected to the IP cameras, located in the annex room of the Neuro-surgery Department, as can be seen from figure 3.

3. The software platform

In order to disseminate learning materials to the student, as well as to meet the requirements of the project, an e-learning platform based on Moodle Learning Management System v.3.7.2 [4] was implemented. Moodle provides the most flexible tool-set to support both blended learning and 100% online courses. Configure Moodle by enabling or disabling core features, and easily integrate everything needed for a course using its complete range of built-in features, including external collaborative tools such as forums, wikis, chats and blogs. It has been secured using various levels of access as well as by customizing the modules used to eliminate possible vulnerabilities. Modules needed to embed audio / video streams from your own server or YouTube have been added.

Because it was intended to be independent of public content sharing platforms, a Wowza Streaming Engine licensed server was installed [5]. The media server software is a robust, customizable, and highly extensible Java-based platform that powers live and on-demand single-bitrate and adaptive bitrate streaming to any device, anywhere. It takes over the two RTSP streams from IP cameras, transcodes the audio component from MP2 to MP4 for compatibility with most web browsers and supports a large and scalable number of clients. In this way, data streams can be created as pre-YouTube events or integrated into web pages or the Moodle e-learning platform, as can be seen in Figure 4.

The e-learning platform allows access on various levels of permissions to guest users, enrolled students, teachers and system administrators. Through it, course materials and announcements can be published; evaluation sessions can be carried out, as well as collaborative activities such as chat or conference, encompassing all the specific functionalities of such applications. An overview of its web interface is illustrated in Figure 5.

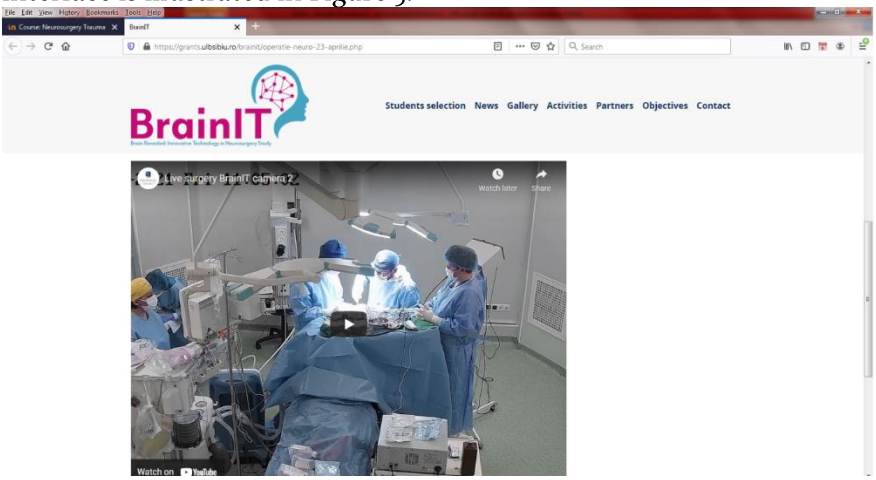

Figure 4. Embedded stream from the second camera on the webpage of the project.

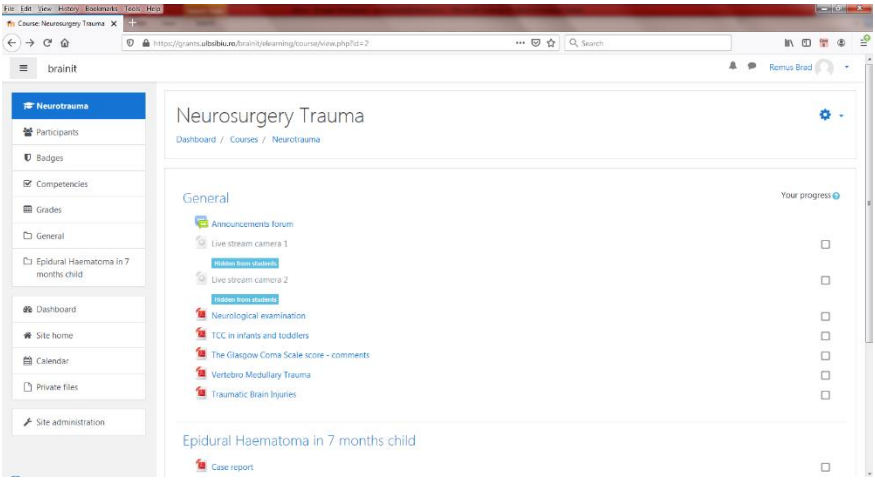

Figure 5. The e-learning platform based on Moodle.

4. Conclusions

Through the developed tele-medicine system, the following functionalities were achieved:

- Create a user-friendly online platform
- Employ the latest ICT technologies in teaching
- Telemedicine approach in the form of live-transmission
- Interactive teaching and training
- Access for graduates, residents and others medical personnel

Also, the use of the IP PTZ cameras in the Operating Room created the opportunity for distance learning teaching and provided an up-to-date way of streaming innovative neuro-surgery procedures during classes, webinars or other medical lectures. Using the local Wowza server of in combination with YouTube streaming live or premiere capabilities enabled a large number of features available in the current pandemic context.

References:

1. Daniel G Eichberg, MD, Gregory W Basil, MD, Long Di, BS, Ashish H Shah, MD, Evan M Luther, MD, Victor M Lu, MD, PhD, Maggy Perez-Dickens, MBA, Ricardo J Komotar, MD, Allan D Levi, MD, PhD, Michael E Ivan, MD, MBS, Telemedicine in Neurosurgery: Lessons Learned from a Systematic Review of the Literature for the COVID-19 Era and Beyond, Neurosurgery, Volume 88, Issue 1, January 2021, Pages E1–E12, https://doi.org/10.1093/neuros/nyaa306
2. Ashry, A.H., Alsawy, M.F. Doctor-patient distancing: an early experience of telemedicine for postoperative neurosurgical care in the time of COVID-19. Egypt J Neurol Psychiatry Neurosurg 56, 80 (2020). https://doi.org/10.1186/s41983-020-00212-0
3. Kim Y, Groombridge C, Romero L, Clare S, Fitzgerald M, Decision Support Capabilities of Telemedicine in Emergency Prehospital Care: Systematic Review, J Med Internet Res 2020; 22(12):e18959, https://www.jmir.org/2020/12/e18959
4. https://docs.moodle.org/310/en/About_Moodle
5. https://www.wowza.com/products/streaming-engine

CLINICAL EXAMINATION IN NEUROLOGY AND NEUROSURGERY

Roman-Filip Corina[1], MD, PhD,
Catană Maria-Gabriela, MD, PhD student[2],
Assist. Prof. Dr. Mircea Vicențiu Săceleanu[2,3]
Dr. Adriana Săceleanu[4]

[1] Department of Neurology, Faculty of Medicine, "Lucian Blaga" University, Sibiu
[2] Department of Neurosurgery, County Clinical Emergency Hospital of Sibiu, Romania
[3] Department of Neurosurgery, Faculty of Medicine, "Lucian Blaga" University, Romania
[4] Faculty of Medicine, "Lucian Blaga" University

CLINICAL DIAGNOSIS

1. **The clinical examination** of the neurosurgical patient always begins with the anamnesis which is most often given by the relatives due to changes in the patient's state of consciousness [1]. Both in the case of the anamnesis and in the case where the patient can give details, they must specify:

- The time of onset of the disease;
- The mode of onset (paroxysmal, chronic);
- Subjective complaints, if possible in evolution;
- Investigations and treatments performed [2].

If the patient is in a coma, there are no relatives who can give the details necessary for the anamnesis, then the next stage is the general clinical examination, the neurological examination (which is equal to the neurosurgical examination), the completion being given by paraclinical investigations [3].

2. **The stabilization** of the neurosurgical patient in the ER is the next step, special attention being paid to the stabilization of vital

functions in the case of patients with craniocerebral trauma or polytraumas, with monitoring of BP, pulse, respiration. Subsequently, the general clinical examination following the same scheme as for any condition shall be performed [4].

3. **Neurosurgical examination** is in fact a **neurological examination** intended to specify ***the level and location of the lesion*** **[5]**.

4. **Intracranial hypertension syndrome** (IH), typically occurs in brain injuries with neurosurgical implications and includes signs and symptoms more or less characteristic of neurosurgical disorders [6]:

a. ***The headache*** is progressive, at first episodic and moderate, later continuous and severe, more pronounced during the night and on awakening. Coughing and sneezing aggravate the headache and it does not yield to the usual painkillers. Mechanism of production: local edema, distortion of blood vessels around the tumor, stretching of the dura mater [7].

b. ***Vomiting*** usually occurs in the morning before breakfast, often being accompanied by headache, it is not preceded by nausea and it is explosive ("projectile vomiting"), often caused by a change in the position of the head, occurs more frequently in tumors of the posterior fossa [6, 7].

c. ***Papillary stasis***, appears at the FE examination, at the beginning - deletion of the nasal, upper and lower edges of the papilla, followed by the deletion of the temporal contour and the arteries form an arch at the papilla edge. In the advanced stages the papilla protrudes, the papillary contour disappears, exudates and retinal hemorrhages appear [7].

d. ***Altered consciousness***, **the most important neurological sign**, is directly related to the severity of trauma and consecutive brain injuries. It is evaluated and graded according to the Glasgow Coma Scale (CGS) (table no. 1), introduced by Jannet and Teasdale, following a study

performed on approximately 2000 patients with craniocerebral trauma. Thus they concluded that to establish the level of consciousness, the best parameters used are [7]:

- ***The best motor response***
- ***The best verbal response***
- ***The best eye opening response***

The obtained score correlates with the severity of the cerebral injury and with the prognosis.

The final GCS score or grade is the sum of these numbers, after which the patient is placed within certain limits, thus establishing the degree of consciousness impairment [8]:

- **GCS 15 points – defines the normal state**
- GCS 14 - 9 points - various degrees of consciousness impairment (confusion, obtundation, temporo-spatial disorientation)
- **CGS < 7 coma state**, the lower the score, the higher the brain suffering.

A GCS of 8 defines the boundary between coma and alertness. It should be noted that CGS is performed after resuscitation in the absence of sedation. If no motor response is obtained, a medullary section must be excluded [7, 8].

The closer the score is to 3, the greater the brain damage, and the deeper the location of the lesions. In patients with CGS score = 3 points, the lesions are located in the brainstem [8].

Glasgow Coma Scale

Eye Opening Response

- Spontaneous--open with blinking at baseline 4 points
- To verbal stimuli, command, speech 3 points
- To pain only (not applied to face) 2 points
- No response 1 point

Verbal Response

- Oriented 5 points
- Confused conversation, but able to answer questions 4 points
- Inappropriate words 3 points
- Incomprehensible speech 2 points

• No response 1 point

Motor Response
• Obeys commands for movement 6 points
• Purposeful movement to painful stimulus 5 points
• Withdraws in response to pain 4 points
• Flexion in response to pain (decorticate posturing) 3 points
• Extension response in response to pain (decerebrate posturing) 2 points
• No response 1 point

e. *Psychiatric disorders* outline a neurasthenic picture, a confusional syndrome. Temporo-spatial disorientation (sometimes the patient urinates in the hospital room), apathy, mental slowness and stupor may occur [7, 8].

f. *Seizures*, more frequent focal seizures, sometimes with secondary generalization, may precede the appearance of a tumor by months or years, especially in benign tumors. Epileptic seizures at onset, especially in the elderly, must be neuroimaging investigated (CT, MRI) [6, 7].

Cerebral herniations include subfalcine herniation, temporal lobe herniation, tonsillar herniation, upper herniation of the cerebellar culmen. Cerebral herniation appear as a complication of IH syndrome. The following forms are described [9]:

➢ *Subfalcine herniation*, through which the central part of the frontal or parietal lobe is pushed under the cerebral falx to the opposite side.

➢ *The temporal lobe herniation* is due to the thrust of the uncus and the hippocampal convolution between the free edge of the cerebellar tentorium and the cerebellar peduncles. The result is compression of the brainstem. The first symptom is represented by the involvement of the common oculomotor nerve with ipsilateral pupil dilatation, diminished pupillary light reflex and palpebral ptosis [8, 9]. The state of consciousness deteriorates rapidly, and in a few hours the coma sets in. Homolateral hemiplegia (Ectors syndrome) frequently occurs due to compression of the cerebellar peduncles at the edge of the cerebral falx

on the opposite side. The nape of the neck becomes stiff, signs of stiffness appear through decerebration (pronation and extension of the upper limbs occur with pain stimuli). Respiratory disorders (Cheyne-Stokes, deep breathing), hyperthermia, hypertension attacks and bilateral pyramidal signs appear [9].

Finally, as the cerebral sufferings spread across the bulb, apnea, tachycardia and cardiac arrest occur.

➢ The *herniation of the cerebellar tonsils* is due to the inferior displacement of the cerebellar tonsils in the foramen magnum. The appearance of the pressure cone can be bilateral (in central supratentorial tumors or massive cerebral edema) or unilateral (cerebellar lobe tumors). Clinically there is a stiffening of the nape of the neck with abnormal positions of the cephalic extremity (torticolis, retrocolis), the appearance of tonic contractions of the upper limbs with their extension and internal rotation, respiratory and cardiac disorders (bradycardia, tachycardia) and loss of consciousness [6, 9].

➢ *Upper herniation of the cerebellar culmen* appears in the tumors of the posterior fossa producing a suffering of the tectal region of the mesencephalon. It occurs in the paralysis of the conjugated upward movements of the eyes (Parinaud syndrome), decreased pupillary light reflex and hearing disorders due to the suffering of the inferior quadrigeminal colliculus [7, 8].

5. **Signs of meningeal irritation** may occur if pathogenic substances enter the CSF: micro-organisms (infections), red blood cells (cerebral hemorrhages, CCT), chemicals (myelography). Characteristically there is photophobia (the patient does not open his eyes because the light bothers him), the stiffness of the nape of the neck, the flexion of the head being painful or limited (figure no. 1) (**the maneuver is NOT performed in case of suspicion of cervical spine injury**). The Kernig and Brudzinski signs complete the clinical picture in the case of meningeal irritation syndrome [9].

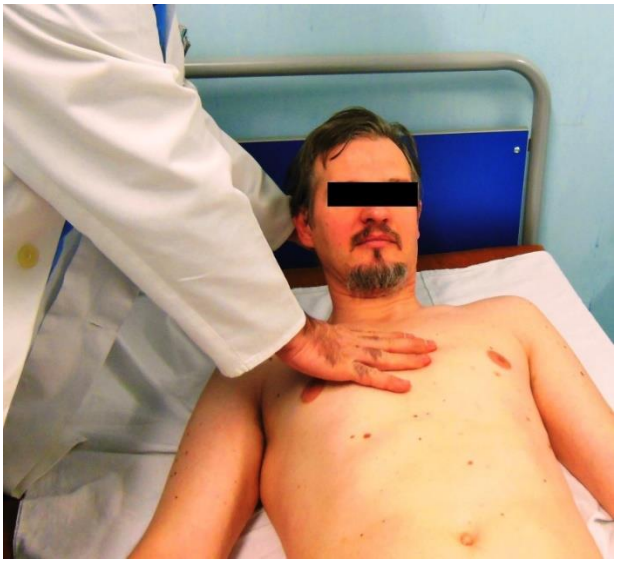

Figure 1. Kernig sign (own collection)
(Personal collection of dr. Vicențiu Săceleanu)

6. Particular positions, antalgic scoliosis, patient in lateral decubitus with hyperextension of the neck and flection of the knees, ceremonial attitude of the head, decerebration, decortication, determine particular positions of the extremities being often suggestive for a certain pathology such as slipped disc, meningeal syndrome, posterior fossa tumor, deep coma [5].

7. **Walking and orthostasism** are also characteristic of certain conditions [3, 4, 6]:

a. Equin gait, in disc herniation with external popliteal sciatic nerve paresis;

b. Spastic gait, in spastic paraparesis;

c. Mowing gait, in motor deficits on a hemibody;

d. Drunken gait, in cerebellar lesions;

e. Broad-based gait in cerebellar-vestibular disorders;

f. Impossible orthostatism in severe motor deficits.

8. **Cranial nerves**, each is examined and the results obtained are recorded separately [10].

I Opthalmic nerve

It is a sensitive nerve and is represented by the axons of the sensitive cells in the nasal mucosa from where it receives the odor impulses that it transmits to the cerebral cortex. It does not belong to the brainstem.

The olfactory function is examined with the eyes closed, separately for each nostril (figure no.2). Substances with known odors (coffee, tobacco, perfume) are used. Devices called olfactometers are used for objective determinations (olfactory threshold, olfactory discrimination) [10].

The terminology used in olfactory disorders is represented by:

- *Hyposmia*, which defines a diminished sense of smell;
- *Parosmia*, which consists in misinterpretation and confusion of odors. Occurs during pregnancy, psychiatric disorders (neurosis, psychosis), drug intoxication (ephedrine), drug use;
- *Cacosmia*, represented by the perception of unpleasant odors, often foul-smelling. It often appears as an aura in temporal epileptic seizures (uncinate);
- *Hyperosmia*, characterized by an increase in olfactory sensitivity. It can be encountered in the first trimester of pregnancy, estrogen treatments, mental disorders (neurosis), hyperthyroidism, migraine;
- *Anosmia*, in which there is a lack of olfactory sense. It may appear in:

- nasal disorders, which prevent the access of air flow to the olfactory area (acute and chronic rhinitis, attrophic rhinitis, septal deviations, polyposis, nasal turbinates hypertrophy, nasal allergy)
- conduction pathway disorders in olfactory meningioma or craniocerebral trauma (due to rupture of the olfactory nerve in the cribriform plate of the ethmoid bone or contusion of the olfactory bulb)
- rhinencephalon diseases due to viral meningoencephalitis (especially influenza, but also herpes, diphtheria, epidemic mumps, etc.) or tumors in the basal area of the frontal lobes
- other causes: diabetes, uremia, leukemia, sarcoidosis, Paget's disease, intoxication (cocaine, lead poisoning, smoking, ephedrine), hypovitaminosis A [9, 10].

➢ *Olfactory hallucinations*, represented by objectless perceptions, usually in the form of cacosmia.

They most often occur in uncinate epilepsy (with an olfactory aura) or mental disorders (psychosis, chronic alcoholism).

II Optic Nerves

They are sensory nerves and originate in multipolar neurons in the retina and transmit the impulse caused by visual excitations to the cortex [11].

➢ Visual acuity is examined using an optotype, before and after lens correction and before using mydriatics.

In the clinic, an approximate assessment can be made by asking the patient to count the fingers or to recognize the examiner's hand at different distances [10, 11].

- amblyopia represents a decrease in visual acuity
- peripheral blindness or amaurosis means total loss of vision. The differential diagnosis is made with cortical blindness in which the patient is not aware of the disease, EF examination is normal, the puppilary light reflex is present and alpha waves are missing on the EEG.
- nyctalopia reveals decreased visual acuity during the day
- hemeralopia refers to loss of visual acuity during the evening. It occurs in vitamin A deficiency, retinitis pigmentosa, chorioretinitis, etc.
- dyschromatopsia indicates color vision disorders (eg color blindness).

➢ *The visual field* is examined in the clinic asking the patient, with his gaze fixed forward, to mention the appearance in the visual field of two fingers moving from the side to the medial. Examine separately for each eye, then with both together. The correct and objective determination of the visual field is done with the help of the campimeter [9].

Visual field defects consist of:

- peripheral blindness or unilateral amaurosis (occurs in lesions of the optic nerve)
- hemianopsia (pierderea unei jumătăţi a câmpului vizual). Se împarte în:

- vertical when it affects the temporal or nasal half of the visual field. It can be heteronym bitemporal or binasal (in lesions of the optic chiasm) or homonymous (on the same side, right or left) in retrochiasmatic lesions (which may occur in the optic tracts, lateral geniculate bodies, optic radiation of Gratiolet or occipital cortex)
- horizontal with loss of vision in the lower or upper half of the visual field (in lesions at the level of the calcarine sulcus in the occipital lobe) [9]

- quadranopsias (loss of vision in a quarter of the visual field). They occur in incomplete lesions of the optic pathways located retrochiasmatically. They can be in the lower, upper, nasal or temporal quadrant [10]
- the scotoma represents a partial deficit of the visual field. Occurs in retinal lesions (chorioretinitis) or lesions of the optic nerve (MS) [10]
- concentric narrowing of the visual field (resulting in "tunnel" vision). Occurs in pigmentary retinopathy, glaucoma, retrobulbar optic neuropathy, optochiasmatic arachnoiditis, hysteria, MS [11].

III, IV, VI Oculomotor nerves

They are motor nerves and have their origin in the cerebral peduncles, activating a part of the eyeballs muscles (superior rectus, inferior rectus, medial rectus, inferior oblique) and raise the upper eyelid (figure no.3) [11].

Oculomotor nerve III

From a clinical point of view, the following are distinguished:

- complete paralysis, when all the innervated muscles (extrinsic and intrinsic) are involved
- incomplete paralysis, when one or more muscles (extrinsic or intrinsic) are involved [10].

Complete paralysis of the oculomotor nerve

The clinical picture is characterized by:

- complete palpebral ptosis. Compensatory there is the wrinkling of the forehead and extension of the head. The eyelid is hypotonic and can be easily lifted by the examiner (differential diagnosis with blepharospasm, in which there is a resistance to eyelid lift)

- divergent strabismus, found in the passive lifting of the upper eyelid, consists in the deviation of the eyeball outwards and downwards (by the compensatory action of the lateral rectus and superior oblique)
- horizontal and heteronymous diplopia (the false image is located on the opposite side of the paralyzed eye). The patient has a tendency to turn his head towards the healthy side
- fixed mydriasis, dilated pupil does not react to light, accommodation or convergence [12].

Incomplete paralysis of the oculomotor nerve

It may involve one or more muscles. The most common is medial rectus paralysis. It consists in limiting or abolishing the adduction of the eyeball with divergent strabismus. Diplopia is horizontal, heteronymous and accentuated when trying to look at the healthy eyeball. Progressive injury of the oculomotor nerve after passing through the dura mater to the base of the skull usually begins with ptosis, followed by motility disorders of the eyeball. In central, nuclear lesions, the rule is reversed, the ptosis appearing last ("eventually the curtain falls") [9, 11].

Etiology

➢ *Troncular paralysis* includes diseases that damage the nerve along the path from the exit of the brainstem to the eyeball:

- basilar skull fractures
- inflammatory processes (meningitis TB, lues, diphtheria, botulism)
- inflammatory-allergic processes (eg Fischer's syndrome, a cerebral form of polyradiculoneuritis characterized by the triad of ophthalmoplegia, ataxia, osteo-tendon areflexia)
- tumors of the base of the skull
- arterial aneurysm (infraclinoid carotid aneurysm, posterior communicating artery)
- cavernous sinus syndrome (in addition to oculomotor nerve damage, there is also paresis of IV, V, VI nerves, exophthalmos and possibly fever)
- neuromuscular junction diseases (myasthenia gravis) [10].

➢ *Nuclear paralysis* can occur in:

- vascular diseases (Weber syndrome)
- MS
- tumors (brainstem glioma)
- encephalitis (Gayet-Wernicke's superior hemorrhagic encephalitis, more common in chronic alcoholics).

Pathetic nerve (trochlear) paralysis, IV.

The pathetic (trochlear) nerve provides the innervation of the superior oblique muscle. Its paralysis results in the lifting of the eyeball and its slight rotation outwards. The result is a homonymous vertical diplopia that appears when looking down (observed especially when descending stairs).

The etiology is given by multiple sclerosis, stroke of cerebral peduncle, basal meningitis (TB, syphilis, pneumococcus), craniocerebral trauma [12].

External oculomotor (abducens) nerve palsy, VI

It is characterized by limiting the abduction of the affected eyeball. From a clinical point of view it results:

- horizontal homonymous diplopia
- convergent strabismus
- compensatory rotation of the head to the affected side.

Etiology

- CCT with basilar skull fracture
- brain and skull base tumors
- MS
- basal meningitis
- cavernous sinus syndromes
- protuberant strokes
- Gradenigo syndrome, which occurs especially in children with inflammatory processes in the petrous temporal bone (most commonly after otitis). It is characterized by paralysis of the abducens, hearing loss, pain in the ophthalmic territory of the trigeminal [13].

Conjugate gaze palsy

- *Lateral gaze palsy*

- superior Foville syndrome, due to the involvement of the cortico-oculogyr tracts above their decussation in the cerebral peduncle. Due to the abolition of the voluntary lateral gaze towards the

paralyzed limbs, a conjugated deviation of them towards the brain injury results ("the patient looks at his injury"). They usually occur in strokes or encephalitis located between the superior part of the cerebral peduncle and the cortex [12].

- inferior Foville syndrome appears in the paralysis of the lateral gaze located below the level of the decussation of the cortico-oculogyr tracts in the cerebral peduncle. The gaze is deflected by the affected side ("the patient is looking at his hemiplegia") [13].
- Internuclear ophthalmoplegia occurs in the lesion of the posterior longitudinal fasciculus, which provides connections between the ponto-mesencephalic oculomotor nuclei. At the lateral gaze one eye remains immobile while for the other only abduction (nistagmus) is possible, performing the so-called "one and a half syndrome". The movements of convergence of the eyeballs can be performed. It occurs in intraneural pontomesencephalic lesions and especially in MS or stroke [13].

➢ *Paralysis of conjugated vertical movements* of the eye is part of Parinaud syndrome. It is more common with the upgaze. The lesion is located at the level of the mesencephalic tegmentum.

➢ *Oculogyr crises (opsoclonus)* are manifested by paroxysmal deviations of the eyes in all directions. They occur in MS, postencephalitic parkinsonism, epilepsy, brainstem glioma, paraneoplastic syndrome 11, 12].

Legend: A. The normal position of the eyelids reported to the cornea

B, D Vertical eyelid movement

B, F Maintaining the parallelism of the gaze to the horizontal and vertical movements

G Convergence accompanied by pupillary contraction

Autonomic dysfunction of the eye

➢ *Argyll-Robertson syndrome* is manifested by the abolition of the pupillary light reflex, the preservation of the accommodation reflex, miosis and / or anisocoria. It occurs in the nervous lues (tabes), brainstem tumors, encephalitis;

➢ *Claude-Bernard-Horner syndrome* occurs in the involvement of the sympathetic fibers (which form the pupillary dilation reflex arc). It consists of the triad: miosis, enophthalmia, palpebral ptosis. It occurs in strokes located in the brainstem, brain tumors or lung apex tumors (by covering the stellate ganglion) [13].

V. Trigeminal nerve

It is a mixed nerve originating in several nuclei of the brainstem (bulb, pons, mesencephalon). It consists of three branches: olfactory, maxillary and mandibular. The first two are sensitive and innervate the skin and facial muscles, and the third is mixed and innervates the masticatory muscles. As a motor nerve, it controls the masticatory muscles and regulates the production of saliva and tears. As a sensory nerve, it provides sensitivity to almost the entire skin of the face and head, teeth, oral cavity, upper eyelid, sinuses and the two anterior thirds of the tongue (figure no. 4) [14].

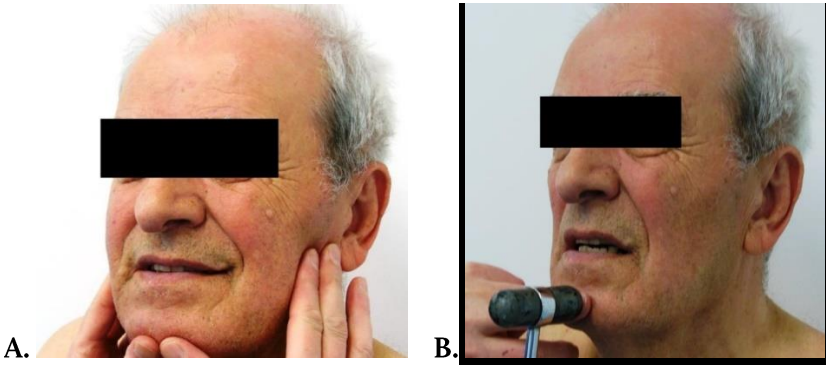

Figure 4. The examination of Vth cranial nerve,
(Personal collection of dr. Vicențiu Săceleanu)

Subjective sensitivity is represented by paresthesias and / or pain in the innervation territory of the nerve. Algic symptoms can be caused and / or exacerbated by compression of the supraorbital, suborbital and mental protruberance points [14].

Objective sensitivity is manifested by tactile, thermal and pain hypoesteshia or anesthesia. Highlighting a thermoalgesic dissociation denotes the existence of a disease at the central level [14].

Examination of motility reveals, in unilateral paralysis, the deviation of the mandible to the affected side (by the action of the external pterygoid muscle on the opposite side). When the mandible is tightened by force, a decrease in the volume and consistency of the masseter muscle can be determined by palpation. In bilateral paralysis the mandible is lowered, with severe damage of the mastication [14].

The *examination of the reflexes* is done by determining:

- corneal reflex, produced by touching the lateral edge of the cornea with a tapered cotton swab. A local sting occurs followed by bilateral blinking. Decreased or abolished reflex may be due to both trigeminal nerve damage (afferent pathway) and facial nerve (efferent pathway)
- the jaw-jerk reflex is elicited by the examiner placing their index finger over the middle of the patient's chin with the mouth slightly open and the jaw relaxed. The index finger is then tapped with a reflex hammer. A contraction of the masseter muscle is obtained delivering a downward stroke. The reflex is diminished or abolished in the lesions of the mandibular nerve and exaggerated in the pseudobulbar syndrome [12, 14]. *Trophic disorders* that occur in the trigeminal nerve impairment are manifested by masticatory muscles hypotonia and / or the appearance of neuroparalytic keratitis.

VII. Facial nerve

It is a mixed nerve and it emerges from the pons of the brainstem. It ensures the innervation of muscles of facial expression, the taste sensitivity and the secretion of the salivary, submandibular and submaxillary glands. Its motor fibers control the muscles of the forehead, face and neck and allow the eyes and mouth to be closed. The sensory fibers transmit the sensations of the sense of taste for the two anterior thirds of the tongue, ensuring the secretion of tears and a part of the saliva. Sensitive fibers innervate the skin of the earlobe and eardrum [15].

Examination of motor function

On inspection, in peripheral facial paralysis the forehead creases disappear, the eyebrow is lowered, the eyelid fissure wider, the blinking absent and the tear secretion gathers in the inner corner of the eye (phenomenon called epiphora and due to eversion of the lacrimal ducts by Horner muscle paralysis). The nasolabial groove appears more erased, the oral commissure is lowered and the saliva flows through the corner of the oral commissure (figure no. 5) [15].

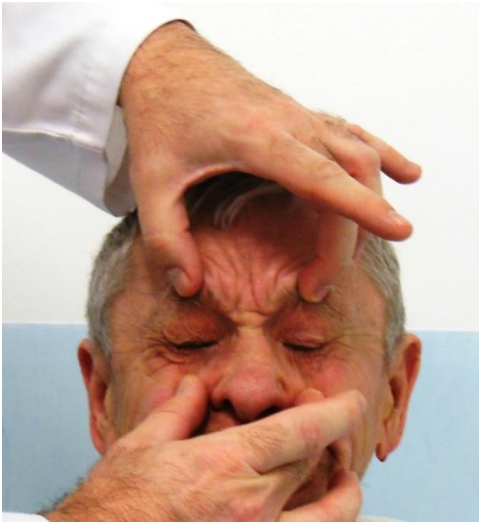

Figure 5.
(Personal collection of dr. Vicențiu Săceleanu)

At the dynamic examination the patient cannot wrinkle the forehead or close the eyelid fissure and at the attempt of voluntary closing the eye it is found that the eye moves involuntarily upwards and outwards (Charles-Bell sign) (figure no. 6). When asking the patient to show the teeth, the oval of the lips is larger on the healthy part, the patient cannot whistle or blow in a candle. Tendons of the skin muscle of the neck (platysma) do not appear [14, 15].

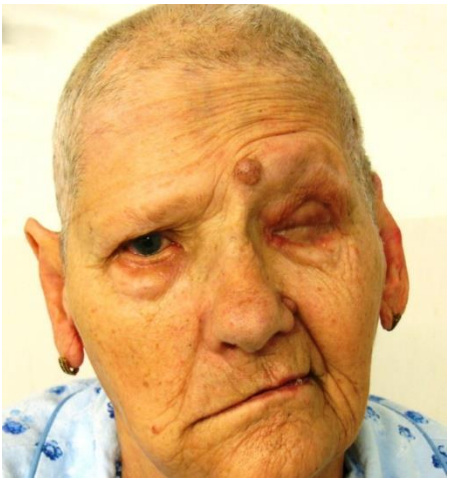

Figure 6. Facial palsy
(Personal collection of dr. Vicențiu Săceleanu)

The corneal reflex is abolished.

During chewing, food stagnates in the buccal vestibule due to paralysis of the buccinator muscle. Speech and laughter accentuate the asymmetry [15].

Examination of the taste

The taste threshold is determined in the anterior 2/3 of the tongue using for the sweet taste a cotton swab soaked in sugar, for the sour taste a cotton with citric acid or lemon and for the salt taste a cotton with sodium chloride [13, 15].

VIII. The vestibulocochlear nerve

It is a mixed nerve and consists of two components: the cochlear branch (acoustic) that collects from the inner ear the impulse produced by auditory excitations and the vestibular branch that also collects information from the inner ear regarding the position of the body in space (balance). It has its origin in the pons of the brainstem [16].

The acoustic nerve pathology

It is manifested by symptoms of irritation and symptoms of deficiency.

➢ *Irritation symptoms* are represented by:

- Tinnitus. It consiss of continuous or paroxysmal abnormal noises perceived in one or both ears. They appear in the syndrome of vertebrobasilar insufficiency, in labyrinthine lesions (after craniocerebral traumas or labyrinthitis), acoustic nerve lesions (acoustic neuritis, toxic neuropathies, neurinomas, arachnoiditis of the pontocerebellar angle). Real "objective" tinnitus it`s also described, which occurs in cerebral angiomas or carotid-cavernous fistulas, usually unilateral with the lesion, which can often be heard with the stethoscope;
- hyperacusis (increased auditory perception) occurs in acoustic neuritis, migraine attacks, epileptic aura, neurosis, etc.
- auditory hallucinations can be elementary (simple noises) or complex (words, songs). They appear paroxysmal in uncinate temporal focal crises [16].

➢ *Deficiency symptoms* consist of total or partial deafness, uni- or bilateral perception type , with or without tinnitus. Perceptive deafness consists in diminishing the air and bone conduction, highlighted in the tuning fork test or by audiometry [15, 16].

Etiology

a. Bilateral hearing loss occurs in:

- intoxications with antibiotic drugs (streptomycin, kanamycin, vancomycin), quinine, etc.
- bacterial and viral infections (scarlet fever, rubella, epidemic mumps, influenza, typhoid fever, syphilis, bacterial meningitis)
- vertebrobasilar circulatory disorders [16]

b. Unilateral hearing loss occurs in:

- tumors (acoustic neurinoma, brainstem tumors, meningiomas)
- vertebrobasilar aneurysms
- craniocerebral trauma with basilar skull fracture
- osteitis deformans (Paget's disease) [16].

The vestibular nerve pathology

➢ *Vertigo* consists in an erroneous sensation of moving objects around in relation to the patient and rarely vice versa. The most common is the rotational type and is exacerbated by changing the position of the head (rotation in bed, transition from clino- to orthostatism). It is often accompanied by nausea, vomiting, anxiety and vasomotor disorders (pallor, sweating, hypotension, bradicardia or tachycardia). The sensation of imbalance is sometimes violent, going as far as falling, but without loss of consciousness (differential diagnosis with epileptic seizures and vago-vagal syncopes) [16].

It appears paroxysmal in Meniere's disease where it is accompanied by tinnitus, nausea, vomiting and progressive deafness.

➢ *Nystagmus* consists of an involuntary movement of the eye composed of a rhythmic succession of a fast jerk, followed by a slow one. The fast jerk gives the sense of the nystagmus (right or left) while the slow jerk is on the same side as the damaged labyrinth [15].

Nystagmus has 3 degrees:

- First degree – the nystagmus is present only in the extreme gaze in the direction of fast component
- Second degree - is observed when looking straight ahead
- Third gaze - it appears both when looking straight ahead and in the two extreme positions of the gaze [15].

There are several forms of nystagmus:

- horizontal per-rotational nystagmus, characteristic of bulbar lesions (by affecting the vestibular nuclei)
- bilateral horizontal nystagmus, characteristic of pontine lesions
- vertical or multidirectional nystagmus (opsoclonus) that occurs in the cerebral peduncles lesion
- dissociated nystagmus in which each eye looks in a different direction and with a different frequency. It occurs in the lesion of the medial longitudinal bundle and is characteristic of multiple sclerosis [14].

Apart from vestibular nystagmus, other forms of nystagmus are described (for their differential diagnosis):

- congenital nystagmus and nystagmus that appears in blind people have horizontal pendular movements equal in amplitude and it appears when looking straight ahead

- fixation nystagmus occurs in healthy people in extreme lateral gaze, is rapidly depletable and of low intensity
- gaze-paretic nystagmus is unilateral and occurs in oculomotor nerves paresis when the patient looks towards the side of the parietal muscle
- optokinetic nystagmus is observed in people who fix a moving object (for example, a colored cylinder with vertical bands that rotates at a constant speed in front of the eye) or when looking at landscapes while traveling by train [13, 16].

Balance disorders

In peripheral vestibular syndrome the tonic deviations of the limbs stretched forward are made towards the side of the injured labyrinth. Balance disorders of vestibular origin are accentuated when the eyes are closed (differential diagnosis with cerebellar ataxia). Static and dynamic tests are used to highlight balance disorders when the clinical examination is conducted [16].

➢ *Static tests*

- the Romberg test in which the patient is standing, with his feet together. When the eyes are closed, the body is constantly tilted to the side of the injured labyrinth;
- the test with the outstretched arms of the patient with the legs close together. When closing the eyes, the arms deviate to the side of the injured labyrinth. In the clinic, usually both tests are combined into one [15].

➢ *Dynamic tests*

- indication test (Barrany). The patient sits down and performs with his eyes closed a few vertical movements of his outstretched arms. There is a deviation of the arms towards the affected side.
- star pattern walking test. The patient walks with his eyes closed 4-5 meters forward and an equal distance backward, performing a star pattern walking.
- Utemberg test. The patient steps on the spot with his knees slightly raised. In pathological cases, the patient rotates to the side of the injured labyrinth [16].

IX and X Glossopharyngeal and vagus nerves

The glossopharyngeal nerve is a mixed nerve and originates from the medulla oblongata. It ensures taste sensitivity, innervation of the laryngeal muscles and secretion of the parotid glands. Its sensory fibers provide the sense of taste for the posterior third of the tongue and the sensitivity of the pharynx. Its motor fibers control some muscles of the pharynx and the secretion of part of the saliva to the parotid gland [17].

The examination of the motor function is done on the patient pronouncing a vowel with his mouth open while the examiner presses the tongue with a spatula. In unilateral lesions, the curtain sign is observed, which consists in the unilateral traction, on the healthy side, of the posterior wall of the pharynx. Swallowing disorders also occur for solid foods [17].

The examination of the exteroceptive sensitivity is done by touching with a spatula the posterior wall of the pharynx and / or the amygdala. Normally, the pharyngeal reflex occurs, which consists of a contraction of the pharyngeal muscles accompanied by nausea and vomiting.

The examination of the taste sensitivity is made by means of a tampon soaked in bitter solution (quinine) with which the posterior third of the tongue is reached.

The examination of the vegetative function is done by determining the salivary secretion of the parotid gland. The carotid sinus reflex is also investigated. Its compression causes vegetative changes: bradycardia, decreased BP and peripheral vasodilation. In atherosclerosis, hyperexcitability of the carotid sinus often occurs [16, 17].

The vagus nerve is a mixed nerve originating in the medulla elongata and has the longest trajectory; it has sensitive, motor and vegetative fibers and controls the activity of most internal organs (heart, lungs, stomach, etc.). This nerve, both sensory and motor, is able to release acetylcholine, which causes a contraction of the bronchi or a slowing of the heartbeat. It can also increase gastric and pancreatic secretions, it can act on the gallbladder, it can control variations in the voice, it can interfere in swallowing (it partially ensures the motility of the pharynx and palatal veil), in coughing, sneezing and peristalsis. movements of the cavitary organs, in particular those of the intestine) [17].

The examination of the somatic motor function is carried out in the open-mouthed patient by pressing the tongue with a spatula. When pronouncing the vowel "a" there is a symmetrical lifting of the uvula and the palatal veil.

In the unilateral damage there is an asymmetry of the palatal veil with its fall and deviation together with the uvula on the healthy side [17].

In bilateral lesions, a fall of the palatal veil on both sides, with the uvula touching the base of the tongue is observed. When pronouncing the vowels, there is no muscular contracture of the palatal veil.

- the motor function of the pharynx is evaluated by swallowing, giving the patient to swallow a small amount of water. In unilateral lesions there is a significant impairment of fluid swallowing, which flows back to the nose. Due to the concomitant penetration of fluids into the trachea, a cough reflex occurs. In bilateral paralysis it is found that the larynx (Adam's apple) does not rise during swallowing.
- the motor function of the larynx is done by analyzing the voice, which in unilateral paralysis becomes hoarse, bitonal, with the loss of high tones. The cough reflex is preserved. Bilateral paralysis is accompanied by aphonia, lack of cough reflex and inspiratory dyspnea [15].

The examination of the somatic sensory function is carried out by searching the cutaneous and mucous sensitivity of the nerve innervation area (the retroauricular cutaneous area, the posterior wall of the external auditory canal, the base of the uvula and the palatal veil area near the uvula) [14].

Examination of the gag reflex. The palatine reflex is examined by touching with the spatula the anterior wall of the palatal veil. The result is muscle contraction and nausea. The center of the reflex arc is in the medulla oblongata. Both nerves (IX and X) participate in the reflex.

XI. The accessory nerve

It is a motor nerve and originates in the bulb, innervates the sternocleidomastoid and trapezius muscles, which take part in the movements of the head and neck.

The clinical examination for the internal branch is similar to that presented for the vagus nerve.

For the examination of the external branch, the motility and trophicity of the sternocleidomastoid and trapezius muscles are analyzed.

The sternocleidomastoid muscle flexes the head on the contracted side and rotates it to the opposite side. The trapezius muscle tilts the head towards the contracted side, lifts and brings the shoulder back, elevates, depresses, and retracts the scapula. Consequently, for the examination of the internal branch of the patients, the aim is to perform the movements of tilting and flexion of the head, lifting and projecting the shoulder backwards [17].

XII The hypoglossal nerve

It is a motor nerve originating in the medulla ablongata and innervates the base of the tongue, whose movements it controls.

The clinical examination aims:

- motility of the tongue. At rest, unilateral lesions cause a slight deviation of the tongue towards the healthy side. The anterior projection of the tongue results in its deviation to the affected side by the action of the genioglossal muscle on the healthy side. To test the existence of a lateral paralysis, the patient is asked to press the inside wall of the cheek with the tip of his tongue. The examiner tests the force of this movement with his finger. On the paralyzed side there is a tongue atrophy often accompanied by muscle fasciculations [18].

In bilateral paralysis, the motility of the tongue is severely affected, its protrusion or lateral movements not being possible. Muscular atrophy is bilateral and is accompanied by fasciculations. Mastication and swallowing disorders occur along with dysarthria with difficulty pronouncing the labial consonants (l, d, t).

9. Motility, both active and passive motility are examined, also noting the involuntary movements.

Active segmental motility, paresis, plegia, paraparesis, paraplegia, is examined comparatively bilaterally. The examination is performed by asking the patient to perform active, segmental movements, the examiner opposing these movements (figure 7-14) [17].

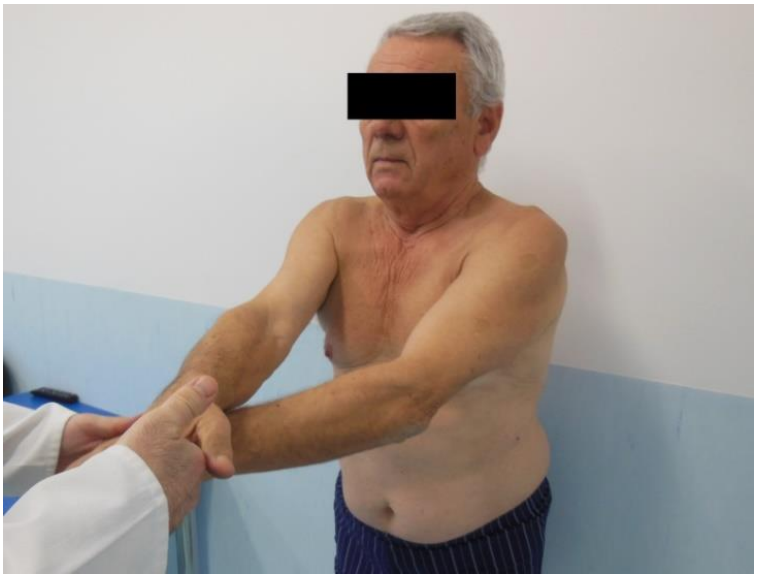

Figure 7. Examination of motility in the upper limbs

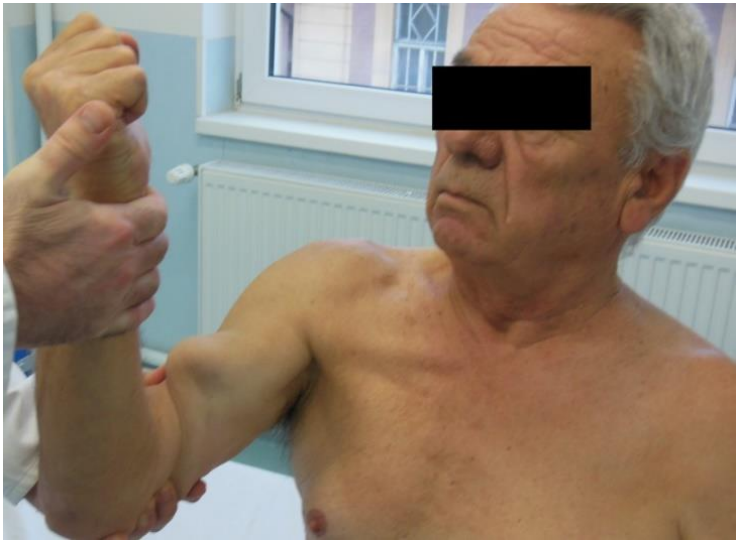

Figure 8. Segmental motility test (biceps),
(Personal collection of dr. Vicențiu Săceleanu)

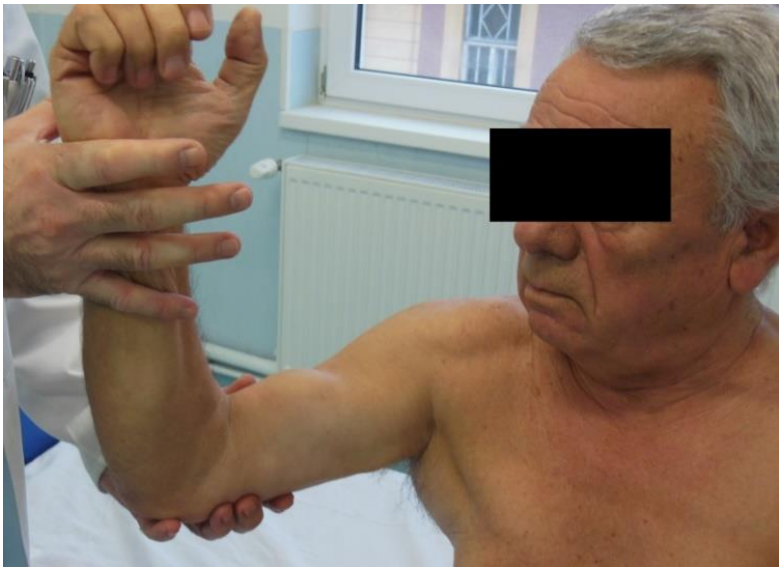

Figure 9. Segmental motility test (triceps),
(Personal collection of dr. Vicențiu Săceleanu)

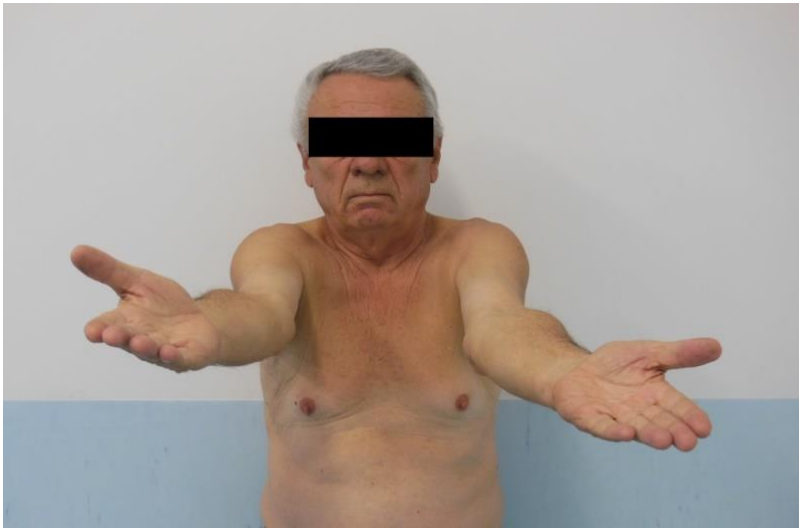

Figure 10. Stretched arms test
(Personal collection of dr. Vicențiu Săceleanu)

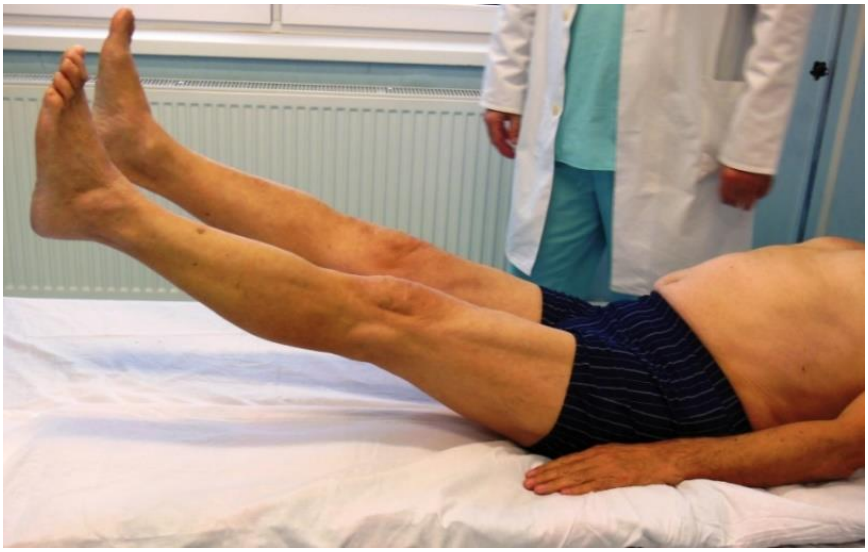

Figure 11. Lower limb motility test
(Personal collection of dr. Vicențiu Săceleanu)

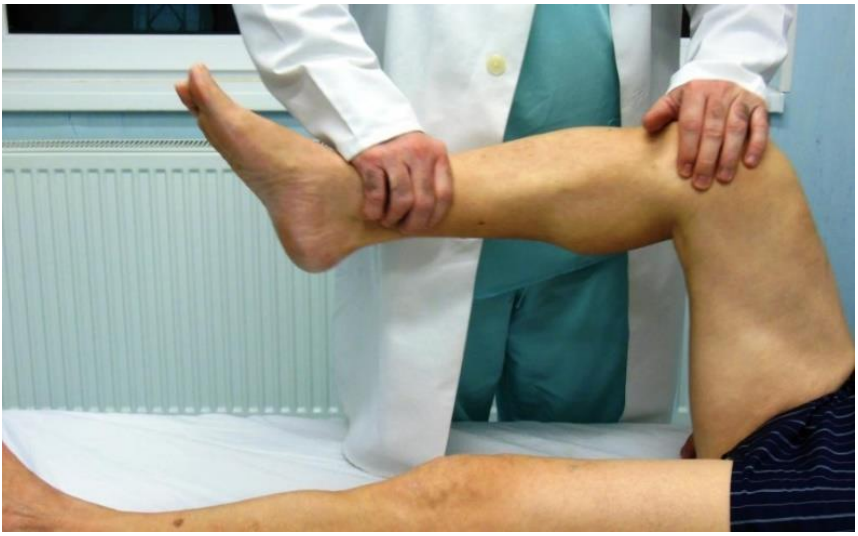

Figure no. 12. Segmental motility in the lower limbs,
(Personal collection of dr. Vicențiu Săceleanu)

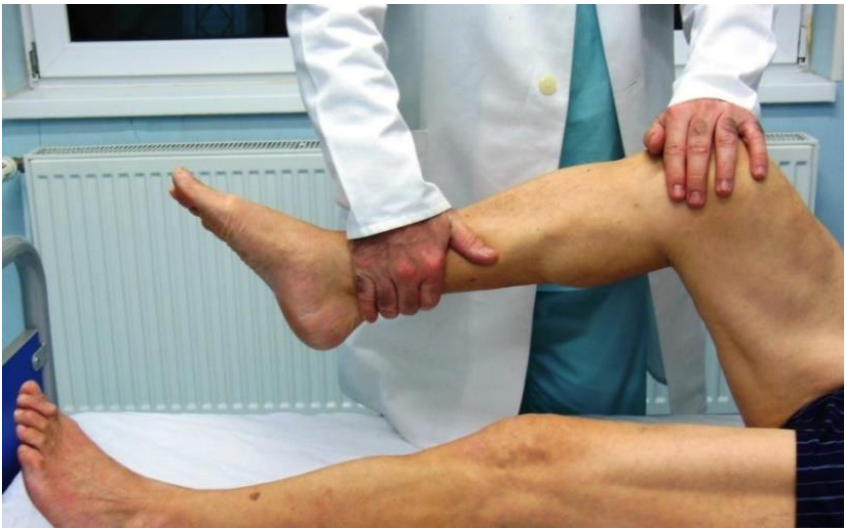

Figure no. 13. Segmental motility in the lower limbs,
(Personal collection of dr. Vicențiu Săceleanu)

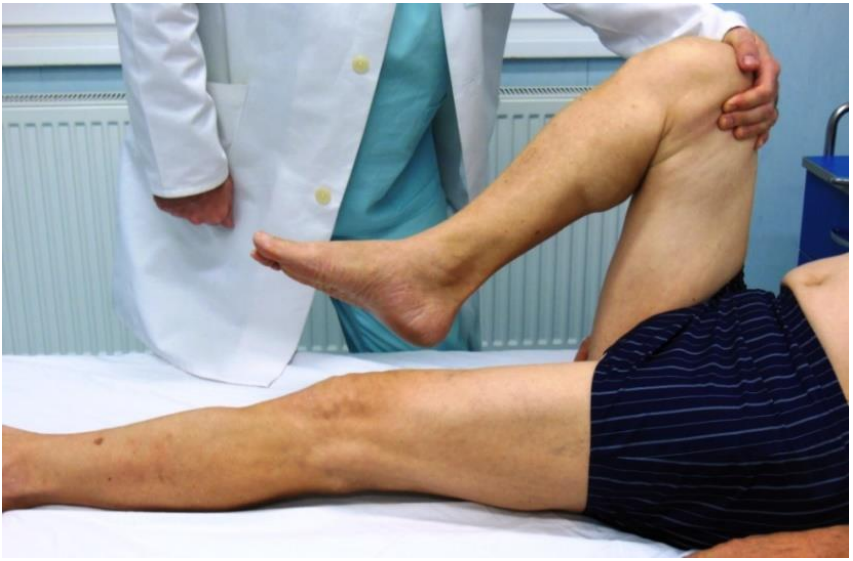

Figure no. 14. Segmental motility in the lower limbs,
(Personal collection of dr. Vicențiu Săceleanu)

Passive motility, which is dependent on the muscle tone, is altered in cerebellar disorders or spastic syndromes.

Involuntary movements include tremors, tonic clonic seizures, generalized seizures [18].

10. Sensitivity should be examined for both objective and subjective sensitivity.

Pain, paresthesias, are expressions of subjective sensitivity changes and are recorded as localization, irradiation territory. During the examination, the terms used by the patient must be interpreted correctly because under the same name they can understand various symptoms. Sometimes the patient through numbness understands the paralysis of a limb and often terms must be used in order for the patient to understand, for example instead of paresthesias, tingling [19].

It is important to delimit the territory of paresthesia as well as the mode of onset. The presence of paresthesias can indicate a condition of the peripheral nerves, a spinal cord injury, but also a neurosis when the topography of the paresthesias is unsystematized. Pain should be investigated, specifying the mode of onset, location, nature and duration of painful seizures, their intensity, as well as the phenomena of association of motor or vegetative time. Pain can be classified into [19]:

- Neuralgia - is pain in the distribution of a nerve or nerves, being called in direct contact with the affected nerve, and can often be the only symptom of suffering of that nerve.
- Radicular pain - has the character of accompanying the territory of dermatomes, that irradiates along the limbs (radicular territory) and at the level of the chest the characteristic of the pain is that it irradiates "in belt". Characteristic is the way of propagation from proximal to distal with exacerbation when increasing the CSF pressure on the injured root (cough, sneezing).
- Cordonal pain - occurs in damage of the lateral or posterior columns of the spinal cord. It has a dull character, it is imprecisely localized, with a wide distribution and accompanied by objective sensitivity disorders distributed on a hemibody or "level" in a medullary segment.

- Thalamic pain - it is located on the opposite hemibody of the injured thalamus, predominantly the face and upper limb, accompanied by objective sensitivity disorders and occurs through lesions of the lateral nuclear groups of the thalamus.
- Headache - "the disease of the seven specialties" is a pain located at the level of the head extremity and is often the reason why the patient goes to the doctor.
- Migraine - is a paroxysmal hemicrania with left / right localization, with a throbbing character and variable duration from a few hours to a few days, accompanied by intense autonomic phenomena [19].

Objective sensitivity should be tested for all forms (tactile, thermal, painful), throughout the body, from the head extremity to the torso and limbs, compared to the two halves of the body.

Differences in sensitivity are noted both left and cranio-caudal. In order to facilitate the determination of sensitivity levels, the following guide points can be used [17]:

- C4 – the tip of the shoulder
- C5 - the lateral side of arm (above deltoid insertion)
- C6 – the thumb
- C7 – the middle finger
- C8 – the baby finger
- T1 - the lateral edge of the forearm
- T2 - the medial face of the arm
- T3 – the axilla
- T4 – the nipple line
- T6 - the xiphoid process
- T10 – the linea alba
- T12 – the groin fold
- L1 – superior 1/3 of the anterior face of the thigh
- L2 - middle 1/3 of the anterior face of the thigh
- L3 - inferior 1/3 of the anterior face of the thigh
- L4 - medial malleolus
- L5 – the hallux
- S1 – the lateral side of the foot

- S2 - the plantar surface of the foot
- S3 – the gluteal region

Superficial sensation [18]

- The tactile sensitivity is examined with a piece of cotton wool applied symmetrically in order to determine the affected territory. Its quantification is done in the form: normesthesia, hyperesthesia, hypoaesthesia, anesthesia.
- Thermal sensitivity is examined by successively applying two test tubes (hot water, cold water) to the skin surface.
- Pain sensitivity is examined by lightly puncturing the skin in the territory of dermatomas alternately and comparatively.

Deep sensation [17]

- Proprioceptive sensitivity is examined by printing slight movements of various limb segments, the patient sitting with his eyes closed and telling the type of movements imprinted.
- Vibratory sensitivity is examined using a vibrating tuning fork placed on the patient's bony prominances.
- The paresthetic sensitivity is examined by placing the patient with objects of the same shape or size but with a different weight, the patient being asked to identify the object with a higher or lower weight.

11. Reflexes testing, includes the examination of deep tendon reflexes (ROT) (figure 15-19), cutaneous reflexes, as well as pathological ones.

DTR change both in the sense of their accentuation (brain and spinal cord disorders) and in the sense of diminishing or abolishing (peripheral nerve damage).

Abdominal skin reflexes are suggestive for spinal cord compressions, especially if they occur unilaterally modified, in the sense of their reduction or abolition.

The Babinski reflex is part of the group of pathological reflexes that appear both in brain and spinal cord diseases (figure no. 20, 21,22) [19].

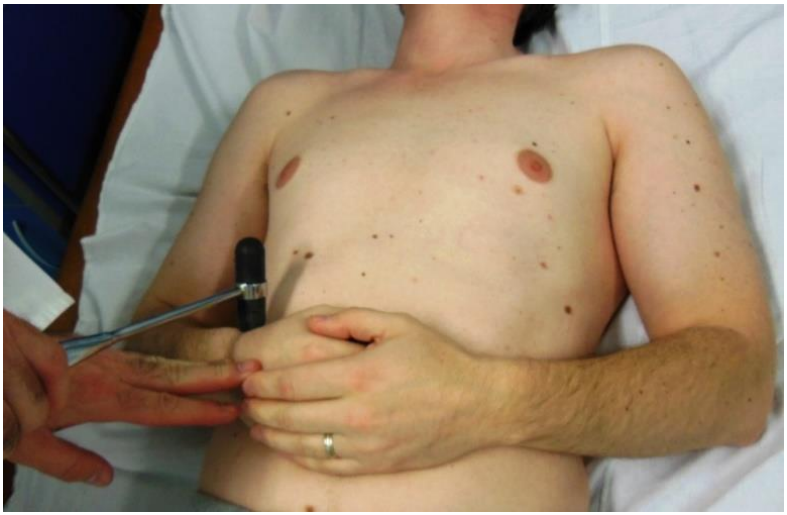

Figure 15. Radial style reflex
(Personal collection of dr. Vicențiu Săceleanu)

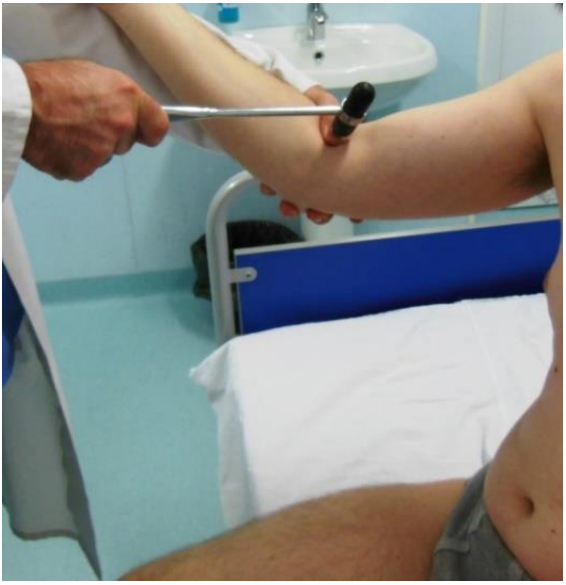

Figure no. 16 Bicipital reflex
(Personal collection of dr. Vicențiu Săceleanu)

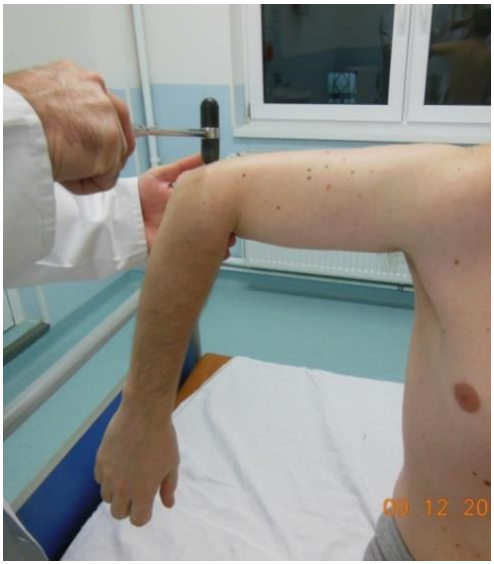

Figure 17. Tricipital reflex
(Personal collection of dr. Vicențiu Săceleanu)

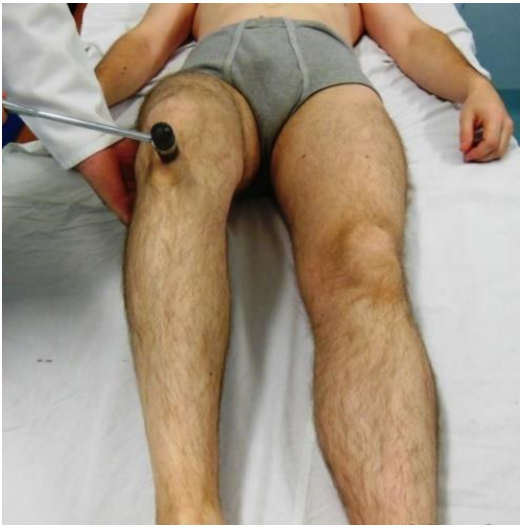

Figure 18. The patellar reflex
(Personal collection of dr. Vicențiu Săceleanu)

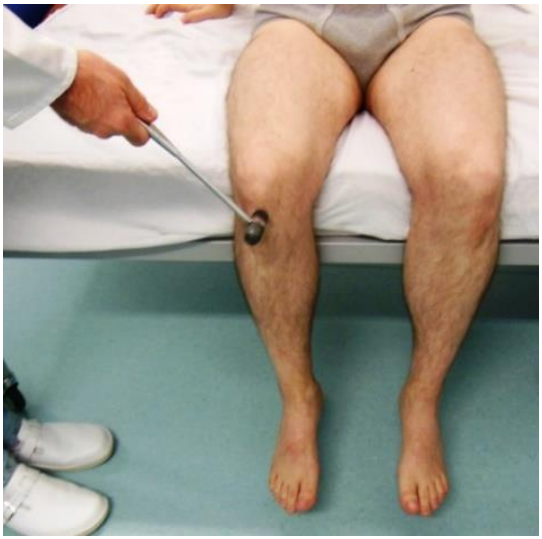

Figure 19. The patellar reflex
(Personal collection of dr. Vicențiu Săceleanu)

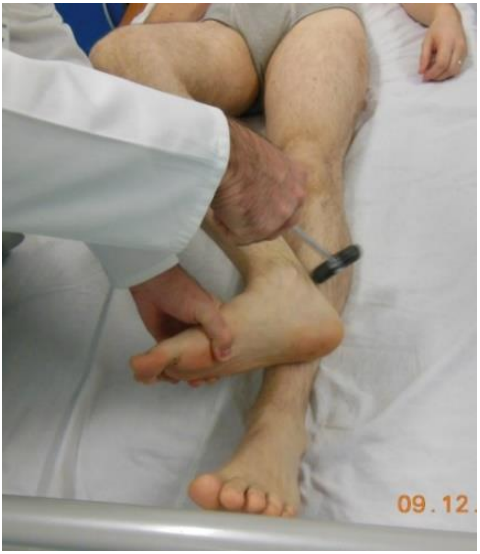

Figure 20. The Achilles reflex
(Personal collection of dr. Vicențiu Săceleanu)

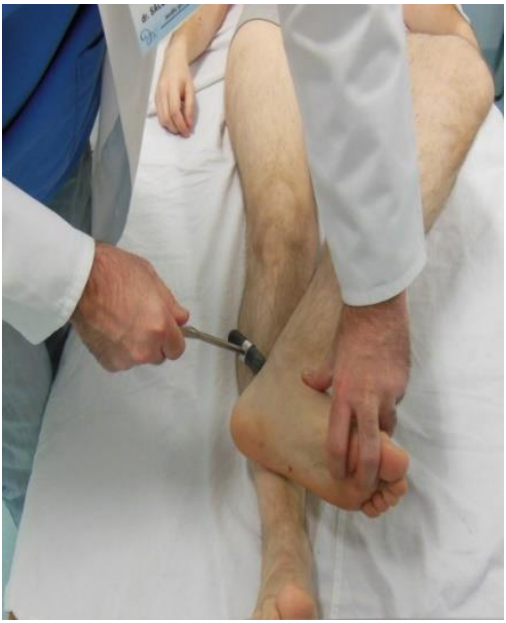

Figure 20. The Achilles reflex
(Personal collection of dr. Vicențiu Săceleanu)

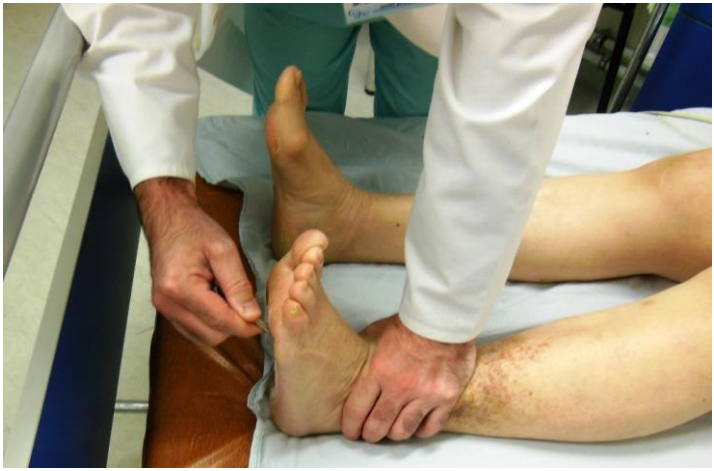

Figure 21. Babinski sign
(Personal collection of dr. Vicențiu Săceleanu)

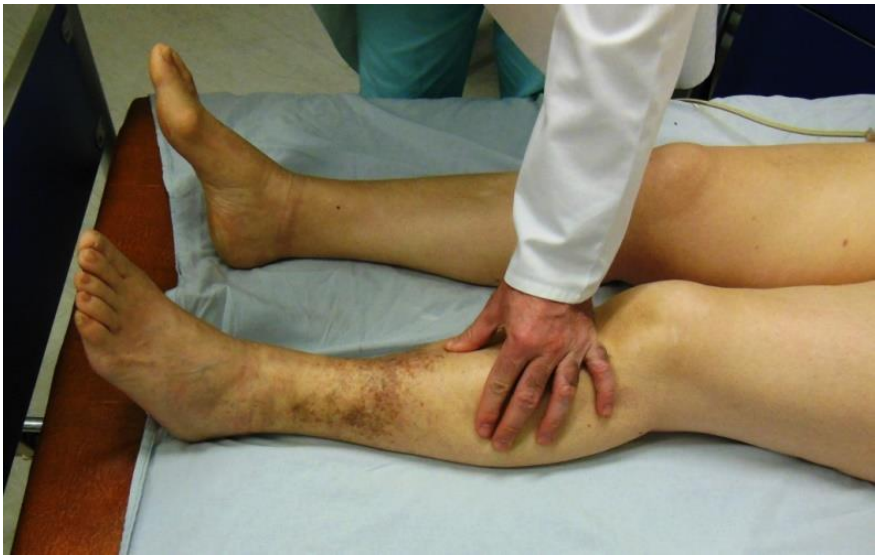

Figure 22. Oppenheim Maneuver,
(Personal collection of dr. Vicențiu Săceleanu)

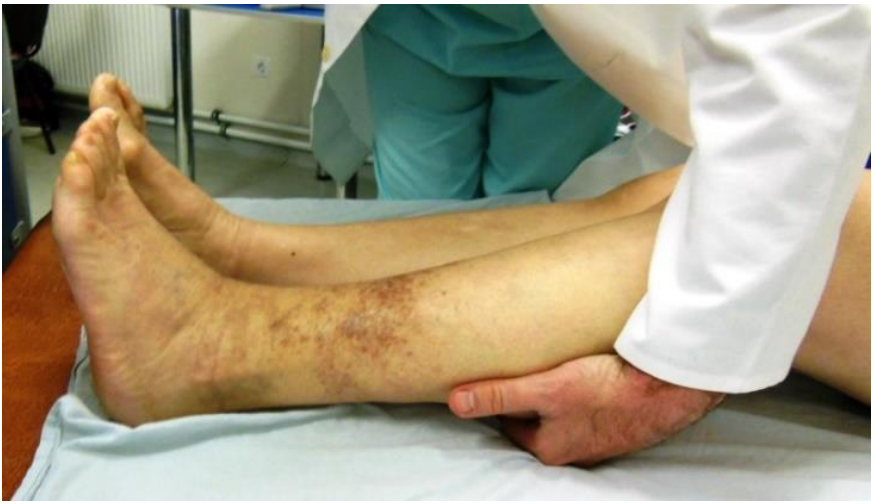

Figure 23. Gordon Maneuver
(Personal collection of dr. Vicențiu Săceleanu)

12. Coordination

Due to the structures involved in coordinating the activity of the muscular system (cerebellum, motor cerebral cortex, reticular formation, vestibular system) the voluntary movements are harmonious and fluent, adapting to any situation [19, 20].

The coordination systems are interconnected with the peripheral receptors through the ascending pathways of proprioceptive sensitivity and the central vestibular pathways, providing continuous information on the position of the segments and the functional state of the myo-arthro-kinetic apparatus. It follows the appreciation of the cerebellum function through the known tests, finger-to-nose test (figure no. 23), finger-to-finger test, Romberg test, puppet test [20].

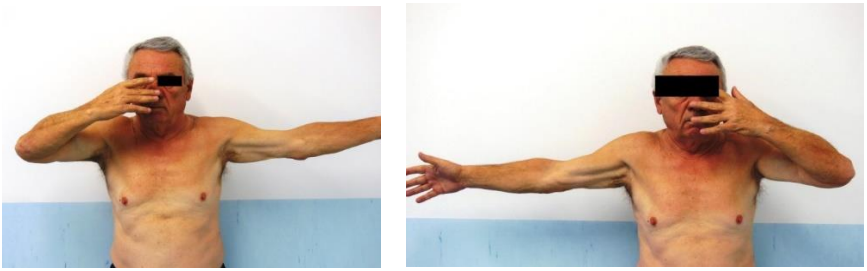

Figure 23. Nose index test
(Personal collection of dr. Vicențiu Săceleanu)

Coordination disorders such as ataxia (jerky movement, difficulty reaching a target), are characteristic of diseases of the cerebellar hemispheres (positive on the same side), and balance disorders (lateropulsion, antero-retropulsion), are characteristic of the pathology of the midline of the cerebellum [19].

The term ataxia only includes active movements coordination disorders:

- Tabetic ataxia is most often caused by a posterior, luetic meningo-radicular lesion. It is the consequence of a disorder of conscious deep sensation. It manifests itself in the form of static ataxia and dynamic ataxia.
- Cerebellar ataxia.

- Frontal ataxia, encountered in frontal lesions, consists of a body balance disorder, lateropulsion on the side of the lesion and retropulsion, which occurs both while standing and while walking [18].

13. Speech, examined only in the conscious patient, it shows a condition of the dominant hemisphere.

Aphasia is an acquired speech disorder that results in damage to specific brain regions. They are most often of vascular or traumatic origin. In the case of polyglots, the speech of all languages is affected, the extent of the disorder depending on certain factors [17].

Global aphasia occurs after a damage to the territories irrigated by the trunk of the middle cerebral artery. All elements of the speech are affected, comprehension is abolished, the patient has difficulty naming objects, reading and writing, copying letters or words with great difficulty.

Motor or expressive aphasia occurs in lesions of the Broca area, the patient being unable to express himself in words even though he understands perfectly [18].

Sensory, receptive aphasia occurs in lesions of the temporo-parieto-occipital junction (Wernicke area). In this case the patient does not understand what he is being told but may present the so-called echolalia in which he repeats the words of the examiner.

It will be examined:

- Spontaneous speech
- Naming objects
- Speech comprehension
- Repeating
- Reading
- Writing

In dysarthria, speech is affected by mispronunciation, which makes comprehension difficult. The cause is the inadequate coordination of the functions necessary for speech. The pronunciation is evaluated [19].

Agraphia consists of an acquired deficit of the ability to express through writing. Word syllabification can also be affected. The examination is performed as follows: the patient is asked to write

sentences, longer words or numbers after dictation, to spell / transcribe words [20].

14. The mental state is examined during the anamnesis and by observing the patient's behavior [18, 20].

The following shall be assessed:

- Behavior (excessive slowness, signs of anxiety)
- Type of verbal activity (speech rhythm, logorrhoea)
- Thoughts of self- or hetero-aggression
- Laughter and ideas of grandeur
- Beliefs (about oneself, one's body, other people and about the future or abnormal beliefs)
- Unusual sensations or hallucinations
- Orientation in time and space
- Discernment [20]

Memory disorders

Memory includes the brain's processes of retrieving, storing, remembering, and rendering information. Memory functions are taken over by the limbic system and the areas of the brain with which it is connected [20].

Hypermnesia, hypomnesia and amnesia which represents permanent or temporary memory loss [19, 20].

References:

1. Glick, T. Neurologic skills: examination and diagnosis, Blackwell Scientific Publication, 2003, pg 194-198.
2. Mayo Clinic. Clinical Examination in Neurology, Mayo Clinic Department of Neurology, 1997, pf 20-45.
3. DeJong, R. Revised By Haerer, A.F. DeJong's The Neurologic Examination, 2014, ed, Wolter Kluwers, pg 74-100.
4. Gilman, S. Newman W. Manter and Gatz Essentials of Clinical Neuroanatomy and Neurophysiology, 10th edition, 2009, pg 124-154.
5. Aids to the examination of the peripheral nervous system. WB Saunders, 2010, Saunders Ltd., pg 236-275.

6. Săceleanu MV, Clinical Neurosurgery for students, Literatur Stolz, 2015, pg. 7,10,21,26-29.
7. Adam D. Compendiu de neurotraumatologie, Didactic and Pedagogical ed, Bucharest. 2009, 26-28.
8. Florian lSt. Neurochirurgie. Curs pentru studenți, Cluj-Napoca, Edit.Srima, 2003, pg. 4-5,12-13.
9. Ciurea AV, Constantinovici A. Ghid practic de Neurochirurgie, Medical Ed, 1988, pag. 35.
10. Arseni C, Al. Constantinescu, M. Maretsis, Semiologie Neurochirurgicală, Bucharest, 1977.
11. Miller DJ, Traumatic brain swelling and edema. In: Cooper RP, Head Injury, Williams and Wilkins, 1993, p. 137-158.
12. Ciurea AV, Davidescu HB, Traumatologie cranio-cerbrală,. In: Popescu Irinel (sub red.), Tratat de Chirurgie, Neurochirurgie, Vol.II, Edit. Romanian Academy ed, Bucharest, 2007.
13. Ciurea AV. Tratat de Neurochirurgie, vol. 1, Medical ed, Bucharest, 2010, pag.159-160.
14. Teasdale GM, Jennet B, Assesment of coma and impaired consciuosness. Lancet.1974;ii:103I-4.
15. Teasdale GM, Murray G, Parker L, Jennet WB, Adding up the Glasgow coma score. Acta Neurochir (Paris). 1979; 1(suppl28):13-16.
16. Lăcrămioara Perju- Dumbravă, Ştefania Kory Calomfirescu, Ioan Florian Ştefan: Neurologie curs pentru studenţi, University Medical Ed „Iuliu Haţieganu" Cluj-Napoca, 2002.
17. Mohan D, Ciurea AV, Mohan AG. Curs de Neurochirurgie, Univeristy Ed Oradea 2014
18. Băjenaru O. Ghid de diagnostic si tratament în neurologie, Bucharest, 2010.
19. Van Allens, Pictorial manual of Neurologic Test, 1988, pag. 16-17.
20. Pendefunda Gh, Sftefanache F, Pendefunda L, Semiologie neurologică, lnternational Contact Ed, Iași, 1992, pag. 39-45,68-75,84-99,137-139.

IMAGISTIC ASPECTS IN CRANIOCEREBRAL PATHOLOGIES

Conf. Dr. Grosu Florin[1,2]
Dr. Adriana Săceleanu[1]

[1] Faculty of Medicine, "Lucian Blaga" University, Sibiu
[2] Sibiu Emergency Clinical Hospital, Sibiu

Imagistic aspects in cerebral neoplasms

The intracranial tumors represents a heterogenic group, being localised especially at the supra- or infranevraxial level of the brain. The age of occuring is a very important factor especially in the course of a differential diagnosis. Some brain tumors occur at the age below 2 years, such as teratomas, choroid plexus papillomas; other brain tumors occur at the age below 10 years, such as ependimomas, astrocytomas, medulloblastomas or craniopharyngiomas. In the adulthood the most frequent types of brain tumors ar the metastases, the gliomas, the meningiomas and the schwanomas. The multiform glioblastoma is characteristic to the elderly people.

The purpose of imaging in cerebral tumors:

- Intracranial pathology confirmation
- Lesion characterization
- Biopsy guiding and determining the therapeutic conduct
- Follow-up.

The MRI is the gold standard tool for diagnosing a brain tumor.

Clasification according to the tumor location:

– intranevraxial tumors in pediatric population:

- infratentorial: pilocytic astrocytoma, ependimoma, brainstem glioma, medulloblastoma

- supratentorial: astrocitoma, primitive neuroectodermal tumor, dysembryoplastic neuroepitelial *tumor*

– intranevraxial tumors in adulthood:

- infratentorial: - metastases and hemangioblastoma
- supratentorial: metastases, gliomas

- extranevraxial tumors – derived from adiacent structures of the brain (in the most frequent cases- schwanomas and meningiomas).

Primary brain tumors:

- **3rd GRADE ANAPLASTIC ASTROCYTOMA**
  - 50 year old pacient with headache, dysarthria and confusion
  - Left temporal brain tumor with a well-circumscribed shape with a heterogeneous signal in T2, T1 and Flair, especially when there are necrosis areas and hematic residues in interior with brain edema and mass effect on the parenchymal tissue
  - After contrast enhancement it presents periferic and central heterogeneous gadolinophilia

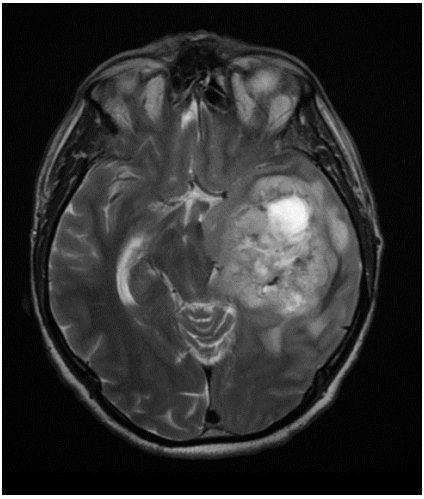

AXIAL T2

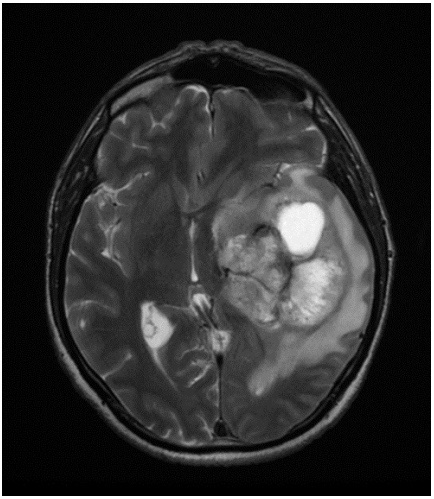

AXIAL T2

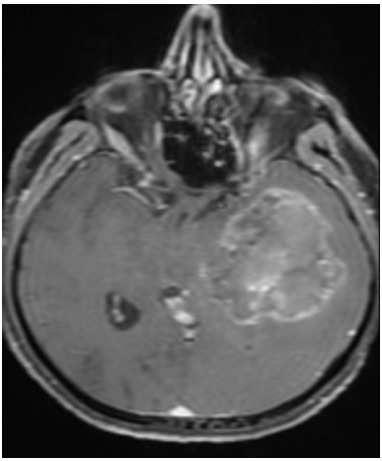

CORONAL T1 +Contrast

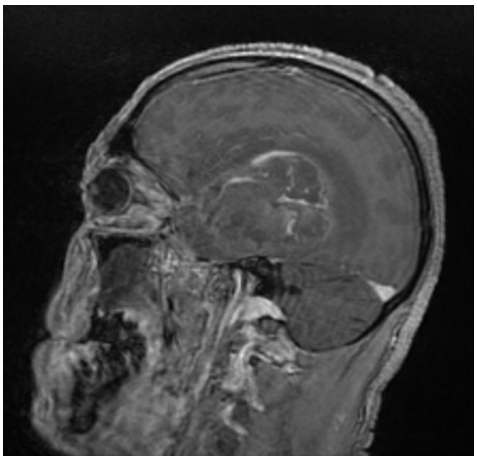

AXIAL T1 +Contrast

- **74 year** patient with headaches and left hemiplegia
- Heterogeneous tisular mass with central necrotic areas, fluid signal, heamtic residues, localised in the left frontal lobe with heterogeneous gadolinophilia at the tisular level, with marked perilesional vasogenic edema with compresive effect on the lateral ventricle and median shift of the brain parenchyma.

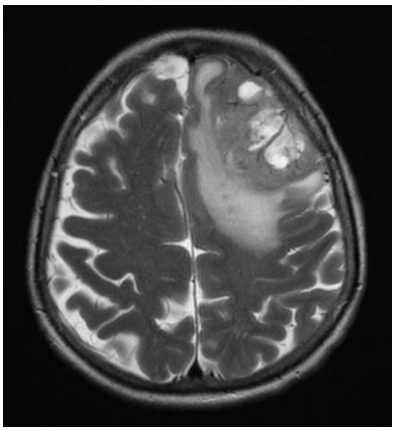

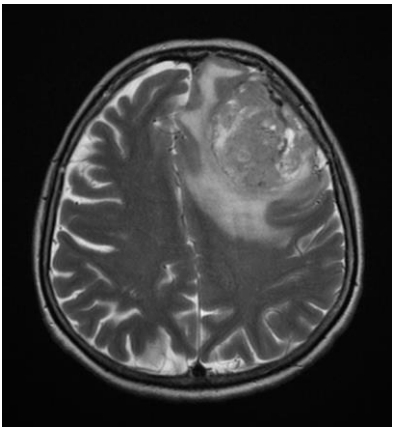

AXIAL T2

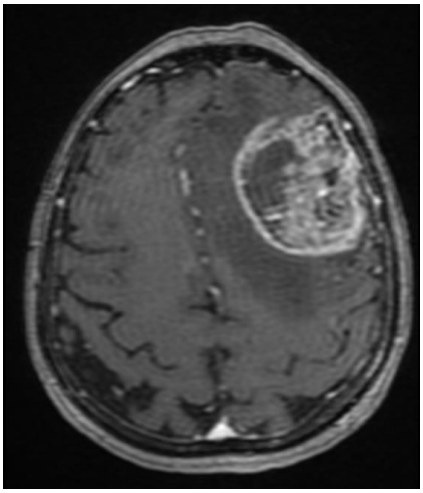

AXIAL T1+Contrast

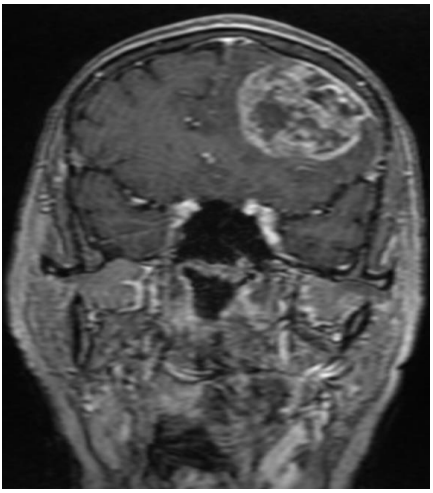

AXIAL T1+Contrast

- **4th GRADE GLIOBLASTOMA**

  - **59 year** patient with headaches and pronounced fatigability
  - Deep tisular mass localised in the right temporo-parietal aspect of the brain at the level of lentiform nucleus, right posterior arm of the internal capsule, the thalamic nuclei, the splenium, with an irregular shape, polilobular shape with gadolinophilia enhancement and hematic residues with vasogenic edema and median line shift on the parenchymal tissue.

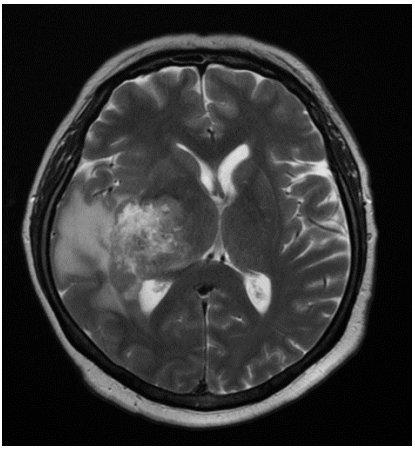

AXIAL T2

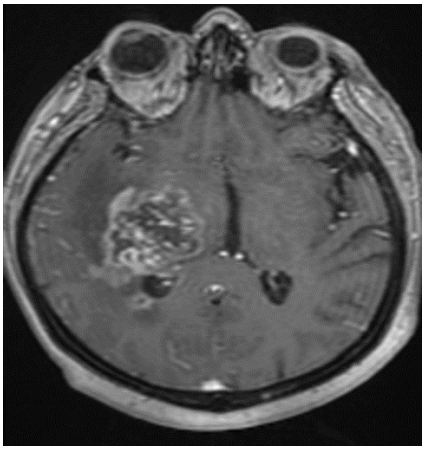

AXIAL T1 +Contrast

- **FIBRILLARY ASTROCYTOMA**
  - **40 year** patient with headache and a loss of consciousness episode
  - On a CT scan performed there is hypodense area in the left frontal cortico-subcortical region without mass effect on the parenchymal tissue with heterogeneous aspect that include partially the left superior frontal gyrus . It's shape is iregullar, heterogeneous with multiple blood petechiae.

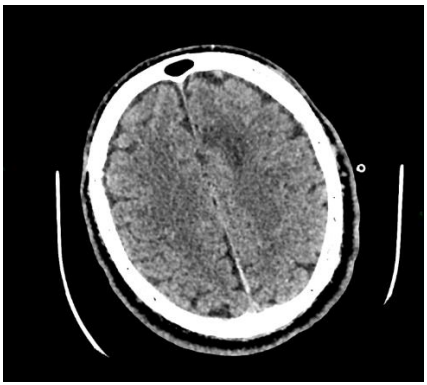

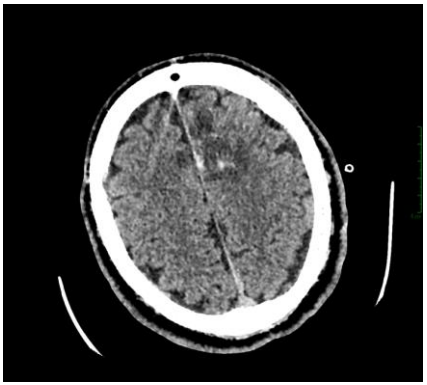

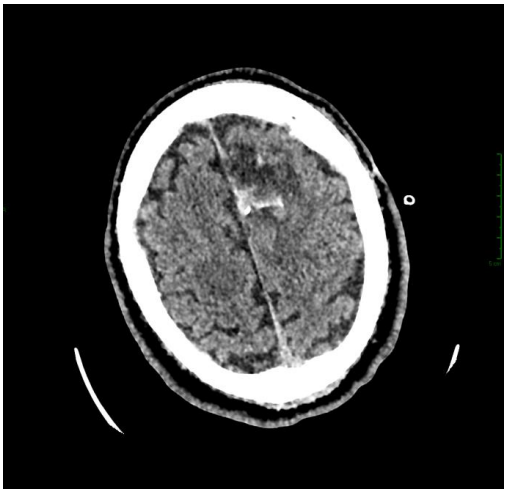

- **CEREBELLAR MEDULOBLASTOMA**
  - **42** year patient with headaches and vertigo
  - On the MRI and CT-scan images the left cerebellar hemisphere presents an anarchic tissular organization with heterogenous hypersignal in T2, hyposignal in T1, intensively restricted in DWI/ADC sequences, with nodular gadolinophilia, mostly emphasized in the perifery in the contact with the cerebellar parenchyma. The lesion described doesn't produce cerebellar edema, but has a compressive effect on the brainstem and the 4^{th} ventricle, with inferior displacement of the cerebellar amygdala and moderate supratentorial hydrocephalus with periventricular hypersignal in T2/FLAIR (transependimar edema).

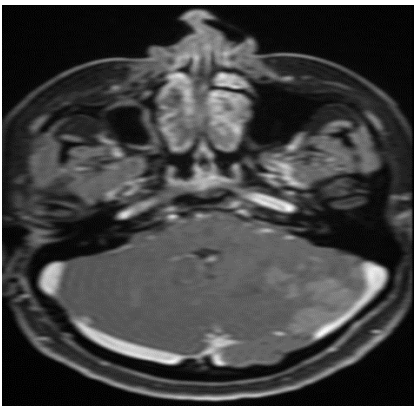

AXIAL T2+Contrast

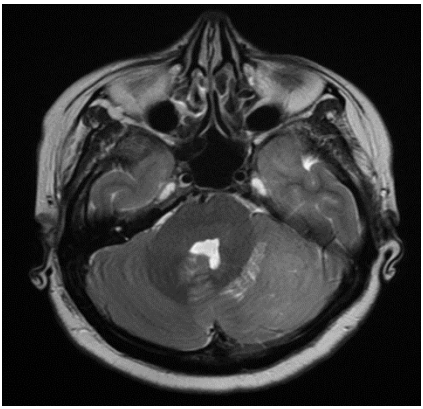

AXIAL T2

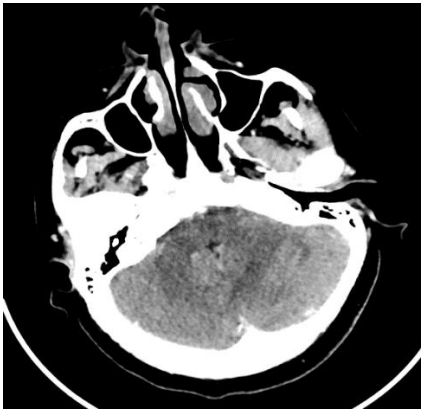

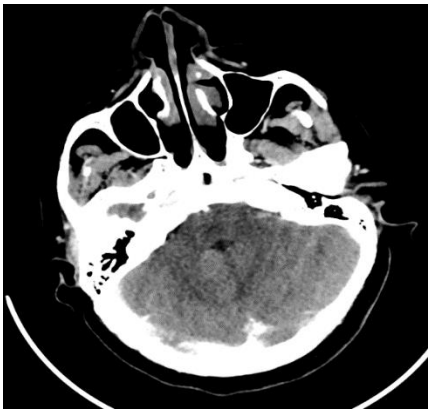

- **<u>CEREBRAL METASTASES</u>**
  - **73 year old** patient known with malign melanoma
  - On the right periventricular , right frontal, posterior temporal and right temporal aspect of the brain are highlighted some nodular formations: the frontal one is heterogenous with hyper-hypo signal in T2, T1, FLAIR with a small restrictive peripheric bud, with peripheric gadolinophilia, parenchymal edema and compresive effect on the frontal portion of the right lateral ventricle. The

temporal lesions present hyposignal in all sequences with focal edema and ring-like gadolinophilia.

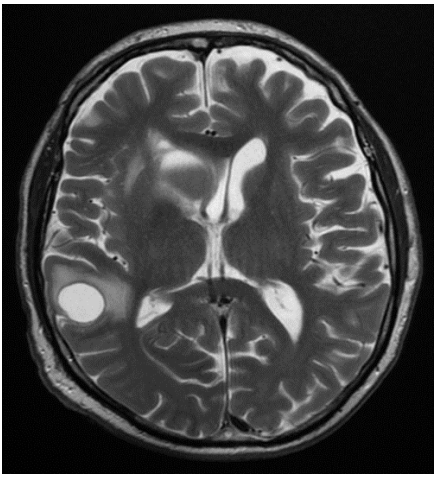

AXIAL T2

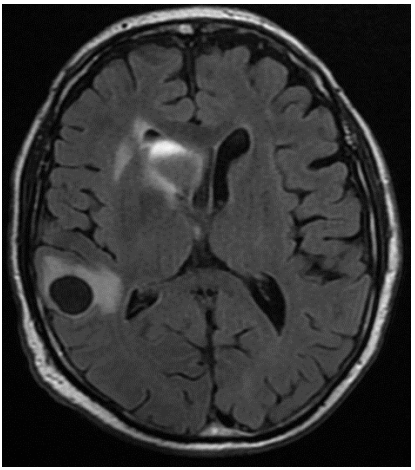

AXIAL T2 FLAIR

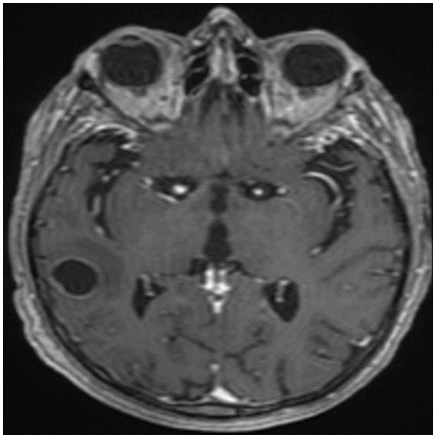

AXIAL T1+Contrast

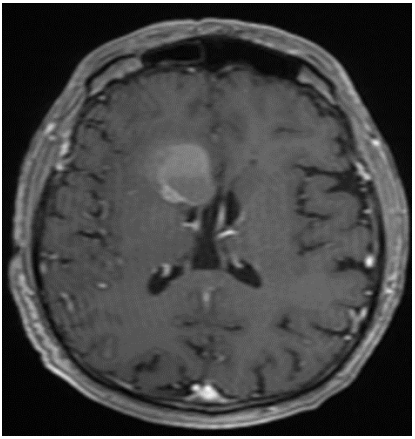

AXIAL T1+Contrast

- **43 year old** patient known with mammary cancer
- At the level of the left frontal lobe is highlighted o gigantic nodular mass, with heterosignal in T2, FLAIR and T1, with cetral

necrotic areas and hematic residues; the mass described presents intense gadolinophilia, inhomogeneous especially in the periphery, on the internal shape of the mass described is highlighted a tissular bud, and in the proximity of the posteromedial shape there is another nodular mass similar to the lesion anteriorly described, having an important mass effect on the left lateral ventricle which appears with a compressed frontal horn and a subfalciform herniation of the median line structures shifting to the right with a left transtentorial herniation in contact with the left antero-lateral face of the pons

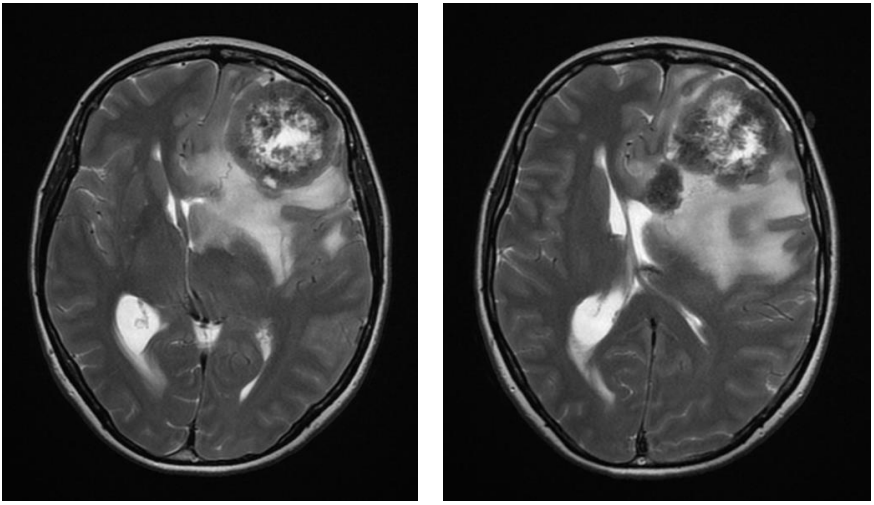

AXIAL T2

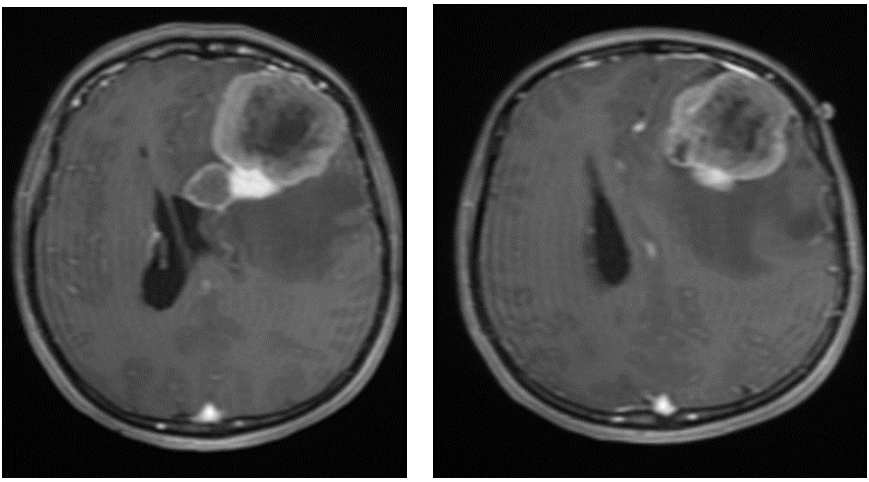

AXIAL T1+Contrast

- **42 year old** patient with malign melanoma, adresses to the emergency room with dyzartria
- On the radiologic findings there are multiple lesions with dense structures and parenchymal edema, some of them inhomogeneous, localized supra- and infratentorial.

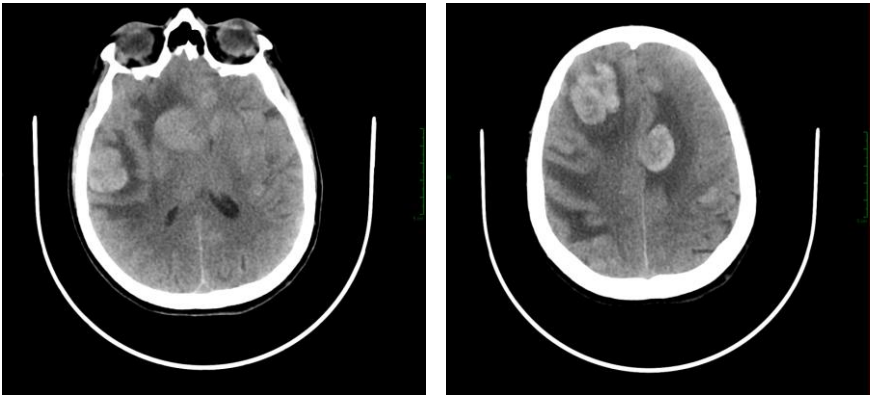

- **68 year old** patient known with laryngian cancer adresses the emergency room for left hemiparesis
- On the radiologic findings there are multiple spontaneous hyperdense nodular formations, with massive finger-like edema in the right cerebral hemisphere with an important compression on the right lateral ventricle and a minimum shift of the cerebral structures to the left and diffuse edema in the right cerebral hemisphere.

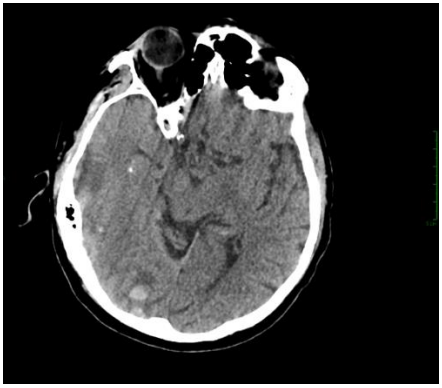

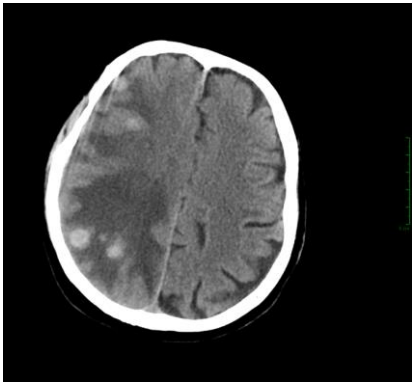

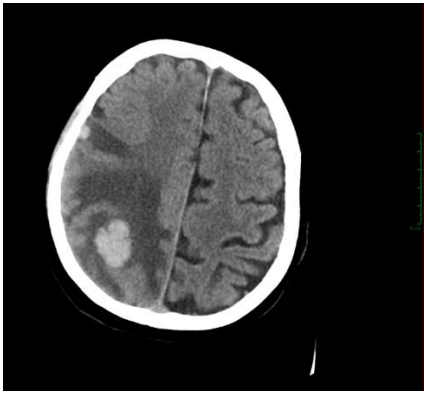

➢ **PSEUDOTUMOR LESIONS – CEREBRAL HYDATID CYST**

- **23 year old** patient known with hepatic hydatidosis adresses the

emergency room for headaches, vomiting and blindness.

- On the imagistic findings at the high left frontal aspect there is gigantic mass with fluid signal, nonrestrictive, with an interior septum; on the postcontrast aspect the lesion appears with a very fine peripheral load at the lesion wall, without parietal iodophilic buds or intralesional, with the shift of the adjacent vascular structures.

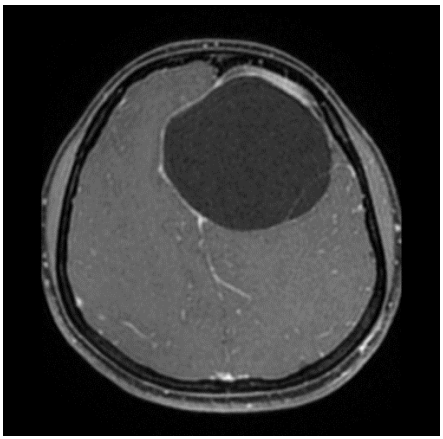

AXIAL T1+Contrast

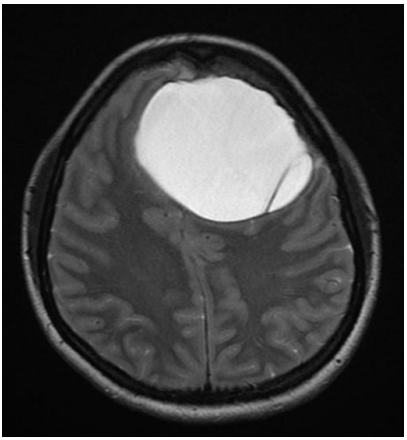

AXIAL T2

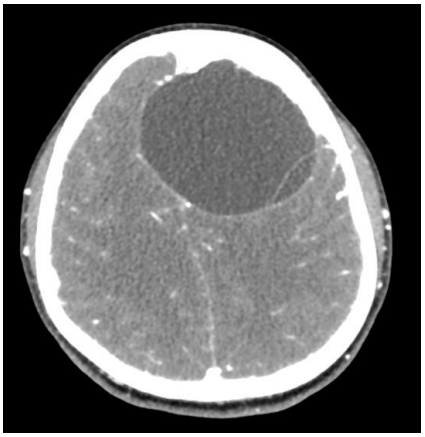

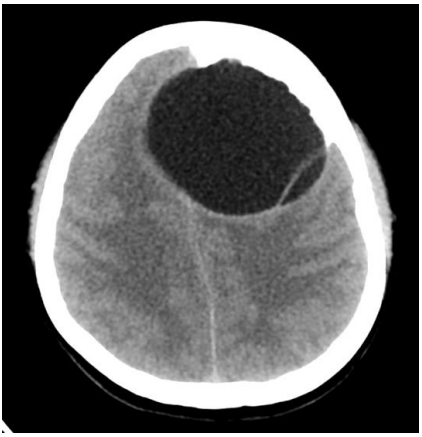

CT

- **MENINGIOMAS**
  - Non-glima extrenevraxial tumors
  - Classified in: - primary intradural
    - primary epidural
  - Many of them are benign, but a small percentage of them can be malign
  - Simptomatology: - asimptomatic
    - headaches
    - paresthesia
- **76 year old** patient adresses the emergency room for right inferior limb paresthesias with a suddenly onset
- On the radiologic findings there is a left high parietal mass very dense on FLAIR, lightweighted signal on T1 and T2, with a regular shape.

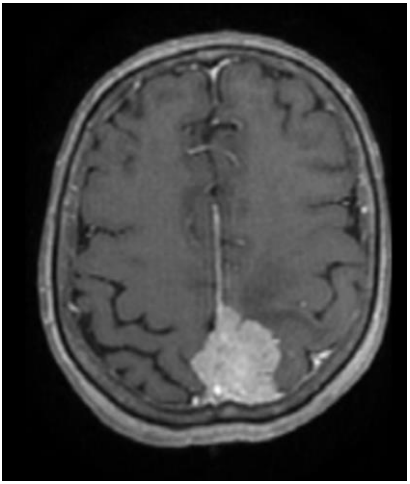

AXIAL T1+Contrast

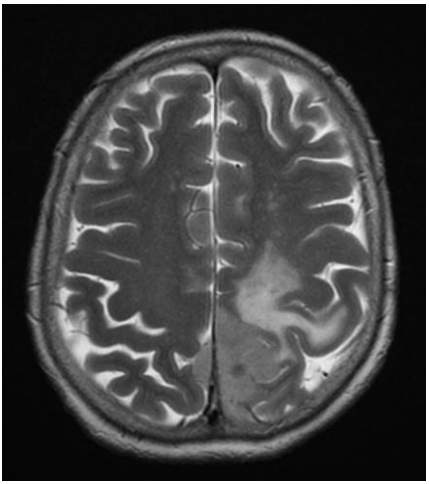

AXIAL T2

- **61 year old** adresses the emergency room for tonico-clonico ictus, loss of consciousness followed by temporo-spatial dezorientation and confusion.
- On the radiologic findings there is a multi lobular mass with parenchyma-like signal in T2/FLAIR, hyposignal in

T1, restrictive in DWI and ADC, with heamtic residues, intense gadolinophilic and at the high frontal level exceedind the median line.

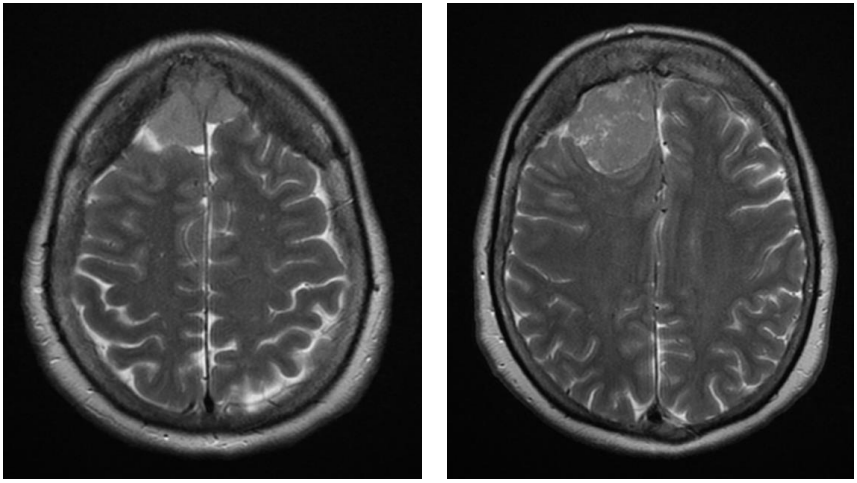

AXIAL T2

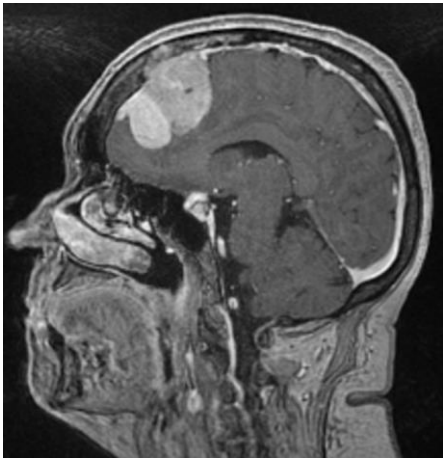

SAGITAL T1+Contrast

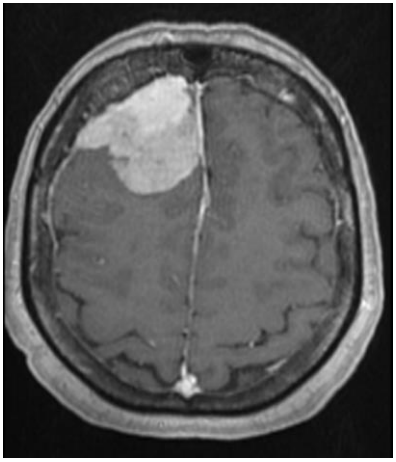

AXIAL T1+Contrast

- **<u>SCHWANNOMAS</u>**
  - Benign tumors with axonal sheath origin
  - Well circumscribed mass with mass effect on the adjacent structures, without infiltration or invasion of the parechyma

    - **64 year old** patient adresses the emergency room for a postictal condition

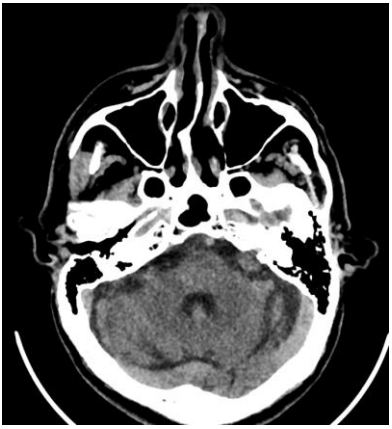

AXIAL – SCHWANOM VESTIBULO-COHLEAR STANG

    - **62 year old** patient adresses the emergency room for headaches
    - On the imagistic findings there is a right ponto-cerebellar angle extranevraxial tissular mass, light inhomogeneous, spontaneous hyperdense, with T2 and FLAIR hypersignal, T1 hyposignal as against the cerebellar parenchyma, with hematic residues localised intralesional .

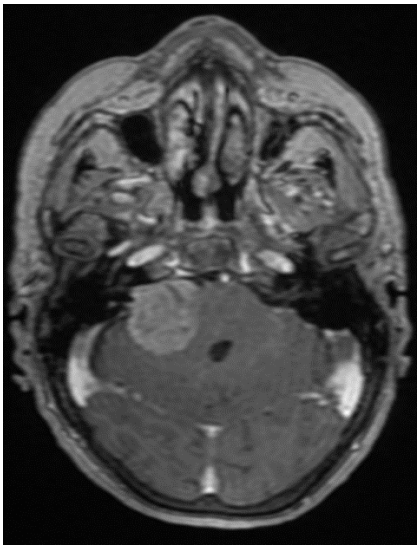

AXIAL T1+Contrast

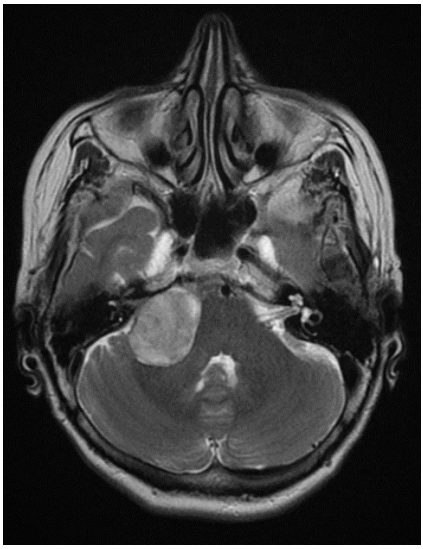

AXIAL T2

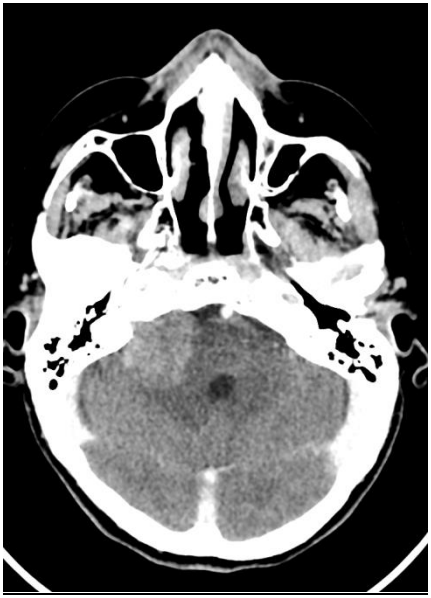

IMAGISTIC ASPECTS IN TRAUMATIC BRAIN INJURIES

The cerebral hemorrhages are classified in traumatic (with or without fractures discernable on CT-scan or radiography) and non - traumatic (hemorrhagic stroke and the subarachoid hemorrhage caused by the rupture of a microaneurysm).

- **Cranian fractures**
  - Caused by a high energy force applied on the bone, that will deform it beyond its elastic limit.

Cranian fractures classification:

- According to how the bone is interested (totally or partially): ca be full or partial (fissures);
- According to the topography: fractures of neurocranium or viscerocranium;
- According to how they communicate with the exterior: can be opened or closed;
- According to the shape: liniar, cominutive, diastatic, depressed in the subjacent structures;
- According to the disposition of the bone fragments in the fracture locus: can be intrusive and extrusive (projectile outlet).

- ***The posttraumatic brain hemorrhages*** are:

  Extranevraxial:
  - Subdural hematoma (SDH)
  - Epidural hematoma (EDH)
  - Subarachnoid hemorrhage (SAH)

  Intranevraxial:
  - Hemorrhagic contusions from coup or "contre coup"
  - Diffuse axonal injury (DAI)

  - **50 year old** patient addresses the emergency room for headaches and vomiting started following a traumatic brain injury occurred as a result of a car accident

- On the radiologic findings there is a right mastoid fracture with multiple left temporal fractures and a left large sphenoid wing fracture.

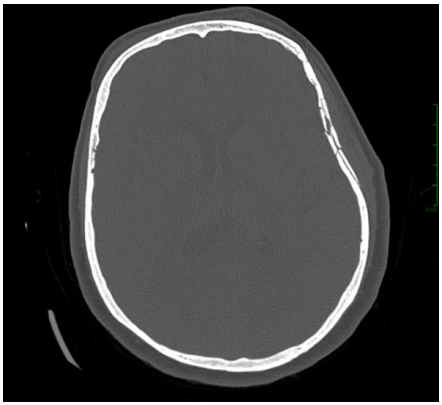

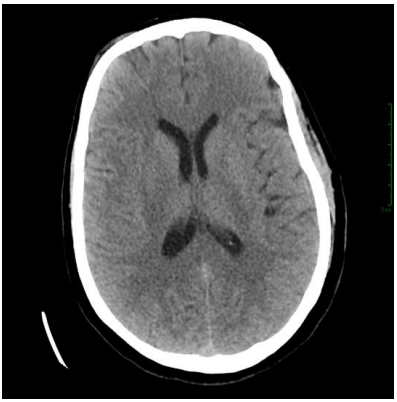

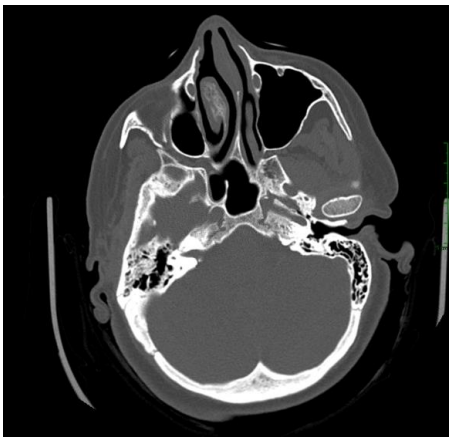

- **33 year old** patient addresses the emergency room for an ictal status that produced a traumatic brain injury
- On the imagistic findings there is a fracture with a ramified right temporal-parietal trajectory; left frontal-parietal subdural hematoma, hematic contusions and a left frontal-parietal

subarachnoid hemorrhage with diffuse edema in the left cerebral hemisphere.

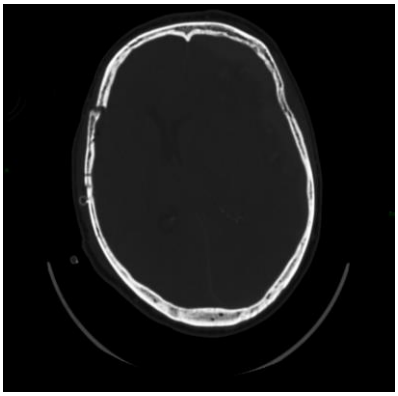

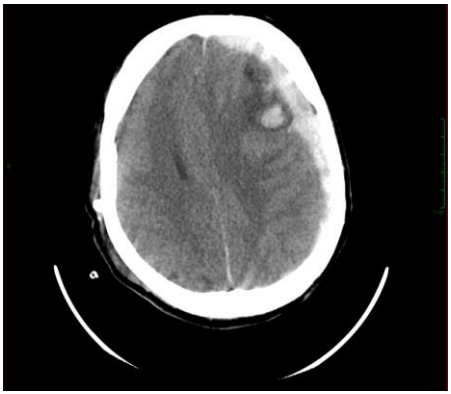

➢ **HEMATOMAS:**

- **The epidural hematoma** is a hemorrhagic collection formed in the virtual space between dura mater and the internal plate of the cranium being associated often with cranial fractures. The hemorrhagic source in most cases is arterial, from a rupture of the middle meningeal artery.
- The shape is biconvex or lentiform and the CT-scan shows a hyperdense heterogeneous fluid structure that can or cannot have mass effect.
    - ❖ **31 year old** patient addresses the emergency room for a traumatic brain injury with loss of consciousness followed after a forehead blow
    - ❖ The CT-scan shows a left frontal epidural hematoma

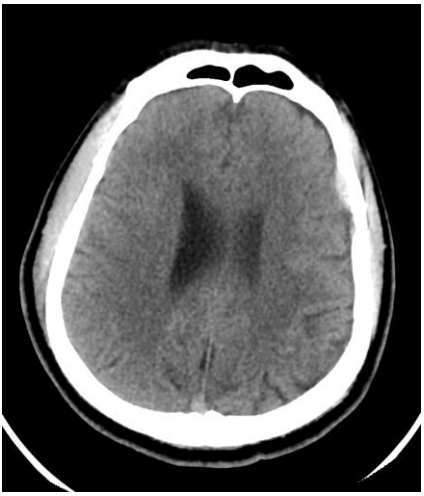
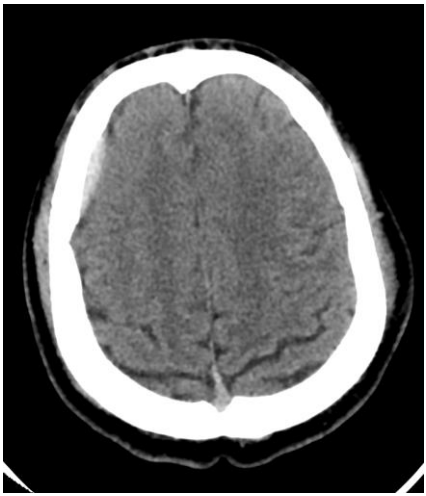

- **The subdural hematoma** is a hemorrhagic collection formed in the space between the dura mater and arachnoid layer often produced after a traumatic brain injury. The CT-scan shows a crescent-like hemorrhage with hyper intensity.
    - **68 year old** patient addresses the emergency room for headache and confusion.
    - The CT-scan shows an acute subdural hematoma in the left T-O aspect.

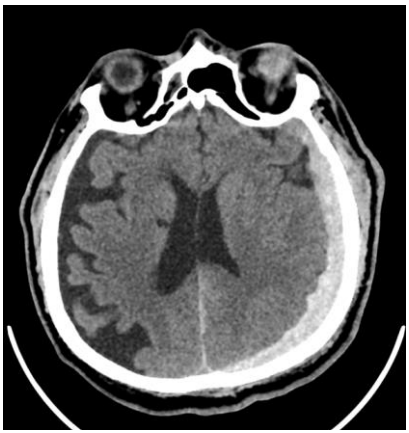
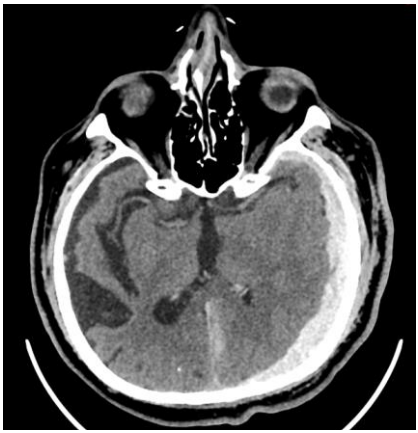

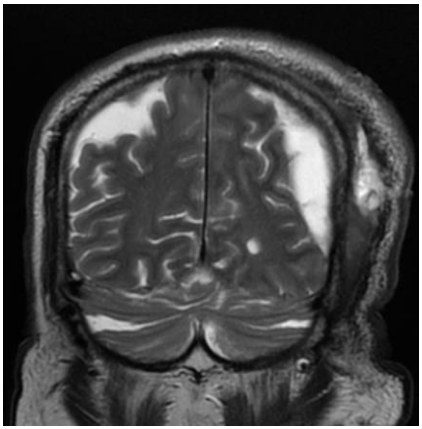
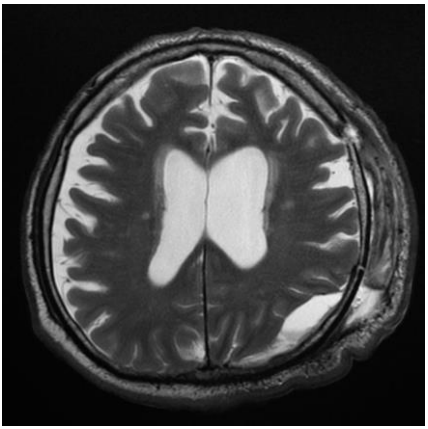

- **The subarachnoid hemorrhage** is an acute, sudden bleeding, in subarachnoid space, most frequently observed after a traumatic brain injury or a ruptured aneurysm. The CT-scan sensitivity is highly influenced by both the quantity of the blood and of the time elapsed since the onset of the hemorrhage. The CT-scan shows a hyper intense image that fills the subarachnoid space.

    - **77 year old** patient addresses the emergency room for a traumatic brain injury
    - The CT-scan shows a left high parietal epidural hematoma, with serpiginous hyper intense spots in the left high frontal, right temporal and left temporal aspects of the brain, where it associates small hematic petechiae.

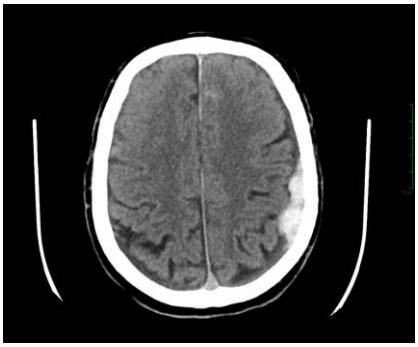
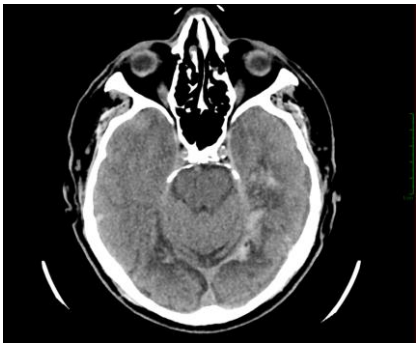

- **The parenchymatous hematoma** is formed in the cerebral hemispheres parenchyma as a result of a traumatic brain injury. Is characterized by a well circumscribed hemorrhage, localized in the white matter of the cerebral hemispheres.
    - **61 year old** patient known with hypertension addresses the emergency room for headache and vertigo
    - On the right superficial parieto-occipital aspect is evidentiated an intrecerebral lesion with T2 and T1 heterosignal, with peripheric edema.

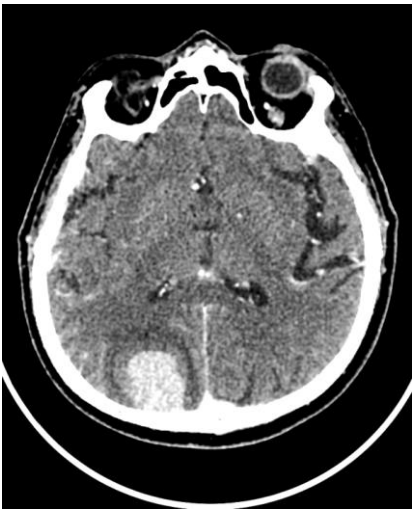
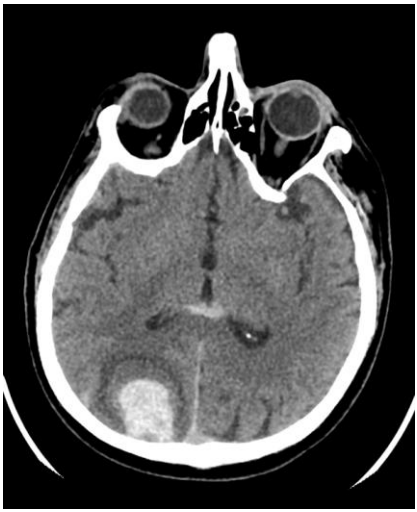

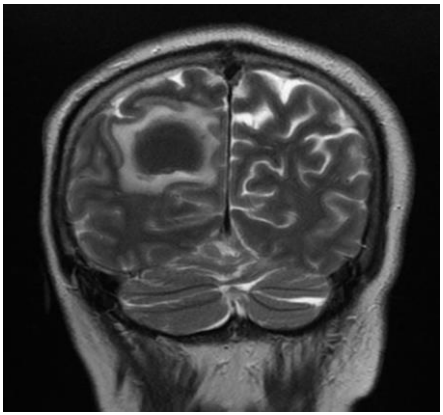
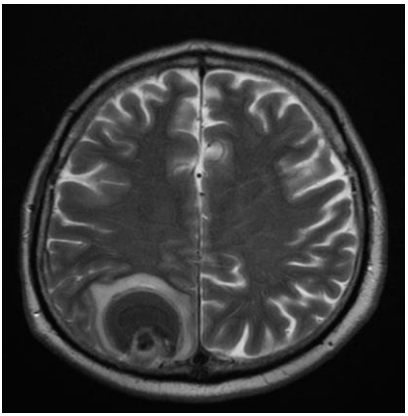

- ❖ **76 year old** patient that presents a right hemiparesis
- ❖ The CT-scan shows a left thalamo-capsulo-lenticular intraparenchymatous hematoma with edema and contact with the 3rd ventricle and minimum hemorrhage in the posterior horns of the lateral ventricle.

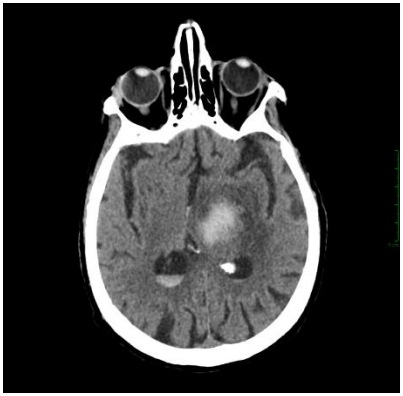
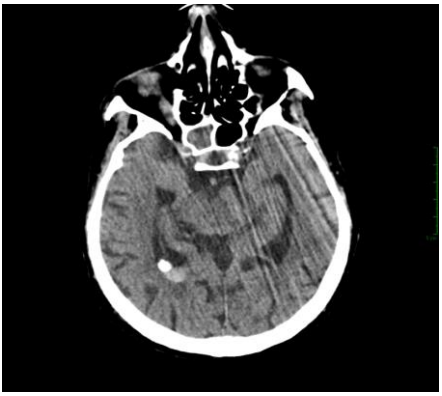

- **HEMORRHAGIC CONTUSIONS** – are small cortical bleedings produced by coup or countercoup, most frequently localized in the fronto-basal and temporal anterior aspect of the brain.

- **80 year old** patient presents confusion after a traumatic brain injury
- The CT-scan shows hemorrhagic contusions bilaterally fronto-temporal, with peripheral edema, bilateral fronto-temporal subarachnoid hemorrhage, subdural hematoma bilaterally in the fronto-temporo-parietal aspect.

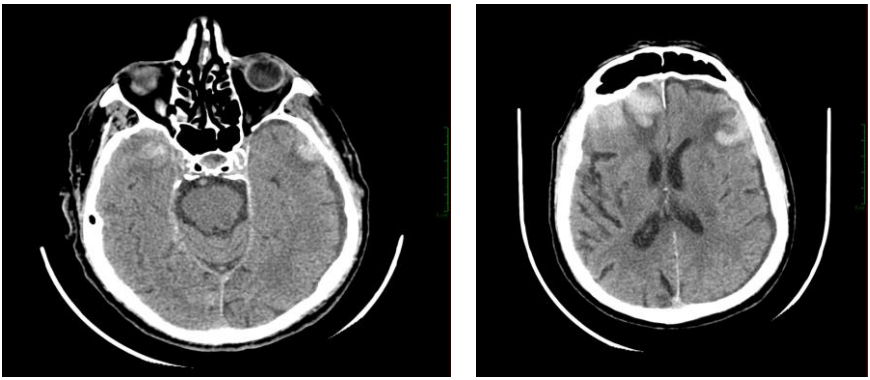

Tumoral mass that causes falx herniation with contralateral displacement of the median line.

- **THE CEREBRAL HERNIATION** is reffering to the displacement of the cerebral tissue from its normal location, in an adjacent space, as a result of a mass effect. Is a life threatening affliction and requires a prompt diagnostic.
  - The cerebral herniation is clasiffied as intracranial or extracranial. An intracranial herniation can be subfalciform (the most frequent type), transtentorial (ascended or descended), transsphenoidal or amygdalian. The brain herniation can have compressive effects on the nerves and arteries of the brain (causing hemorrhage or ischaemia) or circulatory obstruction of CSF resulting in a hydrocephaly.

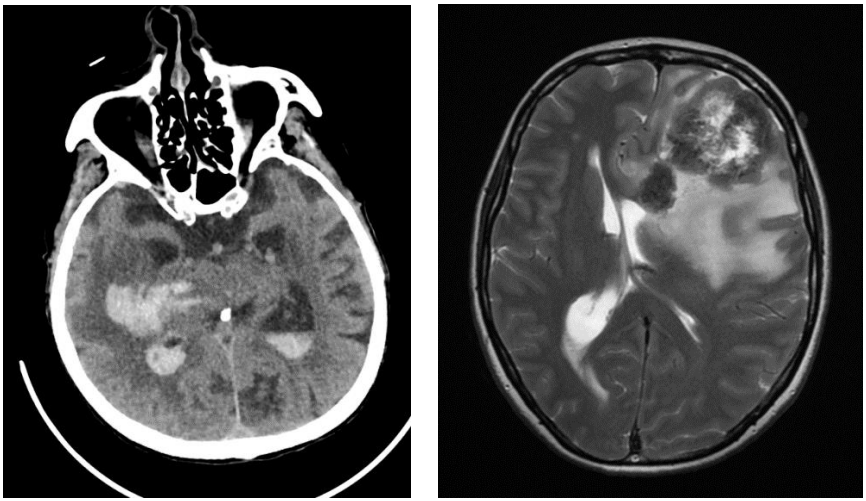

Intraparenchymatous hematoma that causes descending transtentorial herniation (uncal).

Figures: Personal collections of dr. Grosu

References:

1. Osborn AG, Heaston DK, Wing SD. Diagnosis of ascending transtentorial herniation by cranial computed tomography. AJR Am J Roentgenol. 1978;130 (4): 755-60.
2. W Dahnert. Radiology Review Manual. Lippincott Williams & Wilkins. (2011)
3. Provenzale JM. Imaging of traumatic brain injury: a review of the recent medical literature. AJR Am J Roentgenol. 2010;194 (1): 16-9.
4. Davis PC. Head trauma. AJNR Am J Neuroradiol. 2007;28 (8): 1619-21.
5. Lee B, Newberg A. Neuroimaging in traumatic brain imaging. NeuroRx. 2005;2 (2): 372-83.
6. Maas A, Stocchetti N, Bullock R. The Lancet Neurology. 2008;7 (8)
7. Diagnostic Imaging. Brain. Anne G. Osborn [et al.], First Edition
8. CT and MRI of the whole body. John R. Haaga/ Daniel T . Boll [et al.], Sixth Edition
9. https://radiopaedia.org/
10. https://radiologyassistant.nl/
11. The images are from the personal collection of the Radiology department from SCJU Sibiu.

CEREBROSPINAL FLUID

Prof. Dr. Alexandru Vlad Ciurea[1],
Assist. Prof. Dr. Mircea Vicențiu Săceleanu[2,3]

[1] "Carol Davila" University of Medicine and Pharmacy, Bucharest
Sanador Clinical Hospital, Bucharest
[2] Department of Neurosurgery, Faculty of Medicine, "Lucian Blaga" University, Sibiu
[3] Department of Neurosurgery, County Clinical Emergency Hospital of Sibiu, Romania

"The three essential things to do something worthwhile are: hard work, perseverance, and common sense."
Thomas Edison (1847-1931)

Contents

1. General Data

Around brain and spinal cord, as well as in the ventricles and ependymal canal there is cerebrospinal fluid (CSF). At the level of the brain, four ventricles are described: two lateral ventricles, the third ventricle (V. III) and the fourth ventricle (V. IV). These ventricles

communicate with each other with the medullary ependymal canal and the subarachnoid space surrounding the central nervous system.

Classically, CSF is defined as the biological fluid in the cerebral ventricles, central medullary canal and subarachnoid spaces. It is now known that the cerebrospinal fluid and the extracellular fluid or interstitial fluid in the brain tissue are identical and are in fact a single fluid that is the physiological environment of the central nervous system.

CSF is mostly the product of ventricular choroidal plexuses and its resorption is done mainly through the arachnoid villi to the dural venous sinuses. The volume of cerebrospinal fluid is approximately **125-150 ml in adults**, of which **25-30 ml are in the ventricular system**, **30 ml of CSF is in the spinal subarachnoid space** and the rest of the CSF is contained in the cranial subarachnoid space and basal cisterns.

The total production of CSF is about **400 - 500 ml / day, about 0.35-0.4 ml/min**.

The pressure of the cerebrospinal fluid is equal to the intraparenchymal pressure and constitutes the intracranial pressure; has normal values between **5-10 mm Hg**, reaching a maximum of 15 - 20 mm Hg, or between **80 - 150 mm H2O** (1).

CSF runs in two main compartments - one is represented by the ventricular system and the ependymal canal while the second one by the subarachnoid space. The surface of the endo-neural fluid space, except for the choroid plexuses, is bordered by ependymal cells. The subarachnoid space is delimited by arachnoid and pia mater and extends along cranial nerves, around the roots of the spinal nerves and through the Virchow-Robin perivascular spaces, which surround the arterioles and venules, penetrating deep into the cerebral parenchyma (2)(3).

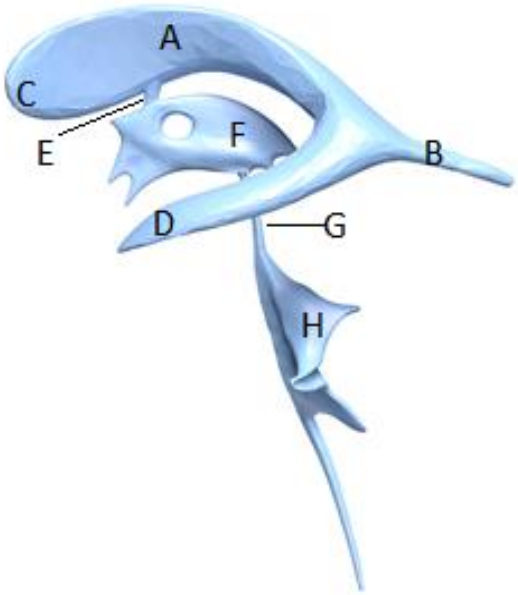

Figure 1. Representation of the ventricular system
A. Central part (pars centralis) of lateral ventricle.
B. Occipital horn of the lateral ventricle
C. Frontal horn of the lateral ventricle
D. Temporal horn of lateral ventricle
E. Interventricular foramina of Monro
F. IIIrd ventricle
G. Sylvius aqueduct.
H. IVth Ventricle.
(Image source: Modified after BodyParts3D, © The Database Center for Life Science licensed under CC Attribution-Share Alike 2.1 Japan)

CSF provides the homeostasis necessary for the development of nervous activity through its functions:

- nutritional role by participating in the metabolic exchanges in the nerve tissue;

- ensures the biochemical stability of the nerve tissue;
- allows the removal of catabolites resulting from the activity of the nervous system;
- allows the neuroendocrine integration of the stages of the central nervous system through hormonal circulation;
- has an informational role through the circulation of chemical mediators / neuropeptides with a role in modulating nerve influx at the synapses;
- has a role in mediating the immune response: the drainage of the CSF to the cervical lymphatics transfers some of its own substances (such as proteins from periventricular cells, with antigenic properties) or foreign substances that can induce an antigenic response;
- CSF maintains together with the meningeal structures the special anatomical shape and consistency of the CNS;
- CSF has a hydrostatic (antigravitational) role ensuring the buoyancy of the brain: the weight of the brain in CSF is about **50 grams;**
- has the role of mechanical protection, by absorbing shocks during movement;
- maintains endocranial volume constant by adjusting the production / resorption ratio of CSF according to variations in brain parenchyma volume and intracranial blood volume, according to the Monro-Kellie relationship;
- has a role in maintaining the temperature of the central nervous system.

Pathological processes that disrupt the physiology of CSF and parenchymal interstitial fluid cause significant disorders in the functioning of the central nervous system in relation to the level of interest (production, circulation or resorption), often more pronounced in children, where compensatory mechanisms are less effective (4,5).

The basic function of the cerebrospinal fluid is tetravalent. CSF has the function of **preventing cerebral ischemia.** The mechanism is simple and refers to compensation (within certain limits) for the increase in intracranial pressure by migrating fluid from the cranial box. Second, according to Archimedes' principles, the brain has a density almost equal to that of the CSF (the liquid in which it is immersed) and will

have almost neutral buoyancy, in other words the **brain floats in the CSF**. Third, CSF ensures the **chemical balance** by clearing the catabolism products of neurons and glial cells while correctly dispersing neuroendocrine factors. A concrete example is that of *glycine* which, if not removed correctly and sufficiently, will cause alterations in the temperature control mechanisms. Finally, the CSF has the function of **a dynamic barrier dissipating shock waves** (within tolerated physiological limits) that would damage the brain substance (4)(5).

2. Brain barriers

The extraparenchymal fluid spaces, the ventricular system, subarachnoid space, intraparenchymal extracellular space and interstitial fluid are separated from the endocranial intravascular space by two morphological and functional barriers: the blood-fluid barrier (BFB) and the blood-brain barrier (BBB). These "barriers" are in fact dynamic interfaces that allow fluid exchanges that ensure homeostasis of the central nervous system.

2.1. Blood-brain barrier

The blood-brain barrier (BBB) separates the blood circulation from the nerve parenchyma and allows brain homeostasis. The blood-brain barrier is an anatomical barrier involving a complex of biochemical and chemical mechanisms of membrane transport that creates **a dynamic interface with the role of regulating the exchanges between blood circulation and nervous system fluids**. The blood-brain barrier protects the nerve parenchyma from harmful substances in the circulating blood and allows the central nervous system to be supplied with the necessary nutrients (7).

2.2. Blood-spinal cord barrier

In the spinal cord, the blood-spinal cord barrier (BSCB) is equivalent to BBB. Minor differences were found between the blood-brain barrier and the blood-bone marrow barrier: for example, the endothelial cells of the medullary capillaries contain **glycogen deposits**, which are not normally found in the brain capillaries, and another difference is the

increased permeability of the medullary capillaries. cerebral capillaries (2-5).

2.3. Blood-fluid barrier

CSF is separated from the intraparenchymal bloodstream by a structure called the blood-fluid barrier (BFB). The blood-fluid barrier consists of the epithelium of the choroid plexuses, the external meningoblastic layer of the arachnoid, the epithelium of the arachnoid villi, and the endothelium of the vessels that cross the subarachnoid space. The cerebrospinal fluid is mostly developed by the choroid plexuses in the cerebral ventricles, which is a major component of the blood-fluid barrier. Choroidal plexuses are formed by capillarization of choroidal arteries, capillaries are surrounded by connective tissue and in contact through the basement membrane with the ependymal epithelium (2-5).

3. Mechanism of formation and CSF composition

The choroid plexus at the blood-CSF border is the main component of fluid dynamics in central nervous system. The choroid plexus in the lateral ventricles produce roughly 60-70% of all CSF. The capillaries of the choroidal plexuses have fenestrations through which substances pass from the capillary lumen to the ependymal epithelium. Ependymal cells covering the choroidal capillaries are joined by circumferential occlusion junctions that ensure selective permeability. Structurally and functionally the choroid plexus epithelium resembles the kidney proximal tubule (4,5).

Fluid formation is primarily generated by net secretion of Na, Cl and HCO_3; water osmotically follows ion transport across the apical membrane. CSF production is directly proportional to the net transfer of Na and Cl from blood to ventricles. The driving force for ion movements across choroid plexus membranes is a downhill concentration or electrochemical gradient (8-10).

Na moves from plasma across the basolateral membrane into choroid plexus epithelium through the epithelial sodium channel (ENaC) and Na-inward transport coupled with HCO_3. At the other side of the choroid cell, K, Cl and HCO_3 move downhill across the apical

membrane into CSF. This transfer is preceded by active transport, ATP-dependent, through the Na/K ATP pump. Active Na pumping into CSF maintains a low gradient in choroid plexus epithelium Na concentration, hence establishing a basolateral inward driving force for Na transport from plasma to epithelium – Figure 2 (8-10).

Cl is the main anion in CSF secretion. It is actively transported across the basolateral membrane in exchange for cellular HCO_3. This attracts Cl into the choroid epithelium which then diffuses into CSF through Na-K-Cl cotransporter. However, the gradient created at the apical membrane is the main trigger of Cl secretion into CSF – Figure 2 (8-10).

Bicarbonate reaches the CSF from 2 main sources. First, carbon anhydrase catalyzes the hydration of CO_2 to form H and HCO_3 ions in choroid plexus epithelial cells. Second, HCO_3 is transported intra-epithelial through Na-HCO_3 cotransporter. HCO_3 release into the CSF is carried out either by downward diffusion through an anion channel or through an electrogenic Na-coupled HCO_3 co-transporter at the apical membrane – Figure 2 (11-14).

Water represents 99% of CSF; it chases osmotically active ions (Na, Cl, HCO_3) by diffusing down its chemical potential gradient through aquaporin (AQP1) channels in the apical membrane – Figure 2 (11-14).

Minerals make up the majority of CSF dissolved substances. Organic substances are in lower concentrations: glucose represents 2/3 of plasma glucose, total proteins 0.15-0.50 g/L, urea 10-40 mg%, total lipids 1.25 mg%, creatinine 1.2 mg%. Normally the cell density is below 5 elements / mm3 in lumbar CSF, 3 elements / mm3 in cisternal CSF and 2 elements / mm3 in ventricular CSF – Neutrophils = 0, Lymphocytes <5. Exceeding 10 elements / mm3 in lumbar CSF is pathological. Only in the newborn can the number of elements exceed 10 elements / mm3 (even up to 30 elements / mm3) (2,3,5)

Table 1. Concentration of solutes in plasma and cerebrospinal fluid

Substance	CSF	Plasma
Na (mEq /l)	147	150
K (mEq /l)	2,86	4,6
Cl (mEq /l)	113	101
HCO3 (mEq /l)	23.3	23
Glucose (mg/100ml)	60	90
Proteins (mg/100ml)	20 – 30	7000
pH	7,30	7,4
Osmolality (mOsm/l)	289	289

4. CSF Dynamics

The cerebrospinal fluid developed in the lateral ventricles then passes into the third ventricle and then through the Sylvius aqueduct reaches the fourth ventricle; from here, it passes into the magna cistern through Magendie's foramen and circulates in the subarachnoid space. CSF is mostly resorbed in the dural venous sinuses through the arachnoid villi (2,3,5)

From the magna cistern the cerebrospinal fluid follows three directions:

- to the cerebellar subarachnoid space;
- to the prepontine, interpeduncular and suprasellar basal cisterns;
- to the spinal subarachnoid space.

5. CSF Resorption

Absorption of cerebrospinal fluid occurs in a proportion of up to 60-80% in the dural venous sinuses through arachnoid villi. Arachnoid villi, called Pacchioni's corpuscles or granules, are arachnoid extensions in the thickness of the dura mater and venous sinuses, which hypertrophy in time and can imprint the internal cranial bone. The passage of CSF from the subarachnoid space into the venous sinuses is done through a unidirectional valvular mechanism and by transcellular transport mediated by vesicles (2,3,5)

The resorption of cerebrospinal fluid depends on the pressure difference between the subarachnoid space and the venous blood in the upper longitudinal sinus. Normally the pressure gradient is 3-4 mmHg, but usually the pressure in the superior sagittal sinus is negative. The pressure difference called **"critical opening pressure"** is about **5 mmHg**, ensuring constant resorption of cerebrospinal fluid. In this way, the absorption depends only on the pressure values of the CSF at the level of the arachnoid villi; hence, CSF circulation relies more on CSF absorption rather than production (which is constant) (2-5)

6. CSF Investigation

The biochemical and cytological exploration of the CSF is done by evacuation and collection of CSF by lumbar puncture (PL); this procedure is contraindicated in case of increased intracranial pressure (ICP). If there is a suspicion of an increase in intracranial pressure, the lumbar puncture can be done only after a cerebral computed tomography which indicates the absence of a cranial cause of intracranial hypertension. One of the possible complications of lumbar puncture may be intracranial hypotension with consecutive engagement of the cerebellar tonsils by foramen magnum and compression of medulla (2-5).

Lumbar puncture (LP) can highlight:

- the value of the intracranial pressure, measured with a manometer;
- increase in the number of leukocytes in meningeal infections;
- the value of proteins;
- the existence of a subarachnoid hemorrhage, traumatic or non-traumatic;
- the existence of markers for certain diseases:
  - increased gamma globulin in some demyelinating diseases, etc.
  - decreased glucose levels in TB meningitis, meningeal carcinomatosis.

The macroscopic appearance of the CSF may indicate:

- bacterial meningitis when CSF is cloudy,
- subarachnoid hemorrhage - hemorrhagic CSF, or in case of PL defect,

- subarachnoid hemorrhage older than 3 days or in proteinorrhea, CSF has a citrine appearance.

CSF cultures can be performed to highlight microorganisms responsible for CNS infections. The specific marker for CSF is beta-2 transferrin, which is found only in CSF, and its detection is important in CSF fistulas (2-5).

The normal biochemical and cellular values of the CSF obtained by PL are:

- clear, colorless appearance;
- proteins: 15-45 mg%,
- gamma-globulins: 3-12% of the plasma proteins;
- glucose: 50-80 mg/dl (approximately 2/3 of the blood sugar),
- chlorides: 110-125 mEq/l;
- cellularity: 0-5 leukocytes, absence of red blood cells.

Changes in the composition of the CSF can occur in various conditions: meningitis, encephalitis, brain tumors, arachnoiditis, subarachnoid hemorrhage, spinal cord compression, CNS degenerative diseases, etc. In spinal tumors, the composition of the CSF can change by increasing proteinuria, slowing down and blocking the spinal circulation of the CSF. Increased proteinuria leads to blockage of the peripheral CSF drainage pathway and obstruction of arachnoid villi, with the possible occurrence of hydrocephalus and increased intracranial pressure (2-5).

Table 2. CSF in bacterial, viral and tuberculous meningitis

	Bacterial meningitis	Tuberculosis	Viral meningitis
Colour	Yellow & turbid	Fibrin web & turbid	Clear
Neutrophils	↑↑↑	↓	↓
Lymphocytes	↓	↑↑↑	↑↑↑
Glucose	< 50% of plasmatic glucose	< 50% of plasmatic glucose	> 50% of plasmatic glucose
Proteins	↑↑	↑↑↑	↑

7. Conclusions

CSF is mostly the product of ventricular choroidal plexuses and its resorption is done mainly through the arachnoid villi to the dural venous sinuses. The volume of cerebrospinal fluid is approximately **125-150 ml in adults**, of which **25-30 ml are in the ventricular system**, **30 ml of CSF is in the spinal subarachnoid space** and the rest of the CSF is contained in the cranial subarachnoid space and basal cisterns - the total production of CSF is about **400 - 500 ml / day, about 0.35-0.4 ml/min**.

Absorption of cerebrospinal fluid occurs in a proportion of up to 60-80% in the dural venous sinuses through arachnoid villi called Pacchioni's corpuscles or granules (arachnoid extensions in the thickness of the dura mater and venous sinuses). The passage of CSF from the subarachnoid space into the venous sinuses is done through a unidirectional valvular mechanism and by transcellular transport mediated by vesicles.

The resorption of cerebrospinal fluid depends on the pressure difference between the subarachnoid space and the venous blood in the upper longitudinal sinus. Normally the pressure gradient is 3-4 mmHg, but usually the pressure in the superior sagittal sinus is negative. The pressure difference called **"critical opening pressure"** is about **5 mmHg**, ensuring constant resorption of cerebrospinal fluid.

Abbreviations

CSF - cerebral spinal fluid, **BBB** - blood brain barrier, **BFB** - blood fluid barrier, **BSCB** - blood spinal cord barrier; **ENaC** - epithelial sodium channels, **AQP1** - aquaporin 1, **ICP** - intracranial pressure, **LP** - lumbar puncture.

Disclaimer: the authors declare no conflict of interests.

References:

1. Johanson CE, Duncan JA 3rd, Klinge PM, et al. Multiplicity of cerebrospinal fluid functions: New challenges in health and disease. Cerebrospinal Fluid Res. 2008;5:10.

2. Ciurea A.V. Tratat de Neurochirurgie Vol. 1, Editura Medicală, București, 2010.
3. Ciurea A.V. Tratat de Neurochirurgie Vol. 2, Editura Medicală, București, 2011.
4. Constantinovici A., Ciurea A.V. Ghid practic de neurochirurgie, Ed. Medicală, Bucureşti, 1998.
5. Mohan D., Ciurea A.V. Mohan A.G. Curs de neurochirurgie, Editura Universitatii din Oradea, 2014.
6. Ballabh P., Braun A., Nedergaard M. The blood-brain barrier: An overview: Structure, regulation and clinical implications., Neurobiol Dis, 16:1-13, 2004.
7. Ballabh P., Braun A., Nedergaard M. The blood-brain barrier: An overview: Structure, regulation and clinical implications., Neurobiol Dis, 16:1-13, 2004.
8. Smith QR, Johanson CE. Effect of ouabain and potassium on ion concentrations in the choroidal epithelium. Am J Physiol. 1980;238(5):F399-F406
9. Brown PD, Davies SL, Speake T, et al. Molecular mechanisms of cerebrospinal fluid production. Neuroscience. 2004;129(4):957-970.
10. Millar lD, Brown PD. NBCe2 exhibits a 3 HCO3(–):1 Na+ stoichiometry in mouse choroid plexus epithelial cells. Biochem Biophys Res Commun. 2008;373(4):550-554.
11. Johanson CE. Fluid-forming functions of the choroid plexus: What is the role of aquaporin-1? In: Dorovini-Zis K, ed. The Blood-Brain Barrier in Health and Disease, Vol. 1. 1st ed. Enfield, New Hampshire: Science Publishers; 2015:140-171.
12. Johanson C. Choroid plexus-CSF circulatory dynamics: Impact on brain growth, metabolism and repair. In: Conn P, ed. Neuroscience in Medicine. Totowa, New Jersey: The Humana Press; 2008:173-200.
13. Oshio K, Song Y, Verkman AS, et al. Aquaporin-1 deletion reduces osmotic water permeability and cerebrospinal fluid production. Acta Neurochir Suppl. 2003;86:525-528.
14. Huber VJ, Tsujita M, Nakada T. Aquaporins in drug discovery and pharmacotherapy. Mol Aspects Med. 2012;33(5–6):691-703.

INTRACRANIAL HYPERTENSION

Prof. Dr. Alexandru Vlad Ciurea[1],
Assist. Prof. Dr. Mircea Vicențiu Săceleanu[2,3]

[1] "Carol Davila" University of Medicine and Pharmacy, Bucharest, Sanador Clinical Hospital, Bucharest
[2] Department of Neurosurgery, Faculty of Medicine, "Lucian Blaga" University, Sibiu
[3] Department of Neurosurgery, County Clinical Emergency Hospital of Sibiu, Romania

"There are successes that degrade you and defeats that elevate you".
Nicolae Iorga (1871-1940)

Contents

1. General Data

Intracranial hypertension (HIC) represents an increase in intracranial pressure due to disorders of pressure balance mechanisms. The intracranial pressure balance is maintained by keeping constant the volumes of the cerebral parenchyma, the cerebrospinal fluid and last but not least of the blood content (1).

The increase in intracerebral compartments and / or the addition of an extrinsic pathological volume determines the increase of the intracranial pressure above the normal values. Increased intracranial pressure (ICH) induces pathophysiological disorders that result in characteristic symptoms and paraclinic changes, correlated with the causal condition.

2. Classification

Classically, ICH has been divided into two main groups:

- intracranial hypertension as a result of intracranial expansive processes and
- pseudo-ICH, which occurs in diseases other than intracranial expansive processes, also known as pseudotumor cerebri.

Currently, considering the etiology and the mechanisms of volume-pressure disturbance, several types of HIC are mentioned (2):

2.1. Parenchymal ICH occurs in intracranial expansive processes (brain tumors, intracranial hematomas, brain abscesses, etc.), in traumatic cerebral edema, in cerebral ischemia with hypoxic cerebral edema, in general intoxications with neurotoxins, etc.

2.2. Vascular ICH occurs when increased PIC is secondary to blood, cerebral, or extracerebral circulation disorders. The increase in the volume of the cerebral parenchyma in vascular HIC is caused by cerebral edema or by an increase in cerebral blood volume ("congestive brain"). Cerebral edema and / or congestive cerebral parenchyma increase intracranial pressure. The increase in cerebral blood volume occurs in the case of an increased intracranial arterial blood supply or in the decrease or blockage of venous drainage.

2.3. ICH due to CSF dynamics disorders. CSF dynamics disorders can be:

- disorders of CSF circulation from formation to resorption and
- disorders of the passage of the CSF in the venous drainage system (resorption).

2.4. Idiopathic ICH or essential ICH, formerly known as cerebral pseudotumor cerebri. The etiology is not clearly established. It occurs in endocrine diseases, metabolic disorders or various hematological diseases, etc. The current pathogenic hypothesis is based on the disorder of the blood-brain barrier as well as the disturbance of the dynamics of the intracranial fluid circuits but with the maintenance of the self-regulation of the cerebral circulation.

3. Intracranial Pressure

Intracranial pressure is defined as the pressure developed by the intracranial structures (nervous tissue, blood and CSF), resulting from the effect of the tension forces developed by intracranial contents on the dural limiting sheath. The determining factor of intracranial pressure is the volume and distribution of fluid in the intracranial and spinal space.

Normally, the intracranial pressure (ICP) has average values between **5-10 mmHg**, with maximum values up to **15-20 mmHg**, corresponding to values of **80-150 mm H2O**. *The young child* has lower normal ICP values, with maximum values up to about 10 mmHg. (3)

Arterial pressure can vary around average normal values of 100 mmHg, with maximum values allowed up to 150 mmHg; parenchymal pressure is in balance with CSF pressure in the ventricular system and subarachnoid spaces. (4)

Intra-parenchymal pressure = Vascular pressure + intra-parenchymal fluid pressure = Interstitial pressure = CSF pressure

Interstitial pressure which results is equal to ventricular/subarachnoid CSF pressure; hence, intracranial pressure (ICP) can be identified by measuring each one of the aforementioned ones.

ICP = Interstitial pressure = CSF pressure

Intracerebral blood flow is maintained by the difference between cerebral perfusion pressure (CPP) and ICP. CPP results from the following relationship:

CPP = MAP – ICP (MAP = mean arterial pressure)

Intracranial pressure may have negative values depending on the position of the body and head or may show physiologic increases for extremely short periods of time (during sneezing, etc.). (5)

We mention that since the end of the XVIIIth century and later in XIXth century Monro [6] (1783) and then Kellie (7) (1824) established the relationships between the skull and its contents and postulate that the subdural intracranial volume is constant. The intracranial contents consist of the brain, the blood contents and the CSF (Monro-Kellie's Law). Any change in the volume of one of these components is immediately offset by changes in the volume of the other components.

4. Intracranial Contents

Intracranial contents are represented by:

- Cerebral parenchyma – 80-83.5%
- CSF – 10%
- Blood in the cerebral circulation – 7-10%

Monro-Kellie law states the following:

$\mathbf{V_{CSF}+V_{BLOD}+V_{BRAIN}+V_{OTHER}=VI_{NTRACRANIAL\ SPACE}=constant}$

V = volume

Any modification of one of the above components will be made, at first, to the detriment of the other components within the intracranial content. Therefore, the appearance of an expansive intracranial process will lead to reduction and ischemia of the cerebral vascular bed and to the obstruction of the CSF circulation, and later to obstructive hydrocephalus (8).

5. Increase in Intracranial Pressure

From the beginning we mention that this increase in ICP produces the major symptom, namely headache.

In physiological conditions for short periods of time by increasing the intracranial blood volume in the effort of coughing, sneezing, defecation, compensation for increased PIC may be at the limit. In pathological situations, even a small increase in intracranial volume exceeds compensation limits with the appearance of HIC.

Alteration of pressure control mechanisms occurs in cases such as (9):

- Intracranial expansive processes: tumors, hematomas, intracranial abscesses, etc.
- Diffuse cerebral edema in traumatic brain injury, encephalitis, asphyxia.
- Cerebral edema in intoxications, etc.
- Blockage of CSF circulation, etc.

The following values are accepted for normal and pathological intracranial pressure:

- Normal intracranial pressure has values up to **5-10 mmHg**,
- Values between **15 - 20 mmHg** correspond to the compensation limits but also to a degree of instability in pathological situations,
- Intracranial pressure **above 20 mmHg** causes brain damage in relation to the duration of these increased values.

Accurate assessment of ICH is mandatory, mainly to prevent increase beyond the limits that causes severe, vital brain suffering. ICH monitoring allows highlighting increases in intracranial pressure and changes in the appearance of ICH waves that correspond to decreased brain compliance.

Figure 1 depicts a normal intracranial pressure waveform. The baseline pressure level is affected by rhythmic components due to cardiac and respiratory activity. Fluctuations of MAP is responsible for small amplitude rapid pulsation while respiration causes larger-amplitude fluctuations of lower frequency. To accurately describe ICP, both baseline and pulsatile components needs to be evaluated.

If the ICP waveform is examined at higher velocities, then the waveform of highest frequency can be seen to consist of as many as five peaks. Three of these peaks are relatively constant: the percussion wave (W1), the tidal wave (W2) and dicrotic wave (W3) – Figure 2. The percussion wave is the result of pulsation in the large intracranial vessels while tidal wave is the result of brain elastance.

Several types of pressure increases can be described in relation to the above characteristics and depending on the clinical evolution (10):

- Superacute increase in ICP with rapid decompensation which occurs in supra-acute cases of intracranial hematoma, cerebral edema, etc.
- Acute increase in ICP, preceded by a prolonged infraclinical period. The period in which the intracranial pressure reaches and then exceeds the normal pressure values, is long, with a slow rate of increase of the intracranial pressure, occurs in brain tumors, etc.
- Slow increase in ICP with prolonged infraclinical period and with a long period of pathological increase of ICP, is found in cases of decreased CSF resorption in acute meningitis, subarachnoid hemorrhage, cerebral venous thrombosis, etc.

6. Measurement of Intracranial Pressure

Measurement of intracranial pressure was initially performed by determining lumbar CSF pressure by lumbar puncture. In lateral decubitus, the pressure of the ventricular CSF is equal to the pressure of the lumbar spinal CSF. In a sitting position, the intraventricular pressure is lower than the pressure of the lumbar CSF. In adults, the normal pressure of the lumbar CSF is approximately **100-200 mmH2O**. Lumbar manometry is no longer used due to the risk of cerebral hernia.

Currently, the ICP measurement is done by invasive means, establishing a connection through a drill hole between the intracranial space and the external measurement system (transducer-pressure sensor) and recording the ICP values. The most common procedure for monitoring ICP is through the intraventricular catheter, which also allows CSF drainage as needed and can be recalibrated. Catheter obstruction incidences can be easily resolved and infectious risks can be prevented.

7. Mechanisms of intracranial pressure decompensation

From the moment of exceeding the compensatory capacities of the PIC increases, the intracranial hypertension evolves as a disease and corresponds to the cerebral pathology for which the volume-pressure imbalance is an etiologic factor (12).

Increased ICP has two intracranial consequences:

- cerebral circulation disorder with impaired cerebral blood flow
- displacements of cerebral substance with hernias between the supratentorial, subtentorial and spinal compartments, through the pressure gradient.

The increase in pressure is related to intracranial volume changes and compensation mechanisms. The symptoms depend on the initial cause of HIC, development rate (expansion, pressure increase, cerebral distortion) and individual characteristics (CSF volume, width of tentorial communications, etc.).

The clinical picture of decompensated intracranial hypertension is threatening or severe. The consequences of HIC occur by affecting the cerebral circulation and / or by cerebral hernias and occur due to ischemia, hemorrhage and direct compression of the vital centers in the brainstem.

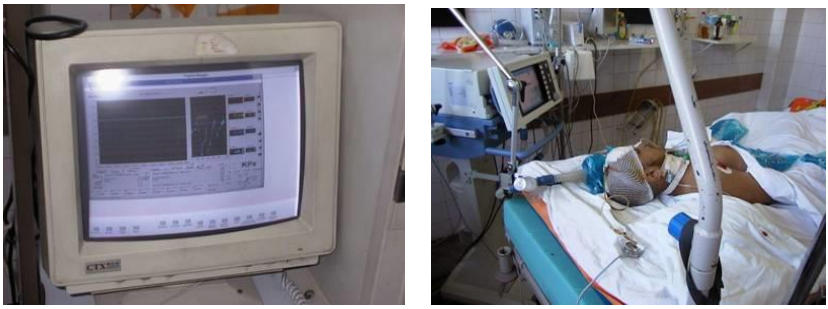

Figure 1. ICP monitoring using ventriculostomy on a patient in a comatose patient after severe traumatic brain injury. Image source: Personal case of Prof. Dr. AV Ciurea

8. Cerebral ischemia secondary to intracranial hypertension

Moderate increase in PIC does not induce marked changes in cerebral blood flow. Higher PIC increases initially cause capillary closure with blood flow reduction but maintaining CPP. (13)

Vital signs may also change under ICH. The Cushing response, defined as arterial hypertension and bradycardia, arise as a result or either generalized central nervous system ischemia or of focal ischemia due to pressure on the brain stem; bradycardia is possibly a consequence of vagus nerve stimulation which may occur independently to hypertension.

Marked increase in ICH causes extremely low CPP, cerebral vascular collapse and cerebral blood flow to cease. Ischemic areas exacerbate cerebral edema and progressively expand manifested by a clinical syndrome of progressive aggravation.

9. Brain herniation

Brain herniation is the movement of the cerebral parenchyma from its normal location to neighboring regions or over other intracranial structures. The pressure conflict between the intracranial content and the container is manifested by the cerebral hernia at the moment of the appearance of a marked pressure gradient between intracranial and spinal compartments (5).

This situation corresponds to the intracranial hypertension, the acute form with a rapid uncompensated increase of the PIC at the level of an intracranial compartment or in the chronic form with the progressive increase of the PIC until the compensatory mechanisms are exceeded. Herniated expansion affects vital centers in the brainstem indirectly or through direct injury.

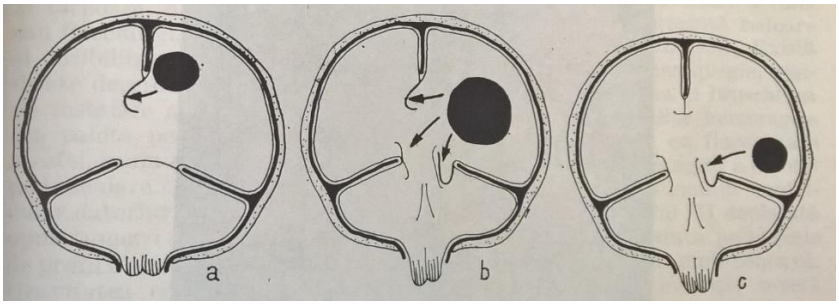

Figure 2. A. Subfalcine herniation in case of frontal expansive process; B. Subfalcine, uncal and central herniation; C. Uncal heniation
(Image source: Arseni C., Constantinescu Al.I., Maretsis M., Semiologie Neurochirurgicală, Ed. Didactică și Pedagogică, București, 1977.)

Central transtentorial herniation represents a downward shift of cerebral hemispheres and basal ganglia which compress and displace the diencephalon through the tentorial incisura. Subsequent displacement of the brain stem causes blood flow impairment in the paramedian branches of the basilar artery which leads to altered levels of consciousness and abnormal respiration. Pupils become small, with low reactivity to light. As the brain stem being more and more involved, respiration becomes tachypneic and pupils fall into a midline fixed position. Internuclear ophthalmoplegia may also arise (medial longitudinal fasciculus being affected) associated with decerebrate posturing. Respiration remains rapid and shallow in pons involvement while it becomes irregular, with prolonged sighs and gasps in medullary involvement. As hypoxia ensues, pupils dilate and brain death follows.

Uncal herniation is represented by the medial shift of the uncus and hippocampal gyrus to the tentorial notch, with significant brain stem involvement. Firstly, ipsilateral to uncal herniation the pupil becomes dilated with poor reactivity to light. It then fully dilates as the oculomotor ophthalmoplegia develops. If midbrain compression occurs, consciousness may be impaired, followed by contralateral decerebrate posture. If the uncal compression progresses, extensor plantar reflexes appear bilaterally, along with dilation of the

contralateral pupil. Finally, patients develop hyperpnea, midposition pupils, impaired oculovestibular response and bilateral decerebrate rigidity. From this point the progression is similar to that of central herniation.

Subfalcine herniation of the cingulate gyrus is caused by expansion of one hemisphere that causes a movement of the cingulate gyrus under falx cerebri. This type of hernia leads to compression of the internal cerebral veins and/or ipsilateral anterior cerebral artery.

Upward transtentorial herniation is a type of brain herniation which appears in posterior cerebral fossa lesions. Lesions with similar location may as well lead to **downward transforaminal herniation** – when cerebellar tonsils move towards and eventually through foramen magnum which leads to medullary compression. The latter is the most frequently encountered and it represents the highest risk of all.

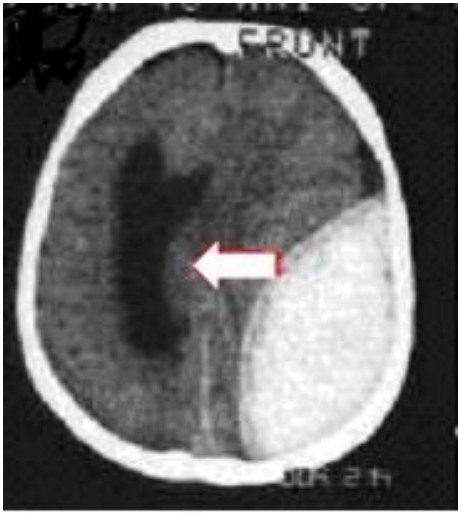

Figure 3. Parietal-temporal-occipital epidural hematoma with subfalcine herniation.
(Personal collection of Prof. Dr. AV Ciurea)

10. Clinical symptoms of intracranial hypertension

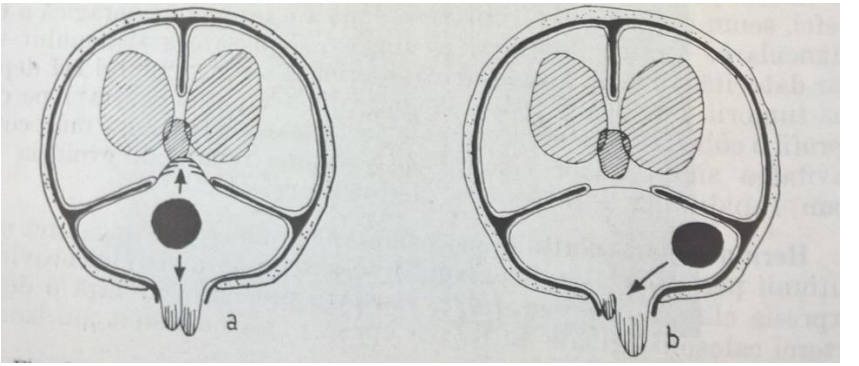

Figure 4. A. Upward transtentorial herniation and downward transforaminal herniation of the cerebellar tonsils in a midline intracranial lesion. B. Downward transforaminal herniation of the cerebellar tonsils in a cerebellar hemisphere lesion. (Image source: Arseni C., Constantinescu Al.I., Maretsis M., Semiologie Neurochirurgicală, Ed. Didactică și Pedagogică, București, 1977.)

The clinical picture of intracranial hypertension comprises two groups of symptoms (13):

- Main symptoms are represented by the triad **headache**, **vomiting** and **papillary edema**
- Mental disorders, meningeal irritation, paresis of oculomotor nerves, vegetative disorders and seizures may also occur.

The association between headache and papillary edema is significant for intracranial hypertension. The addition of mental disorders and / or vomiting is a pathognomonic clinical picture for intracranial hypertension. Vomiting without any associated nausea is especially suggestive of intracranial disease. Varying degrees of cranial nerve palsies may be present due to the pressure of brainstem nuclei (abducens nerve palsy is one of the most common cranial nerve palsies).

11. Investigations

The investigations are made according to the clinical stage of the intracranial hypertension specified by patient's history and clinical signs. (14,15).

In the case of a ICH syndrome with a slow clinical picture, with uncommon headache, without a clear neurological syndrome:

- a complete ophthalmological examination is performed;
- a craniocervical radiographic examination is performed;
- a computed tomography brain scan is performed.

Any ICH syndrome is mandatory to investigate and based on MRI – it provides most of the paraclinical information and it is also a non-invasive method. If the patient presents with a history of seizures, an electroencephalographic examination is performed, which may reveal a focal lesion. Because slowly expanding hemispheric brain lesions can often cause insignificant EEG changes and infratentorial lesions do not produce EEG abnormalities, this exploration does not provide useful data for the diagnosis of ICH.

Suspicion of decompensated intracranial hypertension is raised in the case of a patient with altered state of consciousness (severe condition), in whom the history and neurological examination leads to the suspicion of a brain injury, urgent CT scan or MRI (and cranial radiography and cervical in trauma) are performed.

12. Treatment

The treatment of intracranial hypertension depends on the mechanism of ICH and the evolutionary stage of the disease. The treatment is primarily etiological - to remove the cause which induced the increase in intracranial pressure as well as pathogenic – interrupting the mechanisms by which the nerve structures are affected; a symptomatic treatment is also applied to reduce the intensity of the clinical syndrome (16,17).

The term etiological treatment refers to the etiology of intracranial hypertension, such as the immediate cause that increases the ICP: for example, in the case of a brain metastasis leading to HIC, the meaning of etiological treatment is given to the action of removing the metastasis and is not related to the etiology and home neoplasia

therapy. The treatment of intracranial hypertension can be complex by combining the three therapeutic modalities applied simultaneously or successively (3).

The specification of the type of intracranial hypertension determines the therapy to be applied:

12.1. Etiologic treatment

- intracranial expansive processes: brain tumors, intracranial hematomas, brain abscesses, hydatid cyst, etc.,
- hypertensive encephalopathy due to vascular intracranial hypertension,
- thrombosis of intracranial vessels, venous or arterial, from vascular intracranial hypertension,
- CSF circulation disorders due to the existence of a ventricular or paraventricular tumor with obstructive hydrocephalus,
- CSF resorption disorders in acute meningitis.

12.2. Pathogenic treatment

- all cases of ICH with known etiology, in order to stop the evolution of pathogenic mechanisms that have already been triggered (18,19),
- parenchymal intracranial hypertension due to post-traumatic cerebral edema, hypoxic cerebral edema due to post-traumatic secondary cerebral ischemia or subarachnoid hemorrhage, general intoxication with neurotoxins (endogenous or exogenous), etc.,
- vascular intracranial hypertension due to cerebral venous thrombosis, superior sagittal sinus thrombosis with decreased venous drainage and blockage of CSF absorption, or in secondary ischemic cerebral edema from ischemic stroke caused by occlusion or stenosis of large cerebral vessels (20),
- intracranial hypertension by disturbing the dynamics of the CSF,
- idiopathic intracranial hypertension, especially to block the evolution of some complications.

- an important role in the pathogenic treatment of ICH is the decompressive flaps. Their indication was initially in cranio-cerebral trauma with major edema, in which in the first 6 hours the decompressive component together with the other measures performed in intensive care managed to significantly improve the prognosis of ICH cases, sometimes with severe evolution (22,23). These decompressive patches have also extended to cerebral edema due to other causes (such as vascular) (18).
-

12.3. Symptomatic treatment

All cases of intracranial hypertension to which etiological therapy is applied and / or pathogenic benefits from symptomatic treatment in relation to the symptoms presented.

13. Conclusions

The whole ICH syndrome, with all the aspects described above, represents a diagnostic and therapeutic neurosurgical emergency. This is due to the fact that in the narrow frame of the cranial box, the three elements (cerebral parenchyma, cerebrospinal fluid and blood compartment) must be in perfect balance (15, 21).

Any alteration of this balance by the appearance of an especially intracranial expansive process leads to the creation of a pressure cone, such as a cerebral hernia, that will affect the brain stem. After the failure of the compensatory means, the neural structures will highly suffer, so that the therapeutic sanction must be extremely fast and effective.

Abbreviations:

ICH - intracranial hypertension, **CSF** - cerebral spinal fluid, **ICP** - intracranial pressure, **CPP** - cerebral perfusion pressure, **MAP** - mean arterial pressure, **CT** - Computed Tomography.

Disclaimer: the authors declare no conflict of interests.

References:

1. Ciurea A.V., Tratat de Pediatrie - Hipertensiunea intracraniană, sub redacţia Prof. Dr. E.P. Ciofu, Dr. Carmen Ciofu, Editura Medicală, Bucureşti, 2001.
2. Iencean St M A new classification and a synergetical pattern in intracranial hypertension Medical Hypotheses, 2002;**58**:159-63.
3. Iencean St M, Ciurea AV. Hipertensiunea intracraniana. In Prof dr Irinel Popescu (ed general), Prof dr AV Ciurea (ed vol Neurochirurgie) (eds.), Tratat de Chirurgie , vol II, Neurochirurgie. Ed Academiei Romane, 2007.
4. Ciurea A.V., Tratat de Neurochirurgie Vol. 1, Editura Medicală, Bucureşti, 2010.
5. Constantinovici A, Ciurea AV Ghid practic de neurochirurgie, Ed Medicală, Bucureşti, 1998
6. Dunn LT. Raised intracranial pressure.J Neurol Neurosurg Psychiatry. 2002 ;**73**: i23-7.
7. Kellie, G. (1824) An account of the appearance. Transactions of the medico-chirurgical society of Edinburgh. 1:84
8. Iencean St M Classification and essential conditions of decompensation in intracranial hypertension, Rom J Neurosurgery 2004, **I**, pp. 3-13
9. Iencean St M Actual state in intracranial hypertension, Ed. „Gh. Asachi" Iaşi 2003
10. Iencean St M Hipertensiunea intracraniană, Ed Institutul European, Iaşi, 2006
11. Arseni C., Constantinescu Al.I., Maretsis M., Semiologie Neurochirurgicală, Ed. Didactică şi Pedagogică, Bucureşti, 1977.
12. Iencean St.M., Ciurea A.V., Intracranial hypertension classification, Journal of Medicine and Life, Vol.1, No.2, pp. 101 - 107, 2008.
13. Ciurea A.V., Tratat de Neurochirurgie Vol. 2, Editura Medicală, Bucureşti, 2011.
14. Arseni C, Constantinescu Al I Hipertensiunea intracraniană Ed Academiei Române, Bucuresti 1972
15. Mohan D., Ciurea AV, Mohan AG; Curs de neurochirurgie; Ed. Univ. din Oradea; 2014
16. Dunn LT. Raised intracranial pressure.J Neurol Neurosurg Psychiatry. 2002 ;**73** :i23-7.
17. Marmarou A. The pathophysiology of brain edema and elevated intracranial pressure. Cleve Clin J Med. 2004;**71** Suppl 1:S6-8.

18. Adamson DC, Dimitrov DF, Bronec PR. Upward transtentorial herniation, hydrocephalus, and cerebellar edema in hypertensive encephalopathy. Neurologist. 2005 ;**11** :171-5.
19. Ciurea AV, Arseni Aurelia, Alexianu D şa Edemul cerebral acut, factor agravant în politraumatisme la copii. Neurologia, Psihiatria, Neurochirurgia , 1988, **23**, 267-276.
20. Rajpal S, Niemann DB, Turk AS. Transverse venous sinus stent placement as treatment for benign intracranial hypertension in a young male: case report and review of the literature. J Neurosurg. 2005;**102**:342-6.
21. Iencean St M Pattern of increased intracranial pressure and classification of intracranial hypertension. Journal of Medical Sciences, 2004, **4** :52- 58
22. Schneider GH, Bardt T, Lanksch WR, Unterberg A. Decompressive craniectomy following traumatic brain injury: ICP, CPP and neurological outcome. Acta Neurochir Suppl. 2002;**81**:77-9.
23. Jiang JY, Xu W, Li WP, Xu WH, et al Efficacy of standard trauma craniectomy for refractory intracranial hypertension with severe traumatic brain injury: a multicenter, prospective, randomized controlled study. J Neurotrauma. 2005;**22**:623-8 py. Mol Aspects Med. 2012;33(5–6):691-703.

Contents
vol. 1